Measurements, Modeling and Analysis of High Pressure Gas Sorption in Shale and Coal for Unconventional Gas Recovery and Carbon Sequestration

Xu Tang

Dissertation submitted to the faculty of the Virginia Polytechnic Institute and State University in partial fulfillment of the requirements for the degree of

Doctor of Philosophy
In
Mining Engineering

Nino S. Ripepi, Chair
Gerald H. Luttrell
Kramer D. Luxbacher
Matthew R. Hall
Cheng Chen

November 28, 2016
Blacksburg, Virginia

Keywords: adsorption, shale, coal, high pressure, methane, carbon dioxide, thermodynamics, kinetics

Measurements, Modeling and Analysis of High Pressure Gas Sorption in Shale and Coal for Unconventional Gas Recovery and Carbon Sequestration

Xu Tang

ABSTRACT

In order to exploit unconventional gas and estimate carbon dioxide storage potential in shale formations and coal seams, two key questions need to be initially answered:

1) What is the total gas-in-place (GIP) in the subsurface reservoirs?
2) What is the exact ratio between bulk gas content and adsorbed gas content?

Both questions require precise estimation of adsorbed phase capacity of gases (methane and carbon dioxide) and their adsorption behavior in shale and coal. This dissertation therefore analyzes adsorption isotherms, thermodynamics, and kinetics properties of methane and carbon dioxide in shale and coal based on experimental results to provide preliminary answers to both questions.

It was found that the dual-site Langmuir model can describe both methane and carbon dioxide adsorption isotherms in shale and coal under high pressure and high temperature conditions (up to 27 MPa and 355.15K). This allows for accurate estimation of the true methane and carbon dioxide GIP content and the relative quantity of adsorbed phases of gases at in situ temperatures and pressures representative of deep shale formations and coal seams. The concept of a deep shale gas reservoir is then proposed to optimize shale gas development methodology based on the successful application of the model for methane adsorption in shale.

Based on the dual-site Langmuir model, the isosteric heat of adsorption is calculated analytically by considering both the real gas behavior and the adsorbed phase under high pressure, both of which are ignored in the classic Clausius–Clapeyron approximation. It was also found that the isosteric heat of adsorption in Henry's pressure region is independent of temperature and can serve as a quantified index to evaluate the methane adsorption affinity on coal.

In order to understand the dynamic response of gas adsorption in coal for carbon sequestration, both gas adsorption kinetics and pore structure of coal are investigated. The pseudo-second order model is applied to simulate the adsorption kinetics of carbon dioxide in coals under different pressures. Coal particle size effects on pore characterization of coal and carbon dioxide and nitrogen ad/desorption behavior in coal was also investigated.

Measurements, Modeling and Analysis of High Pressure Gas Sorption in Shale and Coal for Unconventional Gas Recovery and Carbon Sequestration

Xu Tang

GENERAL AUDIENCE ABSTRACT

Shale gas is natural gas that is found trapped within subsurface shale formations, and the in-situ pressure and temperature of shale formations can go up to 27MPa and 86℃. Shale gas, the main component of which is methane, mainly consists of adsorbed phase and free compressed gas in shale formations. The adsorbed phase accounts for 20-85% of the total gas-in-place resource. Thus, the estimation of amount of methane adsorbed in shale under in-situ conditions are extremely important for determining the total gas-in-place quantity and the working life of a shale gas production well and its economic viability. This work provides a method for accurate estimation of the shale gas-in-place resource under in-situ shale formation conditions. The method is based on laboratory methane adsorption test data in shale at high pressure (up to 27MPa) and high temperature (up to 82℃) conditions. According to this method, it was found that for depths greater than 1000 m (> 15 MPa) in the subsurface, the shale gas resources have historically been significantly overestimated. For Longmaxi shale (2500 – 3000 m in depth), classical approaches overestimate the GIP by up to 35%. The ratio of the adsorbed phase compared to the free gas has been significantly underestimated.

Shale gas production follows pressure depletion of shale formations. The pressure depletion process allows methane in the adsorbed phase to become free gas, which is known as the physical desorption process. Desorption is an endothermic process while adsorption is an exothermic process, both of them are reversible. Thus, the heat transfer process during shale gas production requires a thermodynamic analysis of methane adsorption in shale. This work investigates the isosteric heat of adsorption for methane in shale by considering both the real gas behavior and the volume effect of the adsorbed phase, not previously considered for methane in shale. The temperature dependence as well as the uptake dependence of the isosteric heat can be readily investigated by the applied method. This study lays the foundation for future investigations of the thermodynamics and heat transfer characteristics of the interaction between high pressure methane and shale.

This work also investigates gas adsorption kinetics properties in coal and the particle size effect on pore characterization of coal using the gas adsorption approach. Results show that particle size of coal samples can significantly influence the sorption behavior of gas in coal, which finally affects pore characterization of coal. It is difficult to characterize the pore structure of coal using only one coal particle size. Carbon dioxide adsorption kinetics in coal, which can be modelled by the pseudo-second order model, is a combination of both bulk diffusion-controlled and surface interaction-controlled processes; the former dominates the initial stage while the latter controls the majority of the overall process.

DEDICATION

This dissertation is dedicated to my father, Yinghai Tang, and my mother, Xiangniu Wang.

ACKNOWLEDGEMENT

First, I would like to thank my advisor, Dr. Nino S. Ripepi for giving me the opportunity to complete this dissertation and for providing me the best study and research conditions in Virginia Tech. Without his continuous encouragement and extensive discussion on this topic, this work cannot be completed.

I am very thankful to Dr. Gerald H. Luttrell, Dr. Kray Luxbacher, Dr. Matthew Hall and Dr. Cheng Chen for being the examiners of my dissertation. I would also like to give my special thanks to Dr. Matthew Hall (University of Nottingham, UK) for supervising me when I was an exchange student in the University of Nottingham. His tremendous knowledge and friendliness helped me to understand the fundamental principle of gas adsorption.

Furthermore, I would like to thank my colleges in the mining department and VCCER (Virginia Center for Coal & Energy Research) and for their help and support in the laboratory works: Charles Schlosser, Kyle Louk, Ellen Gilliland, Scott Jeter, Cigdem Keles, Joseph Amante, Flora Lado, Marina Rossi, Biao Li, Ming Fan, Kaiwu Huang. I gratefully acknowledge Dr. Alex O. Aning (Materials Science and Engineering, Virginia Tech), Dr. Emily Sarver and Dr. Roe-Hoan Yoon for their permission to use their laboratory instruments.

I would also like to thank several collaborators for their help in conducting the high pressure gas adsorption tests in shale and coal and for their valuable discussions on this work: Dr. Zhaofeng Wang, Mr Lingjie Yu and Dr. Nicholas P. Stadie.

Finally, I would like to thank and dedicate this dissertation to my family for their constant supports throughout all those years. Special thanks go to my wife, Min Chu, for all her encouragement and support all the time.

TABLE OF CONTENTS

TABLE OF CONTENTS vi
LIST OF FIGURES viii
LIST OF TABLES xii
PREFACE xiii
Chapter 1 Introduction 1
1.1 Background 1
1.1.1 Gas adsorption phenomenon 2
1.1.2 Gibbs excess adsorption concept 3
1.1.3 Thermodynamics of adsorption 5
1.1.4 Kinetics of adsorption 7
1.2 Problem statement 7
1.3 Objectives of this dissertation 8
References 9
Chapter 2 High pressure methane adsorption in shale for deep shale gas resource estimation 13
2.1 Comparison of adsorption models for high pressure methane adsorption in shale 13
2.1.1 Introduction 14
2.1.2 Adsorption model review 15
2.1.3 Model evaluation criteria 19
2.1.4 Test results and data processing method 20
2.1.5 Results and discussion 21
2.1.6 Conclusions 27
References 27
2.2 A dual-site Langmuir equation for accurate estimation of high pressure deep shale gas resources 33
2.2.1 Introduction 34
2.2.2 Dual-site Langmuir adsorption model 36
2.2.3 Materials and methods 39
2.2.4 Results and discussions 39
2.2.5 Conclusions 49
References 50
2.3 Deep means different: concept of the deep shale gas reservoir and its influence on shale gas development 55
2.3.1 Introduction 56
2.3.2 Current fundamentals for shale gas development 57
2.3.3 Concept of deep shale gas reservoir and its implication 62
2.3.4 Implications for shale gas development 64
2.3.5 Conclusions 67
References 67
Chapter 3 Thermodynamic analysis for gas adsorption in shale and coal 73
3.1 Adsorption affinity of different types of coal: mean isosteric aeat of adsorption 73
3.1.1 Introduction and background 74
3.1.2. Isothermal adsorption tests: from 243.15K to 303.15K 75

3.1.3 The mean isosteric heat of adsorption 79
3.1.4 Results analysis and discussion 81
3.1.5 Conclusions 85
References 86
3.2 Thermodynamic analysis of high pressure methane adsorption in Longmaxi shale 91
3.2.1 Introduction 92
3.2.2 Adsorption model and thermodynamic calculations 94
3.2.3 Experimental data and analysis 99
3.2.4 Thermodynamic analysis and discussion 101
3.2.5 Discussion 105
3.2.6 Conclusions 107
References 108
3.3 High pressure supercritical carbon dioxide adsorption in coal: adsorption model and thermodynamic characteristics 112
3.3.1 Introduction 113
3.3.2 Absolute adsorption model 116
3.3.3 Gibbs excess adsorption model and isosteric heat of adsorption 117
3.3.4 Data set acquisition and processing 120
3.3.5. Modeling results and discussions 121
3.3.6 Implications for geological carbon dioxide storage 126
3.3.7 Conclusions 127
References 128
Chapter 4 Gas adsorption kinetics analysis and pore characterization of coal 136
4.1 Isothermal adsorption kinetics properties of carbon dioxide in crushed coal 136
4.1.1 Background and introduction 137
4.1.2 PSO sorption kinetics model 138
4.1.3 Experimental section 140
4.1.4 Test results 144
4.1.5 Discussion 146
4.1.6 Conclusions 154
References 155
4.2 How different coal particle sizes generate unreliable pore characterization from gas adsorption test 161
4.2.1 Introduction 162
4.2.2 Experimental methodology 163
4.2.3 Test results and discussion 165
4.2.4 Conclusions 171
References 172
Chapter 5 Conclusions and future work 179
5.1. Conclusions 179
5.2. Future work 181
Appendix A Supplemental materials for Section 2.2 183
Appendix B Supplemental materials for Section 4.1 191
Appendix C Copyright releasing documents from publishers 194

LIST OF FIGURES

Figure 1.1.1 Concept of Gibbs surface excess sorption for gas adsorption on solid. V_{tot} is the sum of V_a*and V_{gas}* which can be measured by non-adsorbed gas (Helium) intrusion test. The density file shows the hypothetical density profile near the solid surface. 4

Figure 1.1.2 Compressibility of methane and carbon dioxide under different pressures and temperatures. (Data is obtained from the NIST Standard Reference Database 23 (REFPROP: Version 8.0.)) 6

Figure 2.1.1 Depiction of the physical modelling approach from real world to conceptual world (revised from Dym et al., 2004) 19

Figure 2.1.2 High pressure methane adsorption test in shale (a: observed adsorption uptake as a function of pressure; b: observed adsorption uptake as a function of bulk gas density) 21

Figure 2.1.3 Comparison between fitting curve and test data for each model: symbols represent test data, solid lines represent fitting curves. 22

Figure 2.1.4 Relative error between fitting data and test data for each method for all raw data 23

Figure 2.1.5 Modelled values of the density of gaseous (solid color lines, left axial), adsorbed and liquid methane (solid black lines, left axial) and the coefficient of equation (7) ($(n_{\max} - \rho_g V_{\max})$, dotted lines, right axial) on Longmaxi shale as a function of pressure 24

Figure 2.1.6 Surface coverage of the methane in shale 24

Figure 2.1.7 Adsorption model fitting results: Gibbs excess adsorption content as a function of bulk methane density 25

Figure 2.1.8 Extrapolated Gibbs excess adsorption isotherms of methane on Longmaxi shale (dashed lines) and as a function of bulk methane density (Note: Method 6 cannot be used to predict isotherms because there is no consistent empirical relationship between fitting parameters and temperature) 26

Figure 2.2.1 Gibbs excess adsorption isotherms of methane on Longmaxi shale (symbols) and dual-site Langmuir model fits (lines) 40

Figure 2.2.2 Modelled values of the volume of adsorbed methane (V_a) (solid lines, filled symbols, left major axis) and the volume-density term (V_a*ρ_g) (dotted line, hollow symbols, right minor axis) on Longmaxi shale as a function of pressure 41

Figure 2.2.3 Gibbs excess adsorption isotherms of methane on Longmaxi shale (symbols) and dual-site Langmuir equation fits (lines) as a function of bulk methane density 42

Figure 2.2.4 Gibbs excess adsorption (solid lines, filled symbols) and absolute adsorption (dashed lines) isotherms of methane on Longmaxi shale as fitted by a dual-site Langmuir equation (measured up to 355.15 K), extrapolated up to 415.15 K (gradual grey lines) 43

Figure 2.2.5 Schematic depiction of the quantities relevant to gas-solid adsorption in two distinct regimes: in the dilute limit (left) and at high pressures (right) of the bulk gas 44

Figure 2.2.6 Directly calculated shale GIP content as a function of pressure using the measured data at 355.15 K 45

Figure 2.2.7 Comparison of the Gibbs excess adsorbed methane content (solid line) to two estimates of absolute adsorbed methane (dashed lines) on Langmaxi shale, at geological conditions of one completion well (353.15 K and up to 37.69 MPa (34)). 47

Figure 2.2.8 Comparison of methane adsorption capacity in Fuling region shale formations under geological temperature and pressure conditions as they vary with depth. Predictions are based on the following adsorption quantities: observed Gibbs excess adsorption, modeled absolute adsorption uptake (this work) and the "Conventional Absolute Prediction" (refer to Supplemental Materials). 47

Figure 2.2.9 Shale GIP content in Fuling region shale formations under geological conditions, where temperature and pressure are varied as a function of depth. The Correct Method uses Eq. 8 where n_e is calculated using Eq. 6; Incorrect Method 1 uses Eq. 9 where n_a is calculated using Eq. 5; Incorrect Method 2 uses Eq. 9 where n_a is calculated using the Conventional Absolute Prediction (refer to Supplemental Materials). 48

Figure 2.2.10 Comparison of the estimated contribution to total GIP content by adsorbed methane in Longmaxi shale by three methods: where the actual adsorbed amount is estimated as the excess uptake (solid red), absolute uptake (by a dual-Langmuir fit, dashed red), and by a conventional prediction of absolute uptake (dashed black). For demonstration purposes, the correct total GIP content is used in all cases (via Eq. 8). 49

Figure 2.3.1 Conceptual model for shale gas phases in formations: both V_{shale} (skeletal volume of shale) and V_{tot} (total volume of pore space) can be measured using Helium intrusion tests; V_a (volume of adsorbed layers) and V_{free} (free gas volume existing in the shale formation) are unmeasurable using current technologies. 58

Figure 2.3.2 Conventional shale gas research methodology 61

Figure 2.3.3 High pressure methane adsorption isotherms under different temperatures; solid squires are measured data, solid color lines are fitting curves using equation (6), dotted color lines are fitting curves using equation (7), black solid and dotted lines are extrapolated adsorption isotherms beyond test data .. 63

Figure 2.3.4 Fundamentals for shale gas development 64

Figure 3.1.1 Schematic setup for low temperature isothermal sorption-diffusion comprehensive device; 1-Gas Chromatograph (GC), 2-Data recording module, 3-Vaccum pump, 4- Vaccum gage, 5- Water injection pump, 6-Measuring cylinder, 7-Sample cell; the low temperature control system can control the temperature between 225.15K and 373.15K with fluctuation of ±0.5 K. 76

Figure 3.1.2. Sorption pressure decreases with time in low temperature control system 78

Figure 3.1.3. Isothermal adsorption of methane in different types of coal under different temperatures ... 79

Figure 3.1.4 Relationship between ln(K') and the reciprocal of temperature for coal 81

Figure 3.1.5 Relationship between ln(P/n) and n 82

Figure 3.1.6 The isosteric heat of adsorpion acquired via the Clausius-Clapeyron equation (after [41] Yue, G. et al, 2014) 85

Figure 3.2.1. Equilibrium adsorption uptake of methane on Longmaxi shale between 303-355 K and 0.5-25 MPa: solid symbols are measured Gibbs excess uptake, solid lines are modeled Gibbs excess uptake (equation (4)), and open symbols and dashed lines are modeled absolute uptake (equation (2)). The data are reproduced from a previous study [36]. 100

Figure 3.2.2. Isosteric heat of adsorption of methane on shale between 303-355 K (blue to red) as a function of absolute adsorption uptake up to 30 MPa (solid lines). For comparison, the isosteric heat calculated by including experimental data from restricted ranges of pressure and temperature is also shown (as small and large dashes, respectively). 102

Figure 3.2.3. Isosteric heat of adsorption of methane on shale as calculated using four different methods: $\Delta H_{ads(na),\ IGL\text{-}OV}$ (equation (12)) as solid lines, $\Delta H_{ads(na),\ RGL\text{-}0V}$ (equation (14)) as dashed lines, $\Delta H_{ads(na),\ IGL}$ (equation (11)) as single dotted lines, and $\Delta H_{ads(na),\ RGL}$ (equation (13)) as double dotted lines. The isosteric

heat of adsorption calculated in the C-C approximation (equation (9)) is also shown as filled black symbols. 103

Figure 3.2.4. Comparison of isosteric heat of adsorption of methane on shale: $\Delta H_{ads(na),\ IGL\text{-}OV}$ (equation (12)) as solid lines, $\Delta H_{ads(na),\ IGL}$ (equation (11)) as single dotted lines, $\Delta H_{ads(na),\ RGL\text{-}0V}$ (equation (14)) as dashed lines and $\Delta H_{ads(na),\ RGL}$ (equation (13)) as double dotted lines. The isosteric heat of adsorption calculated in the C-C approximation (equation (9)) is also shown as filled black symbols..... 104

Figure 3.2.5. Equilibrium adsorption uptake of methane on shale (n_a) between 303-355 K and 0.5-25 MPa, as measured (solid symbols) and as fitted by a virial-type equation (solid lines, equation (19)). (left) Adsorption uptake is shown as a product of n_a and $1\text{-}P/P_{max}$, as a function of P/P_{max}. (right) Adsorption uptake is shown in the linear region for $\ln(P/n_a)$ as a function of n_a. 105

Figure 3.2.6. Mean isosteric heat of adsorption calculated by equation (17) 105

Figure 3.3.1 Deviation behavior of the CO_2 under different temperatures and pressures (Data is obtained from the NIST Standard Reference Database 23 (REFPROP: Version 8.0.)) 116

Figure 3.3.2 The difference of CO_2-coal sorption system before and after CO_2 adsorption..... 117

Figure 3.3.3 Experimental data retrieved from Song et al.(2015), Ottiger et al.(2006); the dotted line is to connect data points for visualization..... 120

Figure 3.3.4 Fitting adsorption isotherms using dual-site Langmuir model for five coals; solid line: Gibbs excess fitting (equation (8)) and dotted line: absolute adsorption uptake (equation (5))..... 121

Figure 3.3.5 Surface coverage (solid line, left axial) and the term ($n_{max}\text{-}V_{max}*\rho$ (P,T)) (dotted lines, right axial) with increasing pressure (density) for both Chinese and Sulcis coals 122

Figure 3.3.6 Prediction of adsorption isotherms (black lines) beyond test data; left: adsorption uptake as a function of pressure, right; adsorption uptake as a function of bulk density. 124

Figure 3.3.7 Adsorption isotherms comparison between fitting data using three low temperature isotherms (dotted dark lines) and fitting data using four temperature adsorption isotherms (solid color lines). Solid symbol represents test data. 125

Figure 3.3.8 Comparison of different isosteric heats of adsorption for $scCO_2$ in coal: isosteric heat of adsorptions using ideal gas law (dotted lines) and real gas law (solid lines), and the gas phases are supercritical and liquid in the magnified area. 125

Figure 3.3.9 Density of liquid and $scCO_2$; dotted line represents liquid carbon dioxide and solid line represents $scCO_2$ 126

Figure 4.1.1 Schematic of high temperature and pressure (HTHP) isothermal test setup 142

Figure 4.1.2 Time dependent sorption data recording process 143

Figure 4.1.3 Relation between isothermal sorption content and time at 50℃ for bituminous and subbituminous coal 145

Figure 4.1.4 Isothermal adsorption curves for bituminous and subbituminous coal at 50℃..... 145

Figure 4.1.5 Measurement error of the pressure transducer..... 146

Figure 4.1.6 Linear relationship between t/Qt and t: stage (1) and stage (8) for bituminous 147

Figure 4.1.7 Linear relationship between t/Qt and t: stage (1) and stage (8) for sub-bituminous coal..... 147

Figure 4.1.8 Relationship between pressure and kinetics parameter Qe..... 149

Figure 4.1.9 Relationship between pressure and kinetics parameter k_2..... 150

Figure 4.1.10 Isothermal adsorption curves and error analysis; Q_{tc} is the predicted value using PSO value, Q_{tm} is the measured test value. 152
Figure 4.1.11 Comparison between predicted values and measured test data 152
Figure 4.1.12 Generalized pore system in coal 153
Figure 4.2.1 Adsorption behavior of carbon dioxide and nitrogen 165
Figure 4.2.2 Knudsen number of CO_2 and N_2 in different size of pore under different test conditions ... 166
Figure 4.2.3 N_2 BET surface area comparison of different sizes of coal particles 167
Figure 4.2.4 Comparison of micropore size distribution of different coal particles from CO_2 adsorption test 168
Figure 4.2.5 Comparison of pore size distribution of different coal particle size from N2 adsorption test 168
Figure 4.2.6 Hysteresis behavior of carbon dioxide in coal 169
Figure 4.2.7 Hysteresis behavior of nitrogen in coal 170
Figure A-1 Blank test results 186
Figure A-2 Helium test results 186

LIST OF TABLES

Table 2.1.1 Comparison of methane adsorption models in shale and coal 18
Table 3.1.1 Physical parameters of coal sample 75
Table 3.1.2 Henry's coefficient (K') determination 82
Table 3.1.3 Determination of the mean isosteric heat of adsorption in coal 83
Table 3.2.1. Definition of various isosteric heats of adsorption 102
Table 3.3.1 Fitting parameters (equation (7)) for coal samples 121
Table 3.3.2 Fitting parameters (equation (7)) for observed adsorption isotherms using only three adsorption isotherms 124
Table 4.1.1 Comparison of different adsorption kinetics models for gas in coal 138
Table 4.1.2 Proximate and ultimate analysis of coal (Unit: %) 141
Table 4.1.3 Test parameters for isothermal sorption system 142
Table 4.1.4 PSO model fitting data 148
Table 4.2.1 Different coal particle sizes used in low temperature gas adsorption analyses 163
Table 4.2.2 Composition of coal samples 164
Table 4.2.3 Microfluidic regime classified by Knudsen number (revised from [56]) 166
Table A-1 Properties of shale 185
Table A-2 Test data under 303.15K, 318.15K, 333.15K, and 355.15K 188
Table A-3 Fitting parameter using two parameter Langmuir equation 189
Table B-1 Comparison between the predicted sorption content and measured data for bituminous coal 192
Table B-2 Comparison between the predicted sorption content and measured data for subbituminous coal 193

PREFACE

This dissertation is submitted as a completion of the degree of Doctor of Philosophy at Virginia Polytechnic Institute and State University. The research described here was conducted by the author, Xu Tang, under the supervision of Dr. Nino S. Ripepi in the Department of Mining & Minerals Engineering at Virginia Polytechnic Institute and State University.

This dissertation mainly comprises three fundamental works for high pressure methane adsorption in shale for deep shale gas resource estimation (Chapter 2), thermodynamic analysis for high pressure gas adsorption in shale and coal (Chapter 3), as well as gas adsorption kinetics analysis and pore characterization of coal (Chapter 4).

In Chapter 1, the basic concepts for adsorption related phenomenon are briefly discussed for shale gas development and geological sequestration of carbon dioxide in unconventional gas reservoirs. The objective of this dissertation is also presented.

Chapter 2 represents a compilation of three separate manuscripts focusing on the methane adsorption model in shale and its application for shale GIP resource estimation in deep formations. First, analysis of laboratory data for methane adsorption in shale (303 - 355 K and up to 27 MPa) proves the single-site Langmuir model becomes invalid under high pressure conditions. Thus, a new concept, the deep shale gas reservoir, is introduced for the shale gas industry based on the observed methane adsorption behavior in shale under high pressure conditions. The deep shale gas reservoir study requires a new high pressure adsorption model. A dual-site Langmuir model is then introduced to interpret observed methane adsorption behavior in shale. This model can not only interpret all observed test phenomena but also is superior to available adsorption models in literature. The proposed model herein allows accurate estimations of the true shale GIP resource and the relative quantity of adsorbed methane at in situ temperatures and pressures representative of deep shale formations.

Chapter 3 is composed of three manuscripts focusing on thermodynamic feature of methane adsorption in shale and carbon dioxide adsorption in coal. On the one hand, the isosteric heat of adsorption within Henry's region is calculated for methane adsorption in coal, which can be used to describe the adsorption affinity of different types of coal. On the other hand, the isosteric heat of adsorption, considering both the real gas behavior and the contribution of adsorbed gas phase,

is calculated analytically for high pressure methane adsorption in shale based on the dual-site Langmuir adsorption model. Both the adsorption model and thermodynamic analysis for supercritical carbon dioxide adsorption in coal are also explored in order to support an on-going carbon dioxide sequestration field test in unminable coal seams.

Chapter 4 contains two manuscripts. The first one studies the carbon dioxide adsorption kinetics properties of crushed coal using the pseudo-second order (PSO) model. Understanding both the pore feature of coal and the dynamic response of coal to carbon dioxide sorption are important for optimizing carbon dioxide injection methods in unconventional reservoirs such as coal seams and shale formations to enhance natural gas production. The second exhibits how different coal particle sizes used in the low pressure gas adsorption methods affects the pore characterization of coal samples.

In Chapter 5, conclusions from this dissertation are summarized. Suggestions for future work, that have not been covered in this work but deserve attention in future research, are presented.

The Appendix section contains both supplemental materials for this dissertation and the copyright release documents from publishers for three published papers.

Part of this dissertation has been published in the following peer-reviewed journals:

- Tang, X., Ripepi, N., Stadie, N. P., Yu, L., & Hall, M. R. (2016). A dual-site Langmuir equation for accurate estimation of high pressure deep shale gas resources. Fuel, 185, 10-17.
- Tang, X., Wang, Z., Ripepi, N., Kang, B., & Yue, G. (2015). Adsorption affinity of different types of coal: mean isosteric heat of adsorption. Energy & Fuels, 29(6), 3609-3615.
- Tang, X., Ripepi, N., & Gilliland, E. (2015). Isothermal adsorption kinetics properties of carbon dioxide in crushed coal. Greenhouse Gases: Science and Technology. DOI: 10.1002/ghg.1562.

Chapter 1 Introduction

1.1 Background

Unconventional gas now plays a significant role in the world energy profile because of the boom in shale gas production over the past ten years. With the development of horizontal drilling technology coupled with hydraulic fracturing, shale gas (primarily methane) has become the major component of the total natural gas production in the United States [1-6]. Based on the successful experience in the United States, different countries have launched a variety of projects to explore their shale gas resource potential [7-8]. The principle of shale gas exploration and production has followed the methodology developed for coalbed methane (CBM) because shale gas and coalbed methane have some similar features. For example, gas in shale formations and coal seams under reservoir conditions are mainly composed of adsorbed methane and bulk methane, which makes them distinguishable from other gases like tight gas and conventional natural gas. Since the adsorbed methane makes up a large portion of the total gas-in-place (GIP) resource for both shale gas and CBM, it is imperative to understand the relationship between the adsorbed methane quantity and the free methane quantity at reservoir conditions. Thus, the methane adsorption behavior in shale and coal needs to be fully understood in order to accurately estimate the CBM/shale gas resource.

In order to decrease greenhouse gases in the atmosphere like carbon dioxide, geological sequestration of carbon dioxide in unconventional natural gas reservoirs like coal seams and shale formations is likely a promising option [9-12]. The injected carbon dioxide can displace methane in coal and shale and enhance natural gas recovery, which can help offset the cost of carbon capture and storage. In order to initiate the carbon dioxide sequestration project in shale formations and coal seams, the carbon dioxide storage capacity needs to be evaluated. Thus, the states of carbon dioxide under reservoir conditions, such as adsorbed, bulk gas and dissolved phases, must be investigated. Since the dissolved amount of carbon dioxide in reservoir water can usually be neglected compared to the adsorbed and bulk phases, an accurate estimation of the adsorbed phase becomes critical. This therefore requires a thorough understanding of carbon dioxide adsorption behavior under reservoir conditions.

Based on the above discussions, it is noted that the adsorption phenomenon is extremely important for the process of CBM/shale gas development and carbon dioxide sequestration. Thus, the basic concepts for adsorption related phenomena are briefly reviewed in this section.

1.1.1 Gas adsorption phenomenon

Adsorption is a surface phenomenon where the density of a fluid near the surface of solid increases as a condensed phase. The adsorption process is governed by not only the unique properties of the solid (surface heterogeneities, etc.) but also the specific energy of the fluid (temperature, etc.). Physical adsorption can be attributed to the weak van der Waals forces. Methane adsorption in coal and shale belongs to physisorption.

In order to model gas adsorption behavior, different models have been proposed such as Henry's model [13], Langmuir's model [14], BET (Brunauer–Emmett–Teller) model [15] and pore-filling model [16-17]. Among these models, the Langmuir model is the most widely used one because of its simplicity, effectiveness, and the reasonable explanation of its parameters. The Langmuir equation was developed by Irving Langmuir in 1916, which is based on the following assumptions: 1) the adsorption sites are monolayer, independent, unique, and the same at the solid surface, 2) there is no interaction between adsorbed gas molecules, and 3) the dynamic equilibrium state is reached between adsorbed gas molecules and free gas molecules. Langmuir's model can be shown as the following form,

$$n = \frac{n_{\max} KP}{1 + KP} \qquad (1)$$

where n is the adsorbed amount under equilibrium temperature and pressure, n_{max} is the maximum adsorbed capacity, P is the adsorption pressure, K is the Langmuir constant which is a function of temperature. In the limit of low pressure, Langmuir's model is equivalent to Henry's model,

$$n = \lim_{P \to 0} \frac{n_{\max} KP}{1 + KP} = KP \qquad (2)$$

As supported by numerous experimental data for methane in coal and shale, the Langmuir model is routinely used to model methane adsorption in coal and shale for estimating adsorbed methane content at reservoir conditions for the CBM and shale gas industry.

1.1.2 Gibbs excess adsorption concept

In the laboratory, measurements of adsorption using either manometric or gravimetric approaches cannot measure the true adsorbed amount because both methods, in principle, ignore the occupied volume of the adsorbed phase. Under low pressure conditions (<10MPa), this assumption works well, however, this assumption becomes invalid under high pressure conditions (>15MPa) because it is observed that the measured adsorption uptake increases up to a maximum and then decreases with increasing pressure. This observation contradicts the fact that the true adsorbed amount monotonically increases with pressure. In order to solve this issue, Josiah Willard Gibbs introduced the concept of "excess sorption" (also called "Gibbs excess sorption,") where he gives a simple geometric explanation of the measured adsorbed quantity by considering the finite volume of adsorbed phase [18],

$$n_e = n_a - V_{ad} \cdot \rho_g = n_a \cdot (1 - \frac{\rho_g}{\rho_{ad}}) \qquad (3)$$

where n_e is the Gibbs excess adsorbed amount, n_a is the true adsorbed amount (absolute adsorbed amount), V_{ad} is the volume of adsorbed phase, ρ_{ad} is the density of adsorbed phase, and ρ_g is the bulk gas density. The Gibbs excess sorption concept is illustrated in Figure 1. Figure 1 shows a simplified equilibrium sorption system with a single component gas adsorbed on the porous solid at pressure (P) and temperature (T). The density of "gas" (also called "adsorbed phase") near the solid surface is higher than the bulk gas density and decreases with the distance away from the solid surface. At a certain distance, the surface can no longer influence the bulk gas, and the density is equal to bulk gas density.

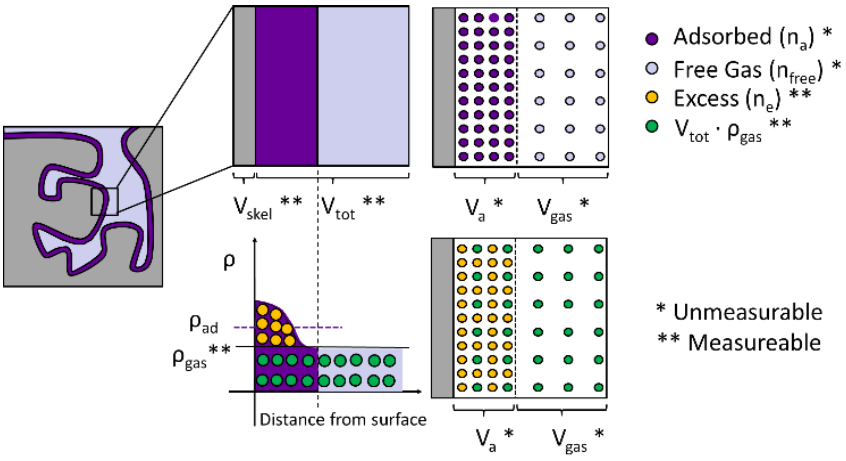

Figure 1.1.1 Concept of Gibbs surface excess sorption for gas adsorption on solid. V_{tot} is the sum of V_a*and V_{gas}* which can be measured by non-adsorbed gas (Helium) intrusion test. The density file shows the hypothetical density profile near the solid surface.

According to Gibbs excess concept, if the volume of the adsorbed phase is extremely small or the density of adsorbed phase is much higher than the bulk gas under low pressure, the Gibbs excess adsorbed amount is almost equivalent to the true adsorbed amount,

$$n_e \approx n_a \qquad (4)$$

This also explains why both the manometric and gravimetric method approximate the true adsorbed amount, therefore, the Langmuir equation (equation (1)) works well for modeling gas adsorption behavior at low pressure conditions.

Under high pressure conditions there will be distinguishable differences between the measured data and the true adsorbed amount, especially when the measured adsorption uptake increases up to a maximum and then decreases with increasing pressure. In this situation, the Langmuir model loses its power, and the Gibbs excess sorption concept needs to be applied. Since the measurement of true physical properties of the adsorbed phase such as density and volume is not possible using current technology, assuming either the density or the volume of the adsorbed phase as a constant may provide a solution.

If the Langmuir model (equation (1)) can describe the relationship between the true adsorbed amount and pressure (most cases for a homogenous surface), the relationship between Gibbs excess adsorbed amount and the true adsorbed amount can be obtained,

$$n_e = \frac{n_{\max} KP}{1+KP} - V_{ad} \cdot \rho_g \qquad (5)$$

For real adsorbents, the heterogeneous surface may offer two (or more) types of adsorption sites with different characteristic energies [19-21]. Under this situation, the single site Langmuir model can be extended to a dual-site Langmuir model corresponding to different adsorption sites,

$$n = n_{\max} \cdot [(1-\alpha)\frac{K_1 P}{1+K_1 P} + \alpha \frac{K_2 P}{1+K_2 P}] \qquad (6)$$

where K_1 and K_2 corresponds to each type of adsorption sites weighted by a coefficient α ($0<\alpha<1$). In this way, another relationship between Gibbs excess adsorbed amount and true adsorbed amount can be obtained,

$$n_e = n_{\max} \cdot [(1-\alpha)\frac{K_1 P}{1+K_1 P} + \alpha \frac{K_2 P}{1+K_2 P}] - V_{ad} \cdot \rho \quad (7)$$

Since equations (5) and (7) consider the volume effect of the adsorbed phase, either of them could provide a practical way to obtain the true adsorbed uptake based on measured data, especially when the measured adsorption uptake increases up to a maximum and then decreases with increasing pressure.

1.1.3 Thermodynamics of adsorption

When a gas molecule is adsorbed on a surface, it changes from free gas to the adsorbed film and therefore results in an energy release. At equilibrium, the change in enthalpy of the system due to adsorption at a specific state of surface occupancy is referred to as the isosteric heat of adsorption (ΔH_{ads}). Generally, the isosteric heat of adsorption can vary as a function of the amount of adsorbate and the system conditions. It therefore serves as an important descriptor of the physisorption system, and is directly related to the strength of the interaction between the gas adsorbate and the solid adsorbent.

The isosteric heat of adsorption can be determined via the Clapeyron relationship which is relevant to the equilibrium between two phases in a closed system,

$$\Delta H_{ads} = (\frac{dP}{dT})_{n_a} \cdot T \cdot \Delta v = (\frac{dP}{dT})_{n_a} \cdot T \cdot (v_a - v_g) \quad (9)$$

Where v_a is the volume of adsorbed phase, v_g is the volume of bulk gas phase, T is temperature. Since the pressure in a closed system is a function of temperature and quantity adsorbed, a general expansion of $(\frac{dP}{dT})_{n_a}$ can be made such that [22],

$$(\frac{dP}{dT})_{n_a} = (\frac{\partial P}{\partial n_a})_T \frac{dn_a}{dT} + P(\frac{\partial(\ln P)}{\partial T})_{n_a} \quad (10)$$

If the bulk fluid is approximated as an ideal gas, $Pv_g = RT$, it follows that,

$$-\Delta H_{ads(n_a)} = RT^2[(\frac{\partial(\ln P)}{\partial T})_{n_a}] + \frac{RT^2}{P}\cdot(\frac{\partial P}{\partial n_a})_T \frac{dn_a}{dT} - [(\frac{\partial P}{\partial n_a})_T \frac{dn_a}{dT} + P(\frac{\partial(\ln P)}{\partial T})_{n_a}]\cdot T\cdot v_a \quad (11)$$

In right hand side (RHS) of equation (8), the second term, $\frac{RT^2}{P}\cdot(\frac{\partial P}{\partial n_a})_T \frac{dn_a}{dT}$, includes the behavior of the adsorbed phase mass, and the third term, $[(\frac{\partial P}{\partial n_a})_T \frac{dn_a}{dT} + P(\frac{\partial(\ln P)}{\partial T})_{n_a}]\cdot T\cdot v_a$, considers the volume effect of the adsorbed phase.

If the volume of the adsorbed layer is taken to be negligible and the influence of the adsorbed mass is therefore ignored, the routinely used Clausius-Clapeyron (C-C) relationship is obtained,

$$\Delta H_{ads} = \Delta H_{ads,c-c} = RT^2[(\frac{\partial(\ln P)}{\partial T})_{n_a}] \qquad (12)$$

Equation (12) is only valid when the gas behaves like ideal gas and the influence of the adsorbed phase can be ignored. In low pressure conditions like Henry's range, equation (12) is applicable. However, when the gas behavior deviates from ideal gas or the influence of the adsorbed phase cannot be neglected, equation (12) is not reliable. Figure 1-1 shows how the real gas like methane and carbon dioxide deviates from ideal gas. Under this situation, equation (12) cannot be applied to explore the true behavior of the isosteric heat of adsorption.

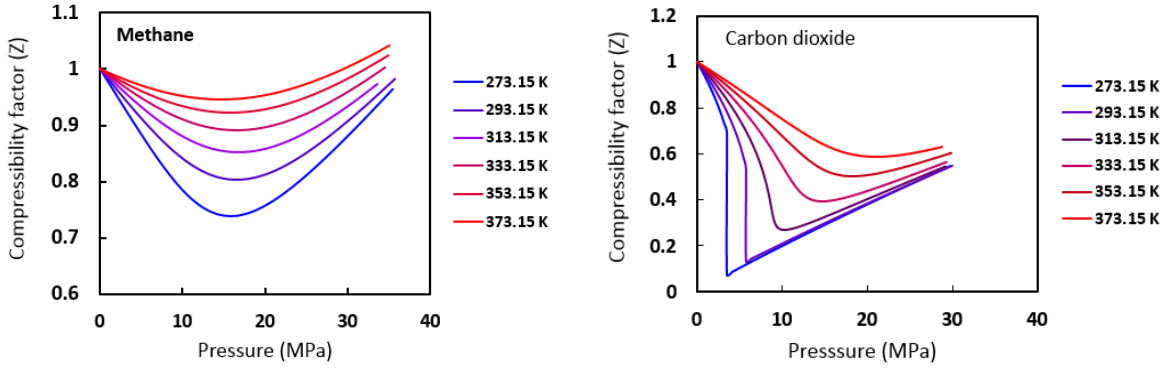

Figure 1.1.2 Compressibility of methane and carbon dioxide under different pressures and temperatures. (Data is obtained from the NIST Standard Reference Database 23 (REFPROP: Version 8.0.))

1.1.4 Kinetics of adsorption

Numerical modeling of both the recovery process for CBM and shale gas and the carbon dioxide injection process requires the kinetics information of the sorption process. The kinetics behavior of gas usually determines the rate of methane desorption in shale and coal for primary recovery and the rate of carbon dioxide adsorption in coal/shale for carbon dioxide storage.

Several sorption kinetics models have been applied for gas and solid interactions: the unipore model [23], the bidisperse model [25-26], the dynamic diffusion model [27-30] and other semi-empirical models [31-32]. Among these models, the unipore model is the most widely used. The unipore model is established based on the following four assumptions: 1) coal particles are spherically symmetric, homogeneous and isotropic, 2) all the pores are of the same size, 3) at the surface of the spheres gas concentrations are constant throughout the sorption process, and 4) gas diffusion process follows mass conservation law and the continuity principle. Based on Fick's second law and the above four assumptions, the unipore model for spherically symmetric flow is,

$$\frac{\partial \mathrm{C}}{\partial t} = D\left(\frac{\partial^2 C}{\partial r^2} + \frac{2}{r}\frac{\partial C}{\partial r}\right) \qquad (13)$$

where r is the radius, C *is* the adsorbate concentration, D *is* the diffusion coefficient, and t is time. The solution of equation (6) for a constant surface concentration of the diffusing gas can be expressed as follows [33],

$$\frac{Q_t}{Q_\infty} = 1 - \frac{6}{\pi^2}\sum_{n=1}^{\infty}\frac{1}{n^2}\exp\left(-\frac{Dn^2\pi^2 t}{r^2}\right) \qquad (14)$$

where Q_t is the total volume of gas desorbed in time t and Q_∞ is the total gas adsorbed or desorbed in infinite time. Note, there is no analytical solution for equation (9) but the approximate numerical solution has been applied by different researchers to obtain the constant diffusion coefficient to evaluate the gas diffusion process [23, 24, 34-37].

1.2 Problem statement

A unique characteristics of shale gas is its high temperature and high pressure reservoir condition (up to 27MPa and 360 K), which differentiates it from coal seam gas. This feature has resulted in the Gibbs excess adsorption behavior of methane in shale, where the observed adsorption uptake of methane first increases and then decreases with increasing pressure [38]. Under this situation,

the single-site Langmuir model losses its power to model the methane adsorption behavior. Therefore, a new adsorption model is needed for describing methane adsorption behavior under high pressure conditions in order to obtain the true adsorbed gas amount. The same problem also existes in carbon dioxide sequestration field, where an adsorption model in needed to model supercritical carbon dioxide adsorption behavior in coal and shale.

Considering the heat change is always associated with the physical adsorption process, the thermodynamics feature of gas adsorption in shale and coal is necessary in order to understand the adsorption process. Unfortunately, the classic Clausius–Clapeyron approximation cannot be used to obtain isosteric heat of adsorption under high pressure conditions because it does not account for the real gas behavior and the volume effect of the adsorbed phase [20-21, 39-40]. Furthermore, it is also inappropriate to calculate the isosteric heat of adsorption by using experimental data (Gibbs excess sorption data) especially under high pressure conditions because experimental data usually underestimate the true adsorbed amount. Therefore, isosteric heat of adsorption for high pressure gas adsorption in shale and coal needs to be further studied by considering the real gas behavior and the volume effect of the adsorbed phase, and a uniform approach for obtaining the absolute quantity of adsorption from measured adsorption isotherms is also needed.

There also existed many key research questions surrounding the geological sequestration process related to the dynamic interaction between carbon dioxide and coal. For example, how quickly the injected CO_2 plume will migrate through a coal seam during injection, how the sorption process will affect the transportation of carbon dioxide in the coal seam, and whether continuous injection or intermittent injection is more effective for maximizing storage. Therefore, the interaction between gases (carbon dioxide, nitrogen and methane) and coal are analyzed to study the pore characterization of coal, gas adsorption kinetics behavior in coal, and adsorption thermodynamics.

1.3 Objectives of this dissertation

In order to accurately estimate the CBM/shale GIP and carbon dioxide storage capacity under in situ reservoir conditions, the following studies were carried out:

- Model and analyze high pressure methane adsorption in shale
- Develop a methodology for accurate estimation of shale GIP
- Model and analyze supercritical carbon dioxide adsorption in coal
- Develop a methodology for accurate estimation of carbon dioxide storage capacity

To obtain adsorption thermodynamic characterization of gas in shale/coal, the following topics were studied:

- Investigate how coal rank will influence the isosteric heat of adsorption under low pressure conditions (Henry's pressure range)
- Calculate isosteric heat of adsorption by considering the real gas behavior and the influence of adsorbed phase under high pressure conditions
- Investigate how the real gas behavior and adsorbed phase influence the isosteric heat of adsorption

To study pore characterization of coal and gas transport behavior in coal, the following topics were addressed:

- Investigate how coal particle size will influence the pore characterization of coal via low pressure and low temperature nitrogen and carbon dioxide adsorption approach
- Investigate how coal particle size will influence the ad/desorption behavior of gas in coal
- Measure, model and analyze adsorption kinetics behavior of carbon dioxide in crushed coal

References

1. Curtis, J. B. (2002). Fractured shale-gas systems. AAPG bulletin, 86(11), 1921-1938.
2. Montgomery, S. L., Jarvie, D. M., Bowker, K. A., & Pollastro, R. M. (2005). Mississippian Barnett Shale, Fort Worth basin, north-central Texas: Gas-shale play with multi–trillion cubic foot potential. AAPG bulletin, 89(2), 155-175.
3. King, G. E. (2010). Thirty years of gas shale fracturing: what have we learned? In SPE Annual Technical Conference and Exhibition. Society of Petroleum Engineers. http://dx.doi.org/10.2118/133456-MS.
4. Kuuskraa, V., Stevens, S. H., & Moodhe, K. D. (2013). Technically recoverable shale oil and shale gas resources: an assessment of 137 shale formations in 41 countries outside the United States. [J]. Natural Gas Industry, 5, 003.
5. NETL (National Energy Technology Laboratory). (2009). Modern shale gas development in the United States: A primer. US Department of Energy, Office of Fossil Energy. https://www.netl.doe.gov/File%20Library/Research/Oil-Gas/shale-gas-primer-update-2013.pdf.

6. EIA, 2016. http://www.eia.gov/dnav/ng/ng_prod_sum_dcu_NUS_a.htm
7. Wang, Q., Chen, X., Jha, A. N., & Rogers, H. (2014). Natural gas from shale formation–the evolution, evidences and challenges of shale gas revolution in United States. Renewable and Sustainable Energy Reviews, 30, 1-28.
8. Andrews, I. J. (2013). The Carboniferous Bowland Shale gas study: geology and resource estimation.
9. White, C. M., Smith, D. H., Jones, K. L., Goodman, A. L., Jikich, S. A., LaCount, R. B., ... & Schroeder, K. T. (2005). Sequestration of carbon dioxide in coal with enhanced coalbed methane recovery a review. Energy & Fuels, 19(3), 659-724.
10. Busch, A., Alles, S., Gensterblum, Y., Prinz, D., Dewhurst, D. N., Raven, M. D., ... & Krooss, B. M. (2008). Carbon dioxide storage potential of shales. International Journal of Greenhouse Gas Control, 2(3), 297-308.
11. Kang, S. M., Fathi, E., Ambrose, R. J., Akkutlu, I. Y., & Sigal, R. F. (2011). Carbon dioxide storage capacity of organic-rich shales. Spe Journal, 16(04), 842-855.
12. Middleton, R. S., Carey, J. W., Currier, R. P., Hyman, J. D., Kang, Q., Karra, S., ... & Viswanathan, H. S. (2015). Shale gas and non-aqueous fracturing fluids: Opportunities and challenges for supercritical CO2. Applied Energy, 147, 500-509.
13. Henry, W. (1803). Experiments on the quantity of gases absorbed by water, at different temperatures, and under different pressures. Philosophical Transactions of the Royal Society of London, 93, 29-276.
14. Langmuir, I. (1918). The adsorption of gases on plane surfaces of glass, mica and platinum. Journal of the American Chemical society, 40(9), 1361-1403.
15. Brunauer, S., Emmett, P. H., & Teller, E. (1938). Adsorption of gases in multimolecular layers. Journal of the American chemical society, 60(2), 309-319.
16. Dubinin, M. M. (1965). Modern state of the theory of gas and vapour adsorption by microporous adsorbents. Pure and Applied Chemistry, 10(4), 309-322.
17. Dubinin, M. (1960). The potential theory of adsorption of gases and vapors for adsorbents with energetically nonuniform surfaces. Chemical Reviews, 60(2), 235-241.
18. Gibbs, J. W. (1878). On the equilibrium of heterogeneous substances. American Journal of Science, (96), 441-458.

19. Graham, D. (1953). The characterization of physical adsorption systems. I. The equilibrium function and standard free energy of adsorption. The Journal of Physical Chemistry, 57(7), 665-669.
20. Mertens, F. O. (2009). Determination of absolute adsorption in highly ordered porous media. Surface Science, 603(10), 1979-1984.
21. Stadie, N. (2012). Synthesis and thermodynamic studies of physisorptive energy storage materials (Doctoral dissertation, California Institute of Technology).
22. Chakraborty, A., Saha, B. B., Koyama, S., & Ng, K. C. (2006). On the thermodynamic modeling of the isosteric heat of adsorption and comparison with experiments. Applied physics letters, 89(17), 171901.
23. Smith D. M., & Williams F. L. Diffusion models for gas production from coal: determination of diffusion parameters. Fuel, 63(2), 256-261 (1984a).
24. Yang Q. & Wang Y. Theory of methane diffusion from coal cuttings and its application. Journal of China Coal Society. 3:87-94 (1986).
25. Ruckenstein E., Vaidyanathan A. S., & Youngquist G. R. Sorption by solids with bidisperse pore structures. Chemical Engineering Science, 26(9), 1305-1318 (1971).
26. Yi J., Akkutlu, I. Y., & Deutsch C. V. Gas transport in bidisperse coal particles: investigation for an effective diffusion coefficient in coalbeds. Journal of Canadian Petroleum Technology, 47(10), 20-26 (2008).
27. Li Z., Wang D., Song D. Influence of temperature on dynamic diffusion coefficient of CH4 into coal particles by new diffusion model [J]. Journal of China Coal Society, 40(5):1055-1064.
28. Yue, G., Wang, Z., Xie, C., Tang, X., & Yuan, J. (2016). Transp Porous Med. doi:10.1007/s11242-016-0776-x.
29. Jian, X., Guan, P., & Zhang, W. (2012). Carbon dioxide sorption and diffusion in coals: Experimental investigation and modeling. Science China Earth Sciences, 55(4), 633-643.
30. Kang, J., Zhou, F., Xia, T., & Ye, G. (2016). Numerical modeling and experimental validation of anomalous time and space subdiffusion for gas transport in porous coal matrix. International Journal of Heat and Mass Transfer, 100, 747-757.

31. Plazinsk, W., Rudzinski W., & Plazinska A. Theoretical models of sorption kinetics including a surface reaction mechanism: a review. Advances in Colloid and Interface Science, 152(1), 2-13 (2009).
32. Busch A., & Gensterblum Y. (2011). CBM and CO2-ECBM related sorption processes in coal: a review. International Journal of Coal Geology, 87(2), 49-71 (2011).
33. Crank, J. (1975). The Mathematics of Diffusion: 2d Ed. Clarendon Press.
34. Yang Q. & Wang Y. Theory of methane diffusion from coal cuttings and its application. Journal of China Coal Society. 3:87-94 (1986).
35. Guo Y.Y., Wu S.Y. Study on the measurement of coal particle gas diffusion and diffusion coefficient. Shanxi Mining Institute Journal, 15(1), 15-19 (1997).
36. Nie B., Guo Y. Mathematical Physics Model of Gas Diffusion through Coal Particle. Journal of Liaoning Technical University (Natural Science), 18(6), 582-585 (1999).
37. Charrière, D., Pokryszka, Z., & Behra, P. (2010). Effect of pressure and temperature on diffusion of CO 2 and CH 4 into coal from the Lorraine basin (France). International Journal of Coal Geology, 81(4), 373-380.
38. Gašparík, M. (2013). Experimental investigation of gas storage properties of black shales (Doctoral dissertation).
39. Pan, H., Ritter, J. A., & Balbuena, P. B. (1998). Examination of the approximations used in determining the isosteric heat of adsorption from the Clausius-Clapeyron equation. Langmuir, 14(21), 6323-6327.
40. Sircar, S., Mohr, R., Ristic, C., & Rao, M. B. (1999). Isosteric heat of adsorption: theory and experiment. The Journal of Physical Chemistry B, 103(31), 6539-6546.

Chapter 2 High pressure methane adsorption in shale for deep shale gas resource estimation

2.1 Comparison of adsorption models for high pressure methane adsorption in shale

Xu Tang*, Nino Ripepi*,†, Kray Luxbacher*,†

(*Department of Mining and Minerals Engineering & †Virginia Center for Coal and Energy Research, Virginia Polytechnic Institute and State University, Blacksburg, Virginia, 24060, U.S)

Abstract: Describing true supercritical methane adsorption behavior in shale under high pressures (>15 MPa) is challenging because the density or volume of adsorbed methane cannot be measured directly. There are several models available to describe the observed adsorption isotherms, but a consensus model has not been reached by researchers. Based on the assumption that the density of the adsorbed methane is an unknown constant, the authors successfully describe observed adsorption isotherms of methane in shale for pressure up to 27MPa and temperature up to 355.15K using a dual-site Langmuir equation, and the density of the adsorbed methane in shale is found to be 17.7 mmol/mL. This work then compares the nine currently available adsorption models for describing high pressure methane adsorption behavior in shale in order to assess the efficacy of each model. Three aspects of the adsorption model are compared: (1) the goodness-of-fit of each adsorption model, (2) interpretation of the observed test phenomena, and (3) predicted isotherms beyond test data. Comparison results show that even though the goodness-of-fit for each model is comparable, the dual-site Langmuir model is still superior to other available models because it can not only reasonably address all observed test phenomenon but can also extrapolate adsorption isotherms without using an empirical relationship. The dual-site Langmuir model is recommended for describing high pressure methane adsorption in shale, especially when the Gibbs excess adsorption phenomenon is observable.

Key words: Methane, adsorption, shale, Langmuir model, high pressure

2.1.1 Introduction

Shale gas has been considered as one of the most important energy resources in the world and countries have launched different programs to estimate shale gas resources (Wang et al., 2014; Andrew et al., 2013; Kuuskraa et al., 2013). Shale gas, the most significant component of which is methane, exists in three different states in the subsurface: free gas, adsorbed gas and dissolved gas. Current studies have shown the adsorbed gas accounts for 20-85% of the total shale gas-in-place (GIP) content (Curtis, 2002). Therefore, it is important to understand the adsorption behavior of methane in shale in order to accurately estimate shale gas resources in shale formations. Knowing the exact ratio between adsorbed and free shale gas is also fundamental to understand shale gas transport behavior and predict shale gas well production behavior (Tang, 2016). Since most of shale formations are at depths from 1000m to 3000 m, the reservoir pressure of deep shale formations can go up to 27MPa (Curtis, 2002). This in-situ feature of shale formations requires high pressure methane adsorption studies for shales. Unfortunately, because of instrument limitation, there are limited data for high pressure methane adsorption in shale (Rexer et al., 2013; Luo et al., 2015; Weniger et al., 2010; Tian et al., 2016) which makes investigation and characterization of methane adsorption in shale challenging.

In order to understand methane adsorption in shale under reservoir conditions it is essential to have an accurate model for high pressure supercritical gas adsorption in shale. In order to build a methane adsorption model in shale, the challenge is to describe observed adsorption isotherms showing Gibbs excess phenomena (Zhou et al., 2000 & 2009). Some researchers use the molecular simulation approach to simulate methane adsorption behavior in shale and synthetic materials (Ambrose et al., 2012; Luo et al., 2011; Mosher et al., 2013; Zhang et al., 2014; Chareonsuppanimit et al., 2012; Fitzgerald et al., 2003; Sudibandriyo et al., 2010; Bourrelly et al., 2005; Aukett et al., 1992; Snurr et al., 1991; Wang, 2007; Chen et al., 1997; Akkutlu et al., 2013). These studies are important to understanding the methane adsorption mechanism at a molecular scale. However, since the simplified, homogeneous pore structure of the computational approach does not represent the heterogeneous properties of shale, the molecular simulation method has not been widely used in engineering applications. In addition, molecular simulation has not been used to interpret the isothermal adsorption phenomenon such as the crossover of the isotherms under different temperatures observed in experimental data. Other researchers have attempted to build a physical model from observed adsorption isotherms based on either known constant density (density of

liquid methane) or constant volume assumptions of the adsorbed methane phase (Rexer et al., 2013; Bae et al., 2006; Sakurovs et al., 2007; Luo et al., 2015; Ottiger et al., 2006; Herbst et al., 2002; Weniger et al., 2010; Zhou et al., 2000 & 2001; Do et al., 1997; Tian et al., 2016; Bruns et al., 2016). Unfortunately, most of the proposed adsorption models in the literature do not provide satisfactory interpretation of the experimental data, and the assumptions used are uncertain. For example, the crossover of the observed adsorption isotherms at high pressures has not been reasonably explained, where the observed adsorption content increases with increasing temperature beyond the Gibbs excess maximum. In addition, none of the models can be used to extrapolate adsorption isotherms beyond test data without using empirical relationships. Therefore, an optimized model is needed for accurately describing the adsorption behavior of methane in shale.

In order to simulate the true methane adsorption behavior in shale under high pressure conditions, the authors introduced a dual-site Langmuir model to describe high pressure methane adsorption behavior in shale for temperatures up to 355.15K and pressures up to 27 MPa (Tang et al, 2016). This work compared this model with other available models in literature to present the specific characteristics of each model using the test data, which provides a clearer picture of the strengths and weaknesses of each model. This study compares adsorption models used for engineering applications, especially for the shale gas industry; therefore, molecular simulation for methane adsorption in shale is not part of this work.

2.1.2 Adsorption model review

2.1.2.1 Dual-site Langmuir model

In any pure gas-solid adsorption system, the observed adsorption quantity, also called the Gibbs excess adsorption uptake, is given by the Gibbs equation (1),

$$n_e = n_a - \rho_g V_a = n_a\left(1-\frac{\rho_g}{\rho_a}\right) \qquad (1)$$

where the excess adsorption quantity (n_e) refers to the difference between the absolute adsorption quantity (n_a) and the quantity of adsorbate that would be present in the same volume (V_a) of the adsorbed phase at the density of the bulk gas phase (ρ_g). When V_a is very low or the density of

the adsorbed phase (ρ_a) is much higher than the bulk gas phase density (ρ_g), the excess adsorption quantity is approximately equal to the actual adsorbed amount. However, this relation is invalid at high pressure where the density of the adsorbed phase is similar to the density of the bulk fluid, the point at which the observed adsorption quantity reaches a maximum and then decreases. This Gibbs excess maximum phenomenon has also been observed in many other gas-solid adsorption systems (Rexer et al., 2013; Bae et al., 2006; Sakurovs et al., 2007; Luo et al., 2015; Ottiger et al., 2006; Herbst et al., 2002; Weniger et al., 2010; Zhou et al., 2000 & 2001; Do et al., 1997; Tian et al., 2016; Bruns et al., 2016). Under such conditions, the conventional adsorption models that neglect the real volume of the adsorbed phase cannot reasonably explain such adsorption behavior. Therefore, it is imperative to use a more sophisticated approach to obtain the absolute isotherms from observed Gibbs excess isotherms at high pressures.

For heterogenous adsorbent sites, the dual-site Langmuir model is more suitable than the single-site Langmuir model for describing the gas adsorption behavior (Graham et al., 1953; Mertens, 2009; Stadie et al., 2013 & 2015). The dual-site Langmuir model assumes two different adsorption sites in the heterogenous adsorbent. The adsorption energy of the adsorption sites will vary, where the strongest adsorption energy sites will be filled first, followed by the weak adsorption energy sites. When both sites reached equilibrium with the same adsorbed phases, each site can be modelled by two separate equilibrium constants $K(T)_1$ and $K(T)_2$ ($K(T)_1 = A_1 \cdot \exp(\frac{E_1}{RT})$ and $K(T)_2 = A_2 \cdot \exp(\frac{E_2}{RT})$, A_1, and A_2 are prefactors, E_1 and E_2 are the binding energy of the two different adsorption sites, R is universal gas content, T is temperature) with a weighting coefficient for two different adsorption sites in the Langmuir type relationship (Graham et al., 1953). Thus, the single site Langmuir equation can be superposed as the following form (equation 2), where α is the fraction of two different adsorption sites ($0<\alpha<1$),

$$n_a(P,T) = n_{\max} \cdot \left[(1-\alpha)\left(\frac{K(T)_1 P}{1+K(T)_1 P}\right) + \alpha\left(\frac{K(T)_2 P}{1+K(T)_2 P}\right) \right] \qquad (2)$$

Based on the assumption that the density of adsorbed methane is an unknown constant under test conditions, the volume of the adsorbed layer can be obtained in equation (3),

$$V_a = \frac{n_a}{\rho_a} \qquad (3)$$

Similarly, we can obtain the maximum volume of the adsorbed phase, Vmax,

$$V_a = \frac{n_{\max}}{\rho_a} \qquad (4)$$

By combining equation (2) and (4), the volume changes of the adsorbed layer in different adsorption sites can obtained in equation (5),

$$V_a = \frac{n_{\max}}{\rho_a} \cdot \left[(1-\alpha)\left(\frac{K(T)_1 P}{1+K(T)_1 P}\right) + \alpha\left(\frac{K(T)_2 P}{1+K(T)_2 P}\right) \right] \qquad (5)$$

Combining equation (1), (2) and (5), the excess adsorption equation for dual sites adsorbates can be obtained as shown in equation (6) and the surface coverage (θ) is shown in equation (7),

$$n_e(P,T) = (n_{\max} - \rho_g V_{\max}) \cdot \left[(1-\alpha)\left(\frac{K(T)_1 P}{1+K(T)_1 P}\right) + \alpha\left(\frac{K(T)_2 P}{1+K(T)_2 P}\right) \right] \qquad (6)$$

$$\theta = \frac{n_a(P,T)}{n_{\max}} = (1-\alpha)\left(\frac{K(T)_1 P}{1+K(T)_1 P}\right) + \alpha\left(\frac{K(T)_2 P}{1+K(T)_2 P}\right) \qquad (7)$$

It is clear that if the experimental adsorption (Gibbs excess adsorption) isotherms are obtained through isothermal adsorption tests, the unknown parameters in equation (6) can be easily obtained via curve fitting. The absolute adsorption uptake can then be calculated by equation (2). In addition, the density of adsorbed methane can be obtained using equation (4).

2.1.2.2 Review of adsorption models

In order to describe the observed methane adsorption behavior in shale and coal under high pressures, several researchers have proposed different models based on experimental data summarized in Table 2.1.1. These models can be classified into three different groups: (1) unknown constant density of adsorbed methane layers with changing volume of adsorbed layer with increasing adsorption uptake: ④; (2) known density assumption of adsorbed methane layers: ①②③⑦⑧⑨, and; (3) constant volume assumption of adsorbed methane layers: ⑤⑥. These models can also be classified as Langmuir-style equations, Toth-style equations, and Dubinin–

Radushkevich (D-R) (or Dubinin–Astakhov (D-A)) equations based on adsorption potential theory as shown in Table 2.1.1.

Table 2.1.1 Comparison of methane adsorption models in shale and coal

Classification	No.	Fitting model	Assumptions	Variables	Data processing	Isotherms prediction	Reference
Langmuir-style model	①	$n_{ex}=\frac{n_{\max}K_0\rho_b}{1+K_0\rho_b}(1-\frac{\rho_b}{\rho_{ad}})$	$\rho_{ad}=420kg/m^3$	ρ_b (density)	Independent fitting	Empirical prediction	Sakarovs et al, 2007; Weniger et al, 2010.
	②	$n_{ex}=\frac{n_{\max}K_0\rho_b}{1+K_0\rho_b}(1-\frac{\rho_b}{\rho_{ad}})+k\rho_g$	$\rho_{ad}=420kg/m^3$	ρ_b (density)			
	③	$n_{ex}=\frac{n_{\max}K_0\rho_b}{1+K_0\rho_b}(1-\frac{\rho_b}{\rho_{ad}})+k\rho_g(1-\frac{\rho_b}{\rho_{ad}})$	$\rho_{ad}=420kg/m^3$;	ρ_b (density)			
	④	$n_e(P,T)=n_{\max}(1-\frac{\rho_b}{\rho_a})\cdot\left[(1-\alpha)(\frac{K(T)_1P}{1+K(T)_1P})+\alpha(\frac{K(T)_2P}{1+K(T)_2P})\right]$	Unknown constant density of adsorbed layer	P (Pressure)	Global Fitting	Intrinsic prediction	This work, Tang et al, 2016
	⑤	$n_{ex}=\frac{n_{\max}K_0\rho_b}{1+K_0\rho_b}-\rho_bV_{ad}$	Constant volume of adsorbed layer	ρ_b (density)	Independent fitting	Empirical prediction	Pini et al, 2010; Bae et al, 2006; Ottiger et al, 2006.
Toth model	⑥	$n_{ex}=\frac{n_{\max}K_0f}{[1+(K_0f)^t]^{1/t}}-\rho_bV_{ad}$	Constant volume of adsorbed layer	P (fugacity)			Bae et al, 2006.
D-R (or D-A) style model	⑦	$n_{ex}=n_o(1-\frac{\rho_b}{\rho_{ad}})e^{-D[\ln(\frac{\rho_{ad}}{\rho_b})]^2}$	$\rho_{ad}=420kg/m^3$	ρ_b (density)			Sakarovs et al, 2007; Day et al, 2008; Pini et al, 2010; Song et al, 2015.
	⑧	$w_{ex}=n_o(1-\frac{\rho_b}{\rho_{ad}})e^{-D[\ln(\frac{\rho_{ad}}{\rho_b})]^2}+k\rho_b$	$\rho_{ad}=420kg/m^3$	ρ_b (density)			
	⑨	$w_{ex}=n_o(1-\frac{\rho_b}{\rho_{ad}})e^{-D[\ln(\frac{\rho_{ad}}{\rho_b})]^2}+k\rho_b(1-\frac{\rho_b}{\rho_{ad}})$	$\rho_{ad}=420kg/m^3$	ρ_b (density)			

In practice, it is impossible to measure all isotherms under in-situ conditions in order to predict shale GIP content. Therefore, the use of limited test data to extrapolate isotherms under different temperatures has been researched. Researchers have attempted to use D-R or its revised form to predict isotherms under different temperatures, because the characteristic curve is unique under different temperatures for gas adsorption in microporous media like activated carbon (Dubinin et al., 1960; Dubinin et al., 1971; Amankwah et al., 1995). However, when D-R methods are applied for describing methane adsorption in coal or shale, the characteristic curve is not unique (Huan, et al., 2015; Xiong et al., 2015). This can be attributed to (1) the heterogenous properties of natural geo-materials; (2) the fact that methane is a supercritical gas under reservoir conditions, and the empirical saturation pressure assumption is invalid, and; (3) the fitting parameters of D-R equation and its revised form are non-unique which contradicts its assumptions. Therefore, other researchers use an empirical approach to predict isotherms under different temperatures (Tian et al., 2016; Hildenbrand et al., 2006; Kronimus et al., 2008; Busch et al., 2016). First, each isotherm is fitted independently using the proposed model. Then, the relationship between fitting parameters and temperature is obtained empirically. Based on this empirical relationship, the isotherms beyond

test pressures and temperatures are predicted. Since this approach highly depends on the obtained empirical relationship, only limited information can be obtained from the predicted data and these results should also be treated with caution.

2.1.3 Model evaluation criteria

A physical model is typically developed by scientists and engineers to simplify the complexity of the real world to better understand the real phenomena. Generally, the best models represent a simplification, but are still complex enough to help one understand the phenomena and to solve the problem. The best model should simplify complexity of real world phenomena while retaining the most important parameters. Figure 2.1.1 shows the way a model can be developed in order to better understand the real world phenomena. From this flowchart, one can gain several intuitive perspectives about the development of the model. First, the model should describe the observed phenomena based on real world observations. Second, the model should give one a reasonable interpretation of the real phenomena. Third, the model should provide predictable capacity, which can be validated by more real phenomena. If the model is developed following these three approaches, it will become a reliable model.

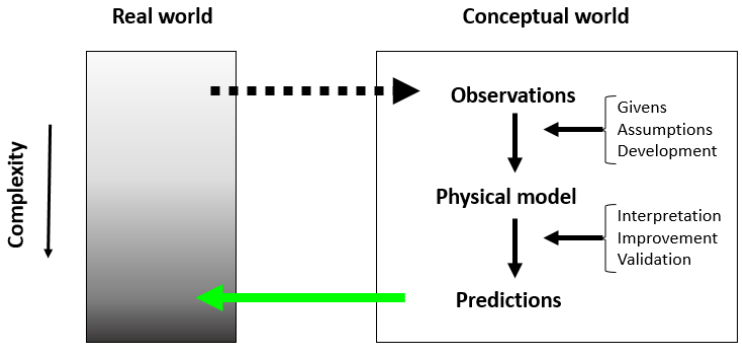

Figure 2.1.1 Depiction of the physical modelling approach from real world to conceptual world (revised from Dym et al., 2004)

In order to compare the current available adsorption model, the first and crucial step is to set comparison criteria for each model. Three general criteria are used here. First, the goodness-of-fit of the model to test data will be evaluated. This is a straightforward approach to show whether the proposed model can describe the experimental measurements. An accurate model should closely match the data using the minimal but the most significant assumptions. It should be noted that goodness-of-fit should reflect such a physical fact that the experimental results are not only

determined by the experimental parameters but also influenced by experimental errors. This means too precise fitting may not be the best result for a good model. If the proposed model has too many fitting parameters, higher fitting precision can be achieved, but the whole model can lose its physical meaning. Secondly, the proposed model should interpret part or all observed phenomenon in the test and should improve one's understanding of the mechanisms of methane adsorption mechanism in shale. Lastly, the prediction ability of the model will be compared, where isotherm adsorption curves are predicted beyond test temperature and pressure. The predicted isotherms should show similar properties with the observed test phenomena. This means a good model should extrapolate to situations or data beyond those originally described in the model. If the proposed model meets the all of the above three standards, the model should be treated as valid.

2.1.4 Test results and data processing method

Shale samples from the Lower Silurian Longmaxi Formation (2400.8 meters deep) were obtained from the Fuling #1 well in the Fuling region, Sichuan Province, China. The vitrinite equivalent reflectance (Ro) of the sample is 2.2% - 2.5% (Tang et al, 2016). Methane adsorption measurements were conducted using a Rubotherm Gravimetric Sorption Analyzer IsoSORP. The methane density is obtained via the NIST package using Setzmann & Wagner equation (Setzmann et al., 1991).The instrument is rated up to pressures of 35 MPa and temperatures up to 150°C±0.2℃, and pure methane gas (99.99%) is used as the adsorbate. Equilibrium was determined as when the adsorption time was longer than 2 hours or when the weight change of the sample was within 30 μg over a span of 10 min. The detailed characteristics of the instrument have been extensively described elsewhere (Keller & Staudt, 2005). The test results are shown in Figure 2.2.2, where test data are retrieved from Tang et al, 2016. All raw data can be reached at the Supplemental Material file.

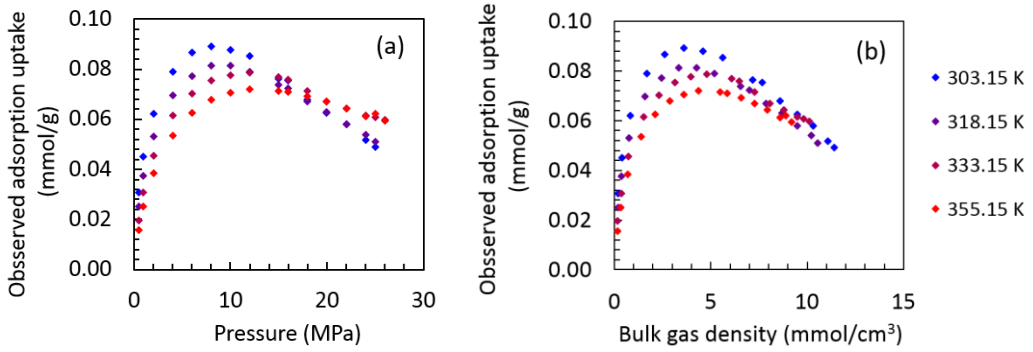

Figure 2.1.2 High pressure methane adsorption test in shale (a: observed adsorption uptake as a function of pressure; b: observed adsorption uptake as a function of bulk gas density)

The least squares residual method is used to fit nine different models in Table 1,

$$\text{Residual} = \sum_{i=1}^{N} [(n_{e,i}^{fitted} - n_{e,i}^{tested})^2] \qquad \text{with i=1, 2, 3, …..,j} \quad (7)$$

For method ④, the global fitting method is used, which means the four Gibbs excess adsorption isotherms under different temperatures are fitted simultaneously to the dual-site Langmuir model (equation 6) by a least-squares residual minimization algorithm. This means the j in equation (6) is equal to 63, corresponding to the total measured points from all four isotherms. The seven independent fitting parameters were varied to achieve the global minimum of the residual squares value within the following limits: $0<n_{max}<100$ mmol/g, $0< V_{max}<10$ cm^3/g, $0<\alpha<1$, $0< E_1 <100$ kJ/mol, $0< E_2 <100$ kJ/mol, $A_1 > 0$, $A_2 > 0$). Minimization was performed in excess of 100 times by changing the random seed in order to assure that a global minimum was achieved.

For methods ①-③ and ⑤-⑨, the conventional independent fitting method is used, which means each isotherm under different temperatures is fitted independently using the corresponding equation by a least-squares residual minimization algorithm. The best fitting parameters for each isotherm can be obtained by achieving the local minimum of the residual squares value without using a boundary constraint. This means j is equal to either 15, 16, or 17, corresponding to the measured points from each isotherm.

Since the least squares residual method cannot reflect the fitting error for individual measured points from each isotherm, the fitted relative error is used here in order to evaluate the difference between the predicted data and test data,

$$\text{Relative Error} = \frac{\left| n_e^{fitted} - n_e^{tested} \right|}{n_e^{tested}} \% \qquad (8)$$

The relative error reflects how the predicted value deviates from the measured data in a straightforward way, and it can be used to evaluate the fitting goodness of the model.

2.1.5 Results and discussion

2.1.5.1 Goodness-of-fit evaluation

As illustrated in Figure 2.1.3, more fitting parameters allow for better fitting results. Method ① and ⑦ are the poorest fit, with only two fitting parameters in their models. The other methods have three or more fitting parameters and all have similarly improved results. All fitting models show that there are crossovers of the isotherm beyond the maximum Gibbs excess adsorption content. However, only method ④ shows a clear trend that after the crossover point the increasing temperature results in higher observed adsorption uptake. This trend was reported for methane adsorption in activated carbon up to 50 MPa (Herbst et al, 2002).

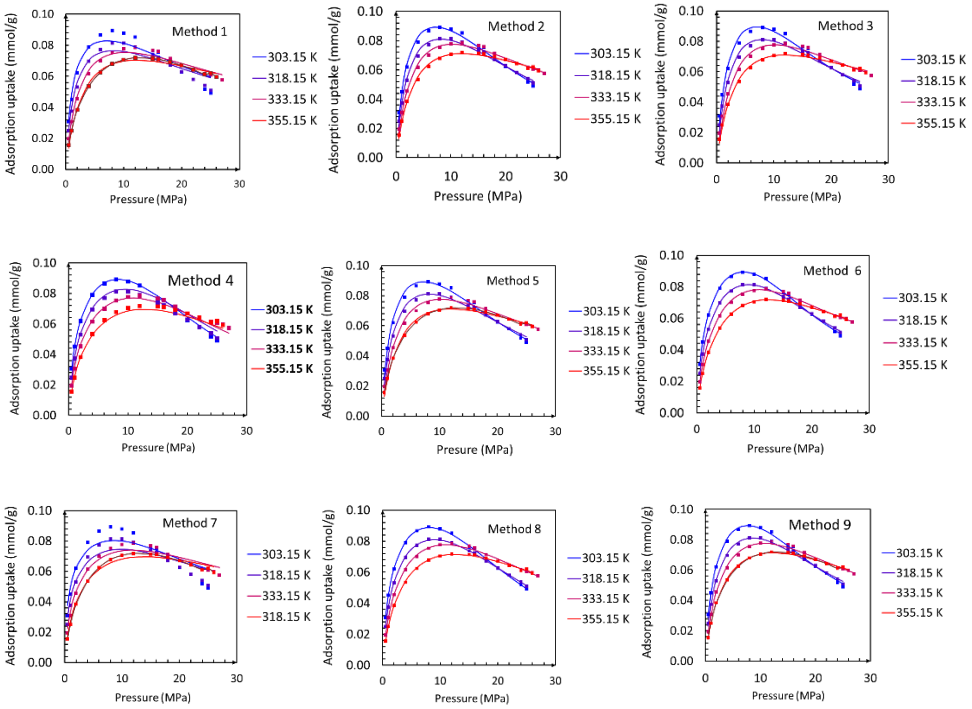

Figure 2.1.3 Comparison between fitting curve and test data for each model: symbols represent test data, solid lines represent fitting curves.

Using equation (8), the relative error for each fitting model is shown in Figure 2.1.4. The relative error for method ④ is comparable to the error of other methods. Furthermore, it is difficult to distinguish which method is better only by the relative fitting error (Figure 2.1.4). The fitting error can only show the goodness of a fitting model but cannot reflect the physical meaning of each model. However, whether the proposed model can be used to interpret the observed phenomena is the critical criteria.

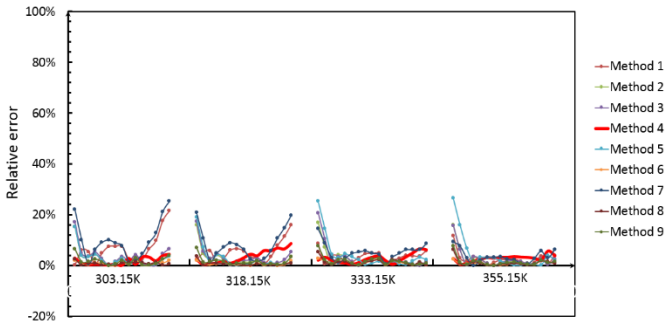

Figure 2.1.4 Relative error between fitting data and test data for each method for all raw data

2.1.5.2 Interpretation of test phenomena

The adsorption model is built in order to explain the test phenomena. For adsorption isotherms under different temperatures, the most distinguishable phenomena is the crossover of the isotherms under different temperatures as shown in Figure 2.1.2(a). At pressures below the Gibbs excess maximum, the excess adsorption is always lower at higher temperatures. However, at a point somewhere beyond the Gibbs excess maximum, the isotherms crossover and higher temperatures result in higher excess uptake at equivalent pressures.

Method ④ gives a reasonable interpretation for this crossover phenomenon. A reasonable interpretation of the crossover phenomenon can be made by examining the change of the coefficient of equation (6). As pressure increases, the density of gaseous methane increases, but the density of the adsorbed phase stays constant based on the assumption in equation (3); further, the density of gaseous methane approaches the density of the adsorbed phase (shown in Figure 2.1.5). This results in a decrease of the coefficient, $(n_{max} - \rho_g V_{max})$, as pressure goes up. Temperature also has a positive effect on the coefficient: the higher the temperature the higher the value of the coefficient. Figure 2.1.6 shows the temperature has a negative effect on the surface coverage (equation (7)): the higher the temperature the lower the surface coverage. As we multiply the coefficient ($(n_{max} - \rho_g V_{max})$) and the surface coverage using equation (6), we obtain the observed (excess) adsorption content with the crossover of the isotherms under high pressure conditions. Therefore, the observation of the crossover phenomenon in the measured data supports the assumption that the density of the adsorbed phase is constant and the volume of adsorbed phase changes with temperature and pressure following a dual-site Langmuir-like equation.

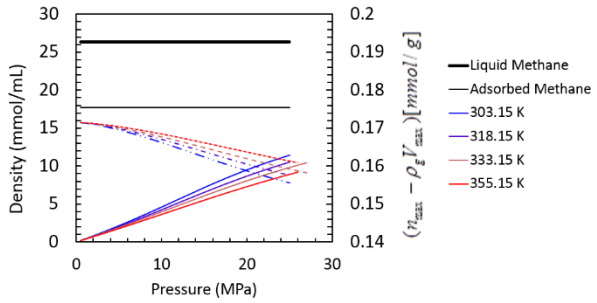

Figure 2.1.5 Modelled values of the density of gaseous (solid color lines, left axial), adsorbed and liquid methane (solid black lines, left axial) and the coefficient of equation (7) ($(n_{max} - \rho_g V_{max})$, dotted lines, right axial) on Longmaxi shale as a function of pressure

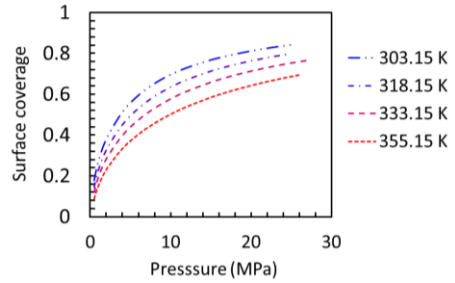

Figure 2.1.6 Surface coverage of the methane in shale

Generally, adsorption isotherms show the relationship between Gibbs excess adsorption content and pressure, where pressure is the independent variable for most of the adsorption isotherms under intermediate pressures (10-15MPa). Under high pressure conditions (>15MPa), density is suggested as the independent variable (Ottiger et al., 2006; Pini, 2014). The observed adsorption isotherms as a function of gas density clearly show the temperature dependent properties of adsorption isotherms. The crossover of the excess uptake isotherms will not be observed when the isotherms are plotted as a function of bulk gas density instead of pressure. The measured isotherms show the same temperature dependence at all pressures, i.e. increasing excess uptake with decreasing temperature. As shown in Figure 2.1. 7, only Method ④ can reproduce this phenomena even though the test data fluctuates slightly. Figure 2.1.2(b) shows a slight fluctuation of the test data under 318.15K, which is caused by some measurement errors. All fitting curves in the other methods still show crossover of the isotherms, which cannot overcome the fluctuation from the raw data. This on the other hand confirms the robustness of Method ④, which is relatively immune to fluctuations in the raw data.

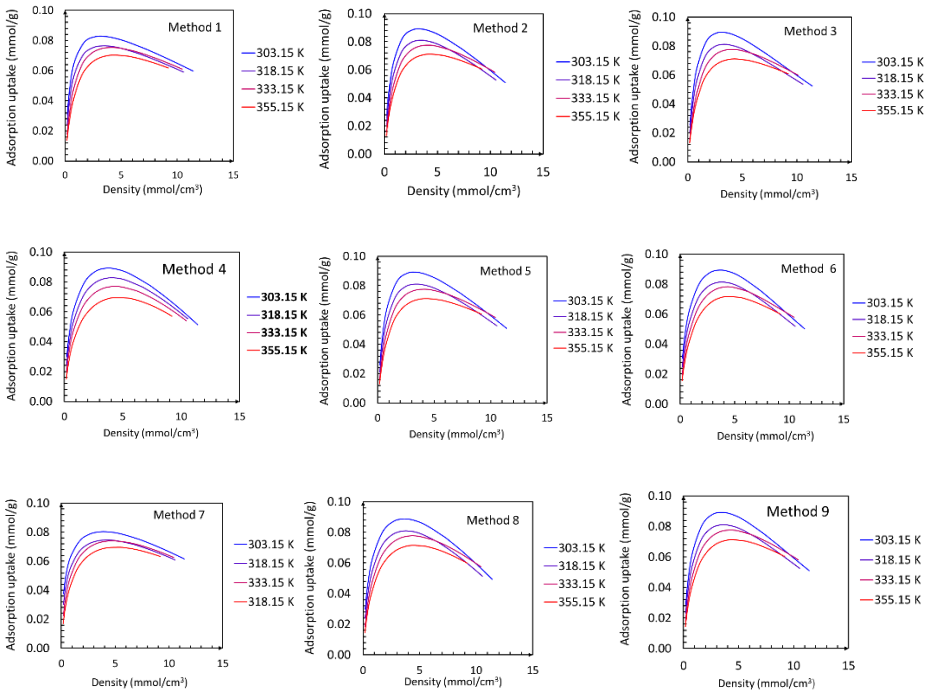

Figure 2.1.7 Adsorption model fitting results: Gibbs excess adsorption content as a function of bulk methane density

2.1.5.3 Evaluation of predicted isotherms beyond test data

In the shale gas industry, due to laboratory instrument limitations, adsorption isotherms are typically measured under intermediate pressures (10-15MPa) and temperatures higher than room temperature. The high pressure (>15 MPa) adsorption test typically requires higher reliability and accuracy of the instrument (Tang et al., 2015). The widely used approach is to use methane adsorption measurements at intermediate pressure conditions (10-15 MPa) to predict the methane adsorption behavior in the higher pressure region (>15 MPa). In addition, the commonly used technique for constant temperature is to use a water bath which can maintain room temperature to about 100℃, but it is difficult to reach temperatures lower than room temperature. For shallow coalbeds and shale formations, the temperature is typically lower than room temperature. It is also impractical to measure all adsorption isotherms at all in-situ geological conditions. Engineers usually use isotherms under intermediate temperatures to predict both low temperature (lower than room temperature) and high temperature adsorption isotherms based on an empirical relationship between fitting parameters and temperatures. Since a good physical model can not only help one

interpret the observed phenomena but also has predictive capability, we present the predicted isotherms beyond test data in this section.

As mentioned previously, predicting adsorption isotherms at different temperatures is of fundamental interest for reservoir characterization of coalbed and shale formations. Therefore, the temperature within and beyond the test ranges is extrapolated for each model at temperatures of 353.15K, 375.15K, 395.15K and 415.15K. As shown in Figure 2.1.8, all isotherms are plotted as a function of bulk gas density. It is clear that the predicted Gibbs excess adsorption isotherms using Method ④ are the only isotherms exhibiting similar properties for both the observed adsorption isotherms and predicted isotherms. Method ① and ⑦ also show a clear trend but they are not immune to errors in the raw data, where the isotherms still crossover. This conflicts with the fact that temperature always has a negative effect on the true (absolute) adsorption uptake.

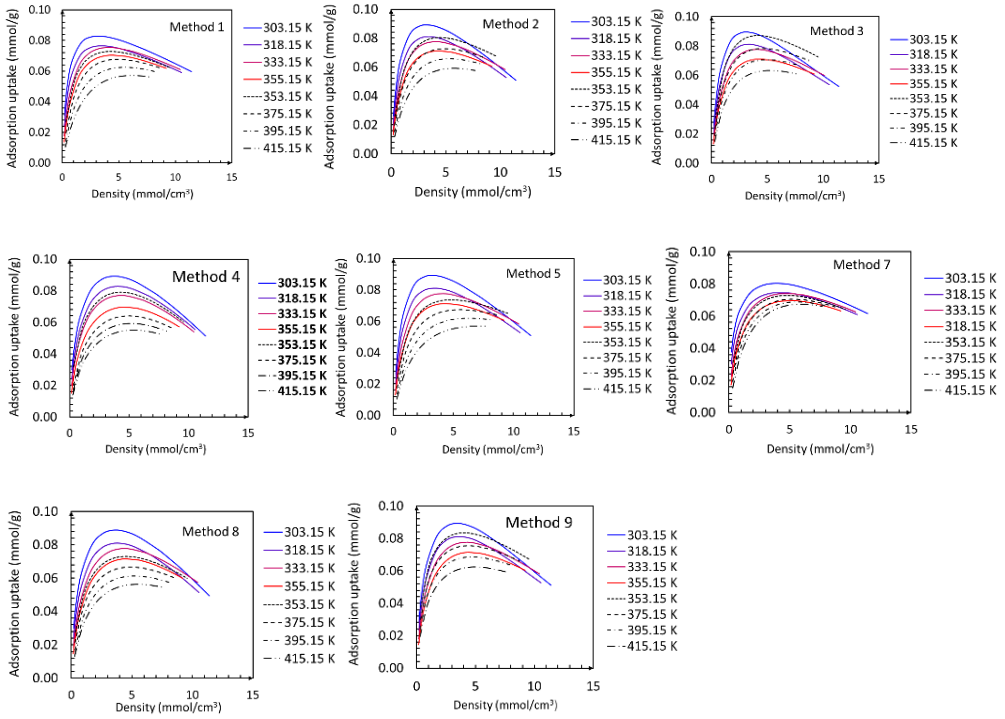

Figure 2.1.8 Extrapolated Gibbs excess adsorption isotherms of methane on Longmaxi shale (dashed lines) and as a function of bulk methane density (Note: Method 6 cannot be used to predict isotherms because there is no consistent empirical relationship between fitting parameters and temperature)

From the previous discussions, it is noted that the dual-site Langmuir model is the only model that passes the three criteria. This supports the hypothesis that the dual-site model (Method ④) is

superior when compared with the other models (①-③ and ⑤-⑨). The successful application of the dual-site Langmuir model also sheds light on the true behavior of the adsorbed phase for methane in shale: the volume of the adsorption layer depends on temperature and pressure and the density of the adsorbed layer can be treated as a constant value.

2.1.6 Conclusions

This work compares nine adsorption models for high pressure methane adsorption in shale using isotherm data at four temperatures (303.15 K, 318.15 K, 333.15 K and 355.15 K) and high pressures (up to 27 MPa) based on three evaluation criteria: (1) fitting goodness of the adsorption model for describing experimental raw data, (2) interpretation of the observed test phenomena, and (3) prediction capability of the adsorption models beyond the test data. The dual-site Langmuir model is the only one that passes these three criteria, which supports the robustness of the dual-site Langmuir model. Therefore, the dual-site Langmuir model is recommended to use for methane adsorption in shale under high pressure conditions, especially when the Gibbs excess adsorption phenomenon is observable.

Acknowledgements

This research was supported in part by the U.S. Department of Energy through the National Energy Technology Laboratory's Program under Contract No. DE-FE0006827. The authors would like to thank Dr. Nicholas P. Stadie for the help in curve fitting and Mr. Lingjie Yu for conducting isothermal adsorption experiments.

References

Ambrose, R. J., Hartman, R. C., Diaz Campos, M., Akkutlu, I. Y., & Sondergeld, C. (2010, January). New pore-scale considerations for shale gas in place calculations. In SPE Unconventional Gas Conference. Society of Petroleum Engineers.

Amankwah, K. A. G., & Schwarz, J. A. (1995). A modified approach for estimating pseudo-vapor pressures in the application of the Dubinin-Astakhov equation. Carbon, 33(9), 1313-1319.

Andrews, I. J. (2013). The Carboniferous Bowland Shale gas study: geology and resource estimation.

Aukett, P. N., Quirke, N., Riddiford, S., & Tennison, S. R. (1992). Methane adsorption on microporous carbons—a comparison of experiment, theory, and simulation. Carbon, 30(6), 913-924.

Akkutlu, I. Y., & Didar, B. R. (2013, April). Pore-size dependence of fluid phase behavior and properties in organic-rich shale reservoirs. In SPE International Symposium on Oilfield Chemistry. Society of Petroleum Engineers.

Bae, J. S., & Bhatia, S. K. (2006). High-pressure adsorption of methane and carbon dioxide on coal. Energy & Fuels, 20(6), 2599-2607.

Busch, A., Bertier, P., Gensterblum, Y., Rother, G., Spiers, C. J., Zhang, M., & Wentinck, H. M. On sorption and swelling of CO2 in clays (2016). Geomechanics and Geophysics for Geo-Energy and Geo-Resources, 1-20. DOI: 10.1007/s40948-016-0024-4.

Bruns, B., Littke, R., Gasparik, M., Wees, J. D., & Nelskamp, S. (2016). Thermal evolution and shale gas potential estimation of the Wealden and Posidonia Shale in NW-Germany and the Netherlands: a 3D basin modelling study. Basin Research, 28(1), 2-33.

Bourrelly, S., Llewellyn, P. L., Serre, C., Millange, F., Loiseau, T., & Férey, G. (2005). Different adsorption behaviors of methane and carbon dioxide in the isotypic nanoporous metal terephthalates MIL-53 and MIL-47. Journal of the American Chemical Society, 127(39), 13519-13521.

Curtis, J. B. (2002). Fractured shale-gas systems. AAPG bulletin, 86(11), 1921-1938.

Rexer, Thomas FT, Michael J. Benham, Andrew C. Aplin, and K. Mark Thomas. "Methane adsorption on shale under simulated geological temperature and pressure conditions." Energy & Fuels 27, no. 6 (2013): 3099-3109.

Chen, X. S., McEnaney, B., Mays, T. J., Alcaniz-Monge, J., & Linares-Solano, A. (1997). Theoretical and experimental studies of methane adsorption on microporous carbons. Carbon, 35(9), 1251-1258.

Chareonsuppanimit, P., Mohammad, S. A., Robinson, R. L., & Gasem, K. A. (2012). High-pressure adsorption of gases on shales: Measurements and modeling. International Journal of Coal Geology, 95, 34-46.

Dubinin, M. (1960). The potential theory of adsorption of gases and vapors for adsorbents with energetically nonuniform surfaces. Chemical Reviews, 60(2), 235-241.

Dubinin, M. M., & Astakhov, V. A. (1971). Development of the concepts of volume filling of micropores in the adsorption of gases and vapors by microporous adsorbents. Bulletin of the Academy of Sciences of the USSR, Division of chemical science, 20(1), 3-7.

Dym, C. (2004). Principles of mathematical modeling. Academic press.

Do, D. D., & Do, H. D. (1997). A new adsorption isotherm for heterogeneous adsorbent based on the isosteric heat as a function of loading. Chemical engineering science, 52(2), 297-310.

Fitzgerald, J. E., Sudibandriyo, M., Pan, Z., Robinson, R. L., & Gasem, K. A. M. (2003). Modeling the adsorption of pure gases on coals with the SLD model. Carbon, 41(12), 2203-2216.

Graham, D. (1953). The characterization of physical adsorption systems. I. The equilibrium function and standard free energy of adsorption. The Journal of Physical Chemistry, 57(7), 665-669.

Hildenbrand, A., Krooss, B. M., Busch, A., & Gaschnitz, R. (2006). Evolution of methane sorption capacity of coal seams as a function of burial history—a case study from the Campine Basin, NE Belgium. International Journal of Coal Geology, 66(3), 179-203.

Huan X., Zhang, X., & Wei, H.. Research on parameters of adsorption potential via methane adsorption of different types of coal. Journal of China Coal Society, 2015,40(8):1859-1864. doi:10. 13225 / j. cnki. jccs. 2014. 1220.

Herbst, A., & Harting, P. (2002). Thermodynamic description of excess isotherms in high-pressure adsorption of methane, argon and nitrogen. Adsorption, 8(2), 111-123.

Keller, J. U., & Staudt, R. (2005). Gas adsorption equilibria: experimental methods and adsorptive isotherms. Springer Science & Business Media.

Kronimus, A., Busch, A., Alles, S., Juch, D., Jurisch, A., & Littke, R. (2008). A preliminary evaluation of the CO 2 storage potential in unminable coal seams of the Münster Cretaceous Basin, Germany. International Journal of Greenhouse Gas Control, 2(3), 329-341.

Kuuskraa, V., Stevens, S. H., & Moodhe, K. D. (2013). Technically recoverable shale oil and shale gas resources: an assessment of 137 shale formations in 41 countries outside the United States. Natural Gas Industry, 5, 003.

Luo, X., Wang, S., Wang, Z., Jing, Z., Lv, M., Zhai, Z., & Han, T. (2015). Adsorption of methane, carbon dioxide and their binary mixtures on Jurassic shale from the Qaidam Basin in China. International Journal of Coal Geology, 150, 210-223.

Luo, J., Liu, Y., Jiang, C., Chu, W., Jie, W., & Xie, H. (2011). Experimental and modeling study of methane adsorption on activated carbon derived from anthracite. Journal of Chemical & Engineering Data, 56(12), 4919-4926.

Mertens, F. O. (2009). Determination of absolute adsorption in highly ordered porous media. Surface Science, 603(10), 1979-1984.

Mosher, K., He, J., Liu, Y., Rupp, E., & Wilcox, J. (2013). Molecular simulation of methane adsorption in micro-and mesoporous carbons with applications to coal and gas shale systems. International Journal of Coal Geology, 109, 36-44.

Murialdo, M., Stadie, N. P., Ahn, C. C., & Fultz, B. (2015). Observation and Investigation of Increasing Isosteric Heat of Adsorption of Ethane on Zeolite-Templated Carbon. The Journal of Physical Chemistry C, 119(2), 944-950.

Ottiger, S., Pini, R., Storti, G., Mazzotti, M., Bencini, R., Quattrocchi, F., ... & Deriu, G. (2006). Adsorption of pure carbon dioxide and methane on dry coal from the Sulcis Coal Province (SW Sardinia, Italy). Environmental Progress, 25(4), 355-364.

Pini, R. (2014). Interpretation of net and excess adsorption isotherms in microporous adsorbents. Microporous and Mesoporous Materials, 187, 40-52.

Sakurovs, R., Day, S., Weir, S., & Duffy, G. (2007). Application of a modified Dubinin-Radushkevich equation to adsorption of gases by coals under supercritical conditions. Energy & fuels, 21(2), 992-997.

Sudibandriyo, M., Mohammad, S. A., Robinson, R. L., & Gasem, K. A. (2010). Ono–Kondo lattice model for high-pressure adsorption: Pure gases. Fluid Phase Equilibria, 299(2), 238-251.

Snurr, R. Q., June, R. L., Bell, A. T., & Theodorou, D. N. (1991). Molecular simulations of methane adsorption in silicalite. Molecular Simulation, 8(1-2), 73-92.

Stadie, N. P., Murialdo, M., Ahn, C. C., & Fultz, B. (2013). Anomalous isosteric enthalpy of adsorption of methane on zeolite-templated carbon. Journal of the American Chemical Society, 135(3), 990-993.

Stadie, N. P., Murialdo, M., Ahn, C. C., & Fultz, B. (2015). Unusual Entropy of Adsorbed Methane on Zeolite-Templated Carbon. The Journal of Physical Chemistry C, 119(47), 26409-26421.

Setzmann, U., & Wagner, W. (1991). A new equation of state and tables of thermodynamic properties for methane covering the range from the melting line to 625 K at pressures up to 100 MPa. Journal of Physical and Chemical reference data, 20(6), 1061-1155.

Tang, X., Ripepi, N., Stadie, N. P., Yu, L., & Hall, M. R. (2016). A dual-site Langmuir equation for accurate estimation of high pressure deep shale gas resources. Fuel, 185, 10-17.

Tang, X. (2016). Comments on paper "Langmuir slip-Langmuir sorption permeability model of shale". Fuel, 181, 1095.

Tang, X., Ripepi, N., & Gilliland, E. (2015). Isothermal adsorption kinetics properties of carbon dioxide in crushed coal. Greenhouse Gases: Science and Technology. DOI: 10.1002/ghg.1562

Tian, H., Li, T., Zhang, T., & Xiao, X. (2016). Characterization of methane adsorption on overmature Lower Silurian–Upper Ordovician shales in Sichuan Basin, southwest China: Experimental results and geological implications. International Journal of Coal Geology.156, 36-49.

Weniger, P., Kalkreuth, W., Busch, A., & Krooss, B. M. (2010). High-pressure methane and carbon dioxide sorption on coal and shale samples from the Paraná Basin, Brazil. International Journal of Coal Geology, 84(3), 190-205.

Wang, Q., Chen, X., Jha, A. N., & Rogers, H. (2014). Natural gas from shale formation–the evolution, evidences and challenges of shale gas revolution in United States. Renewable and Sustainable Energy Reviews, 30, 1-28.

Wang, S. (2007). Comparative molecular simulation study of methane adsorption in metal-organic frameworks. Energy & fuels, 21(2), 953-956.

Xiong, J., Liu, X., Liang, L. & Lei, M. Improved Dubibin-Astakhov model for shale-gas supercritical adsorption. Acta Petrolei Sinica, 2015, 36(7): 849-857.

Zhou, Y., & Zhou, L. (2009). Fundamentals of high pressure adsorption. Langmuir, 25(23), 13461-13466.

Zhou, L., Li, M., & Zhou, Y. (2000). Measurement and theoretical analysis of the adsorption of supercritical methane on superactivated carbon. Science in China Series B: Chemistry, 43(2), 143-153.

Zhang, J., Clennell, M. B., Dewhurst, D. N., & Liu, K. (2014). Combined Monte Carlo and molecular dynamics simulation of methane adsorption on dry and moist coal. Fuel, 122, 186-197.

2.2 A dual-site Langmuir equation for accurate estimation of high pressure deep shale gas resources

Xu Tang[*], Nino Ripepi[*,†], Nicholas P. Stadie[‡], Lingjie, Yu[§,¶], Matthew R Hall[#,‖]

([*]Department of Mining and Minerals Engineering & [†]Virginia Center for Coal and Energy Research, Virginia Polytechnic Institute and State University, Blacksburg, Virginia, 24060, U.S; [‡]ETH Zürich, Laboratory of Inorganic Chemistry, Vladimir-Prelog-Weg 1, 8093 Zürich, Switzerland; [§]Wuxi Research Institute of Petroleum Geology of Sinopec Exploration & Production Research Institute & [¶]Sinopec Key Laboratory of Petroleum Accumulation Mechanisms, Wuxi, Jiangsu, 214151, China; [#]Nottingham Centre for Geomechanics, Faculty of Engineering, University of Nottingham, Nottingham, NG7 2RD UK, [‖]British Geological Survey, Environmental Science Centre, Keyworth, Nottingham, NG12 5GG UK)

Abstract: Adsorbed methane makes up a large portion of the total shale gas-in-place (GIP) resource in deep shale formations. In order to accurately estimate the shale GIP resource, it is crucial to understand the relationship between the adsorbed methane quantity and the free methane quantity of shale gas in shale formations (under high pressure conditions). This work describes and accurately predicts high pressure methane adsorption behavior in Longmaxi shale (China) using a dual-site Langmuir model. Laboratory measurements of high pressure methane adsorption (303 - 355 K and up to 27 MPa) are presented. Our findings show that for depths greater than 1000 m (> 15 MPa) in the subsurface, the shale gas resources have historically been significantly overestimated. For Longmaxi shale (2500 – 3000 m in depth), classical approaches overestimate the GIP by up to 35%. The ratio of the adsorbed phase compared to the free gas has been significantly underestimated. The methods used herein allow accurate estimations of the true shale GIP resource and the relative quantity of adsorbed methane at *in situ* temperatures and pressures representative of deep shale formations.

Key words: Shale gas, methane, absolute adsorption, Langmuir

Published in Fuel: Volume 185, 1 December 2016, Pages 10–17.

2.2.1 Introduction

Shale gas resources are globally abundant and shale gas production has continuously increased over the past ten years as a result of horizontal drilling and hydraulic fracture techniques (1-7). It is now recognized as a promising unconventional natural gas resource, and many countries have attempted to accurately estimate their shale gas resources in an effort to meet their future energy demands (4, 7-8). For example, shale gas production has grown very rapidly in the United States, reaching nearly 40% of total natural gas production in 2013 (6). Despite its widespread importance, substantial uncertainties exist in assessing the quantity of recoverable shale gas, and current resource estimates should be treated with considerable caution (9, 10). This large and continuing uncertainty significantly impacts the total gas-in-place (GIP) estimation at a majority of sites, especially in terms of the often-neglected effects of high pressure and temperature in deeper shale formations, *e.g.* Barnett shale. The future of the shale gas industry and worldwide energy policy therefore depends on the development of a more accurate shale gas resource estimation methodology. In addition, with the development of non-aqueous fracturing fluids such as carbon dioxide in the hydraulic fracturing technique, deep shale formations may become a viable option for carbon dioxide sequestration (11, 12). A reasonable assessment of the carbon dioxide adsorption capacity of shale at high pressure and temperature geological conditions is of parallel interest (13, 14).

Shale gas trapped within shale formations is different from conventional natural gas since the shale formation is often both the source and the reservoir of the natural gas itself. Shale gas exists in three different phases within the shale formation: (i) as free compressed gas, (ii) as adsorbed fluid on the surface, and (iii) as a dissolved component in the liquid hydrocarbon and brine. The most widely used approach for estimating shale GIP is to sum these three components. The adsorbed phase accounts for 20% to 85% of the total amount based on current studies in five major shale formations in the United States (1). Thus, the estimation of the adsorbed amount of natural gas, the largest component of which is methane, significantly influences the final determination of the geological GIP quantity and the working life of the shale gas producing well (9).

Unlike coalbed methane which usually occurs in shallow coal seams (at depths of <1000 m), shale formations are typically much deeper and under significantly different geological conditions. For example, the Barnett shale completions are up to 2500 m deep, where reservoir pressures can reach

27 MPa and the reservoir temperature can be up to 360 K (1). Unfortunately, the effects of these high pressure and temperature conditions on the quantity of adsorbed methane available in shale gas reservoirs have rarely been appropriately considered in both academia and industry. The standard practice for estimating shale GIP is to use methane adsorption measurements at intermediate pressure conditions (10-15 MPa) to predict the methane adsorption behavior in the higher pressure region (>15 MPa) (1, 2, 4, 5, 8). However, the methodology used in the standard practice does not account for the difference between observed and absolute adsorption quantities. This misinterpretation can significantly affect the shale GIP estimation, especially the contribution of the adsorbed methane at high pressure geological conditions (high pressure refers to reservoir pressures above 15 MPa in this work) (9) where the Gibbs excess adsorption phenomenon is very pronounced. Even though this phenomenon has been observed and acknowledged in numerous cases (15-24), several fundamental problems still remain to be addressed. These include the development of physically reasonable methods to (i) accurately describe the observed (excess) adsorption isotherms, (ii) predict the corresponding absolute adsorption isotherms, and (iii) predict adsorption isotherms at pressures and temperatures beyond the measured data. Several adsorption models have been proposed (15, 17-19, 21-23), but these models do not give a satisfactory interpretation of the experimental data and excess adsorption phenomena, and the assumptions used are unphysical in nature. Most notably, a common assumption is to treat the adsorbed layer as having a constant volume independent of the adsorbed amount and/or pressure of the bulk phase (15-19, 21-23). Although in some cases this volume is allowed to vary with temperature (15, 16), it is generally not valid to assume that the volume will not change as the adsorbed phase increases in occupancy. The simplified, homogeneous pore structures used in the computational approach can also not be used to reasonably portray the heterogeneous properties of shale or coal (24- 26). In addition, all of these proposed methods cannot predict adsorption isotherms at arbitrary conditions in a robust and rational way, which inhibits their application for shale gas resource estimation as a function of specific location (e.g., subsurface depth). All of these shortcomings are compounded by a lack of measured data under high pressure conditions (well beyond the Gibbs excess maximum). Therefore, both high-pressure adsorption measurements and an optimized adsorption model are needed to accurately describe the adsorption behavior of methane in shale under relevant subsurface conditions. This will in turn allow an accurate shale GIP estimation for a plethora of worldwide shale resources under actual *in situ* conditions.

In this work, methane adsorption in a sample of Longmaxi shale from China was measured using a gravimetric method at four temperatures (303.15 K, 318.15 K, 333.15 K and 355.15 K) and high pressures (up to 27 MPa). A dual-site Langmuir adsorption model is introduced to describe both the observed and absolute isotherms at high pressure, utilizing the assumption that the volume of the adsorbed phase changes constantly with the number of adsorbed molecules following a dual-site Langmuir-type equation. These results shed light on the true quantity of shale GIP that can be applied over a large range of temperature and pressure, relevant to the geological conditions of actual shale gas resources.

2.2.2 Dual-site Langmuir adsorption model

In any pure gas-solid adsorption system, the observed adsorption quantity, also called the Gibbs excess adsorption uptake, is given by the Gibbs equation,

$$n_e = n_a - V_a \cdot \rho_g = n_a \cdot (1 - \frac{\rho_g}{\rho_a}) \qquad (1)$$

where the excess adsorption quantity (n_e) refers to the difference between the absolute adsorption quantity (n_a) and the quantity of adsorbate that would be present in the same volume (V_a) of the adsorbed phase at the density of the bulk gas phase (ρ_g). When V_a is very low or the density of the adsorbed phase (ρ_a) is much higher than the bulk gas phase density (ρ_g), the excess adsorption quantity is approximately equal to the actual adsorbed amount. However, this relation is invalid at high pressure where the density of the adsorbed phase is similar to the density of the bulk fluid, the point at which the observed adsorption quantity reaches a maximum and then decreases. Under such conditions, the conventional adsorption models that neglect the real volume of the adsorbed phase cannot reasonably explain such adsorption behavior. Therefore, it is imperative to use a more sophisticated approach to obtain the absolute isotherms from observed Gibbs excess isotherms at high pressures. The absolute adsorbed amount (n_a) should always be a monotonically increasing quantity with increasing pressure for a physical adsorption system. A simple description of such a system is the widely used Langmuir equation (equation 2),

$$n_a = n_{\max} \cdot \frac{K(T)P}{1 + K(T)P} \qquad (2)$$

where n_a is the absolute adsorption quantity under equilibrium temperature (T) and pressure (P), n_{max} is the maximum adsorption capacity, K(T) is the temperature-dependent equilibrium constant, which can be expressed as $K(T) = A_0 \cdot \exp(-\frac{E_0}{RT})$, E_0 is the energy of adsorption, A_0 is the pre-exponential coefficient and R is the ideal gas content (where both E_0 and A_0 are independent of temperature).

In order to obtain the absolute adsorption amount from the observed Gibbs excess adsorption isotherms, V_a or ρ_a must be known. However, it is not possible to measure either of these quantities directly. Therefore, the most widely used approach is to estimate the density of the adsorbed layer based on one of numerous empirical relationships (15, 17-23). It is common to assume that the volume of the adsorbed phase is always constant as a function of adsorption uptake, or in some cases only dependent on temperature. This assumption does not have a basis in the physical understanding of adsorption where the volume of the adsorbed phase must increase as uptake increases.

An alternative approach is to assume that the adsorbed phase has a constant density and that its volume is therefore a linear function of adsorbed amount. In this case, the fact that different researchers use different values for the density of the adsorbed phase (e.g., that of the liquid adsorbate) to obtain absolute isotherms from observed Gibbs excess isotherms is a significant issue, and these values cannot be directly validated through laboratory approaches (15-23). The most general approach is to allow the adsorbed density to be an independent parameter of the adsorption model. This is adopted herein as shown in equation (3), by treating the adsorbed layer as constantly increasing as a function of uptake up to a fitted maximum adsorbed phase volume (14, 27-30). This can be expressed as,

$$V_a = V_{max} \cdot \frac{K(T)P}{1 + K(T)P} \quad (3)$$

where V_{max} is the volume of the adsorbed phase at maximum adsorption capacity. This unknown volume (V_{max}) can be left as an independent fitting parameter and varies from system to system but often yields densities of the adsorbed phase that are close to that of the liquid adsorbate.

Combining equations (1), (2) and (3), the excess adsorption uptake can be obtained as shown in equations (4)

$$n_e(P,T) = (n_{\max} - V_{\max} \cdot \rho_g) \cdot \frac{K(T)P}{1+K(T)P} \quad (4)$$

However, this single-site Langmuir equation cannot sufficiently describe a large number of real gas-solid adsorption systems (31-32). For heterogeneous surfaces (as in almost all real-world materials), the adsorption energy at each site will vary, depending on the local chemistry and structure. The single site Langmuir model is limited in this application (31-32). The most favorable sites will be filled first, followed by the less favorable sites. In order to address heterogeneous adsorbents, the most simplified case is where only two different adsorption sites are available. Each site can be modelled by a separate equilibrium constant, $K_1(T)$ and $K_2(T)$ ($K_1(T) = A_1 \cdot \exp(-\frac{E_1}{RT})$ and $K_2(T) = A_2 \cdot \exp(-\frac{E_2}{RT})$), weighted by a coefficient (α). Thus, the dual-site Langmuir equation can be written in the following form (equation 5), where α is the fraction of the second type of site (0<α<1),

$$n_a(P,T) = n_{\max} \cdot \left[(1-\alpha)(\frac{K_1(T)P}{1+K_1(T)P}) + \alpha(\frac{K_2(T)P}{1+K_2(T)P}) \right] \quad (5)$$

In the same way as for the single-site equation, the excess uptake in the dual-site equation can be obtained, shown in (6),

$$n_e(P,T) = (n_{\max} - V_{\max} \cdot \rho_g) \cdot \left[(1-\alpha)(\frac{K_1(T)P}{1+K_1(T)P}) + \alpha(\frac{K_2(T)P}{1+K_2(T)P}) \right] \quad (6)$$

Both the single-site (equation 2, 4) and dual-site equations (equation 5, 6) shown herein are based on the assumption that the volume of the adsorbed layer increases linearly with the adsorbed amount, up to a monolayer completion (V_{max}). Then, the absolute adsorption amount can be obtained from the measured adsorption data *via* a least-squares fitting analysis. It should be noted that the real-world material may have an abundance of different adsorption sites in actuality, but that a two-site model has often been found to be sufficient for describing such a system owing to the large number of independent fitting parameters (28-30), and when using a global fitting method

(see: Section 3 Materials and methods) it is desirable to decrease the number of unnecessary such parameters (30).

2.2.3 Materials and methods

Shale samples from the Lower Silurian Longmaxi Formation (collected at a depth of 2400.8 m) were obtained from the Fuling #1 well in the Fuling region, Sichuan Province, China. The shale specimen was ground and sieved using 0.38-0.83 mm metal sifters and placed in a drying oven at 105 °C for 24 h to dehydrate. After dehydration, the prepared sample was stored in a desiccator prior to adsorption measurements. Methane adsorption measurements were conducted using a Rubotherm Gravimetric Sorption Analyzer (Rubotherm GmbH, Bochum, Germany) with research grade methane gas (99.99%). Detailed experimental procedures and physical parameters of the shale sample are given in the Supplemental Materials.

In this work, four methane adsorption isotherms were obtained at 303.15 K, 318.15 K, 333.15 K and 355.15 K. All isotherms were measured up to 27 MPa and fluctuations in temperature during a given isotherm were < 0.2℃. The data were processed using a previously developed Mathematica script (28-30); the four Gibbs excess adsorption isotherms were fitted simultaneously to the dual-site Langmuir model (equation 6) by a least-squares residual minimization algorithm based on the Differential Evolution method. Each data point was given the same weight and none were discarded. The density of the bulk fluid as a function of temperature and pressure was obtained from the NIST REFPROP database. The seven independent fitting parameters were varied to achieve the global minimum of the residual-squares value within the following limits: $0<n_{max}<100$ mmol/g, $0< V_{max}<10$ cm^3/g, $0<\alpha<1$, $0< E_1 <100$ kJ/mol, $0< E_2 <100$ kJ/mol, $A_1 > 0$, $A_2 > 0$). Minimization was performed in excess of 100 unique times by changing the random seed in order to assure that a global minimum was achieved. Once the seven fitting parameters were determined, absolute and excess adsorption uptake could be easily calculated at any temperature and pressure by use of equations 5 and 6.

2.2.4 Results and discussions

2.2.4.1 Modeling of observed Gibbs excess adsorption at high pressures

Equilibrium excess adsorption uptake of methane measured on Longmaxi shale between 303-355 K and 0.1-27 MPa is shown in Figure 2.2.1. In all isotherms, the observed Gibbs excess adsorption

uptake increases with increasing pressure up to a maximum value and then decreases. At pressures below the Gibbs excess maximum, the excess adsorption is always lower at higher temperatures. However, at a point somewhere beyond the Gibbs excess maximum, the isotherms crossover and higher temperatures now result in higher excess uptake at equivalent pressures. As seen in Figure 2.2.1, the observed maximum Gibbs excess adsorption quantities are 0.0893 mmol/g, 0.0813 mmol/g, 0.0786 mmol/g and 0.0719 mmol/g at 303.15 K (8 MPa), 318.15 K (10 MPa), 333.15 K (12 MPa) and 355.15 K (12 MPa), respectively. As the isotherm temperature increases, higher pressure is needed to reach the Gibbs excess maximum. This is a well-known phenomenon of supercritical gas adsorption (33). The dual-site Langmuir adsorption model (equation 6) gives a good global fit to the observed data, and the corresponding best-fit parameters are: n_{max}=0.1715 mmol/g, V_{max}=0.0097 mL/g, α=0.2640, E_1=16.706 kJ/mol, A_1=0.0002 1/MPa, E_2 =15.592 kJ/mol, A_2=0.0032 1/MPa. It should be emphasized that these seven parameters apply to all the isotherms measured, and that by performing a single global fit to all the data at once, a most general understanding of the properties of the adsorbent-adsorbate system can be achieved.

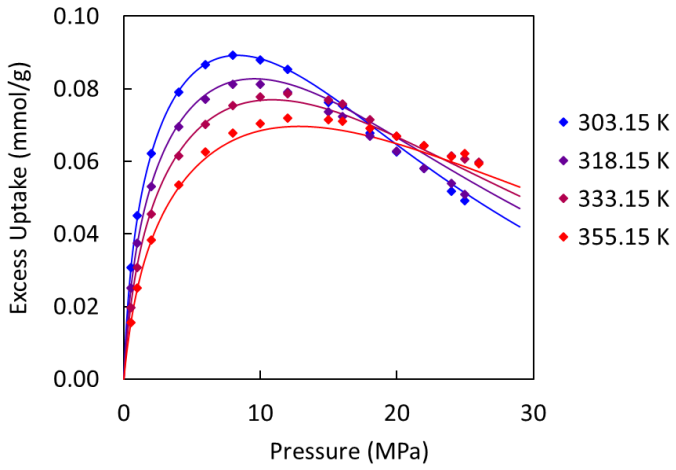

Figure 2.2.1 Gibbs excess adsorption isotherms of methane on Longmaxi shale (symbols) and dual-site Langmuir model fits (lines)

An explanation of the Gibbs excess maximum phenomenon can be made by examining the change in the volume of the adsorbed phase as compared to the volume-density product, as shown in Figure 2.2.2. The volume of the adsorbed methane phase changes with pressure and temperature following a dual-site equivalent of equation 3. Higher temperature decreases the adsorbed quantity of methane, which results in a decreased volume of the adsorbed phase. As pressure increases, the

volume-density term (V_a*ρ_g) of equation (6) always increases but the difference of (V_a*ρ_g) at different temperatures becomes more pronounced. The (V_a*ρ_g) term at low temperature is always higher than that at high temperature and the maximum absolute adsorption quantity (n_{max}) is constant, which results in the crossover of the Gibbs excess adsorption isotherms. Therefore, the observation of the crossover phenomenon in the measured data (Fig. 2.2.1) supports the assumption that the volume of adsorbed methane changes with temperature and pressure following a dual-site Langmuir-type equation. This is in distinct contradiction to the approximation that the adsorbed phase is constant, an often used approximation in other work.

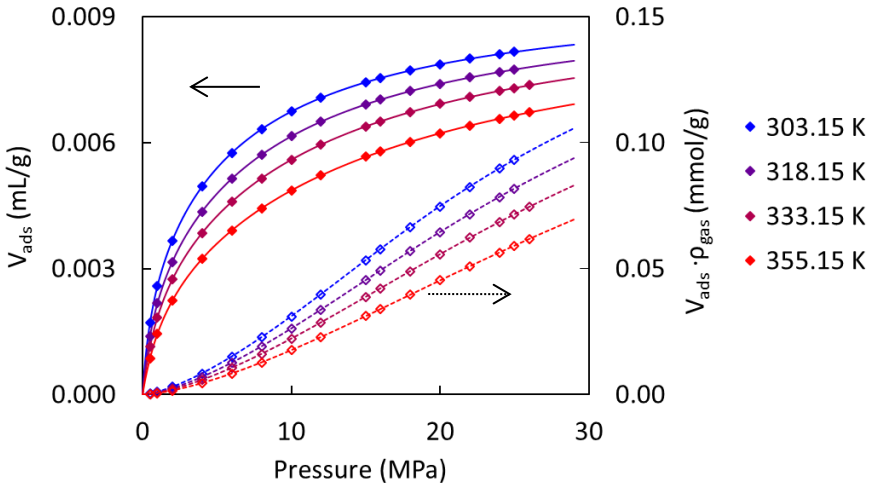

Figure 2.2.2 Modelled values of the volume of adsorbed methane (V_a) (solid lines, filled symbols, left major axis) and the volume-density term (V_a*ρ_g) (dotted line, hollow symbols, right minor axis) on Longmaxi shale as a function of pressure

The crossover of the excess uptake isotherms is not observed when the isotherms are plotted as a function of bulk gas density instead of pressure (Figure 2.2.3). The measured isotherms show the same temperature dependence at all pressures, *i.e.* increasing excess uptake with decreasing temperature. This behavior is also inherently predicted by the dual-site Langmuir equation (see the fits in Figure 2.2.3). The small deviations from this trend in the measured data at 318.15 K can be attributed to experimental error, and the overall trend remains clear. The same phenomenon (seen when plotting excess uptake as a function of bulk fluid density) was also reported for carbon dioxide, methane and nitrogen adsorption in different materials (15, 17, 21).

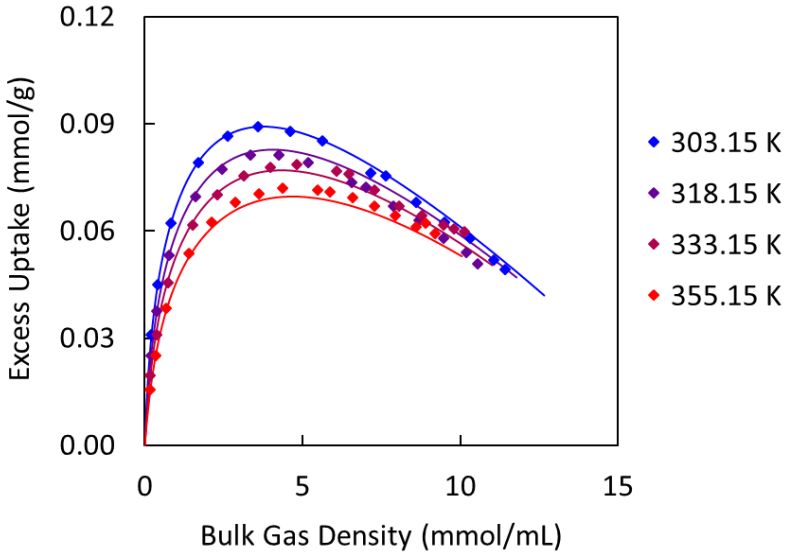

Figure 2.2.3 Gibbs excess adsorption isotherms of methane on Longmaxi shale (symbols) and dual-site Langmuir equation fits (lines) as a function of bulk methane density

2.2.4.2 Prediction of absolute adsorption and extrapolation to higher temperatures

Absolute adsorption isotherms of methane on Longmaxi shale based on equation 5 are shown in Figure 2.2.4. As is characteristic of the Langmuir equation, the adsorption quantity increases monotonically up to 27 MPa, which is consistent with the physical nature of adsorption. The absolute adsorption quantity is significantly higher than the observed Gibbs excess quantity, especially at 27 MPa. This implies the significant contribution of the adsorbed phase volume of methane in shale toward the absolute adsorption content, which is neglected in the observed Gibbs excess adsorption isotherms. Figure 2.2.4 also shows that at higher temperatures, this contribution becomes less pronounced.

Predicting adsorption isotherms at different temperatures is of fundamental interest for shale GIP estimations in the deep subsurface, typically reservoirs at a depth over 1000 m. It is impractical to measure a large number of isotherms at different temperatures for shale gas resource estimation. Thus, another feature of the dual-site Langmuir model used herein is that it can be used to predict isotherms at arbitrary temperatures near the measured isotherms. This is very notably not possible when each isotherm is fitted individually, as is often the case in other studies, and a global fit across numerous isotherms is therefore an extremely desirable feature of a particular model. Interpolation of the measured data (i.e., predictions at temperatures between the measured

isotherms) is expected to be highly accurate, though extrapolation to higher or lower temperatures than measured, while also possible, should be performed with caution. Nevertheless, extrapolation can often shed valuable light on conditions outside of the region where measurement is possible.

Estimated absolute adsorption isotherms of methane on Longmaxi shale are also shown at different temperatures up to 415.15 K in Figure 2.2.4. The predicted Gibbs excess adsorption isotherms exhibit similar properties as the observed isotherms and therefore the extrapolation is determined to be reasonably dependable. As the temperature increases, the contribution of the adsorbed phase volume for the absolute adsorption gradually becomes less pronounced. Notably, the negative effect of temperature on methane adsorption on shale remains clear at all temperatures.

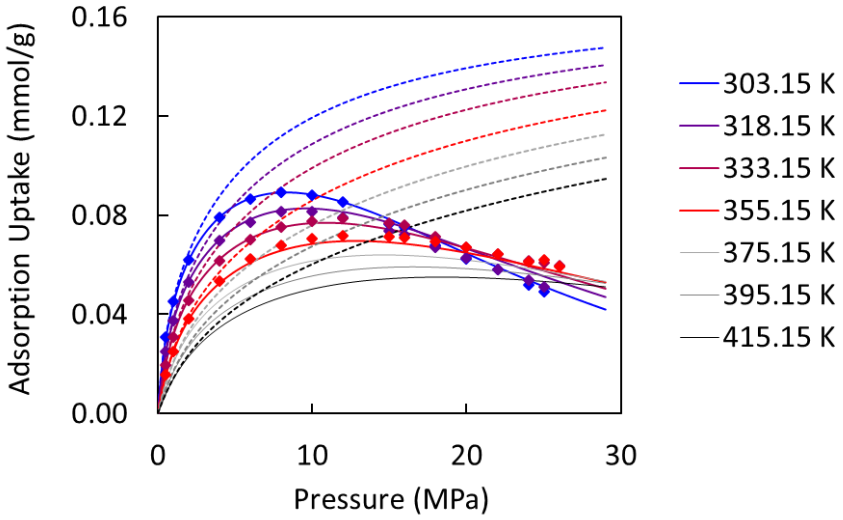

Figure 2.2.4 Gibbs excess adsorption (solid lines, filled symbols) and absolute adsorption (dashed lines) isotherms of methane on Longmaxi shale as fitted by a dual-site Langmuir equation (measured up to 355.15 K), extrapolated up to 415.15 K (gradual grey lines)

2.2.4.3 Accurate shale gas-in-place estimations from adsorption measurements

Equilibrium methane adsorption measurements in shale can be used to estimate the geological gas-in-place (GIP) content of subsurface shale formations. It is important to note that this method does not take into account any moisture present in the shale which can reduce the methane adsorption capacity. In addition, this GIP content does not include any contribution from dissolved methane in the liquid hydrocarbon or brine, and also does not consider the presence of other gaseous components of natural gas (e.g., higher alkanes and hydrogen sulfide).

The geological GIP is estimated herein as the total amount of methane present in the gaseous and adsorbed phases in a homogeneous formation of shale. Conceptually, this amount is accessible via the sum of the free gas phase content, n_{free}, and the absolute adsorbed phase content, n_a.

$$GIP = n_{free} + n_a \quad (7)$$

The amount of gaseous methane is equal to the bulk methane density multiplied by the volume of the gas phase alone (excluding the volume of the adsorbed phase) as shown in Figure 2.2.5. However, the volume accessible to the free gas is not the same as the entire empty volume of the shale since the adsorbed phase occupies a finite volume itself, which is significant at high pressure.

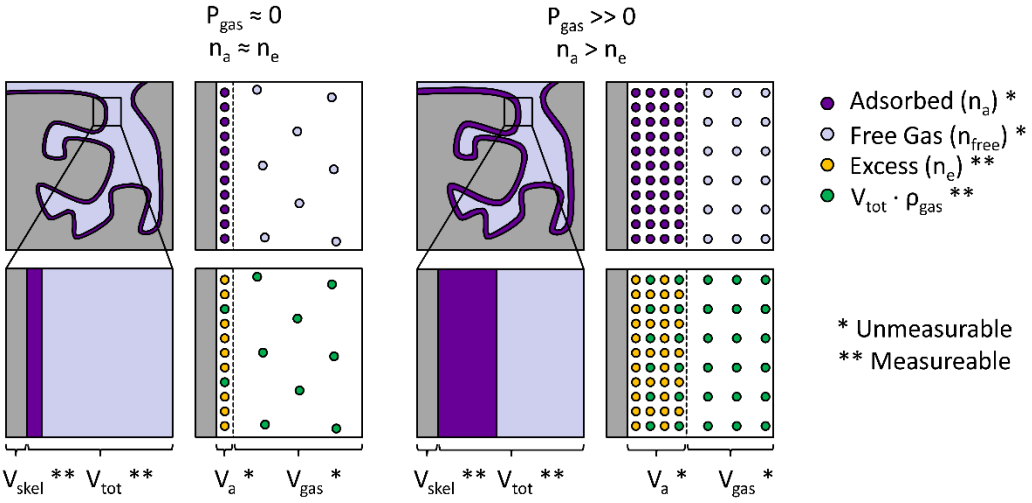

Figure 2.2.5 Schematic depiction of the quantities relevant to gas-solid adsorption in two distinct regimes: in the dilute limit (left) and at high pressures (right) of the bulk gas

The total GIP amount can also be derived in a much simpler way as the sum of the excess adsorbed amount and a product of the entire free volume of the empty shale with the bulk gas phase density, because of the Gibbs definition (from equation 1):

$$GIP = n_{free} + n_e + V_a \cdot \rho_g = V_{tot} \cdot \rho_g + n_e \quad (8)$$

All three of the quantities in the final expression of equation 8 are directly measureable: the total empty volume accessible to gas in the shale formation (V_{tot}), the density of pure gaseous methane at the equilibrium conditions of the formation (ρ_g), and the excess adsorbed amount under these conditions (n_e). In practice, the excluded space within the shale ($V_{tot}=V_{bulk}-V_{skeletal}$) and/or its

skeletal density ($\rho_{shale} = m_{shale}/V_{skeletal}$) are generally measured using pycnometry with a probe gas such as helium, which is assumed to be non-adsorbing, or by other indirect approaches such as well logging. This measurement is required in order to make adsorption measurements, for which the experimental outcome is the excess adsorbed amount (n_e). It must therefore be emphasized that the simplest and most accurate approach to estimate the total shale GIP is *via* equation 8. This is demonstrated in Figure 2.1.6 where the adsorption isotherm of methane on Longmaxi shale measured in this work is directly converted to GIP content as a function of pressure at 355.15 K. No adsorption model is necessary to arrive at the total GIP content in this way.

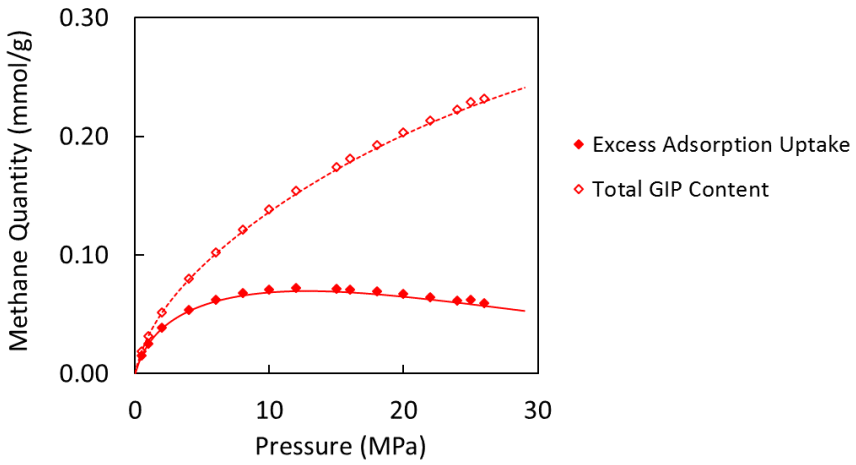

Figure 2.2.6 Directly calculated shale GIP content as a function of pressure using the measured data at 355.15 K

Historically, the precise definition of the measured adsorbed amount has been a matter of confusion. In some reports, the volume of the adsorbed layer is accounted for twice owing to the incorrect method of summing the "free gas content" in the entirety of the empty pore and the absolute adsorption content (9, 34,35), corresponding to:

$$GIP_{incorrect} = V_{tot} \cdot \rho_g + n_a \quad (9)$$

In this approach, where the absolute adsorption isotherms are used in place of the excess quantity for estimating GIP, the total shale gas content will be significantly overestimated.

This may suggest that the effort to extract the absolute adsorption isotherm from the measured data is unnecessary for understanding and estimating total GIP since only the excess adsorption data

are required (9, 34, 35). However, in order to determine the relative amount of adsorbed methane versus gaseous methane in this total figure, the absolute adsorption isotherm is required.

2.2.4.4 Geological gas-in-place resource estimation of a shale gas reservoir in Fuling, China

Generally, coal seams are shallower than shale formations (usually within depths up to 1000 m below the surface), and therefore the pressure (below 10-15 MPa) is low enough that the contribution of the volume of the adsorbed methane phase toward absolute adsorption content has little influence. In this case, employing either the absolute adsorbed amount (equation 9) or the measured Gibbs excess quantity (equation 8) is reasonable to estimate the total GIP content, though it is still simpler to use the directly measured quantity. Methane in deep shales, on the other hand, are in a different geological situation. For example, the Barnett shale completions are up to 2500 m deep, where the reservoir pressure reaches up to 27 MPa and the reservoir temperature can be up to 360 K (1). Therefore, both pressure and temperature effects on the adsorbed methane content cannot be neglected. In addition, the large difference between the observed adsorption uptake and the absolute adsorption uptake at these pressures demonstrates the importance of using an accurate model of methane content in subterranean shale formations. In other reports, the absolute adsorbed amount is estimated by simply fitting the excess adsorption quantities along a single isotherm to a single site (classical) Langmuir isotherm (1, 2, 4, 5, 8), which cannot accurately describe the changing volume of the adsorbed phase that is taking place. In these cases, regardless of whether equation 7 or 9 is used, the estimated GIP will be significantly incorrect. This result is demonstrated in Figure 2.2.7. Logically, there is undeniably a large contribution to the adsorbed amount at high pressures that is undetected by experiment since the bulk gas density approaches that of the adsorbed phase and the excess adsorption quantity is no longer accurate.

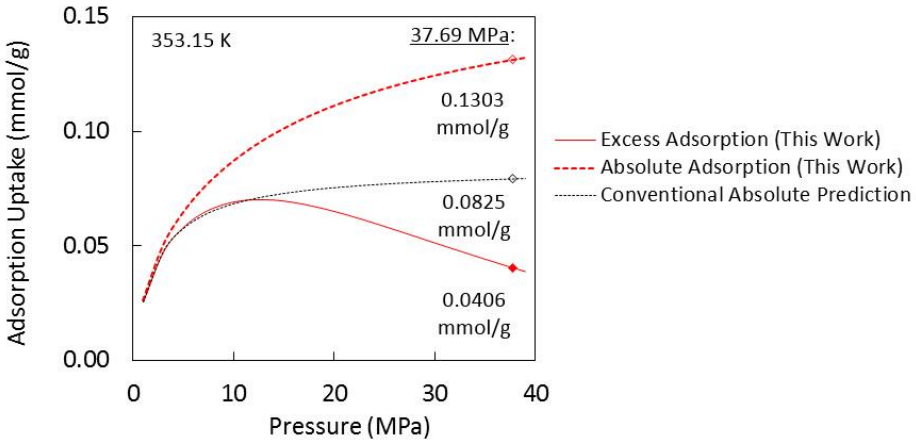

Figure 2.2.7 Comparison of the Gibbs excess adsorbed methane content (solid line) to two estimates of absolute adsorbed methane (dashed lines) on Langmaxi shale, at geological conditions of one completion well (353.15 K and up to 37.69 MPa (34)).

Herein, the geological GIP content of shale gas resources in the Fuling region in China is estimated as an example to determine the magnitude of the difference between conventional methods and those employed in this work. The shale gas wells in the Fuling region are the first commercialized shale gas resource in China (36, 37). The Longmaxi shale formation of the Fuling region is between 2000 to 3000 m deep; the pressure and temperature conditions as a function of depth can be estimated by the pressure coefficient (15 MPa/km) and the geothermal gradient (27.3℃/km). The average porosity and density of the shale rock are 4.5% and 2.4 g/mL, respectively (36, 37).

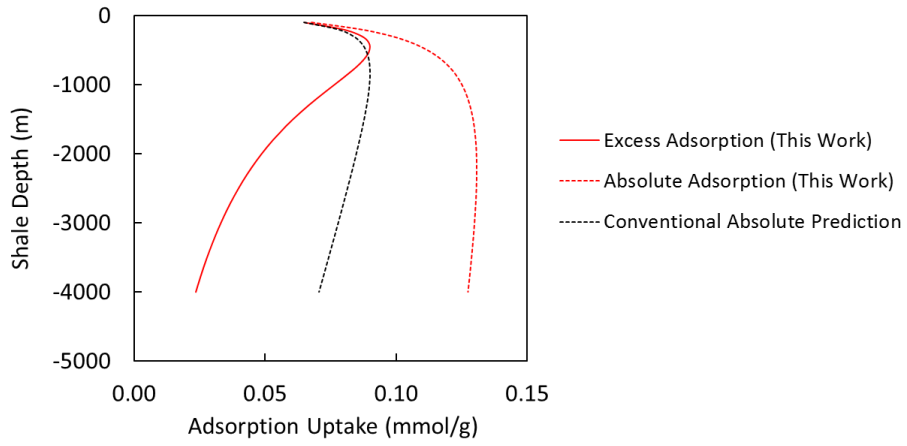

Figure 2.2.8 Comparison of methane adsorption capacity in Fuling region shale formations under geological temperature and pressure conditions as they vary with depth. Predictions are based on the following adsorption quantities: observed Gibbs excess adsorption, modeled absolute adsorption uptake (this work) and the "Conventional Absolute Prediction" (refer to Supplemental Materials).

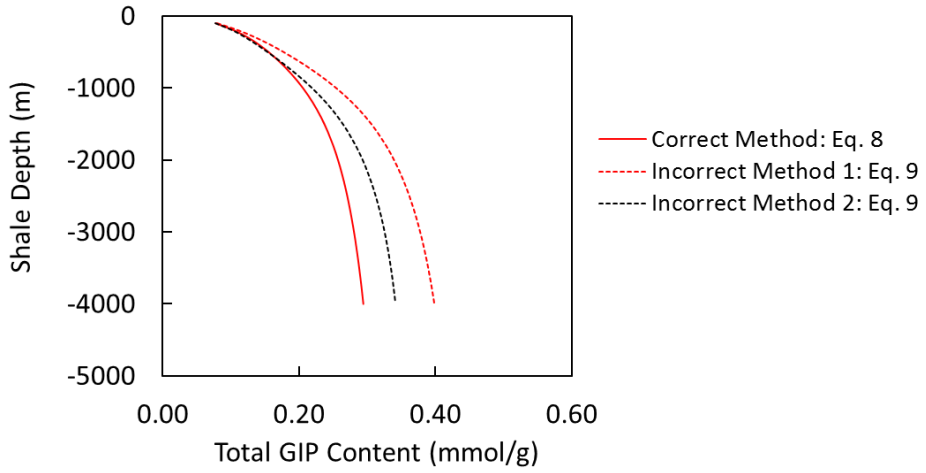

Figure 2.2.9 Shale GIP content in Fuling region shale formations under geological conditions, where temperature and pressure are varied as a function of depth. The Correct Method uses Eq. 8 where n_e is calculated using Eq. 6; Incorrect Method 1 uses Eq. 9 where n_a is calculated using Eq. 5; Incorrect Method 2 uses Eq. 9 where n_a is calculated using the Conventional Absolute Prediction (refer to Supplemental Materials).

In this case, both the temperature and the pressure of the actual shale reservoir at maximum depth are out of the range of data measured in this work. Nevertheless, the dual-site Langmuir model can be used to predict both the Gibbs excess adsorption isotherms and the absolute adsorption isotherms under different temperature and pressures, as previously discussed. Figure 2.2.8 shows that there are significant differences between the observed Gibbs excess adsorption quantity, true absolute adsorption quantity (as determined by the dual-site Langmuir model), and a common oversimplified approach to predict the absolute quantity, especially for formations over 1000 m deep. The oversimplified prediction of absolute adsorption is two times larger or more than the Gibbs excess adsorption amount, and the best estimate of absolute adsorption is three times larger or more. This is because the Gibbs excess adsorption amount and the oversimplified prediction (the "Conventional Absolute Prediction", see Supplemental Materials) are always less than the true (absolute) adsorption amount. When equation 9 is used to incorrectly predict GIP, this leads to a significant overestimation of geological GIP content under real geological conditions as shown in Figure 2.2.9. The correct method to estimate GIP content as a function of depth is *via* equation 8. Using the incorrect method 1 and method 2 (shown in Figure 2.2.9), shale gas resources at a depth of 3000 m are overestimated by 35% and 16%, respectively.

To accurately determine the ratio of adsorbed methane to gaseous methane in the total GIP resource, one must employ an accurate absolute adsorption quantity. If either the measured excess adsorption quantity or an oversimplified absolute adsorption prediction (as in Figure 2.2.7) is used, the result will be a significant underestimation of the contribution to the total GIP from adsorbed methane. The correct method is to consider the absolute adsorption quantity as the total adsorbed amount, modeled by a physically robust method such as the dual-site Langmuir equation used herein. This is shown as a function of formation depth in Figure 2.2.10. The actual adsorbed methane amount still accounts for 46% of the total GIP content at a depth of 4000 m. If only the excess adsorption quantity is taken, the result is a very large underestimation of the contribution of adsorbed methane to the total GIP content: less than 12% at a depth of 3000 m.

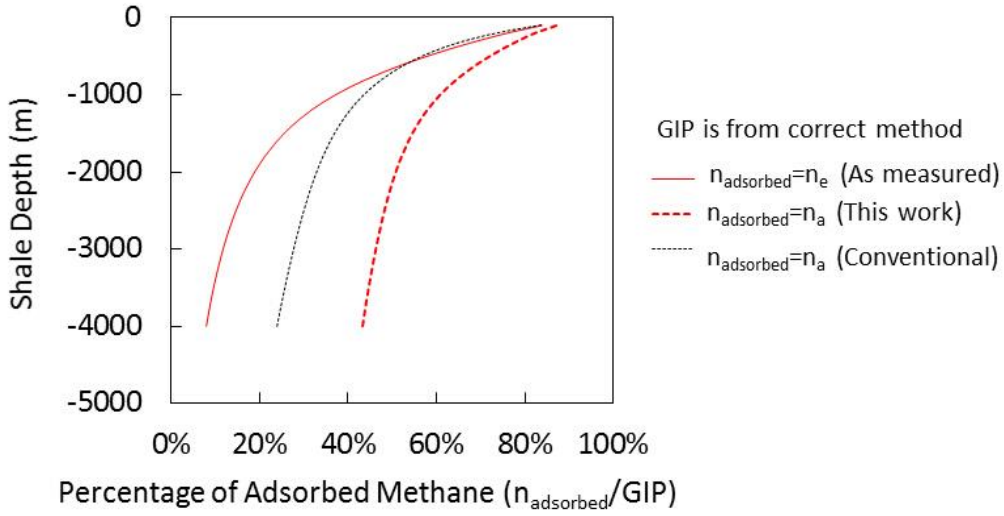

Figure 2.2.10 Comparison of the estimated contribution to total GIP content by adsorbed methane in Longmaxi shale by three methods: where the actual adsorbed amount is estimated as the excess uptake (solid red), absolute uptake (by a dual-Langmuir fit, dashed red), and by a conventional prediction of absolute uptake (dashed black). For demonstration purposes, the correct total GIP content is used in all cases (via Eq. 8).

2.2.5 Conclusions

In this work, laboratory measurements of high pressure methane adsorption (303 - 355 K and up to 27 MPa) are presented. Then, the dual-site Langmuir model is applied to describe and accurately predict high pressure methane adsorption behavior in Longmaxi shale (China). Finally, the shale

GIP resources in deep high pressure shale formation are accurately predicted. Several preliminary conclusions can be made,

(1) The crossover of the adsorption isotherms under high pressures and high temperatures are observed and reasonably interpreted.

(2) Dual-site Langmuir model can not only accurately describes observed adsorption isotherms but also can extrapolate adsorption isotherms beyond test data without using any empirical relationship.

(3) For depths greater than 1000 m (> 15 MPa) in the subsurface, the shale GIP resources have historically been significantly overestimated, and the ratio of the adsorbed phase compared to the free gas has been significantly underestimated.

(4) On the basis of the dual-site Langmuir model, the proposed method allows accurate estimations of the true shale GIP resource and the relative quantity of adsorbed methane at *in situ* temperatures and pressures representative of deep shale formations.

Acknowledgments

Financial assistance for this work was provided by the U.S. Department of Energy through the National Energy Technology Laboratory's Program under Contract No. DE-FE0006827, the State Key Development Program for Basic Research of China (Grant No. 2014CB239102) and Department of Science and Technology at China Petroleum & Chemical Corporation (Grant No.P12002, P14156).

References

41. Curtis, J. B. (2002). Fractured shale-gas systems. AAPG bulletin, 86(11), 1921-1938.
42. Montgomery, S. L., Jarvie, D. M., Bowker, K. A., & Pollastro, R. M. (2005). Mississippian Barnett Shale, Fort Worth basin, north-central Texas: Gas-shale play with multi–trillion cubic foot potential. AAPG bulletin, 89(2), 155-175.
43. King, G. E. (2010). Thirty years of gas shale fracturing: what have we learned? In SPE Annual Technical Conference and Exhibition. Society of Petroleum Engineers. http://dx.doi.org/10.2118/133456-MS.

44. Kuuskraa, V., Stevens, S. H., & Moodhe, K. D. (2013). Technically recoverable shale oil and shale gas resources: an assessment of 137 shale formations in 41 countries outside the United States. [J]. Natural Gas Industry, 5, 003.
45. NETL (National Energy Technology Laboratory). (2009). Modern shale gas development in the United States: A primer. US Department of Energy, Office of Fossil Energy. https://www.netl.doe.gov/File%20Library/Research/Oil-Gas/shale-gas-primer-update-2013.pdf.
46. EIA, 2016. http://www.eia.gov/dnav/ng/ng_prod_sum_dcu_NUS_a.htm
47. Wang, Q., Chen, X., Jha, A. N., & Rogers, H. (2014). Natural gas from shale formation–the evolution, evidences and challenges of shale gas revolution in United States. Renewable and Sustainable Energy Reviews, 30, 1-28.
48. Andrews, I. J. (2013). The Carboniferous Bowland Shale gas study: geology and resource estimation.
49. Ambrose, R. J., Hartman, R. C., Diaz-Campos, M., Akkutlu, I. Y., & Sondergeld, C. H. (2012). Shale gas-in-place calculations part I: new pore-scale considerations. SPE Journal, 17(01), 219-229.
50. McGlade, C., Speirs, J., & Sorrell, S. (2013). Methods of estimating shale gas resources–Comparison, evaluation and implications. Energy, 59, 116-125.
51. Busch, A., Alles, S., Gensterblum, Y., Prinz, D., Dewhurst, D. N., Raven, M. D., ... & Krooss, B. M. (2008). Carbon dioxide storage potential of shales. International Journal of Greenhouse Gas Control, 2(3), 297-308.
52. Kang, S. M., Fathi, E., Ambrose, R. J., Akkutlu, I. Y., & Sigal, R. F. (2011). Carbon dioxide storage capacity of organic-rich shales. Spe Journal, 16(04), 842-855.
53. Middleton, R. S., Carey, J. W., Currier, R. P., Hyman, J. D., Kang, Q., Karra, S., ... & Viswanathan, H. S. (2015). Shale gas and non-aqueous fracturing fluids: Opportunities and challenges for supercritical CO_2. Applied Energy, 147, 500-509.
54. Li, X., Feng, Z., Han, G., Elsworth, D., Marone, C., Saffer, D., & Cheon, D. S. (2016). Breakdown pressure and fracture surface morphology of hydraulic fracturing in shale with H_2O, CO_2 and N_2. Geomechanics and Geophysics for Geo-Energy and Geo-Resources, 2(2), 63-76.

55. Pini, R., Ottiger, S., Burlini, L., Storti, G., & Mazzotti, M. (2010). Sorption of carbon dioxide, methane and nitrogen in dry coals at high pressure and moderate temperature. International Journal of Greenhouse Gas Control, 4(1), 90-101.
56. Weniger, P., Kalkreuth, W., Busch, A., & Krooss, B. M. (2010). High-pressure methane and carbon dioxide sorption on coal and shale samples from the Paraná Basin, Brazil. International Journal of Coal Geology, 84(3), 190-205.
57. Strubinger, J. R., Song, H., & Parcher, J. F. (1991). High-pressure phase distribution isotherms for supercritical fluid chromatographic systems. 1. Pure carbon dioxide. Analytical chemistry, 63(2), 98-103.
58. Bae, J. S., & Bhatia, S. K. (2006). High-pressure adsorption of methane and carbon dioxide on coal. Energy & Fuels, 20(6), 2599-2607.
59. Sakurovs, R., Day, S., Weir, S., & Duffy, G. (2007). Application of a modified Dubinin-Radushkevich equation to adsorption of gases by coals under supercritical conditions. Energy & fuels, 21(2), 992-997.
60. Li, T., & Wu, C. (2015). Research on the abnormal isothermal adsorption of shale. Energy & Fuels, 29(2), 634-640.
61. Moellmer, J., Moeller, A., Dreisbach, F., Glaeser, R., & Staudt, R. (2011). High pressure adsorption of hydrogen, nitrogen, carbon dioxide and methane on the metal–organic framework HKUST-1. Microporous and Mesoporous Materials, 138(1), 140-148.
62. Dreisbach, F., Lösch, H. W., & Harting, P. (2002). Highest pressure adsorption equilibria data: measurement with magnetic suspension balance and analysis with a new adsorbent/adsorbate-volume. Adsorption, 8(2), 95-109.
63. Herbst, A., & Harting, P. (2002). Thermodynamic description of excess isotherms in high-pressure adsorption of methane, argon and nitrogen. Adsorption, 8(2), 111-123.
64. Chareonsuppanimit, P., Mohammad, S. A., Robinson, R. L., & Gasem, K. A. (2012). High-pressure adsorption of gases on shales: Measurements and modeling. International Journal of Coal Geology, 95, 34-46.
65. Fitzgerald, J. E., Sudibandriyo, M., Pan, Z., Robinson, R. L., & Gasem, K. A. M. (2003). Modeling the adsorption of pure gases on coals with the SLD model. Carbon, 41(12), 2203-2216.

66. Yang, K., Lu, X., Lin, Y., & Neimark, A. V. (2011). Effects of CO2 adsorption on coal deformation during geological sequestration. Journal of Geophysical Research: Solid Earth, 116(B8).
67. Zhou, L., Zhou, Y., Bai, S., Lü, C., & Yang, B. (2001). Determination of the adsorbed phase volume and its application in isotherm modeling for the adsorption of supercritical nitrogen on activated carbon. Journal of colloid and interface science, 239(1), 33-38.
68. Stadie, N. P., Murialdo, M., Ahn, C. C., & Fultz, B. (2013). Anomalous isosteric enthalpy of adsorption of methane on zeolite-templated carbon. Journal of the American Chemical Society, 135(3), 990-993.
69. Murialdo, M., Stadie, N. P., Ahn, C. C., & Fultz, B. (2015). Observation and Investigation of Increasing Isosteric Heat of Adsorption of Ethane on Zeolite-Templated Carbon. The Journal of Physical Chemistry C, 119(2), 944-950.
70. Stadie, N. P., Murialdo, M., Ahn, C. C., & Fultz, B. (2015). Unusual Entropy of Adsorbed Methane on Zeolite-Templated Carbon. The Journal of Physical Chemistry C, 119(47), 26409-26421.
71. Graham, D. (1953). The characterization of physical adsorption systems. I. The equilibrium function and standard free energy of adsorption. The Journal of Physical Chemistry, 57(7), 665-669.
72. Do, D. D., & Do, H. D. (1997). A new adsorption isotherm for heterogeneous adsorbent based on the isosteric heat as a function of loading. Chemical engineering science, 52(2), 297-310.
73. Zhou, W., Wu, H., Hartman, M. R., & Yildirim, T. (2007). Hydrogen and methane adsorption in metal-organic frameworks: a high-pressure volumetric study. The Journal of Physical Chemistry C, 111(44), 16131-16137.
74. Tian, H., Li, T., Zhang, T., & Xiao, X. (2016). Characterization of methane adsorption on overmature Lower Silurian–Upper Ordovician shales in Sichuan Basin, southwest China: Experimental results and geological implications. International Journal of Coal Geology.156, 36-49.
75. Bruns, B., Littke, R., Gasparik, M., Wees, J. D., & Nelskamp, S. (2016). Thermal evolution and shale gas potential estimation of the Wealden and Posidonia Shale in NW-Germany and the Netherlands: a 3D basin modelling study. Basin Research, 28(1), 2-33.

76. Sinopec presentation. (2015). Discovery and Characteristics of Fuling shale gas field (Official Release) http://www.cgs.gov.cn/UploadFiles/2015_05/21/20150521091817594.pdf
77. Caineng, Zou, Dazhong, Dong, Yuman, Wang, Xinjing, Li, HUANG, J., Shufang, Wang, ... & Wenhua, Bai. (2015). Shale gas in China: Characteristics, challenges and prospects (Ⅱ). Petroleum Exploration and Development, 42(6), 753-767.

2.3 Deep means different: concept of the deep shale gas reservoir and its influence on shale gas development

Xu Tang[*], Nino Ripepi[*,†], Cheng Chen[*], Lingjie Yu [‡, §]

([*]Department of Mining and Minerals Engineering & [†]Virginia Center for Coal and Energy Research, Virginia Polytechnic Institute and State University, Blacksburg, Virginia, 24060, U.S; [‡] Wuxi Research Institute of Petroleum Geology of Sinopec Exploration & Production Research Institute & [§]Sinopec Key Laboratory of Petroleum Accumulation Mechanisms, Wuxi, Jiangsu, 214151, China)

Abstract: Misunderstanding of methane adsorption behavior in shales under high-pressure conditions has resulted in inappropriate application of shale gas transport models and overestimation of shale gas resources in shale gas reservoirs. This work first reviews current fundamental issues in shale gas development. Then, the concept of the deep shale gas reservoir is proposed to provide a new perspective on shale gas development based on high pressure (up to 27MPa) methane adsorption studies in shales under different temperatures. This concept is on the basis that the dual-site Langmuir model can not only describe the methane adsorption behavior under high pressure conditions but also differentiate the true adsorbed methane content and gaseous methane content in deep shale gas reservoirs. The successful application of the dual-site Langmuir model in describing methane adsorption behavior in shale lays the foundation for understanding methane adsorption behavior in shale, assessing shale GIP resource in deep formations, and optimizing shale gas transport models for deep shale gas reservoirs. Finally, the implications of the deep shale gas reservoir concept on shale GIP resource estimation, thermodynamic analysis of high pressure methane in shale, and shale gas transport model are discussed.

Key words: shale gas, deep, transport, gas-in-place, Langmuir

2.3.1 Introduction

Shale gas has played a major role for the United States natural gas production over the past ten years and there remain significant reserves throughout the world in deep formations up to 2500 m (NETL, 2009; Kuuskraa et al, 2013; Wang et al, 2014; Curtis, 2002; Montgomery et al, 2005). Shale gas typically exists in three different phases within shale formations: (i) as free compressed gas, (ii) as adsorbed fluid on the surface, and (iii) as a dissolved component in kerogen, liquid hydrocarbon and brine. The adsorbed phase accounts for 20% to 80% of the total amount based on current studies from five major shale formations in the United States (Curtis et al, 2002). Thus, the estimation of the adsorbed amount of natural gas, the largest component of which is methane, significantly influences the final determination of the geological GIP resource and the working life of a shale gas producing well (Ambrose et al, 2012; Singh et al, 2016).

Since shale formations are typically deep, in-situ reservoir pressure and temperature can be as high as 27MPa and 76℃, respectively (Curtis et al, 2002). It is still unclear whether the deep in-situ condition (high pressure [>15 MPa] and high temperature [up to 76℃]) can change methane adsorption behavior in shale. Because of the limited data for methane adsorption in shale under high pressures, the shale gas industry still follows the methodology used in shallow coal seams and shale formations to estimate the shale GIP resource in the subsurface without seriously considering the in-situ high-pressure conditions (Curtis, 2002; Montgomery et al, 2005; Kuuskraa et al, 2013; Andrews, 2013). The standard practice for estimating shale GIP is to use methane adsorption measurements under intermediate-pressure conditions (10-15 MPa) modeled by the two-parameter Langmuir equation to predict the methane adsorption behavior in the higher-pressure region (>15 MPa) (Curtis et al, 2002; Montgomery et al, 2005; Kuuskraa et al, 2013; NETL, 2009; Andrews et al, 2013). Whether the commonplace methodology is reasonable or not needs more research. Even though it is known that the neglected volume of adsorbed layers under in-situ conditions results in overestimation of shale GIP (Ambrose et al, 2012), methane adsorption behavior under high-pressure conditions has not drawn researcher's attention from either academia or industry especially in modeling shale gas transport in the subsurface As evidenced by the fact that the two-parameter Langmuir model is still the foundation for developing shale gas transport model (Yu et al, 2014; Akkutlu et al, 2012; Civan et al, 2011; Singh et al, 2016; Wu et al, 2015; Naraghi et al, 2015; Pan et al, 2015; Yang et al, 2015; Wu et al, 2016). The observed adsorption isotherms are typically fitted using two-parameter Langmuir equation to differentiate the adsorbed

gas content and study the contribution of adsorbed gas content on shale gas production (Yu et al, 2014; Akkutlu et al, 2012; Civan et al, 2011; Wu et al, 2015; Singh et al, 2016; Naraghi et al, 2015; Pan et al, 2015; Yang et al, 2015; Wu et al, 2016). However, extending these gas transport models to high-pressure shale formations needs more evidence.

This work reviews studies in shale gas development with emphasis on the fundamentals of shale GIP estimation and gas transport in shale and then points out current issues in shale gas studies. Several misunderstood concepts are also clarified. This paper proposes a new concept, the deep shale gas reservoir, in response to historical studies that describe high pressure methane adsorption by the dual site Langmuir equation. Then, the implication of the deep shale gas reservoir concept in shale gas development are discussed in detail.

2.3.2 Current fundamentals for shale gas development

2.3.2.1 Shale GIP estimation in shale formations

Generally, the geological GIP resource is estimated as the total amount of methane present in the gaseous and adsorbed phases in a shale formation (assuming a negligible contribution from dissolved methane in kerogen, liquid hydrocarbons and brine). Equilibrium methane adsorption measurement in shale is needed in order to estimate the geological GIP content of deep shale formations. It is important to note that this method does not take into account any moisture which can reduce the methane adsorption capacity. In addition, this GIP content does not include any contribution from dissolved methane in kerogens, liquid hydrocarbons and brine, and also does not consider the presence of other gaseous components of natural gas (e.g., higher alkanes and hydrogen sulfide) (Ji et al, 2014 & 2015; Rexer et al, 2013).

Shale GIP resource is calculated via the sum of the free gas phase content, n_{free}, and the absolute adsorbed phase content, n_a (**illustrated in Figure 2.3.2**).

$$GIP = n_{free} + n_a = \rho_{gas} V_{free} + \rho_a V_a \quad (1)$$

where, ρ_{gas} and V_{free} are the free gas density and volume, respectively. ρ_a and V_a are the density and volume of adsorbed gas, respectively, which cannot be measured using current technologies.

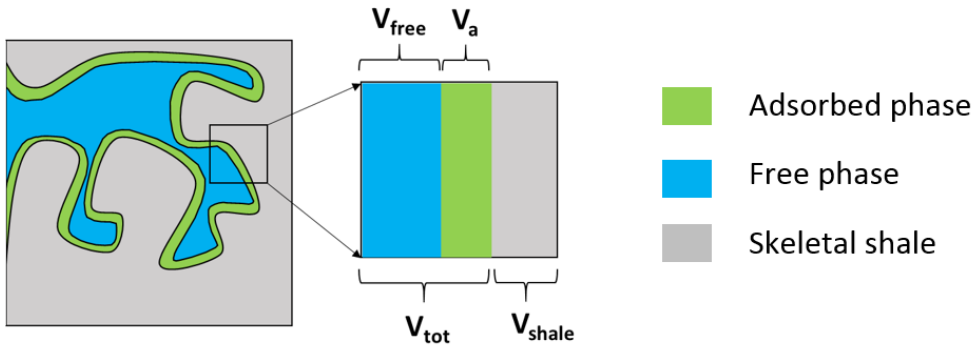

Figure 2.3.1 Conceptual model for shale gas phases in formations: both V_{shale} (skeletal volume of shale) and V_{tot} (total volume of pore space) can be measured using Helium intrusion tests; V_a (volume of adsorbed layers) and V_{free} (free gas volume existing in the shale formation) are unmeasurable using current technologies.

Eliminating V_{free} in equation (1) using volume conservation ($V_{free} = V_{tot} - V_a$), one obtains equation (8):

$$GIP = \rho_{gas} V_{tot} + n_a - \rho_{gas} V_a \quad (2)$$

Under low-pressure conditions (<15 MPa), V_a is very small and thus $\rho_{gas} V_a$ can be ignored. Equation (8) is then rewritten as:

$$GIP \approx \rho_{gas} V_{tot} + n_a \quad (3)$$

Equation (3) is the standard equation for estimating the shale GIP resource (NETL, 2009; Kuuskraa et al, 2013; Wang et al, 2014; Curtis, 2002; Montgomery et al, 2005). For term (n_a), the standard method uses the two-parameter Langmuir equation to fit the isotherm adsorption test data:

$$n_a = n_{\max} \frac{K(T)P}{1 + K(T)P} \quad (4)$$

where n_a is the absolute adsorption quantity under reservoir temperature and pressure, $n_{\max}$ is the maximum single-layer Langmuir adsorption capacity, and $K(T)$ is the temperature-dependent Langmuir equilibrium constant, written as $K(T) = A_0 \cdot \exp(-\frac{E_0}{RT})$, where E_0 is the energy of adsorption and A_0 is the pre-exponential coefficient, both of which are independent of temperature.

As is commonly understood, the two-parameter Langmuir equation is based on the assumption of monolayer adsorption. This means if the adsorption equilibrium pressure increases and multilayer adsorption occurs, the two-parameter Langmuir equation is no longer as accurate as in the low-pressure scenarios. It is critical to find a new model to describe the relationship between the true adsorption content and pressure.

It should be pointed out that under low-pressure conditions (< 10-15 MPa), the volume of the adsorbed layer is very small and the application of equation (3) is acceptable and has been widely used for estimating GIP for shallow coal seams and shale formations. Because of limited data for methane adsorption in shale under high-pressure conditions (>15 MPa), the commonplace approach uses methane adsorption measurements under intermediate-pressure conditions (10-15 MPa), on the basis of Equations (9) and (10), to predict the methane adsorption behavior in the higher-pressure region (>15 MPa).

In practice, we can directly calculate GIP using laboratory-measured data without assuming V_a to be negligible (Tian et al, 2016; Bruns et al, 2016):

$$GIP = \rho_{gas} V_{tot} + n_e \quad (5)$$

where n_e is the observed adsorption quantity under reservoir temperature and pressure, also called Gibbs excess adsorption quantity. Equation (5) indicates that if all the observed adsorption isotherm tests are available, we can accurately estimate the shale GIP resource in the subsurface. Equation (5) is superior since it does not use any assumptions similar to equation (3), and can be used under any pressure. Equation (5) also indicates that if we only want to obtain the shale GIP content in shale formations and do not want to differentiate the exact ratio between adsorbed gas and free gas, the observed adsorption isotherms measured under reservoir conditions is sufficient.

2.3.2.2 Shale gas transport model in shale formations

Existing studies have demonstrated that adsorbed gas accounts for 20-80% of the total shale GIP content (Curtis et al, 2012). Therefore, shale gas production has to consider the adsorbed gas content in both shale gas resource estimation stage and shale gas recovery stage. This also means shale gas transport models for predicting shale gas production should take the adsorbed methane content into consideration.

Shale gas production is a complex, coupled process from nanoscale to reservoir scale. In order to accurately investigate gas transport in shale, the ad/desorption processes of gas in shale must be considered (Yu et al, 2014; Akkutlu et al, 2012; Civan et al, 2011; Singh et al, 2016; Wu et al, 2015; Naraghi et al, 2015; Wu et al, 2016). Since shale is rich in nanopores (Chen et al., 2013), the large surface area strengthens the adsorbed surface diffusion process (Ross et al, 2009; Chalmers et al, 2012). In addition, the volume of the adsorbed layers in nanopores (<10 nm) cannot be neglected. When gas desorbs to free gas, it increases the space for gas transport in these pores (Ambrose et al, 2012; Singh et al, 2016). Several researchers have proposed different gas transport models in shales by considering the gas adsorption effect (Akkutlu et al, 2012; Civan et al, 2011; Yu et al, 2014; Singh et al, 2016; Wu et al, 2015; Naraghi et al, 2015; Wang et al, 2015). All these models have a common characteristic that they employ the two-parameter Langmuir equation (equation 4) to describe the adsorbed methane phase based on observed adsorption isotherms even though it has been found the two-parameter Langmuir equation failed to describe the observed methane adsorption isotherms in shales (Rexer et al, 2013; Tian et al, 2016; Bruns et al, 2016; Gasparik, et al, 2014). This indicates that conclusions from current available models may not be reliable under high pressure conditions since they always use the incorrect ratio between free gas and adsorbed gas in their models.

In order to differentiate the exact ratio between adsorbed gas and free gas under reservoir conditions especially when the Gibbs excess adsorption phenomena becomes obvious, some researchers attempt to use available adsorption models (three or more parameters adsorption model) to predict absolute adsorption isotherms (Rexer et al, 2013; Tian et al, 2016; Bruns et al, 2016; Gasparik, et al, 2014). The typical method is to use available adsorption models to fit observed adsorption isotherms independently and then obtain the empirical relationship between the fitting parameters and temperatures. Based on the obtained empirical relationship, the adsorption isotherm beyond the test data is extrapolated. The absolute adsorption isotherms is also obtained based on either the constant density of the adsorbed layer or the constant volume of the adsorbed layer (Rexer et al, 2013; Tian et al, 2016; Bruns et al, 2016; Gasparik, et al, 2014). However, this commonplace method lacks theoretical support and is problematic because the physical meaning of the fitting parameters has already changed when they fit the observed data independently. One of the obvious and critical defects is that the obtained adsorbed density of methane is higher than the liquid density, which should not occur (Do et al, 2003; Zhou et al, 2000 & 2001). Furthermore,

they have not realized the large difference between observed isotherms and absolute adsorption isotherms for methane in shale under high pressure because of their limited test pressure ranges.

It is helpful to point out a historical misunderstood concept in the shale gas industry for the past twenty years: the definition of free gas and adsorbed gas for shale gas in shale formations. In the shale gas industry, equation (9) is the most widely used, where we call the term ($\rho_{gas}V_{tot}$) as the "true free gas" and (n_a) as the "true adsorbed gas". This is incorrect because the true free gas should be term ($n_{free} = \rho_{gas}V_{free}$) and true adsorbed gas should be ($n_a = \rho_a V_a$). Since V_{tot} is always higher than V_{free}, this results in overestimation of the true free gas content as shown in Figure 2.3.1. That means if we use equation (3) to obtain the ratio between free gas and adsorbed gas, we will miscalculate the ratio between free gas and adsorbed gas, which has been commonly used in published reports of shale GIP resources over the past twenty years making them unreliable.

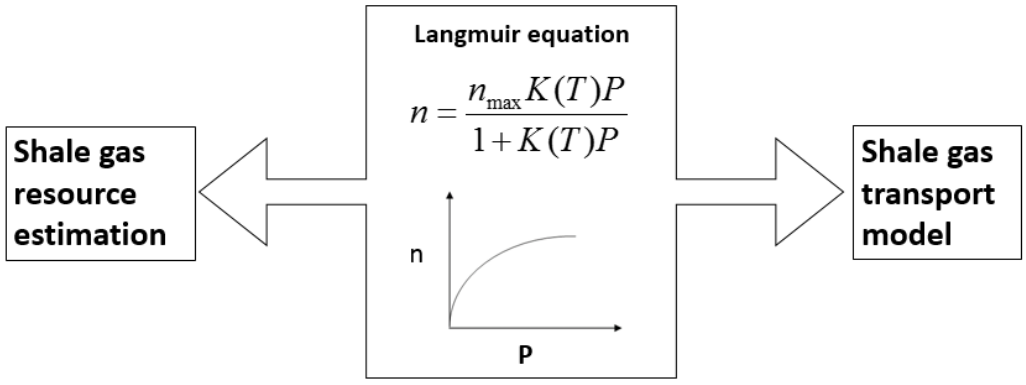

Figure 2.3.2 Conventional shale gas research methodology

From the above discussion, it can be concluded current shale gas development theories are based on the two parameter Langmuir equations as shown in Figure 2.3.2. The reason why two parameter Langmuir equation is widely used is only because of its mathematical simplicity. Under low pressure conditions where the volume of the adsorbed layer can be neglected, the usage of two parameter Langmuir equation produces valid results. However, under high pressure conditions where the Gibbs excess adsorption phenomenon becomes obvious, the usage of the two parameter Langmuir equation to describe observed adsorption isotherms results in many problems, especially in estimating shale gas resource and modelling shale gas transport behavior in shale formations.

2.3.3 Concept of deep shale gas reservoir and its implication

2.3.3.1 Dual-site Langmuir model for describing high pressure methane adsorption in shale

In a previous study, we measured methane adsorption isotherms in Longmaxi shale sample under 303.15, 318.15, 333.15 and 355.15K and up to 27 MPa as shown in Figure 2.3.3 (Tang et al, 2016). It was found that the dual-site Langmuir model can not only describe observed methane adsorption behavior using equation (6) and interpret all observed adsorption phenomenon but also can predict absolute methane adsorption isotherms using equation (7) and extrapolate adsorption isotherms beyond test temperatures (without using any empirical relationship). Detailed discussion of the dual site Langmuir equation refers to Tang et al, 2016. The successful application of the dual site Langmuir model lays the foundation to predict shale gas resource and model shale gas transport behavior in high pressure deep shale formations.

$$n_e = (n_{\max} - V_{\max} \cdot \rho_g) \cdot \left[(1-\alpha)\left(\frac{K_1(T)P}{1+K_1(T)P}\right) + \alpha\left(\frac{K_2(T)P}{1+K_2(T)P}\right) \right] \quad (6)$$

$$n_a = n_{\max} \cdot \left[(1-\alpha)\frac{K_1(T)P}{1+K_1(T)P} + \alpha\frac{K_2(T)P}{1+K_2(T)P}\right) \right] \quad (7)$$

where n_e is the observed adsorption uptake, also called Gibbs excess adsorption uptake, n_a is the absolute adsorption quantity under equilibrium temperature (T) and pressure (P), n_{max} is the maximum adsorption capacity, V_{max} is the volume of the adsorbed phase at maximum adsorption capacity, ρ_g is the bulk gas density, $K_1(T)$ and $K_2(T)$ ($K_1(T) = A_1 \cdot \exp(-\frac{E_1}{RT})$ and $K_2(T) = A_2 \cdot \exp(-\frac{E_2}{RT})$), are equilibrium constants weighted by a coefficient α ($0<\alpha<1$), E_1 and E_2 are the energy of adsorption, and A_1 and A_2 are the pre-exponential coefficient (where both E_0 and A_0 are independent of temperature), P is equilibrium pressure.

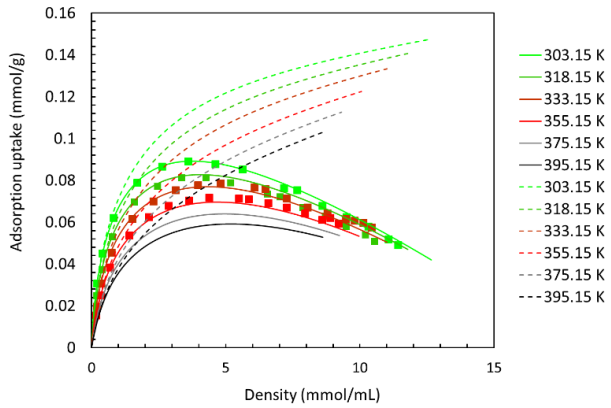

Figure 2.3.3 High pressure methane adsorption isotherms under different temperatures; solid squires are measured data, solid color lines are fitting curves using equation (6), dotted color lines are fitting curves using equation (7), black solid and dotted lines are extrapolated adsorption isotherms beyond test data

2.3.3.2 Concept of deep shale gas reservoir

Shale formations usually have a depth of 500- 3000 meters. A depth deeper than 1000 meters can lead to a high pressure reservoir. Generally speaking, the deeper the shale formation, the higher the reservoir pressure. High pressure is one of the major characteristics of deep shale formations. As discussed previously, the high pressure condition results in the pronounced difference between observed adsorption isotherms (Gibbs adsorption isotherms) and true adsorption isotherms for methane in shale. The two-parameter Langmuir model is no longer valid to describe either the observed adsorption isotherms or true adsorption isotherms. We can no longer use the current shallow shale gas and coalbed methane recovery theory to guide the development of deep, high-pressure shale gas recovery technologies. We have to develop a new theory that is suitable to high-pressure shale gas reservoirs on the basis of the dual site Langmuir equation.

In order to differentiate deep high-pressure shale gas reservoirs and shallow low-pressure shale and coalbed methane reservoirs, we introduce a new concept, the deep shale gas reservoir. Deep shale gas reservoirs specifically refer to deep shale gas formations, where the in-situ reservoir pressure and temperature cause methane adsorption to increase and reach the maximum value and then decrease before the adsorption equilibrium pressures reach the in-situ reservoir pressure (shown in Figure 2.3.4). The inflection pressure in Figure 2.3.4 refers to the corresponding pressure at the maximum observed adsorption content. If the inflection pressure is higher than the reservoir

pressure, the shale gas reservoir is a conventional shallow shale gas reservoir and all current theories are valid. If the inflection pressure is lower than the reservoir pressure, the shale gas reservoir becomes a deep shale gas reservoir. For deep shale gas reservoirs, the two-parameter Langmuir model becomes invalid. The dual-site Langmuir model is available to use for assessing the shale GIP resource and modeling shale gas transport behavior in shale formations.

Previous studies have shown that the occurrence of the pronounced Gibbs excess adsorption behavior also depends on many other physical properties, such as moisture content, kerogens maturity, mineral composition, pore characterization and surface area, et al. Therefore, in order to confirm whether the shale gas reservoir is a deep shale gas reservoir or shallow shale gas reservoir, the very first step is to conduct methane adsorption isotherm measuremens under reservoir conditions. The pronounced Gibbs excess adsorption behavior for methane adsorption isotherms at the reservoir pressure and temperatures (the critical pressure is lower than the reservoir pressure) is the only necessary condition.

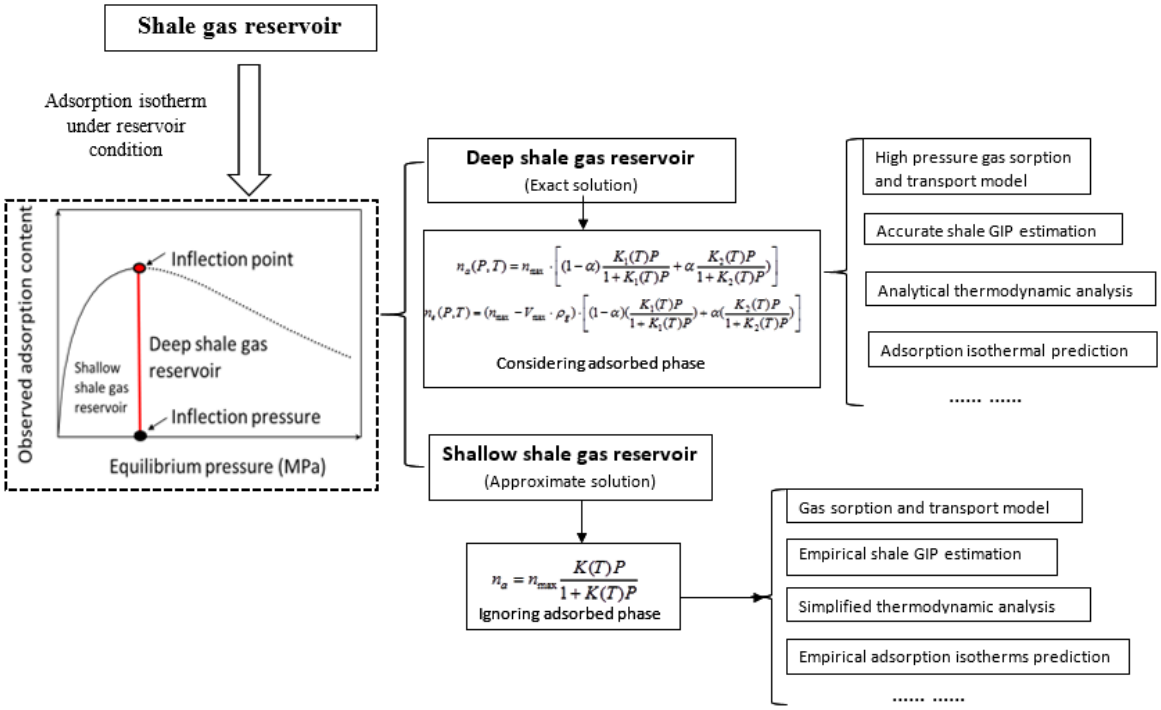

Figure 2.3.4 Fundamentals for shale gas development

2.3.4 Implications for shale gas development

2.3.4.1 Deep shale GIP estimation

As is commonly known, shale gas resources typically exist in deep formations and the reservoir pressure and temperature can be as high as 27MPa and 76 ℃, respectively (Curtis et al, 2002). The high-pressure, high-temperature in-situ condition does affect methane adsorption behavior in shale. If equation (5) is used to estimate the shale GIP resource, there is no need differentiate whether the shale gas reservoir is shallow shale gas reservoir or deep shale gas reservoir. However, there is a significant cost because one must conduct many high pressure methane adsorption tests under different temperatures because of the increasing geothermal effect in the deep subsurface. As revealed in the literature, few labs have the ability to conduct methane adsorption tests in shale up to 27MPa (Zhang et al, 2012; Ji et al, 2012; Tang et al, 2016; Gasparik, et al, 2014). Therefore, in order to assess the shale GIP resource in deep shale formations accurately and decrease the experimental cost, the first step is to determine the type of shale gas reservoir, the shallow shale gas reservoir or the deep shale gas reservoir. The methane adsorption isotherms under reservoir conditions need to be measured to do these assessments. If the shale gas reservoir belongs to shallow shale gas reservoir, the conventional two parameter Langmuir equation methodology approximates the real shale GIP resource. If the shale gas reservoir belongs to a deep shale gas reservoir, the dual-site Langmuir model should be used to describe the methane adsorption behavior and predict shale GIP resource. Another feature of the dual site Langmuir equation is that it can be used to extrapolate adsorption isotherms beyond test temperatures without using an empirical relationship.

It is worth to note that using equation (5) can only show the total shale GIP resource but not the ratio between the bulk gas and free gas. This means one does not know which part contributes more for the shale gas production, the free shale gas or the adsorbed shale gas. As pointed out earlier, it is a historical misunderstanding that we treat the ($\rho_{gas}V_{tot}$) term as the free gas in the subsurface, which results in the overestimation of the free shale gas resource in the subsurface.

2.3.4.2 Thermodynamic analysis for methane in shales

Thermodynamics analysis can reflect the interaction between gas adsorbate and adsorbent for an equilibrium gas sorption system. For example, the thermodynamic index such as the isosteric heat of adsorption reflects how the enthalpy changes when the unit amount of adsorbate is adsorbed on a certain amount of adsorbent molecular (Pan et al, 1998; Sircar et al, 1999; Shen et al, 2000). Previous studies of methane in shales have also reported the isosteric heat of adsorption during the

adsorption process (Zhang et al, 2012; Gasparik et al, 2014; Ji et al, 2012). However, there are several problems associated with these studies in the calculation of the isosteric heat of adsorption (Dejardin et al, 1982; Pan et al, 1998; Stadie et al, 2013 & 2015). First, how to obtain the absolute adsorption isotherms from observed adsorption isotherms (Pan et al, 1998; Stadie et al, 2015). Thermodynamic analysis must use the absolute adsorption uptake instead of the observed adsorption uptake. Generally, the liquid density of methane is used to obtain absolute methane isotherms from observed adsorption isotherms, which is still arguable (Pini, 2010; Bae et al, 2006; Sakurovs et al, 2007; Stadie et al, 2013 & 2015). Second, the classic Clausius–Clapeyron approximation is on the basis of ideal gas assumption and that the contribution of the adsorbed gas phase is ignored (Pan et al, 1998; Stadie et al, 2012; Krishna et al, 2015; Askalany et al, 2015). When the Gibbs excess adsorption phenomenon becomes pronounced, both assumptions are incorrect for gas adsorption isotherms. Previous studies in thermodynamics analysis do not address these questions and there conclusions needs to be treated with cautions (Zhang et al, 2012; Gasparik et al, 2014; Ji et al, 2012).

Fortunately, the dual site Langmuir equation provides an option to solve these problems. As shown in Tang et al 2016, the dual site Langmuir model can reasonably address all observed adsorption phenomenon during the adsorption tests such as interpretation of the crossover of the adsorption isotherms, predicting absolute adsorption isotherms, and extrapolating isotherms beyond test temperatures without using any empirical relationships. Furthermore, it can also be used to calculate the isosteric heat of adsorption for methane in synthetic material, which may be used for thermodynamic analysis of high pressure methane in shales (Stadie et al, 2013 & 2015).

2.3.4.3 Shale gas transport model for deep shale gas reservoir

For shallow shale gas formations, the two parameter Langmuir works well because the observed adsorption isotherms approximate the true adsorption isotherms. Current shale gas transport models can still describe methane transport behavior in shale and predict shale gas well production behavior (Akkutlu et al, 2012; Civan et al, 2011; Yu et al, 2014; Singh et al, 2016; Wu et al, 2015; Naraghi et al, 2015). However, all these models cannot be extended to the deep shale gas reservoirs since the two-parameter Langmuir model does not represent the true adsorbed gas content. In deep shale gas reservoirs, the observed adsorption isotherms no longer approximate the true adsorption isotherms. In fact the observed adsorption content is much lower than the true adsorption content

as illustrated in Figure 2.3.3. Therefore, the dual site Langmuir equation for describing the absolute adsorption isotherms (equation (7)) should be used in these shale gas transport models. By applying the absolute adsorption isotherms, the true ratio between free gas and adsorbed gas can be differentiated. Then, the true contribution of either free gas or adsorbed gas for the total shale gas production can be reasonably investigated.

2.3.5 Conclusions

Based on the Gibbs excess adsorption phenomenon for high pressure methane adsorption in shale, this work introduces a new concept, the deep shale gas reservoir. This concept offers a new theory frame work for shale gas development and calls for more in-depth studies in shale GIP estimation, thermodynamics analysis in high pressure gas adsorption, and shale gas transport models for deep shale gas reservoirs. On the basis that the dual-site Langmuir model can not only describe the methane adsorption behavior under high pressure conditions but also differentiate the true adsorbed methane content and gaseous methane content in deep shale gas reservoirs, the dual site Langmuir model lays the foundation for developing new techniques in deep shale gas development.

Acknowledgements

This research was supported in part by the U.S. Department of Energy through the National Energy Technology Laboratory's Program (No. DE-FE0006827).

References

Akkutlu, I. Y., & Fathi, E. (2012). Multiscale gas transport in shales with local kerogen heterogeneities. SPE Journal, 17(04), 1-002.

Askalany, A. A., & Saha, B. B. (2015). Derivation of isosteric heat of adsorption for non-ideal gases. International Journal of Heat and Mass Transfer, 89, 186-192.

Ambrose, R. J., Hartman, R. C., Diaz-Campos, M., Akkutlu, I. Y., & Sondergeld, C. H. (2012). Shale gas-in-place calculations part I: new pore-scale considerations. SPE Journal, 17(01), 219-229.

Andrews, I. J. (2013). The Carboniferous Bowland Shale gas study: geology and resource estimation.

Bruns, B., Littke, R., Gasparik, M., Wees, J. D., & Nelskamp, S. (2016). Thermal evolution and shale gas potential estimation of the Wealden and Posidonia Shale in NW-Germany and the Netherlands: a 3D basin modelling study. Basin Research, 28(1), 2-33.

Bae, J. S., & Bhatia, S. K. (2006). High-pressure adsorption of methane and carbon dioxide on coal. Energy & Fuels, 20(6), 2599-2607.

Civan, F., Rai, C. S., & Sondergeld, C. H. (2011). Shale-gas permeability and diffusivity inferred by improved formulation of relevant retention and transport mechanisms. Transport in Porous Media, 86(3), 925-944.

Chen, C., D. Hu, D. Westacott, and D. Loveless (2013), Nanometer-scale characterization of microscopic pores in shale kerogen by image analysis and pore-scale modeling, *Geochemistry, Geophysics, Geosystems*, 14(10), 4066-4075, DOI: 10.1002/ggge.20254.

Curtis, J. B. (2002). Fractured shale-gas systems. AAPG bulletin, 86(11), 1921-1938.

Chalmers, G. R., Bustin, R. M., & Power, I. M. (2012). Characterization of gas shale pore systems by porosimetry, pycnometry, surface area, and field emission scanning electron microscopy/transmission electron microscopy image analyses: Examples from the Barnett, Woodford, Haynesville, Marcellus, and Doig units. AAPG bulletin, 96(6), 1099-1119.

Dreisbach, F., Lösch, H. W., & Harting, P. (2002). Highest pressure adsorption equilibria data: measurement with magnetic suspension balance and analysis with a new adsorbent/adsorbate-volume. Adsorption, 8(2), 95-109.

Dejardin, P. (1982). Determination of adsorption isotherms of macromolecules by the depletion method. The Journal of Physical Chemistry, 86(14), 2800-2801.

Do, D. D., & Do, H. D. (2003). Adsorption of supercritical fluids in non-porous and porous carbons: analysis of adsorbed phase volume and density. Carbon, 41(9), 1777-1791.

Gasparik, M., Bertier, P., Gensterblum, Y., Ghanizadeh, A., Krooss, B. M., & Littke, R. (2014). Geological controls on the methane storage capacity in organic-rich shales. International Journal of Coal Geology, 123, 34-51.

Herbst, A., & Harting, P. (2002). Thermodynamic description of excess isotherms in high-pressure adsorption of methane, argon and nitrogen. Adsorption, 8(2), 111-123.

Javadpour, F., Fisher, D., & Unsworth, M. (2007). Nanoscale gas flow in shale gas sediments. Journal of Canadian Petroleum Technology, 46(10).

Ji, W., Song, Y., Jiang, Z., Wang, X., Bai, Y., Xing, J., 2014. Geological controls and estimation algorithms of lacustrine shale gas adsorption capacity: a case study of the Triassic strata in the southeastern Ordos Basin, China. Int. J. Coal Geol. 134, 61e73.

Ji, W., Song, Y., Jiang, Z., Chen, L., Li, Z., Yang, X., & Meng, M. (2015). Estimation of marine shale methane adsorption capacity based on experimental investigations of Lower Silurian Longmaxi formation in the Upper Yangtze Platform, south China. Marine and Petroleum Geology. doi:10.1016/j.marpetgeo.2015.08.012.

Ji, L., Zhang, T., Milliken, K. L., Qu, J., & Zhang, X. (2012). Experimental investigation of main controls to methane adsorption in clay-rich rocks. Applied Geochemistry, 27(12), 2533-2545.

Keller, J. U., & Staudt, R. (2005). Gas adsorption equilibria: experimental methods and adsorptive isotherms. Springer Science & Business Media.

Krishna, R. (2015). Evaluation of procedures for estimation of the isosteric heat of adsorption in microporous materials. Chemical Engineering Science,123, 191-196.

Zhang, T., Ellis, G. S., Ruppel, S. C., Milliken, K., & Yang, R. (2012). Effect of organic-matter type and thermal maturity on methane adsorption in shale-gas systems. Organic Geochemistry, 47, 120-131.

Kuuskraa, V., Stevens, S. H., & Moodhe, K. D. (2013). Technically recoverable shale oil and shale gas resources: an assessment of 137 shale formations in 41 countries outside the United States. [J]. Natural Gas Industry, 5, 003.

Montgomery, S. L., Jarvie, D. M., Bowker, K. A., & Pollastro, R. M. (2005). Mississippian Barnett Shale, Fort Worth basin, north-central Texas: Gas-shale play with multi–trillion cubic foot potential. AAPG bulletin, 89(2), 155-175.

Moellmer, J., Moeller, A., Dreisbach, F., Glaeser, R., & Staudt, R. (2011). High pressure adsorption of hydrogen, nitrogen, carbon dioxide and methane on the metal–organic framework HKUST-1. Microporous and Mesoporous Materials, 138(1), 140-148.

NETL (National Energy Technology Laboratory). (2009). Modern shale gas development in the United States: A primer. US Department of Energy, Office of Fossil Energy. https://www.netl.doe.gov/File%20Library/Research/Oil-Gas/shale-gas-primer-update-2013.pdf.

Naraghi, M. E., & Javadpour, F. (2015). A stochastic permeability model for the shale-gas systems. International Journal of Coal Geology, 140, 111-124.

Pan, H., Ritter, J. A., & Balbuena, P. B. (1998). Examination of the approximations used in determining the isosteric heat of adsorption from the Clausius-Clapeyron equation. Langmuir, 14(21), 6323-6327.

Pan, Z., & Connell, L. D. (2015). Reservoir simulation of free and adsorbed gas production from shale. Journal of Natural Gas Science and Engineering, 22, 359-370.

Pini, R., Ottiger, S., Burlini, L., Storti, G., & Mazzotti, M. (2010). Sorption of carbon dioxide, methane and nitrogen in dry coals at high pressure and moderate temperature. International Journal of Greenhouse Gas Control, 4(1), 90-101.

Rexer, T. F., Benham, M. J., Aplin, A. C., & Thomas, K. M. (2013). Methane adsorption on shale under simulated geological temperature and pressure conditions. Energy & Fuels, 27(6), 3099-3109.

Ross, D. J., & Bustin, R. M. (2009). The importance of shale composition and pore structure upon gas storage potential of shale gas reservoirs. Marine and Petroleum Geology, 26(6), 916-927.

Singh, H., & Javadpour, F. (2016). Langmuir slip-Langmuir sorption permeability model of shale. Fuel, 164, 28-37.

Setzmann, U., & Wagner, W. (1991). A new equation of state and tables of thermodynamic properties for methane covering the range from the melting line to 625 K at pressures up to 100 MPa. Journal of Physical and Chemical reference data, 20(6), 1061-1155.

Sircar, S., Mohr, R., Ristic, C., & Rao, M. B. (1999). Isosteric heat of adsorption: theory and experiment. The Journal of Physical Chemistry B, 103(31), 6539-6546.

Shen, D., Bülow, M., Siperstein, F., Engelhard, M., & Myers, A. L. (2000). Comparison of experimental techniques for measuring isosteric heat of adsorption. Adsorption, 6(4), 275-286.

Stadie, N. (2013). Synthesis and thermodynamic studies of physisorptive energy storage materials (Doctoral dissertation, California Institute of Technology).

Stadie, N. P., Murialdo, M., Ahn, C. C., & Fultz, B. (2013). Anomalous isosteric enthalpy of adsorption of methane on zeolite-templated carbon. Journal of the American Chemical Society, 135(3), 990-993.

Sakurovs, R., Day, S., Weir, S., & Duffy, G. (2007). Application of a modified Dubinin-Radushkevich equation to adsorption of gases by coals under supercritical conditions. Energy & fuels, 21(2), 992-997.

Tang, X. Ripepi, N., Stadie, N., Yu, L., & Hall, M. (2016) A dual-site Langmuir equation for accurate estimation of high pressure deep shale gas resources. Under review, Fuel.

Tian, H., Li, T., Zhang, T., & Xiao, X. (2016). Characterization of methane adsorption on overmature Lower Silurian–Upper Ordovician shales in Sichuan Basin, southwest China: Experimental results and geological implications. International Journal of Coal Geology.156, 36-49.

Wang, Q., Chen, X., Jha, A. N., & Rogers, H. (2014). Natural gas from shale formation–the evolution, evidences and challenges of shale gas revolution in United States. Renewable and Sustainable Energy Reviews, 30, 1-28.

Wu, K., Li, X., Wang, C., Yu, W., & Chen, Z. (2015). Model for surface diffusion of adsorbed gas in nanopores of shale gas reservoirs. Industrial & Engineering Chemistry Research, 54(12), 3225-3236.

Wu, T., & Zhang, D. (2016). Impact of Adsorption on Gas Transport in Nanopores. Scientific Reports, 6.

Yang, T., Li, X., & Zhang, D. (2015). Quantitative dynamic analysis of gas desorption contribution to production in shale gas reservoirs. Journal of Unconventional Oil and Gas Resources, 9, 18-30.

Yu, W., & Sepehrnoori, K. (2014). Simulation of gas desorption and geomechanics effects for unconventional gas reservoirs. Fuel, 116, 455-464.

Zhou, L., Zhou, Y., Bai, S., Lü, C., & Yang, B. (2001). Determination of the adsorbed phase volume and its application in isotherm modeling for the adsorption of supercritical nitrogen on activated carbon. Journal of colloid and interface science, 239(1), 33-38.

Zhou, L., Li, M., & Zhou, Y. (2000). Measurement and theoretical analysis of the adsorption of supercritical methane on superactivated carbon. Science in China Series B: Chemistry, 43(2), 143-153.

Chapter 3 Thermodynamic analysis for gas adsorption in shale and coal

3.1 Adsorption affinity of different types of coal: mean isosteric aeat of adsorption

Xu Tang[*a], Zhaofeng Wang[b,c], Nino Ripepi[a], Bo Kang[b,c], Gaowei Yue[b,c]

(a Department of Mining and Minerals Engineering, Virginia Polytechnic Institute and State University, Blacksburg, Virginia, 24060, U.S.b College of Safety Science and Engineering, Henan Polytechnic University, Jiaozuo, Henan, 454000,China;c the State Key Laboratory Cultivation Base for Gas Geology and Gas Control, Henan Polytechnic University, Jiaozuo, Henan, 454000,China)

Abstract: Understanding the sorption behavior of gas in organic-rich sedimentary rocks, and more specifically recognizing the adsorption properties of methane in coal, is a crucial step for evaluating the coalbed methane (CBM) gas-in-place content, gas quality and CBM recovery potential. However, the adsorption affinity of coal on methane has not been previously considered. This paper introduces the isosteric heat of adsorption in Henry's region, renamed the mean isosteric heat of adsorption, as means to evaluate the adsorption affinity of coal on methane. 18 group isothermal adsorption tests for methane in three different coals were conducted from 243.15K to 303.15K. The mean isosteric heat of adsorption for anthracite, lean coal, and gas-fat coal is -23.31KJ/mol, -20.47 KJ/mol, and -11.14 KJ/mol, respectively. The minus signs indicate the adsorption is an exothermal process. The mean isosteric heat of adsorption is independent of temperature from 243.15K to 303.15K, and shows the overall heterogenous property of different coal. Therefore, the mean isosteric adsorption of heat can serve as a quantified index to evaluate the coal adsorption affinity on methane.

Key words: Coal; Isothermal adsorption; Affinity; Methane; Outburst

Published in Energy Fuels, 29 (6), 2015, pp 3609–3615.

3.1.1 Introduction and background

Methane sorption properties in coal is crucial for coalbed methane (CBM) gas-in-place estimation [1, 2], coal seam degasification in underground coal mines [3, 4], and carbon dioxide sequestration with enhanced CBM recovery [1, 5-7]. Generally, the methane content in the coal seams consists mainly of adsorbed gas and free gas, with the adsorbed gas accounting for 80-90% of the coal seam content. Since the adsorbed gas plays a significant role in determining the coal seam's content, the adsorption properties of methane in coal is an important topic for researchers [1-13]. Even though there are lots of models used to describe the sorption properties of coal [12, 14-17], the affinity of methane on different types of coal has not received as much attention.

For a gas and solid sorption system, when the pressure is low, the gas adsorption is proportional to the equilibrium pressure; this is called Henry's law. This has been validated by classical statistical thermodynamics. Henry's law describes the affinity between the adsorbate molecule and the adsorbent. In Henry's region, each gas molecule can explore the whole adsorbent surface independently, as the interactions among gas molecules are negligible because of low densities [18]. Therefore, the isosteric heat of adsorption in Henry's region obtained via Henry's coefficient become a unique index for evaluating the affinity between an adsorbate molecule and the adsorbent. This relationship has already been considerably studied for gas and solid interaction [18-24] and chromatographic measurements of retention volumes [25-26]. Surprisingly, the isosteric heat of adsorption has not been previously considered for organic materials and gas sorption system such as coal and methane.

The theoretical calculation for Henry's coefficient is based on the assumption that 1) Henry's coefficient is a function of temperature and the interaction energy of one adsorbate molecule with the surrounding adsorbent, and 2) the interaction among adsorbate molecules can be neglected [23, 27]. Generally, the accuracy of Henry's coefficient determines the accuracy of the mean isosteric heat of adsorption. For manmade materials such as carbon nanotube, the Steele's equation can be used to calculate Henry's coefficient based on the energetically homogeneous adsorbent assumption [27, 28] (see Section 4.2). However, this theoretical calculation is not applicable for coal because it is difficult to identify the complex, quantitative-pore system of coal and the heterogeneous properties of coal. Also, the isosteric heat of adsorption in Henry's region cannot indicate the pore features (pore width, pore shape, etc.) of coal as it can with manmade carbon

nanotube [18, 24]. Because of this, the mean isosteric heat of adsorption is introduced to rename the isosteric heat of adsorption in Henry's region for coal in order to distinguish the isosteric heat of adsorption for manmade materials. The mean isosteric heat of adsorption should show the affinity of coal on methane, which results from the integrated effects of the pore size, shape, intersection and the surface area in coal, or the overall heterogeneous property of different coal. This index may serve as a fundamental parameter to evaluate the adsorption affinity of coal theoretically, which requires support from the test data.

In order to explore the coal affinity on methane, 18 isothermal adsorption tests from 243.15K to 303.15K were conducted on three different types of coal (anthracite, lean coal, and gas-fat coal) using in-house low temperature isothermal adsorption equipment. Since the low temperature isothermal adsorption tests for coal and methane (under 273.15K) have not been reported before, the tests are introduced in detail (see Section 2). Then, two approaches for calculating the mean isosteric heat of adsorption are introduced (see Section 3). Finally, the test results are analyzed and discussed (see Section 4).

3.1.2. Isothermal adsorption tests: from 243.15K to 303.15K

3.1.2.1 Sample preparation

The different types of coal used in this study were obtained from the Jiulishan coal mine, the Xinyuan coal mine, and the Panbei coal mine in China. The physical parameters of the coal were evaluated using Chinese national standards (Table 3.1.1). The coal specimen was then ground and sieved using 0.17mm-0.25mm metal sifters and placed in a drying oven at 104 to 110℃ for 1 hour to dehydrate. After dehydration the prepared sample was stored in a dehydrator for later use.

Table 3.1.1 Physical parameters of coal sample

Location	Physical parameters	A_{ad} (%)	V_{ad} (%)	TRD_{20}^{20} (g/cm^3)	ARD_{20}^{20} (g/cm^3)	Porosity (%)
Jiulishan	Anthracite	16.55	8.88	1.62	1.47	9.26
Xinyuan	Lean coal	1.58	11.36	1.39	1.27	8.63
Panbei	Gas-fat coal	1.01	11.01	1.40	1.28	8.52

3.1.2.2 Isothermal test procedure

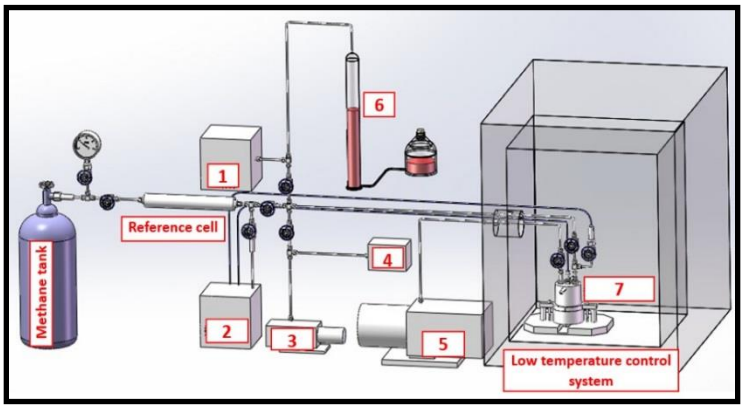

Figure 3.1.1 Schematic setup for low temperature isothermal sorption-diffusion comprehensive device; 1-Gas Chromatograph (GC), 2-Data recording module, 3-Vaccum pump, 4- Vaccum gage, 5- Water injection pump, 6-Measuring cylinder, 7-Sample cell; the low temperature control system can control the temperature between 225.15K and 373.15K with fluctuation of ±0.5 K.

The isothermal test was conducted using the in-house low temperature isothermal instrument based on the volumetric method (Fig. 1). The general test procedures for isothermal adsorption testing are shown below [28],

1) Calibrate the sample cell volume and double-check the tightness of the whole test system.
2) Vacuum the sample cell and then charge the sample cell gas via the reference cell. The adsorption gas content is calculated by the following equation,

$$m_{gas}^{adsorbed} = m_{gas}^{injected} - m_{gas}^{unadsorbed} = (\frac{P\Delta VM}{ZRT})_{pump} - (\frac{PV_{void}M}{ZRT})_{samplecell}$$

where m is the mass of gas, P is pressure, T is temperature, M is the molar mass of the gas species, Z is the compressibility coefficient of methane calculated using the Redlich-Kwong equation (when pressure is less than 9 MPa), R is the universe gas coefficient, $\triangle$V is the volume change of the pump, and V_{void} is the volume of the free gas in the sample cell.

3) Monitor the pressure change of the sample cell to determine the point of the sorption equilibrium state or suspend the time for the sorpiton process. Once the equilibrium point is reached, this phase ends and the sorption content and pressure can be obtained.

4) Repeat step 2) and step 3) until the next defined equilibrium pressure point is reached.
5) Once all the equilibrium points are obtained, the test is suspended and the isothermal adsorption curve can be established.

3.1.2.3 Sorption equilibrium state determination

Sorption equilibrium state determination is very important for the accuracy of test results. The pressure and sorption time monitoring approach are the two most popular approaches for determining the equilibrium state. The pressure monitor approach measures the change of the pressure cell; if the pressure change of the sample cell is within a certain value, the sorption system is treated as having reached a sorption equilibrium state. The sorption time monitor method is an empirical based method, and different research groups use different sorption times for isothermal adsorption testing [29-33]. However, there is no international standard can be referred for sorption equilibrium state determination.

This is the first tentative isothermal adsorption test for coal and methane from 263.15K to 243.15K for coal and methane. Thus, determining the equilibrium state is the key step in obtaining credible and accurate test results. The procedure to determine the equilibrium state is introduced in detail here. First, the sample cell with a sorption equilibrium coal-methane under 293.15 K is reached. Second, the sorption equilibrium sample cell is put into the 253.15 K low temperature control system, and the pressure variation with time inside the cell is recorded (shown in Fig. 3.1.2). Figure 3.1.2 shows the pressure of the sample cell decreasing over time, and a sharp decrease occurs within the first two hours. The pressures of the sample cells at times of 1.84h, 9.49h, and 23.30h are 6.1709, 6.1685, and 6.1660 MPa, and the pressure differences are only 0.08% and 0.04% compared with the pressure at 23.30h. Since there is only a tiny change of the pressure in the sample cell after it stays inside the low temperature system for 2 hours, the authors consider that the sample cell almost approaches the equilibrium status.

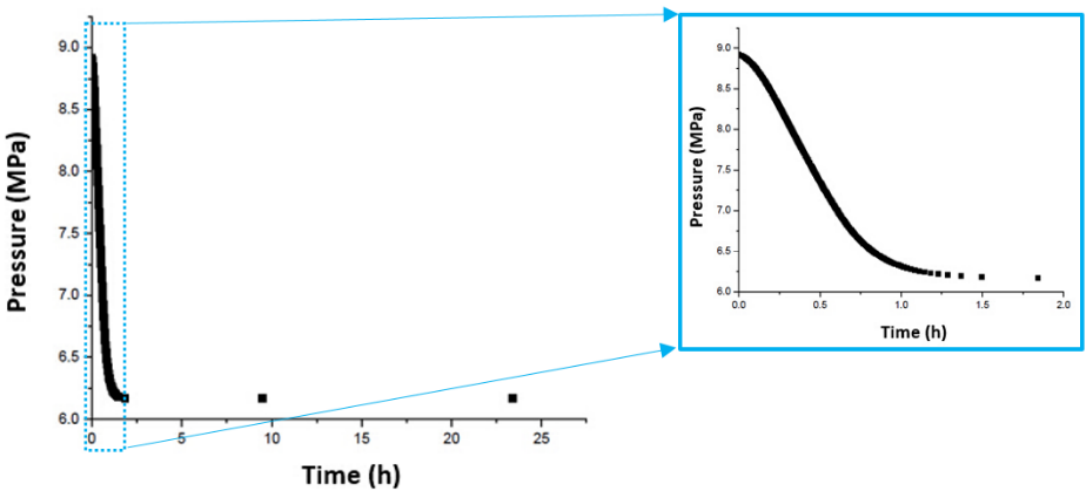

Figure 3.1.2. Sorption pressure decreases with time in low temperature control system

Based on the sorption equilibrium determination test data, the authors take two steps to ensure the equilibrium state of the coal and methane sorption system under low temperatures: 1) the equilibrium coal-methane sorption sample cell under 293.15 K is acquired for 12 hour sorption, and 2) the sample cell obtained in step (1) is then put into the low temperature control system under different temperatures (243.15 K, 253.15 K, 263.15K, 273.15K) for another 12 hours. Once both steps are completed, the authors assume the sample cell has reached an equilibrium state under defined low temperatures.

3.1.2.4 Test results

Figure 3.1.3 shows the isothermal adsorption of methane in anthracite, lean coal, and gas-fat coal under different temperatures ranging from 243.15K to 303.15K. It was found that the adsorbed methane content increases with decreasing temperature, and that coal at the temperatures lower than 273.15K adsorbed more methane than that of above 273.15K. The maximum adsorption content of anthracite, lean coal and gas-fat coal increases at 0.19cm^3/g, 0.15 cm^3/g, and 0.13 cm^3/g respectively, when temperature decreases at 1K.

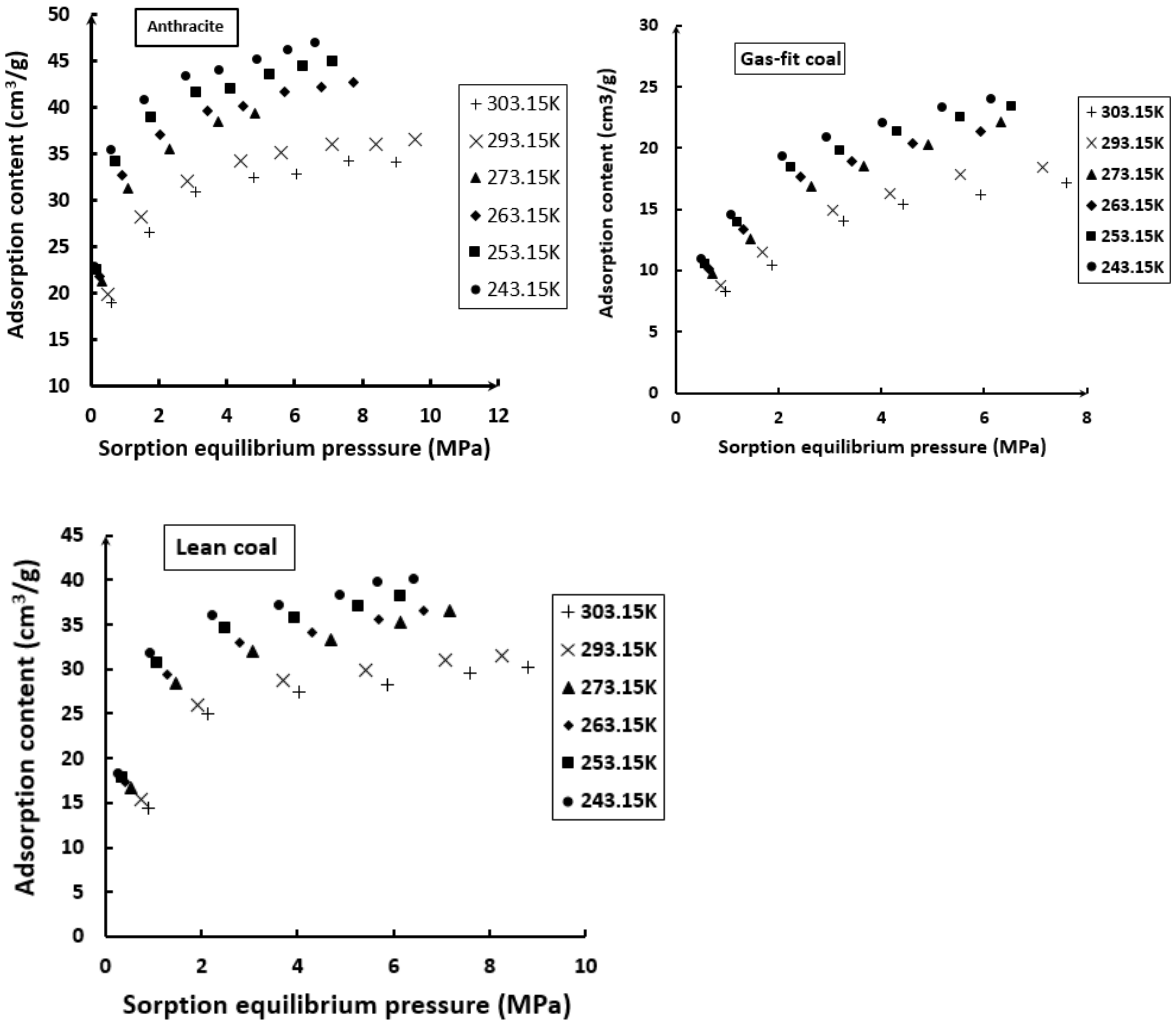

Figure 3.1.3. Isothermal adsorption of methane in different types of coal under different temperatures

3.1.3 The mean isosteric heat of adsorption

For a gas-solid sorption system under low pressure, the gas adsorption behavior follows Henry's law:

$$n = K' \cdot P \qquad (1)$$

where n is the adsorption content, K' is the Henry's coefficient, and the P is sorption pressure.

The relationship between K' and temperature follows Van't Hoff's equation:

$$\frac{d \ln K'}{dT} = \frac{\Delta H_0}{RT^2} \qquad (2)$$

If the mean isosteric heat of adsorption is constant and independent of temperature, the integration of equation (3) is:

$$\ln(K') = -\frac{\Delta H_0}{R} \cdot \frac{1}{T} + \ln(K_0') \quad (3)$$

From equation (3), if the linear relationship between lnK' and 1/T is obtained from equation (3), the mean isosteric heat of adsorption can be calculated using the slope of the linear line.

However, under certain circumstances, the mean isosteric heat of adsorption is influenced by temperature and equation (3) cannot be used. In 2011, T. Galanon & V. David proposed a binomial expression to describe the relationship between Henry's coefficient and temperature (equation (4)) [34], where equation (5) is used to calculate the temperature influenced mean isosteric heat of adsorption [34,35]:

$$\ln(K') = a + \frac{b}{T} + \frac{c}{T^2} \quad (4)$$

$$\Delta H_0 = -R \cdot (a + 2\frac{c}{T}) \quad (5)$$

where a, b and c are fitting parameters. The temperature dependent mean isosteric heat of adsorption can be obtained by the fitting parameters.

In order to determine the mean isosteric heat of adsorption from equation (3) and (4), the Henry coefficient (K') under different temperatures is first calculated. To calculate Henry's law constants, adsorption in the low-pressure region is modeled by a Virial-type equation [36-37]:

$$\ln(\frac{n}{p}) = A_0 + A_1 n + A_2 n^2 + \bullet\bullet\bullet\bullet\bullet\bullet\bullet \quad (6)$$

where n is the content of adsorbed gas at pressure p, and the first virial coefficient A_0 is related to the Henry's law constant, K', and K'=exp(A_0).

When n is small, the high-order term can be neglected, and equation (6) can be written in the following form:

$$\ln(\frac{p}{n}) = -A_0 - A_1 n \quad (7)$$

Equation (7) shows that, if the linear part of the relationship between ln(p/n) and n is obtained, the intercept of the linear relationship easily be found. The linear relationship had already been confirmed under low pressure for a gas-solid sorption system. Once the Henry's coefficient under different temperatures is acquired, the mean isosteric heat of adsorption can easily be calculated via equation (3) or (4 & 5).

3.1.4 Results analysis and discussion

3.1.4.1 Mean isosteric heat of adsorption determination

Based on the isothermal test results under different temperatures (303.15K, 293.15K, 263.15K, 273.15K 253.15K, 243.15K), the relationship between ln(P/n) and n can be described. Figure 3.1.4 shows that the linear curves fit the test data within the low pressure range, confirming Henry's law. The intercept of the curve at n=0 is also attained, and Henry's coefficients under different temperatures are shown in Table 3.1.2.

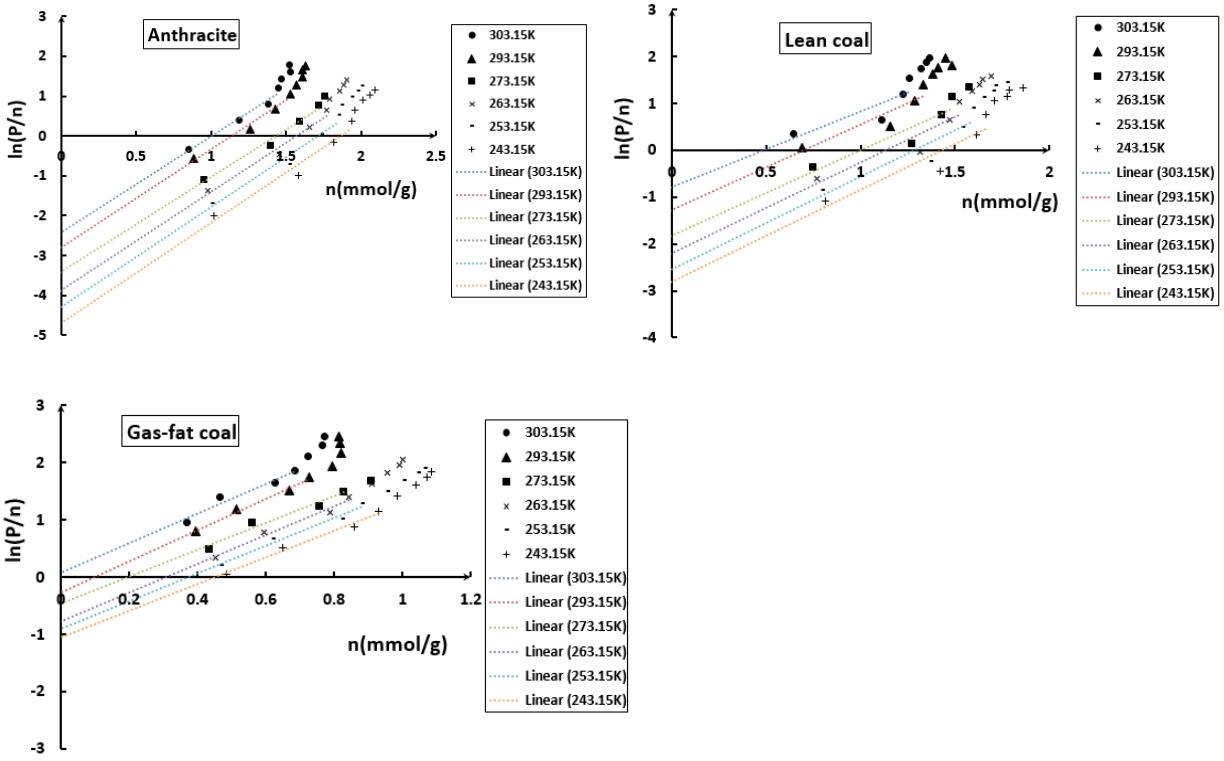

Figure 3.1.4 Relationship between ln(K') and the reciprocal of temperature for coal

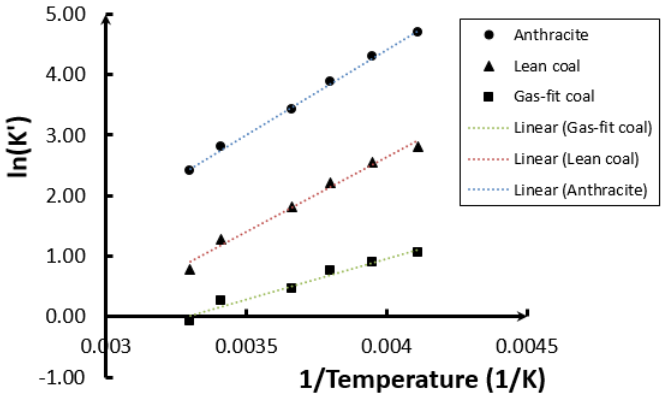

Figure 3.1.5 Relationship between ln(P/n) and n

Table 3.1.2 Henry's coefficient (K') determination

Type of coal	Temperature (K)	Intercept (when n=0)	Henry's coefficient(K') (mmol/ (g MPa))
Anthracite	303.15	-2.4060	11.0895
	293.15	-2.8044	16.5172
	273.15	-3.4168	30.4717
	263.15	-3.8768	48.2695
	253.15	-4.3001	73.7072
	243.15	-4.6916	109.0275
Lean coal	303.15	-0.7824	2.1867
	293.15	-1.2793	3.5941
	273.15	-1.8189	6.1651
	263.15	-2.2209	9.2156
	253.15	-2.5481	12.7828
	243.15	-2.8173	16.7316
Gas-fat coal	303.15	0.0770	0.9259
	293.15	-0.2648	1.3032
	273.15	-0.4675	1.5960
	263.15	-0.7717	2.1634
	253.15	-0.9013	2.4628
	243.15	-1.0545	2.8705

Table 3.1.3 Determination of the mean isosteric heat of adsorption in coal

Coal type	Fitting equation	R^2	ΔH_0 (kJ/mol)
Anthracite	ln(K')=2803.3/T-6.8056	0.9970	**-23.31**
Lean coal	ln(K')=2463.3/T-7.2135	0.9862	**-20.47**
Gas-fat coal	ln(K')=1340.3/T-4.4029	0.9677	**-11.14**

Once the Henry's coefficients are calculated under different temperatures, the relationship between lnK' and 1/T can be described. Figure 3.1.5 shows the linear relationship between ln (K') and the reciprocal of temperature for three different types of coal in the temperature range of 243.15K to 303.15K, which satisfies Equation (3). This also means the mean isosteric heat of adsorption can be treated as a constant and is independent of temperature between 243.15K and 303.15K. The mean isosteric heat of adsorption is shown in Table 3.1.3, and the minus sign means the adsorption is an exothermal process.

It should be pointed out that the volumetric approach for isothermal adsorption testing is preferred for measuring Henry's coefficients. This is because the amount of gas adsorbed is determined by the large difference in between the amount of gas dosed to the system and the amount of gas left in the system after adsorption, instead of by the small weight difference under low pressure [38]. When the pressure is low, the small difference between the weight before and after adsorption increases the experimental error via the gravimetric approach.

3.1.4.2 Discussion

When the temperature of isothermal tests ranges from 243.15K to 303.15K, the value of the mean isosteric heat of adsorption decreases in the following order: anthracite, lean coal and gas-fat coal. This agrees with the general theory that higher rank coal usually has higher adsorption capacity under same sorption conditions [8, 12, 39].

Theoretically, the Henry's coefficient can be obtained based on the energetically homogeneous assumption of adsorbent [40]:

$$H = \frac{S_{BET}}{RT}\int_0^{Z\,max}[\exp(-\frac{\phi(z)}{kT})-1]dz \quad (8)$$

where H is Henry's coefficient, S_{BET} is the BET surface area, Z is the distance perpendicular to the surface, Z_{max} depends on the structure of the solid, T is temperature, and φ(z) is the interaction

energy. Several approaches have been proposed for calculating the interaction energy [27, 28], and most of these approaches are suitable for analyzing the uniform pore of man-made material [18-24]. However, for natural material such as coal, it is hard to acquire the accurate interaction energy $\varphi(z)$ only through simplified assumptions. Surface chemistry plays an important role for the adsorption characteristics; the heterogeneous properties of coal with complex structure, pore size and shape distribution results in the characterized adsorption sites with different energies. The mean isosteric heat of adsorption found using the Henry's coefficient includes the overall effects of heterogeneous coal properties, making it a better option for evaluating the adsorption affinity of coal. The isothermal adsorption approach is more applicable for obtaining the Henry's constant because of the shortcomings of the theoretical approach.

As mentioned earlier, the experimental approach to obtain Henry's coefficient is based on two assumptions that 1) Henry's coefficient is a function of temperature and the interaction energy of one adsorbate molecule with the surrounding adsorbent, and 2) the interaction among adsorbate molecules can be neglected. When temperature ranges from 243.15K- 303.15K, Henry's law is applicable for three different types of coal (Figure 3.1.4). This supports that when the sorption content is low, Henry's coefficient is only dependent on the interaction between the adsorbent surface and the adsorbed gas molecules. According to the kinetic theory of gas, higher temperature means the average kinetic energy of methane molecular is higher, and therefore the interaction among methane molecular in higher temperature system cannot be neglected. For a low temperature system (243.15K- 303.15K), the interaction energy between methane molecular and coal surfaces dominates the process instead of the interaction of methane molecular within Henry's region. This process can be treated as a monolayer adsorption process. Under these conditions the mean isosteric heat of adsorpion remains constant, which is also supported by the constant mean isosteric heat of adsorption acquired from the test results.

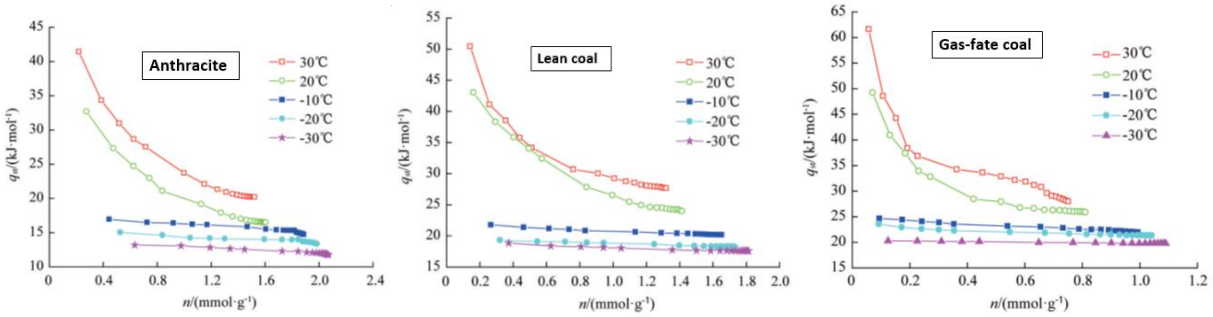

Figure 3.1.6 The isosteric heat of adsorpion acquired via the Clausius-Clapeyron equation (after [41] Yue, G. et al, 2014)

In the previous paper [41], the isosteric heat of the whole adsorption process is found using the Clausius-Clapeyron equation. Figure 3.1.6 shows that 1) the isosteric heat of adsorption is influenced by both temperature and adsorption content, and 2) when the adsorption content is the same, the isosteric heat of adsorption under 265.15K, 253.25K and 243.15K can be treated as a constant value.

The mean isosteric heat of adsorption value is within the isosteric heat of adsorption ranges under different temperatures. Comparing the isosteric heat of adsorption and the mean isosteric heat of adsorption, the mean isosteric heat of adsorption is more useful because it is independent of temperature. This is reasonable because the mean isosteric heat of adsorption reflects the overall heterogenous effect of coal, which should be an independent physical property of different types of coal. The constant mean isosteric heat of adsorption confirms this point. Therefore, the mean isosteric heat of adsorption can be used as an index to for evaluating the affinity of coal on methane.

3.1.5 Conclusions

18 group isothermal adsorption tests for methane and three different coals were conducted from 243.15K to 303.15K. The test results supports the following conclusions:

1) The maximum adsorption content of anthracite, lean coal and gas-fat coal increase at 0.19cm^3/g, 0.15 cm^3/g, and 0.13 cm^3/g when temperature decreases at 1K.

2) The mean isosteric heat of adsorption for anthracite, lean coal, and gas-fate coal is -23.31KJ/mol, -20.47 KJ/mol, -11.14 KJ/mol, respectively, and the minus sign indicates the adsorption is an exothermal process.

3) The mean isosteric heat of adsorption is independent of temperature from 243.15K to 303.15K.

4) The mean isosteric heat of adsorption can serve as an index for evaluating the coal adsorption affinity on methane.

Acknowledgements

The authors want to express their appreciation for the funding provided by both the National Natural Science Foundation of China (No. 51274090) and the State Key Laboratory Cultivation Base for Gas Geology and Gas Control (Henan Polytechnic University) (No. WS2012B01).

References

[1] Seidle, J. (2011). Fundamentals of coalbed methane reservoir engineering. PennWell Books (pp 125-152; pp 347-384).

[2] Bustin, R. M., & Clarkson, C. R. (1998). Geological controls on coalbed methane reservoir capacity and gas content. International Journal of Coal Geology, 38(1), 3-26.

[3] Kissell, F. N. (2006). Handbook for Methane Control in Mining (pp 77-80).

[4] Wang, Z. (2001). Study on the Gas Desorption Laws of Coal in the Media of Air, Water and Drilling Mud and Their Applications [D] (Doctoral dissertation, XuZhou, China: China University of Mining and Technology).

[5] White, C. M., Smith, D. H., Jones, K. L., Goodman, A. L., Jikich, S. A., LaCount, R. B., ... & Schroeder, K. T. (2005). Sequestration of carbon dioxide in coal with enhanced coalbed methane recovery a review. Energy & Fuels, 19(3), 659-724.

[6] Ripepi, N. S. (2009). Carbon dioxide storage in coal seams with enhanced coalbed methane recovery: geologic evaluation, capacity assessment and field validation of the central appalachian basin (Doctoral dissertation, Virginia Polytechnic Institute & State University).

[7] Litynski, J. T., Klara, S. M., McIlvried, H. G., & Srivastava, R. D. (2006). The United States Department of Energy's regional carbon sequestration partnerships program: A collaborative approach to carbon management. Environment international, 32(1), 128-144.

[8] Crosdale, P. J., Beamish, B. B., & Valix, M. (1998). Coalbed methane sorption related to coal composition. International Journal of Coal Geology, 35(1), 147-158.

[9] Mastalerz, M., Gluskoter, H., & Rupp, J. (2004). Carbon dioxide and methane sorption in high volatile bituminous coals from Indiana, USA. International Journal of Coal Geology, 60(1), 43-55.

[10] Laxminarayana, C., & Crosdale, P. J. (2002). Controls on methane sorption capacity of Indian coals. AAPG bulletin, 86(2), 201-212.

[11] Olajossy, A., Gawdzik, A., Budner, Z., & Dula, J. (2003). Methane separation from coal mine methane gas by vacuum pressure swing adsorption. Chemical Engineering Research and Design, 81(4), 474-482.

[12] Busch, A., & Gensterblum, Y. (2011). CBM and CO2-ECBM related sorption processes in coal: a review. International Journal of Coal Geology, 87(2), 49-71.

[13] Weniger, P., Kalkreuth, W., Busch, A., & Krooss, B. M. (2010). High-pressure methane and carbon dioxide sorption on coal and shale samples from the Paraná Basin, Brazil. International Journal of Coal Geology, 84(3), 190-205.

[14] Langmuir, I. (1918). The adsorption of gases on plane surfaces of glass, mica and platinum. Journal of the American Chemical society, 40(9), 1361-1403.

[15] Brunauer, S., Emmett, P. H., & Teller, E. (1938). Adsorption of gases in multimolecular layers. Journal of the American Chemical Society, 60(2), 309-319.

[16] Hutson, N. D., & Yang, R. T. (1997). Theoretical basis for the Dubinin-Radushkevitch (DR) adsorption isotherm equation. Adsorption, 3(3), 189-195.

[17] Sing, K. S. (1998). Adsorption methods for the characterization of porous materials. Advances in colloid and interface science, 76, 3-11.

[18] Schindler, B. J., & LeVan, M. D. (2008). The theoretical maximum isosteric heat of adsorption in the Henry's law region for slit-shaped carbon nanopores. Carbon, 46(4), 644-648.

[19] Vernov, A., & Steele, W. A. (1991). Computer simulations of benzene adsorbed on graphite. 2. 298 k. Langmuir, 7(11), 2817-2820.

[20] Floess, J. K., & Vanlishout, Y. (1992). Calculation of adsorption energies in carbon micropores. Carbon, 30(7), 967-973.

[21] Pikunic, J., Clinard, C., Cohaut, N., Gubbins, K. E., Guet, J. M., Pellenq, R. J. M., ... & Rouzaud, J. N. (2003). Structural modeling of porous carbons: constrained reverse Monte Carlo method. Langmuir, 19(20), 8565-8582.

[22] Jiang, J., Wagner, N. J., & Sandler, S. I. (2004). A Monte Carlo simulation study of the effect of carbon topology on nitrogen adsorption on graphite, a nanotube bundle, C 60 fullerite, C 168 schwarzite, and a nanoporous carbon. Physical Chemistry Chemical Physics, 6(18), 4440-4444.

[23] Do, D. D., Do, H. D., Wongkoblap, A., & Nicholson, D. (2008). Henry coefficient and isosteric heat at zero-loading for gas adsorption in carbon nanotubes. Physical Chemistry Chemical Physics, 10(48), 7293-7303.

[24] Liu, J., & LeVan, M. D. (2010). Henry's law coefficients and isosteric heats of adsorption at zero loading for multi-wall carbon surfaces with different geometries. Carbon, 48(12), 3454-3462.

[25] Kalashnikova, E. V., Kiselev, A. V., Petrova, R. S., Shcherbakova, K. D., & Poshkus, D. P. (1979). Chromatographic measurements and molecular statistical calculations of thermodynamic characteristics of adsorption of aromatic and polycyclic hydrocarbons on graphitized thermal carbon black.Chromatographia, 12(12), 799-802.

[26] Vailaya, A. (2005). Fundamentals of reversed phase chromatography: thermodynamic and exothermodynamic treatment. Journal of liquid chromatography & related technologies, 28(7-8), 965-1054.

[27]Maurer, S., Mersmann, A., & Peukert, W. (2001). Henry coefficients of adsorption predicted from solid Hamaker coefficients. Chemical engineering science, 56(11), 3443-3453.

[28] Steele, W. A. (1973). The physical interaction of gases with crystalline solids: I. Gas-solid energies and properties of isolated adsorbed atoms. Surface Science, 36(1), 317-352.

[29] Goodman, A. L., Busch, A., Duffy, G. J., Fitzgerald, J. E., Gasem, K. A. M., Gensterblum, Y., ... & White, C. M. (2004). An inter-laboratory comparison of CO2 isotherms measured on Argonne premium coal samples. Energy & fuels, 18(4), 1175-1182.

[30] Goodman, A. L., Busch, A., Bustin, R. M., Chikatamarla, L., Day, S., Duffy, G. J., ... & White, C. M. (2007). Inter-laboratory comparison II: CO< sub> 2</sub> isotherms measured on moisture-equilibrated Argonne premium coals at 55° C and up to 15 MPa. International Journal of Coal Geology, 72(3), 153-164.

[31] Gruszkiewicz, M. S., Naney, M. T., Blencoe, J. G., Cole, D. R., Pashin, J. C., & Carroll, R. E. (2009). Adsorption kinetics of CO< sub> 2</sub>, CH< sub> 4</sub>, and their equimolar mixture on coal from the Black Warrior Basin, West-Central Alabama. International Journal of Coal Geology, 77(1), 23-33.

[32] Gensterblum, Y., Van Hemert, P., Billemont, P., Busch, A., Charriere, D., Li, D., ... & Wolf, K. H. (2009). European inter-laboratory comparison of high pressure CO< sub> 2</sub> sorption isotherms. I: Activated carbon. Carbon, 47(13), 2958-2969.

[33] Gensterblum, Y., P. Van Hemert, P. Billemont, E. Battistutta, A. Busch, B. M. Krooss, G. De Weireld, and K-HAA Wolf. "European inter-laboratory comparison of high pressure CO< sub> 2</sub> sorption isotherms II: Natural coals." International Journal of Coal Geology 84, no. 2 (2010): 115-124.

[34] Galaon, T., & David, V. (2011). Deviation from van't Hoff dependence in RP-LC induced by tautomeric interconversion observed for four compounds. Journal of separation science, 34(12), 1423-1428.

[35] Vailaya, A. (2005). Fundamentals of reversed phase chromatography: thermodynamic and exothermodynamic treatment. Journal of liquid chromatography & related technologies, 28(7-8), 965-1054.

[36] Zhao, X. B., Xiao, B., Fletcher, A. J., & Thomas, K. M. (2005). Hydrogen adsorption on functionalized nanoporous activated carbons. The Journal of Physical Chemistry B, 109(18), 8880-8888.

[37] Cole, J. H., Everett, D. H., Marshall, C. T., Paniego, A. R., Powl, J. C., & Rodriguez-Reinoso, F. (1974). Thermodynamics of the high temperature adsorption of some permanent gases by porous carbons. Journal of the Chemical Society, Faraday Transactions 1: Physical Chemistry in Condensed Phases, 70, 2154-2169.

[38] Myers, A. L. (2004). Thermodynamics of adsorption. *Chemical thermodynamics for industry*, 243-252.

[39] Laxminarayana, C., & Crosdale, P. J. (1999). Role of coal type and rank on methane sorption characteristics of Bowen Basin, Australia coals. International Journal of Coal Geology, 40(4), 309-325.

[40] Pierotti, R. A., & Thomas, H. E. (1971). Physical adsorption: The interaction of gases with solids. *Surface and Colloid Science*, *4*, 93-259.

[41] YUE Gaowei,WANG Zhaofeng,XIE Ce. (2014) Experimental Study of Coal Surface Adsorption Uniformity in Low Temperature Environment. Science & Technology Review, 32(31): 71-74.

3.2 Thermodynamic analysis of high pressure methane adsorption in Longmaxi shale

Xu Tang*, Nino Ripepi[*,†], Nicholas P. Stadie[‡], Lingjie, Yu[§,¶]

(*Department of Mining and Minerals Engineering & †Virginia Center for Coal and Energy Research, Virginia Polytechnic Institute and State University, Blacksburg, Virginia, 24060, U.S; ‡ETH Zürich, Laboratory of Inorganic Chemistry, Vladimir-Prelog-Weg 1, 8093 Zürich, Switzerland; § Wuxi Research Institute of Petroleum Geology of Sinopec Exploration & Production Research Institute & ¶ Sinopec Key Laboratory of Petroleum Accumulation Mechanisms, Wuxi, Jiangsu, 214151, China)

Abstract: Thermodynamic analyses of high pressure methane adsorption in shale are rarely reported because of the lack of a reliable approach for obtaining the true adsorption uptake from observed adsorption isotherms and the routinely used, oversimplified Clausius–Clapeyron (C-C) approximation. This work extends our previously proposed dual-site Langmuir adsorption model to calculate the isosteric heat of adsorption analytically from the observed adsorption isotherms for high pressure methane adsorption isotherms on Longmaxi shale from Sichuan, China (up to 27 MPa and 355.15 K). The calculated isosteric heat of adsorption considers both the real gas behavior of bulk methane and the adsorbed phase volume, which are neglected in the C–C approximation. By this method, the temperature dependence as well as the uptake dependence of the isosteric heat can be readily investigated, where the former cannot be revealed using the C–C approximation. The influence of the adsorbed phase and the gas behavior (real gas or ideal gas) on the isosteric heat of adsorption are also investigated, which shows that neglecting either the real gas behavior or the adsorbed phase volume always results in an overestimation of the isosteric heat of adsorption. In the Henry's law regime of low pressure and low adsorption uptake (and up to a surface occupancy of < 0.5), the isosteric heat of adsorption of methane on Longmaxi shale is approximately constant at 15-17 kJ/mol, but then decreases significantly at higher pressures. This work therefore justifies the method to obtain the true isosteric heat of adsorption for high pressure methane in shale, which lays the foundation for future investigations of the thermodynamics and heat transfer characteristics of the interaction between high pressure methane and shale.

Key words: methane, natural gas, shale gas, adsorption, Langmuir isotherm, isosteric heat of adsorption

3.2.1 Introduction

Shale gas has long been recognized as a promising alternative source of natural gas, and increasing demands for energy have led to a widespread international effort to estimate the extent of its resources and develop its production [1, 2]. The gas found in shale formations is fundamentally different from conventional natural gas in that the formation itself is both the source and the reservoir. Within the porous formation, the total shale gas content consists of bulk gas (in larger pore spaces), dissolved gas (in the liquid brine), and adsorbed gas on the solid surface. This adsorbed component varies widely from resource to resource, accounting for 20% to 80% of the total shale gas content in five formations investigated in the United States [3, 4]. Nevertheless, it is clear that the adsorbed quantity is a significant component that must be taken into account in accurate estimations of the total gas-in-place resource and the working life of a producing well. Methane adsorption in carbonaceous shale has been extensively studied over an intermediate range of temperature and pressure but high pressure (>15 MPa) studies have remained less common [5-10]. Furthermore, the thermodynamic characteristics of methane adsorbed on shale have rarely been considered, especially at high pressure. Shale formations at depths of 1500 m to 2500 m below the surface exist under conditions between 330-360 K and up to 38 MPa (given a pressure coefficient of 15 MPa/km and geothermal gradient of 27.3 ℃/km as found in Longmaxi formations) [11], where common approximations as to the ideal nature of the bulk gas are no longer applicable and where the accurate prediction of the true adsorbed amount is not trivial. Understanding the thermodynamic properties of the adsorbed phase is important for evaluating the value of a deep shale resource, as in other adsorption systems such as gas separation and purification applications, adsorption chillers, and adsorptive energy storage [12-17].

Physical adsorption (or physisorption) at the gas-solid interface is the process of gas adsorbate accumulation on the surface of the solid adsorbent as a consequence of the weak van der Waals forces that exist between any two species [18]. The change in heat associated with physical adsorption is negative and significantly lower in magnitude than for chemical adsorption. Methane and shale can only interact via London dispersion forces (neither has a permanent dipole), the weakest type of van der Waals interactions, and the change in enthalpy is typically only 10-22 kJ/mol [5]. In this system, the quantity of adsorbed methane changes as a function of temperature and pressure so that the adsorbed phase and the bulk fluid phase are at the same chemical potential. The specific quantity is not only influenced by material properties of the shale (e.g., organic

components, minerals, and surface structure) but also by the composition of the gas adsorbate (e.g., content of moisture) [5-10]. The isosteric heat of adsorption can also vary as a function of the amount of adsorbate and the system conditions [19-21]. It therefore serves as an important descriptor of the physisorption system, and is directly related to the strength of the interaction between gas adsorbate and solid adsorbent [22, 23]. The isosteric heat of adsorption typically decreases as adsorption uptake increases because of binding site (and therefore binding energy) heterogeneity [20, 24, 25].

Thermodynamic analysis of the properties of the adsorbed phase is possible by measuring the properties of the bulk gas that is in equilibrium with it, and the adsorbed content is measured as a function of bulk gas pressure at various constant temperatures. There are several issues associated with the calculation of the isosteric heat of adsorption directly from observed adsorption isotherms (where the observed adsorption quantity is also called the Gibbs excess adsorption uptake) [19, 26-28]. First, the Gibbs excess adsorption quantity is an underestimation of the absolute amount adsorbed [19, 28]. At low pressure, the experimental adsorption isotherm well approximates the absolute isotherm; however, at high pressure, the observed adsorbed content first reaches a maximum and then decreases with increasing pressure which is not consistent with the physical nature of adsorption [28]. Thus, it is necessary to calculate the isosteric heat of adsorption along absolute isosteres and an effective method for their determination is needed. Second, a direct, uniform approach for obtaining the absolute quantity of adsorption from measured adsorption isotherms has not been developed, and the correct modeling of the physical parameters of the adsorbed phase such as its density are complex issues that remain actively discussed [27-33]. Lastly, a consideration of the deviation of real gas behavior from the ideal gas law is necessary when calculating the isosteric heat of adsorption, especially under high pressure and low temperature conditions. Methane deviates significantly (>10%) from the ideal gas law at pressures above 6 MPa at room temperature, which has a dramatic effect on the calculation of thermodynamic parameters in this regime [27]. For methane adsorption in shale, the C-C approximation is routinely used to calculate the isosteric heat of adsorption. However, since the C-C approximation ignores the adsorbed phase effect and uses the ideal gas law, the calculated results may not reveal the true thermodynamics behavior for methane in shales. In order to reasonably analyze the thermodynamic characteristics of a gas-solid system such as methane in shale, the above issues must be addressed [19, 27, 34, 35].

In previous work, we applied a dual-site Langmuir model to obtain absolute adsorption isotherms from observed Gibbs excess adsorption equilibria utilizing the assumption that the density of the adsorbed phase is an unknown constant [36]. The proposed model gives a reasonable explanation for all observed phenomena in high pressure methane adsorption in shales, which have not been reasonably addressed using the conventional Langmuir model, the potential theory based model, or their revised forms [36]. Considering the justification of its use, the dual-site Langmuir model is therefore extended in this work to calculate the isosteric heat of adsorption analytically for high pressure methane on shale. This method considers both the real gas behavior of the bulk methane and the volume of the adsorbed phase, both of which are neglected in the classic C-C approach. The influence of the adsorbed phase volume and the nature of the gas behavior (real or ideal) on the isosteric heat of adsorption are also investigated. Calculations in the Henry's law region (corresponding to the limit of low pressure) were also performed based on the absolute methane adsorption isotherms to validate the above methodology. Rouquerol's approach [37] is applied in this case to avoid any potential for subjective judgements in determining the properties of the adsorbed phase in the Henry's law pressure range arising from the use of high pressure gas adsorption isotherm data.

3.2.2 Adsorption model and thermodynamic calculations

3.2.2.1 Dual-site Langmuir model

For a pure gas and solid adsorption system, the observed adsorption content, also called the Gibbs excess adsorption uptake (n_e), is given by the Gibbs equation,

$$n_e = n_a - V_a \cdot \rho(P,T) \qquad (1)$$

where n_e refers to the difference between the absolute quantity adsorbed (n_a) and the amount that would be present in the same volume (V_a) of the adsorbed phase at the density of the bulk phase ($\rho(P,T)$). In the limit of low ρ, the excess adsorbed amount well approximates the absolute quantity. At higher pressures where the density of the bulk phase approaches that of the adsorbed phase, the amount of gas that would be present in the volume of the adsorbed layer even in the absence of adsorption cannot be neglected. In order to obtain the absolute quantity of adsorption, the average density (or the total volume) of the adsorbed layer must be obtained.

The Langmuir equation is the simplest model for adsorption at the gas-solid interface that is applicable over the entire range of surface occupancy, making a number of simplifying approximations such as perfect adsorbent binding site homogeneity. For heterogeneous adsorbents, the multi-site Langmuir model is more suitable than the single-site Langmuir model for describing the gas adsorption behavior [28, 38, 39]. The binding energy of the adsorption sites will vary, where the lowest energy sites will be filled first, followed by the higher energy sites. For the purposes of many real-world adsorbents, a dual-site Langmuir model incorporating only two different binding sites is sufficient for fitting experimental data when measured over a wide range of pressures and supercritical temperatures [27, 38, 39]. Each site can be modelled by a separate equilibrium constant, $K_1(T)$ and $K_2(T)$ ($K_1(T) = A_1 \cdot \exp(\frac{E_1}{RT})$ and $K_2(T) = A_2 \cdot \exp(\frac{E_2}{RT})$) [38]. The dual-site Langmuir equation can then be expressed in the following form, where αis the relative fraction of the second site (0<α<1),

$$n_a(P,T) = n_{\max} \cdot \left[(1-\alpha)(\frac{K_1(T)P}{1+K_1(T)_1 P}) + \alpha(\frac{K_2(T)P}{1+K_2(T)P}) \right] \quad (2)$$

The same type of equation can be used to describe the volume change of the adsorbed layer as a function of pressure, as [27, 28, 39],

$$V_a = V_{\max} \cdot \left[(1-\alpha)(\frac{K_1(T)P}{1+K_1(T)P}) + \alpha(\frac{K_2(T)P}{1+K_2(T)P}) \right] \quad (3)$$

By combining equations (1), (2), and (3), the excess adsorption amount and the surface coverage, θ, in the dual-site model can be obtained, giving:

$$n_e(P,T) = (n_{\max} - V_{\max} \cdot \rho(P,T)) \cdot \left[(1-\alpha)(\frac{K_1(T)P}{1+K_1(T)P}) + \alpha(\frac{K_2(T)P}{1+K_2(T)P}) \right] \quad (4)$$

$$\theta = \frac{n_a(P,T)}{n_{\max}} = \left[(1-\alpha)(\frac{K_1(T)P}{1+K_1(T)P}) + \alpha(\frac{K_2(T)P}{1+K_2(T)P}) \right] \quad (5)$$

The dual-site Langmuir model described herein (equations 2, 4, and 5) is based on the assumption that the volume of the adsorbed layer monotonically increases with increased pressure, which is consistent with the physical nature of adsorption and does not necessitate any complex empirical equation for the density of the adsorbed phase. This monotonic increase is further approximated

as linear with respect to the number of adsorbed species, which is a reasonable, simple assumption. The absolute adsorption quantity as a function of temperature and pressure can be obtained via global curve fitting of the entire set of experimental excess uptake isotherms.

3.2.2.2 Isosteric heat of adsorption

The change in enthalpy of the system due to adsorption at a specific state of surface occupancy is referred to as the isosteric heat of adsorption (ΔH_{ads}). It can be determined via the Clapeyron relationship which is relevant to the equilibrium between two phases (in this case the adsorbed phase, a, and the gas phase, g) in a closed system:

$$\Delta H_{ads} = (\frac{dP}{dT})_{n_a} \cdot T \cdot \Delta v = (\frac{dP}{dT})_{n_a} \cdot T \cdot (v_a - v_g) \qquad (6)$$

The derivative of pressure with temperature along an isostere (constant value of adsorption uptake), $(\frac{dP}{dT})_{na}$, can be expanded in various ways for further investigation. Since the pressure in a closed system is a function of temperature and quantity adsorbed, a general expansion may be made such that [40],

$$(\frac{dP}{dT})_{n_a} = (\frac{\partial P}{\partial n_a})_T \frac{dn_a}{dT} + P(\frac{\partial(\ln P)}{\partial T})_{n_a} \qquad (7)$$

If the bulk fluid is approximated as an ideal gas, $Pv = RT$, it follows that,

$$-\Delta H_{ads(n_a)} = RT^2[(\frac{\partial(\ln P)}{\partial T})_{n_a}] + \frac{RT^2}{P} \cdot (\frac{\partial P}{\partial n_a})_T \frac{dn_a}{dT} - [(\frac{\partial P}{\partial n_a})_T \frac{dn_a}{dT} + P(\frac{\partial(\ln P)}{\partial T})_{n_a}] \cdot T \cdot v_a \quad (8)$$

In right hand side (RHS) of equation (8), the second term, $\frac{RT^2}{P} \cdot (\frac{\partial P}{\partial n_a})_T \frac{dn_a}{dT}$, includes the behavior of the adsorbed phase mass, and the third term, $[(\frac{\partial P}{\partial n_a})_T \frac{dn_a}{dT} + P(\frac{\partial(\ln P)}{\partial T})_{n_a}] \cdot T \cdot v_a$, considers the volume effect of the adsorbed phase. If the volume of the adsorbed layer is taken to be negligible and the influence of the adsorbed mass is ignored, the conventional Clausius-Clapeyron (C-C) relationship is obtained:

$$\Delta H_{ads} = \Delta H_{ads,c-c} = RT^2[(\frac{\partial(\ln P)}{\partial T})_{n_a}] \qquad (9)$$

Optionally, if the relationship between the amount adsorbed and the process conditions (pressure and temperature) is known, the derivative can be directly determined. If that relationship is taken to have the form of a Langmuir equation, then the derivative can be expanded into three simpler terms:

$$(\frac{dP}{dT})_{n_a} = (\frac{\partial P}{\partial \theta})_{n_a} \cdot (\frac{\partial \theta}{\partial K})_{n_a} \cdot (\frac{\partial K}{\partial T})_{n_a} \qquad (10)$$

By combining equation (6) with equation (10), the isosteric heat of adsorption is then directly obtained. There are numerous ways to handle the difference between the molar volume of the gas and adsorbate as required to solve equation (6). For example, by applying the ideal gas law ($Pv_g = RT$), one form of the isosteric heat of adsorption can be obtained simply as,

$$-\Delta H_{ads(n_a),IGL} = (\frac{\partial P}{\partial \theta})_{n_a} \cdot (\frac{\partial \theta}{\partial K})_{n_a} \cdot (\frac{\partial K}{\partial T})_{n_a} \cdot T \cdot (\frac{RT}{P} - v_a) \qquad (11)$$

Ignoring the volume of the adsorbed phase (in other words, assuming $v_a << v_g$), another form of the isosteric heat of adsorption can be obtained,

$$-\Delta H_{ads(n_a),IGL-0V} = (\frac{\partial P}{\partial \theta})_{n_a} \cdot (\frac{\partial \theta}{\partial K})_{n_a} \cdot (\frac{\partial K}{\partial T})_{n_a} \cdot T \cdot (\frac{RT}{P}) \qquad (12)$$

If equation (6) and equation (10) are combined and the true gas density is applied (the true gas density can be obtained using NIST REFPROP database) instead of the ideal gas law density, the isosteric heat of adsorption is obtained as:

$$-\Delta H_{ads(n_a),RGL} = (\frac{\partial P}{\partial \theta})_{n_a} \cdot (\frac{\partial \theta}{\partial K})_{n_a} \cdot (\frac{\partial K}{\partial T})_{n_a} \cdot T \cdot (\rho_g^{-1} - v_a) \qquad (13)$$

Ignoring the volume of the adsorbed phase in equation (13), an additional form of the isosteric heat of adsorption can be obtained,

$$-\Delta H_{ads(n_a)RGL-0V} = (\frac{\partial P}{\partial \theta})_{n_a} \cdot (\frac{\partial \theta}{\partial K})_{n_a} \cdot (\frac{\partial K}{\partial T})_{n_a} \cdot T \cdot (\rho_g^{-1}) \qquad (14)$$

Equations (11)-(14) are much easier to solve using an analytical approach than equation (8). The analytical form of $(\frac{\partial P}{\partial \theta})_{n_a} \cdot (\frac{\partial \theta}{\partial K})_{n_a} \cdot (\frac{\partial K}{\partial T})_{n_a}$ in the case of the dual-site Langmuir equation is:

$$\left(\frac{\partial P}{\partial \theta}\right)_{n_a} \cdot \left(\frac{\partial \theta}{\partial K}\right)_{n_a} \cdot \left(\frac{\partial K}{\partial T}\right)_{n_a} = \frac{\frac{(1-\alpha)P}{(1+K_1(T)P)^2} \cdot \frac{-E_1 K_1(T)}{RT^2} + \frac{\alpha P}{(1+K_2(T)P)^2} \cdot \frac{-E_2 K_2(T)}{RT^2}}{\frac{(1-\alpha)K_1(T)}{(1+K_1(T)P)^2} + \frac{\alpha K_2(T)}{(1+K_2(T)P)^2}} \quad (15)$$

The merits of the second approach (equation (10) over equation (7)) are twofold. Firstly, both the true gas behavior and the ideal gas law can easily be implemented as shown in equations (11) and (13), to determine the effect of assuming gas phase ideality in the result. Secondly, the volume of the adsorbed layer can also be taken into consideration, an especially important feature to account for outside of the low-pressure (Henry's law) limit. On the contrary, the conventional C-C equation inherently adopts the ideal gas law and does not consider the density of the adsorbed layer to be significant compared to the bulk gas.

3.2.2.3 The Henry's law limit

An approximate approach is provided here to extrapolate the isosteric heat of adsorption to low pressures (the Henry's law region) from the as-collected high pressure adsorption isotherms. In this way, an unbiased isosteric heat of adsorption can be calculated without the dependence on any model or specific methodology, for comparison to the method described above.

In the limit of low pressure, gas adsorption behavior follows Henry's law,

$$n_a = K_H P \quad (16)$$

where P is the pressure of the bulk gas, n_a is the absolute adsorption content, and K_H is the Henry's law constant. Together with the van't Hoff equation (which relies on the ideal gas law, also applicable in the Henry's law regime), the relationship between K_H and the thermodynamic quantities of adsorption is expressed as,

$$\ln K_H = -\frac{\Delta H_H}{RT} + \frac{\Delta S_H}{R} \quad (17)$$

The isosteric heat of adsorption in the Henry's law region can be obtained from the linear relationship between $\ln(K_H)$ and the reciprocal of T. The key step at this point is to obtain Henry's constant using a reasonable pressure range wherein the linear relationship between absolute adsorption content and pressure is valid.

In order to calculate Henry's law constants, the relationship between adsorption uptake and pressure in the low-pressure region can be expressed by a virial expansion,

$$\ln(n_a / P) = A_0 + A_1 n + A_2 n^2 + \cdots\cdots \quad (18)$$

where n_a is the absolute content of adsorption at bulk gas pressure P, and the first virial coefficient A_0 is related to the Henry's law constant, K_H, as $K_H = \exp(A_0)$. When n_a is small, the higher-order terms can be neglected, and equation (18) can be written as,

$$\ln(P / n_a) = -A_0 - A_1 n \quad (19)$$

From equation (19), A_0 can then be obtained by fitting the linear region of $\ln(P/n_a)$ as a function of n_a, where n_a is approximated by measured n_e isotherms. Rouquerol's recommended approach [37] is applied herein to avoid any subjective judgements in determining the Henry's pressure range:

a. the application of equation (19) should be limited to the pressure range where the term $n_a(1-P/P_{max})$ continuously increases with P/P_{max} (P_{max} is the maximum pressure investigated).
b. an apparent linear relationship must be obtained, i.e., the correlation coefficient (R^2) should be above 0.95.

Once Henry's law constant values are obtained, the isosteric heat of adsorption in Henry's region can be obtained from the linear relationship between $\ln(K_H)$ and the reciprocal of temperature as shown in equation (17).

3.2.3 Experimental data and analysis

Four high-pressure adsorption isotherms of methane on Longmaxi shale (China) were measured using the gravimetric method: at 303.15 K, 318.15 K, 333.15 K, and 355.15 K (Figure 3.2.1) [36]. All four isotherms were then fitted simultaneously to the dual-site Langmuir model (equation 4) by a least-squares residual minimization algorithm. The seven independent fitting parameters were varied to achieve the global minimum of the residual-squares value within the following limits: $0 < n_{max} < 100$ mmol/g, $0 < V_{max} < 10$ mL/g, $0 < \alpha < 1$, $0 < E_1 < 100$ kJ/mol, $0 < E_2 < 100$ kJ/mol, $A_1 > 0$, and $A_2 > 0$. Once the best-fit parameters were determined, absolute and excess adsorption uptake could be expressed at arbitrary temperatures and pressures by use of equations (2) and (4).

As shown in Figure 3.2.1, the dual-site Langmuir adsorption model (equation 4) gives a good global fit to the observed data with the residual sum of squares, 0.000263, and the corresponding best-fit parameters are: n_{max} = 0.1715 mmol/g, V_{max} = 0.0097 mL/g, α = 0.2640, E_1 = 16.706 kJ/mol, A_1 = 0.0002 1/MPa, E_2 = 15.592 kJ/mol, and A_2 = 0.0032 1/MPa. Detailed experimental methods and material properties of the shale are described in our previous work [36].

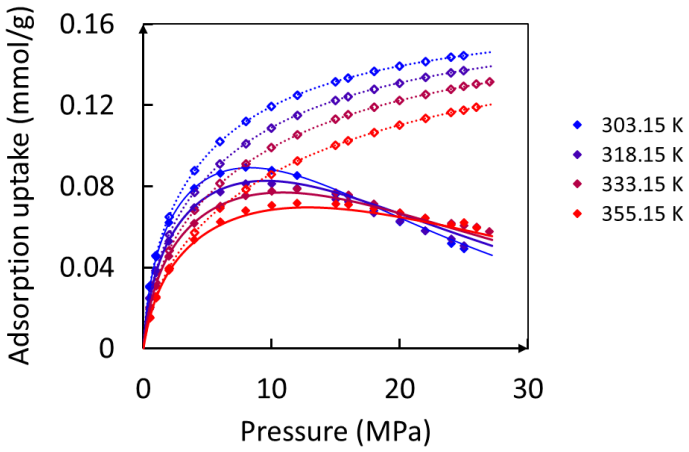

Figure 3.2.1. Equilibrium adsorption uptake of methane on Longmaxi shale between 303-355 K and 0.5-25 MPa: solid symbols are measured Gibbs excess uptake, solid lines are modeled Gibbs excess uptake (equation (4)), and open symbols and dashed lines are modeled absolute uptake (equation (2)). The data are reproduced from a previous study [36].

The well-known phenomenon that the observed Gibbs excess adsorption uptake increases with increasing pressure up to a maximum value and then decreases, as well as the corresponding crossover of isotherms, can be seen in Figure 3.2.1. This is attributed to the increasing volume of the adsorbed phase with increasing pressure, leading to a maximum in the Gibbs excess adsorption at each temperature [36]. This crossover in high pressure methane adsorption isotherms on shale has not been reasonably addressed using other commonly used adsorption models in literature. Furthermore, the temperature dependence of the adsorption uptake is built into the model in this work [36], where previously only empirical relationships or no relationship at all was addressed, making this globally fitted model more descriptive of temperature-related phenomena. As is characteristic of the physical nature of adsorption, the absolute adsorption quantity increases monotonically up to 27 MPa at all temperatures. The temperature dependence of the absolute adsorption uptake is also clear: the higher the temperature the lower the absolute adsorption uptake.

These features ensure that an accurate thermodynamic analysis can be achieved using the absolute adsorption equilibria calculated in this work.

3.2.4 Thermodynamic analysis and discussion

In the thermodynamic analysis of methane adsorption on shale performed in this work, the robustness of the isosteric heat of adsorption is first confirmed. Then, the various quantities describing the isosteric heat of adsorption (equations (11)-(14)) are compared to understand how the real gas behavior and the adsorbed phase volume influence the isosteric heat of adsorption. The temperature influence on the isosteric heat of adsorption is also compared. Finally, the isosteric heat of adsorption within Henry's pressure region is calculated to validate the above methodology using the high pressure methane absolute adsorption isotherms.

3.2.4.1 Robustness of the isosteric heat of adsorption calculation

The isosteric heat of adsorption is best calculated by including all measured adsorption data in the fitting routine, obtaining the best-fit parameters, and then directly solving equation (13) to obtain $-\Delta H_{ads}$, which not only considers the real gas behavior but also takes the volume of the adsorbed phase into consideration. The isosteric heat of adsorption of methane on shale, as a function of absolute quantity of methane adsorbed, is shown as solid isothermal lines in Figure 3.2.2. The isosteric heat varies from 16.5 kJ/mol at low pressure and high temperature (355 K), down to <5 kJ/mol at high pressures, indicating a heterogeneous distribution of adsorption sites in the porous shale structure.

To demonstrate the robustness of the analytical calculation of the isosteric heat of adsorption by our method, the results obtained using different processing approaches are compared: (1) using all measured data, (2) using only the data between 0-15 MPa, and (3) using only the data between 303.15-333.15 K as fitting data to obtain a best fit. Method (1) represents the best approach as described previously, and method (2) and (3) demonstrate the effects of collecting less experimental data (e.g., at <15 MPa as in a majority of previous investigations). As shown in Figure 3.2.3, the resulting isosteric heats are approximately the same except in the low pressure region. While this may seem counterintuitive, it is important to note that subtle changes in the best-fit parameters lead to large changes in the dP/dT term in equation (10) and (15), and the best-fit parameters can only be achieved by using a large range of measured data (typically requiring numerous isotherms and data extending well beyond the Gibbs excess maximum).

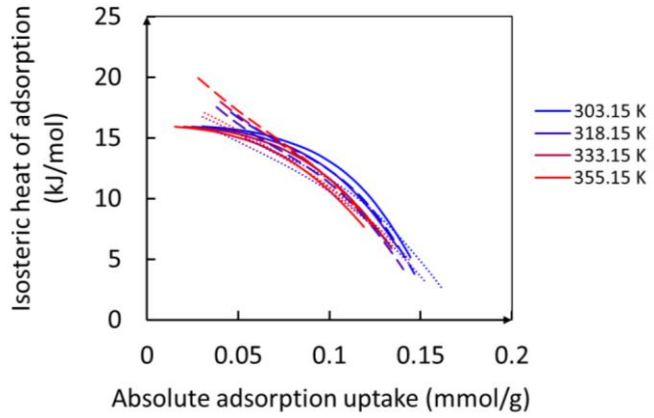

Figure 3.2.2. Isosteric heat of adsorption of methane on shale between 303-355 K (blue to red) as a function of absolute adsorption uptake up to 30 MPa (solid lines). For comparison, the isosteric heat calculated by including experimental data from restricted ranges of pressure and temperature is also shown (as small and large dashes, respectively).

3.2.4.2 Effect of real gas behavior and adsorbed phase volume

The second step is to investigate the effects of real gas behavior and the volume of the adsorbed phase on the isosteric heat of adsorption beyond the Henry's law region. A summary of the assumptions included within each isosteric heat of adsorption investigated herein is shown in Table 3.2.1 and a detailed discussion of the comparison with Henry's law analysis is given in Section 4.4.

Table 3.2.1. Definition of various isosteric heats of adsorption

Isosteric heat of adsorption	Gas behavior	Adsorbed phase volume
Heat of adsorption within the Henry's law region	Ideal gas	No
$\Delta H_{ads,c-c}$: Equation (9)	Ideal gas	No
$\Delta H_{ads(n_a),IGL}$: Equation (11)	Ideal gas	Yes
$\Delta H_{ads(n_a),IGL-0V}$: Equation (12)	Ideal gas	No
$\Delta H_{ads(n_a),RGL}$: Equation (13)	Real gas	Yes
$\Delta H_{ads(n_a)RGL-0V}$: Equation (14)	Real gas	No

A comparison of the isosteric heats of adsorption calculated according to Table 3.2.1 is shown in Figure 3.2.3 The different isosteric heats of adsorption follow a similar behavior irrespective of temperature and the isosteric heat of adsorption at 303.15 K is taken as an example to interpret the

influence of real gas behavior and adsorbed phase volume. The C-C approximation employs the ideal gas law and does not consider the adsorbed phase volume. Both assumptions become less valid with increasing adsorption content and cause a significant overestimation of the isosteric heat of adsorption. Regardless of the gas law employed, the adsorbed phase volume significantly affects the behavior of the calculated isosteric heat of adsorption, especially under high pressure conditions: without considering v_a, the isosteric heat of adsorption is always overestimated. For cases considering the finite volume of the adsorbed phase, the difference between the real gas and ideal gas density also affects the isosteric heat of adsorption significantly: the ideal gas law always corresponds to a higher isosteric heat. Comparing these effects at different temperatures, it can be found that as temperature increases, the influence of both the equation of state of the gas and the volume of the adsorbed phase decreases.

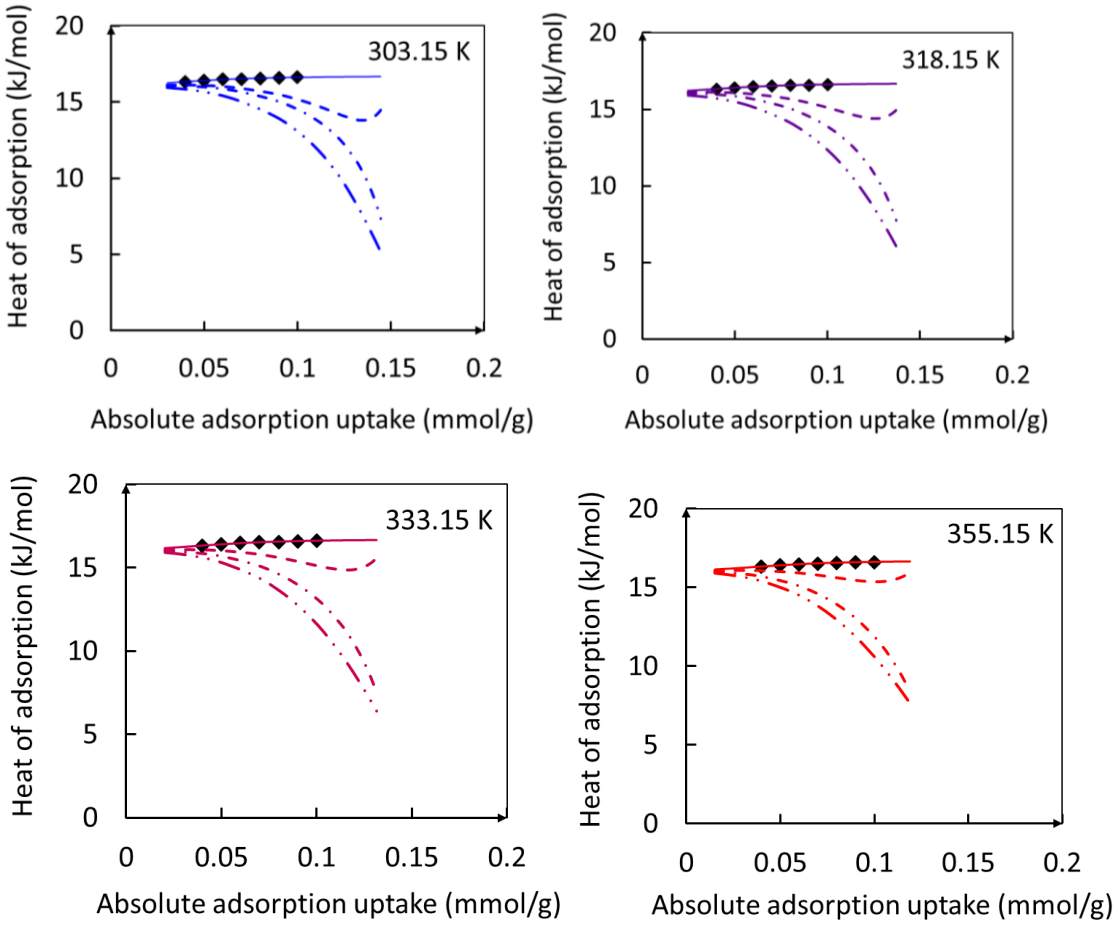

Figure 3.2.3. Isosteric heat of adsorption of methane on shale as calculated using four different methods: $\Delta H_{ads(na),\,IGL\text{-}OV}$ (equation (12)) as solid lines, $\Delta H_{ads(na),\,RGL\text{-}0V}$ (equation (14))

as dashed lines, $\Delta H_{ads(na),\,IGL}$ (equation (11)) as single dotted lines, and $\Delta H_{ads(na),\,RGL}$ (equation (13)) as double dotted lines. The isosteric heat of adsorption calculated in the C-C approximation (equation (9)) is also shown as filled black symbols.

3.2.4.3 Effect of temperature

Isosteric heats of adsorption calculated in different ways (according to equations (9) and (11)-(14)) are shown at all temperatures investigated in Figure 3.2.4. In all cases, temperature generally has a negative effect on the isosteric heat of adsorption for both real gas and ideal gas cases: the higher the temperature, the lower the isosteric heat of adsorption. Using the real gas equation of state, if the adsorbed phase volume is ignored, isosteric heats of adsorption first decrease and then increase and the temperature-dependence reverses at high pressure. In the ideal gas assumption, if the adsorbed phase volume is ignored, the isosteric heat of adsorption becomes the C-C approximation and the temperature-dependence disappears altogether. Figure 3.2.4 also shows that in the low pressure region (i.e., low adsorption uptake), the isosteric heats of adsorption merge at a constant value. However, because limited data were measured in this region, extrapolation to the limiting value is difficult. This problem can be solved using the approach discussed in Section 4.4.

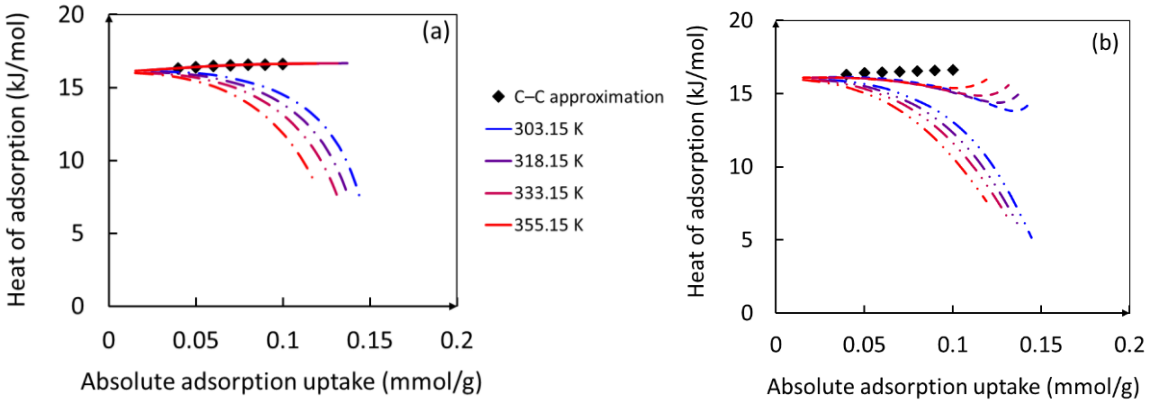

Figure 3.2.4. Comparison of isosteric heat of adsorption of methane on shale: $\Delta H_{ads(na),\,IGL\text{-}OV}$ (equation (12)) as solid lines, $\Delta H_{ads(na),\,IGL}$ (equation (11)) as single dotted lines, $\Delta H_{ads(na),\,RGL\text{-}0V}$ (equation (14)) as dashed lines and $\Delta H_{ads(na),\,RGL}$ (equation (13)) as double dotted lines. The isosteric heat of adsorption calculated in the C-C approximation (equation (9)) is also shown as filled black symbols.

3.2.4.4 Determination of Henry's law limit

The linear range of equation (19) determined using Rouquerol's approach shown in Figure 3.2.5. The mean isosteric heat of adsorption over the entire temperature range, calculated according to equation (17) is 16.5 kJ/mole (see Figure 3.2.6), which is consistent with the value determined by both the analytical and conventional approaches as described above (Figures 3-4).

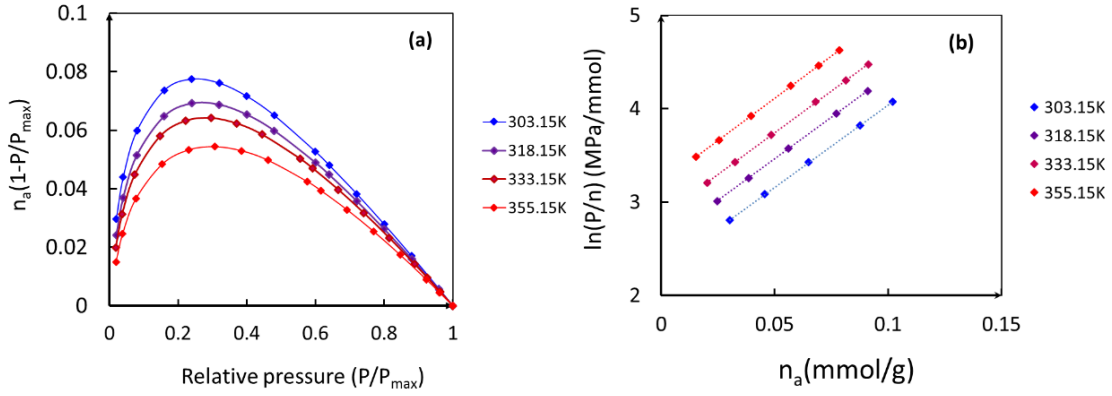

Figure 3.2.5. Equilibrium adsorption uptake of methane on shale (n_a) between 303-355 K and 0.5-25 MPa, as measured (solid symbols) and as fitted by a virial-type equation (solid lines, equation (19)). (left) Adsorption uptake is shown as a product of n_a and $1-P/P_{max}$, as a function of P/P_{max}. (right) Adsorption uptake is shown in the linear region for $\ln(P/n_a)$ as a function of n_a.

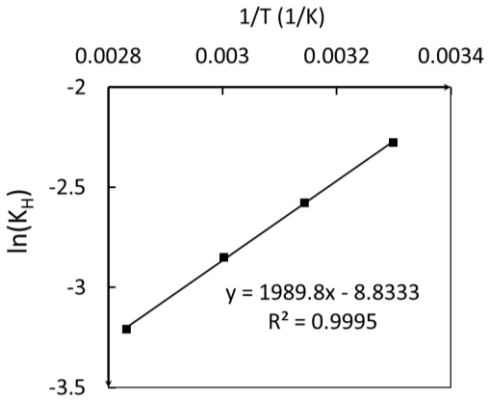

Figure 3.2.6. Mean isosteric heat of adsorption calculated by equation (17)

3.2.5 Discussion

Understanding the isosteric heat of adsorption is useful in accurate estimations of the temperature evolution process during essentially isothermal adsorption processes. It has been previously reported that during methane adsorption on coal, the temperature change induced by adsorption

first shows a sharp increase to a peak, and then a gradual decrease to the environmental (bath) temperature at equilibrium [41]. Moreover, this change in temperature was not the same at different temperatures; at higher temperatures, a smaller temperature change occurred upon adsorption of methane on coal. Considering the fact that the physical adsorption of methane on either coal or shale should exhibit similar characteristics (both are bulk, naturally occurring carbonaceous organic-rich materials), these previous results are readily comparable to those obtained in this work. Herein it is found that the isosteric heat of adsorption decreases with increasing adsorption content for methane in shale, which is also affected by the temperature of the isotherms. Specifically, the isosteric heat of adsorption decreases as a function of temperature, which is qualitatively consistent with the observed temperature change upon methane adsorption on coal. The precise dependence of the isosteric heat of adsorption on both adsorption uptake and temperature must be taken into consideration for accurate modeling of the heat transfer process during methane extraction from shale.

The isosteric heat of adsorption of methane on shale in the Henry's law region is consistent with similar reports on coal samples [42]. In the Henry's law pressure range, each adsorbed molecule can explore the entire adsorbent surface independently because of the extremely low adsorbate concentration at low pressure. The adsorption sites of highest energy will be occupied first (in this work, "highest energy" refers to lowest (negative) absolute energy), and the interactions between adsorbed methane molecules and the gas molecules themselves can both be neglected. When the interaction among adsorbed methane molecules and/or gas molecules becomes significant with increasing pressure, the most accurate calculation of the isosteric heat of adsorption must consider both the real gas behavior and the finite adsorbed phase volume as in equation (13). Then, considering the interaction between the adsorbate molecules and the solid porous adsorbent as the only remaining significant interaction in the system, the evolution of the isosteric heat of adsorption as a function of pressure or adsorption uptake can reflect the overall heterogeneity of the adsorbent which is a very relevant property for comparison between materials [27, 42]. In addition, since the isosteric heat of adsorption in the Henry's law region is independent of temperature, as shown in equation (13), it can be used as a unique index to evaluate the adsorption affinity of the highest energy sites in porous adsorbents such as coal and shale.

3.2.6 Conclusions

In this work, the isosteric heat of adsorption of methane on Longmaxi shale at geologically relevant pressures is obtained by considering both the real gas behavior of bulk methane and the finite adsorbed phase volume. The effects of real gas behavior, adsorbed phase volume, and temperature on the isosteric heat of adsorption are investigated, facilitated by the use of a two-site Langmuir adsorption model. Three conclusions can be drawn.

First, for high pressure methane adsorption on shale, the isosteric heat of adsorption decreases with increasing adsorption uptake (or equilibrium pressure) and the dependence on temperature is negative.

Second, accurate calculations of the isosteric heat of adsorption are always lower than the quantity calculated using the C–C approximation. Neglecting either the real gas behavior or the adsorbed phase volume always results in an overestimation of the isosteric heat. These results are consistent with the temperature evolution phenomenon that occurs during methane adsorption on other carbonaceous adsorbents.

Finally, the isosteric heat of adsorption in the Henry's law region, which is independent of temperature, can be used as a unique index to evaluate the gas adsorption affinity of adsorbents such as coal and shale in the limit of very dilute adsorption. For all thermodynamic analysis outside of this regime, a more sophisticated method such as fitting the data to a two-site Langmuir model must be employed.

Acknowledgements

Financial assistance for this work was provided by the U.S. Department of Energy through the National Energy Technology Laboratory's Program under Contract No. DE-FE0006827, the State Key Development Program for Basic Research of China (Grant No. 2014CB239102) and Department of Science and Technology at China Petroleum & Chemical Corporation (Grant No.P12002, P14156). The first author also wants to thank Prof. Matthew R Hall for his valuable discussions on this work.

References

1. Kuuskraa, V., Stevens, S. H., & Moodhe, K. D. (2013). Technically recoverable shale oil and shale gas resources: an assessment of 137 shale formations in 41 countries outside the United States. [J]. Natural Gas Industry, 5, 003.
2. Wang, Q., Chen, X., Jha, A. N., & Rogers, H. (2014). Natural gas from shale formation–the evolution, evidences and challenges of shale gas revolution in United States. Renewable and Sustainable Energy Reviews, 30, 1-28.
3. Curtis, J. B. (2002). Fractured shale-gas systems. AAPG bulletin, 86(11), 1921-1938.
4. Montgomery, S.L., Jarvie, D.M., Bowker, K.A., Pollastro, R.M., 2005. Mississippian Barnett Shale, Fort Worth basin, north-central Texas: gas-shale play with multietrillion cubic foot potential. AAPG Bull. 89, 155e175.
5. Zhang, T., Ellis, G. S., Ruppel, S. C., Milliken, K., & Yang, R. (2012). Effect of organic-matter type and thermal maturity on methane adsorption in shale-gas systems. Organic Geochemistry, 47, 120-131.
6. Ross, D.J., Bustin, R.M., 2008. Characterizing the shale gas resource potential of Devoniane-Mississippian strata in the Western Canada sedimentary basin: application of an integrated formation evaluation. AAPG Bull. 92, 87e125.
7. Ross, D.J., Bustin, R.M., 2009. The importance of shale composition and pore structure upon gas storage potential of shale gas reservoirs. Mar. Pet. Geol. 26, 916e927.
8. Gasparik, M., Ghanizadeh, A., Bertier, P., Gensterblum, Y., Bouw, S., Krooss, B.M., 2012. High-pressure methane sorption isotherms of black shales from the Netherlands. Energy Fuels 26, 4995e5004.
9. Busch, A., & Gensterblum, Y. (2011). CBM and CO2-ECBM related sorption processes in coal: a review. International Journal of Coal Geology, 87(2), 49-71.
10. Ji, W., Song, Y., Jiang, Z., Wang, X., Bai, Y., Xing, J., 2014. Geological controls and estimation algorithms of lacustrine shale gas adsorption capacity: a case study of the Triassic strata in the southeastern Ordos Basin, China. Int. J. Coal Geol. 134, 61e73.
11. Zou, Caineng, Dazhong, Dong, Yuman, Wang, Xinjing, Li, HUANG, J., Shufang, Wang, ... & Wenhua, Bai. (2015). Shale gas in China: Characteristics, challenges and prospects (Ⅱ). Petroleum Exploration and Development, 42(6), 753-767.

12. Saha, B. B., El-Sharkawy, I. I., Koyama, S., Lee, J. B., & Kuwahara, K. (2006). Waste heat driven multi-bed adsorption chiller: heat exchangers overall thermal conductance on chiller performance. Heat Transfer Engineering, 27(5), 80-87.
13. Jee, J. G., Kim, M. B., & Lee, C. H. (2005). Pressure swing adsorption processes to purify oxygen using a carbon molecular sieve. Chemical engineering science, 60(3), 869-882.
14. Schlapbach, L., & Züttel, A. (2001). Hydrogen-storage materials for mobile applications. Nature, 414(6861), 353-358.
15. Biloe, S., Goetz, V., & Mauran, S. (2001). Dynamic discharge and performance of a new adsorbent for natural gas storage. AIChE Journal, 47(12), 2819-2830.
16. Rahman, K. A., Chakraborty, A., Saha, B. B., & Ng, K. C. (2012). On thermodynamics of methane+ carbonaceous materials adsorption. International Journal of Heat and Mass Transfer, 55(4), 565-573.
17. Jaschik, M., Tanczyk, M., Warmuzinski, K., & Wojdyla, A. (2015). Comments on the paper "On thermodynamics of methane+ carbonaceous materials adsorption". International Journal of Heat and Mass Transfer, 91, 1308.
18. Thommes M, Kaneko K, Neimark, A V, Olivier J P, Rodriguez-Reinoso F, Rouquerol J & Sing K S. Physisorption of gases, with special reference to the evaluation of surface area and pore size distribution (IUPAC Technical Report). Pure and Applied Chemistry, 2015, 87(9-10):1051-1069.
19. Pan, H., Ritter, J. A., & Balbuena, P. B. (1998). Examination of the approximations used in determining the isosteric heat of adsorption from the Clausius-Clapeyron equation. Langmuir, 14(21), 6323-6327.
20. Sircar, S., Mohr, R., Ristic, C., & Rao, M. B. (1999). Isosteric heat of adsorption: theory and experiment. The Journal of Physical Chemistry B, 103(31), 6539-6546.
21. Shen, D., Bülow, M., Siperstein, F., Engelhard, M., & Myers, A. L. (2000). Comparison of experimental techniques for measuring isosteric heat of adsorption. Adsorption, 6(4), 275-286.
22. Murialdo, M., Stadie, N. P., Ahn, C. C., & Fultz, B. (2015). Observation and Investigation of Increasing Isosteric Heat of Adsorption of Ethane on Zeolite-Templated Carbon. The Journal of Physical Chemistry C, 119(2), 944-950.

23. Payne, S. H., Kreuzer, H. J., & Roelofs, L. D. (1991). Isosteric heat of adsorption for repulsive interactions. Surface Science Letters, 259(3), L781-L786.
24. Chung, D. S., & Pfost, H. B. (1967). Adsorption and desorption of water vapor by cereal grains and their products Part I: Heat and free energy changes of adsorption and desorption. Transactions of the ASAE, 10(4), 549-0551.
25. Frost, H., Düren, T., & Snurr, R. Q. (2006). Effects of surface area, free volume, and heat of adsorption on hydrogen uptake in metal-organic frameworks. The Journal of Physical Chemistry B, 110(19), 9565-9570.
26. Dejardin, P. (1982). Determination of adsorption isotherms of macromolecules by the depletion method. The Journal of Physical Chemistry, 86(14), 2800-2801.
27. Stadie, N. P., Murialdo, M., Ahn, C. C., & Fultz, B. (2013). Anomalous isosteric enthalpy of adsorption of methane on zeolite-templated carbon. Journal of the American Chemical Society, 135(3), 990-993.
28. Stadie, N. P., Murialdo, M., Ahn, C. C., & Fultz, B. (2015). Unusual Entropy of Adsorbed Methane on Zeolite-Templated Carbon. The Journal of Physical Chemistry C, 119(47), 26409-26421.
29. Bae, J. S., & Bhatia, S. K. (2006). High-pressure adsorption of methane and carbon dioxide on coal. Energy & Fuels, 20(6), 2599-2607.
30. Pini, R., Ottiger, S., Burlini, L., Storti, G., & Mazzotti, M. (2010). Sorption of carbon dioxide, methane and nitrogen in dry coals at high pressure and moderate temperature. International Journal of Greenhouse Gas Control, 4(1), 90-101.
31. Sakurovs, R., Day, S., Weir, S., & Duffy, G. (2007). Application of a modified Dubinin-Radushkevich equation to adsorption of gases by coals under supercritical conditions. Energy & fuels, 21(2), 992-997.
32. Myers, A. L., & Monson, P. A. (2014). Physical adsorption of gases: the case for absolute adsorption as the basis for thermodynamic analysis. Adsorption, 20(4), 591-622.
33. Marmur, A. (2015). Surface tension and adsorption without a dividing surface. Langmuir, 31(46), 12653-12657.
34. Krishna, R. (2015). Evaluation of procedures for estimation of the isosteric heat of adsorption in microporous materials. Chemical Engineering Science,123, 191-196.

35. Askalany, A. A., & Saha, B. B. (2015). Derivation of isosteric heat of adsorption for non-ideal gases. International Journal of Heat and Mass Transfer, 89, 186-192.
36. Tang, X., Ripepi, N., Stadie, N. P., Yu, L., & Hall, M. R. (2016). A dual-site Langmuir equation for accurate estimation of high pressure deep shale gas resources. Fuel, 185, 10-17.
37. Rouquerol, J., Llewellyn, P., & Rouquerol, F. (2007). Is the BET equation applicable to microporous adsorbents? Studies in surface science and catalysis, (160), 49-56.
38. Graham, D. (1953). The characterization of physical adsorption systems. I. The equilibrium function and standard free energy of adsorption. The Journal of Physical Chemistry, 57(7), 665-669.
39. Mertens, F. O. (2009). Determination of absolute adsorption in highly ordered porous media. Surface Science, 603(10), 1979-1984.
40. Chakraborty, A., Saha, B. B., Koyama, S., & Ng, K. C. (2006). On the thermodynamic modeling of the isosteric heat of adsorption and comparison with experiments. Applied physics letters, 89(17), 171901.
41. Yue, G., Wang, Z., Tang, X., Li, H., & Xie, C. (2015). Physical Simulation of Temperature Influence on Methane Sorption and Kinetics in Coal (II): Temperature Evolvement during Methane Adsorption in Coal Measurement and Modeling. Energy & Fuels, 29(10), 6355-6362.
42. Tang, X., Wang, Z., Ripepi, N., Kang, B., & Yue, G. (2015). Adsorption affinity of different types of coal: mean isosteric heat of adsorption. Energy & Fuels, 29(6), 3609-3615.

3.3 High pressure supercritical carbon dioxide adsorption in coal: adsorption model and thermodynamic characteristics

Xu Tang[a], Nino Ripepi[a,b]

(a.Department of Mining and Minerals Engineering & b Virginia Center for Coal and Energy Research, Virginia Polytechnic Institute and State University, Blacksburg, Virginia, 24060, U.S)

Abstract: This work uses a dual-site Langmuir model to describe supercritical carbon dioxide ($scCO_2$) adsorption in coal up to 20MPa and 253K by considering both the absorbed (penetrated) and adsorbed carbon dioxide phase. The isosteric heat of adsorption for $scCO_2$ adsorption in coal is calculated analytically by considering both the real gas behavior and the behavior of the adsorbed phase, which are ignored in the classic Clausius-Clapeyron approximation. It was found that the proposed model can not only reasonably interpret observed test phenomena but also has the intrinsic ability to extrapolate adsorption isotherms under different temperatures beyond test data. The crossovers of the observed adsorption isotherms under different temperatures are caused by the changing volume of the adsorbed phase during adsorption process. Both the temperature dependence and adsorption uptake dependence of isosteric heat of adsorption are revealed; the higher the temperature and the adsorption uptake, the lower the isothersteric heat of adsorption. Using ideal gas law always overestimates isosteric heat of adsorption for $scCO_2$ adsorption in coal. For $scCO_2$ adsorption in coal, there exists an abnormal phenomenon that the higher the temperature the higher the isosteric heat of adsorption when the adsorption uptake approaches the maximum, which has not been reported in literature. The dual-site Langmuir model and the extended method for calculating heat of adsorption lays the foundation for accurately estimating carbon dioxide storage capacity, differentiating bulk gas phase and adsorbed phase content, and analyzing thermodynamic (heat transfer) characteristic of scCO2 and coal interaction.

Key words: carbon dioxide, adsorption, coal, Langmuir, isosteric heat of adsorption

3.3.1 Introduction

Because of global warming and climate change concerns, global efforts have been made to decrease the concentration of carbon dioxide in the atmosphere (Grubb et al., 1995; Stern, 2009; Morgan et al., 2014; Paris Protocol, 2015). Carbon dioxide capture, utilization and storage are considered crucial ways to meet the carbon dioxide emission reduction targets. Onshore geologic sequestration of carbon dioxide typically involves collecting and placing carbon dioxide into suitable underground formations for storage such as depleted oil and conventional gas reservoirs, unconventional natural gas reservoir (unminable coal seam and shale formation), and deep formations containing salty water and basalt formations (Herzog et al., 2001; White et al., 2003; Metz et al., 2005; Benson et al., 2008; Orr, 2009; Figueroa et al., 2008). Among these geological formations, unminable coal seams are one of the promising sites because of their potential for enhancing coalbed methane (ECBM) recovery while simultaneously sequestering carbon dioxide (White et al., 2005; Mazzotti et al., 2009; Busch et al., 2011; Godec et al., 2014). The enhanced natural gas will help to offset the cost of carbon dioxide sequestration. However, there are still some concerns about the long time effect of the permanent sequestration of CO_2 in the coal seam and its negative effects upon the environments (White et al., 2005; Hedges et al., 2005). Carbon dioxide injection issues may occur along during the field injection process because of the permeability decrease induced by the coal swelling (Reucroft, et al., 1987; Pan et al., 2007 & 2010; Cui et al., 2007; Day et al., 2008). The existing phase of the injected carbon dioxide in the subsurface is also important to know, because it is crucial for the carbon dioxide storage capacity estimation. Therefore, field tests of ECBM with carbon sequestration were and are being conducted across the world, which will be helpful to understand its potential benefits and practical issues (Steven et al., 1998; Yamasaki, 2003; Gunter et al., 2004; Sams et al., 2005; White et al., 2005; Van Bergen, et al., 2006; Wong et al., 2007; Ripepi, 2009; Connell et al., 2013; Gilliland et al., 2013; Wei et al., 2015).

It is well known that the affinity of carbon dioxide in coal is higher than methane and the carbon dioxide adsorbed on coal is always higher than methane. In order to evaluate the carbon dioxide storage potential of unminable coal seam, the first step is to evaluate the adsorption capacity of carbon dioxide in coal via isothermal sorption tests. However, because of the heterogenous properties of coal, $scCO_2$ adsorption behavior in coal has not attracted researcher's attentions like manmade materials. There are inconsistent test phenomena reported regarding $scCO_2$ adsorption

in coal. Some researchers show peculiar test phenomena for $scCO_2$ in coal such as the bimodal Gibbs excess adsorption isotherms (Krooss et al., 2002; Toribio et al., 2004; Busch et al., 2007; Siemons et al., 2007; Busch et al., 2008). Other researchers exhibit smooth CO_2 excess adsorption isotherms in coal when the pressure goes up to 20MPa (Sudibandriyo et al., 2003; Fitzgerald et al., 2005; Bae et al., 2006; Ottiger et al., 2006; Sakurovs et al., 2007; Day et al., 2008; Pini et al., 2010; Weniger et al., 2010; Song et al., 2015; Luo et al., 2015). Since the latter test phenomena can be reproduced and the former cannot, the peculiar test phenomenon is attributed to artificial test errors (Ottiger et al., 2006; Pini et al., 2010). Even though the smooth CO_2 excess adsorption isotherms have been observed, an optimized model for modeling both the Gibbs excess and absolute adsorption uptake is still needed. Despite extensive researches for $scCO_2$ adsorption in manmade materials, a number of semi-empirical models have been adopted by revising the classic D-A, D-R, Langmuir and Toth equations to describe the sorption behavior of $scCO_2$ in coal by fitting each isothermal adsorption curve independently (Sudibandriyo et al., 2003; Fitzgerald et al., 2005; Bae et al., 2006; Ottiger et al., 2006; Sakurovs et al., 2007; Day et al., 2008; Pini et al., 2010; Schell et al., 2012; Weniger et al., 2010; Song et al., 2015; Luo et al., 2015). However, all these models are cling to either the empirical density of adsorbed carbon dioxide (density of liquid carbon dioxide) in coal or the assumed constant volume of adsorbed carbon dioxide in coal. Even though good fitting results are obtained by each researcher, the physical meaning of the obtained parameters from these revised classical equations still needs to be confirmed. Furthermore, even though coal swelling phenomena has been observed, few models take the coal swelling into consideration to obtain absolute isotherms from Gibbs excess isotherms (Ozdemir et al., 2003; Romanov et al., 2006; Pini et al., 2010). Considering both the adsorption and penetration (absorption) CO_2 in coal may explain the coal swelling effect during sorption process. The penetration CO_2 can not only compensate the elastic energy change of coal associated with volume change but also can change the macromolecular structure of coal (Jakubov et al., 2002; Larsen, 2004; Pini et al., 2010). In addition, these models cannot be used to extrapolate isotherms beyond test temperatures. The prediction of adsorption isotherms under high pressure and high temperature geological conditions are critical for carbon dioxide storage capacity estimations in deep subsurface. Therefore, to reasonably interpret the adsorption behavior of $scCO_2$ in coal and predict adsorption isotherms under high temperature and high pressure in-situ conditions, a more concise and robust adsorption model is needed.

As a crucial evaluation index for thermodynamic processes in physical adsorption tests, the isosteric heat of adsorption for $scCO_2$ in coal has rarely been considered by researchers. There are still several issues existing regarding the calculation of this index for $scCO_2$ adsorption in coal (Pan et al., 1998; Chakraborty et al., 2006; Stadie, 2012; Stadie et al., 2013 & 2015). First, the absolute adsorption isotherms must be obtained from the observed adsorption isotherms in order to calculate the isosteric heat of adsorption, where a robust model is needed (Herbst et al., 2002; Bae et al., 2006). Under low pressure conditions, the observed adsorption isotherm approximates absolute adsorption isotherm and there is no need to obtain absolute adsorption isotherms. However, when the Gibbs excess adsorption behavior becomes obvious under higher pressure conditions, a reliable adsorption model is necessary to obtain absolute adsorption uptake from observed adsorption isotherms. Second, even though the absolute adsorption isotherms can be obtained, the classic Clausius-Clapeyron approach is not appropriate because it cannot take the real gas behavior of $scCO_2$ and the adsorbed gas phase into consideration (Pan et al., 1998; Chakraborty et al., 2006; Stadie et al., 2015). Figure 3.3.1 shows the deviation of CO_2 behavior compared with idea gas under different temperatures and pressures. The usage of the Clausius-Clapeyron approach, therefore, will hide the true behavior of the isosteric heat of adsorption because of the ideal gas assumption and the neglect of the volume of the adsorbed gas phase (Chakraborty et al., 2006; Stadie et al., 2015). Therefore, in order to obtain the true behavior of the isosteric heat of adsorption, the above mentioned issues must be reasonably addressed. On the one hand, a robust adsorption model to obtain absolute adsorption isotherms from observed adsorption isotherms is needed. On the other hand, the conventional Clausius–Clapeyron approximation needs to be improved by taking the real gas law of carbon dioxide into consideration to obtain the true isosteric heat of adsorption.

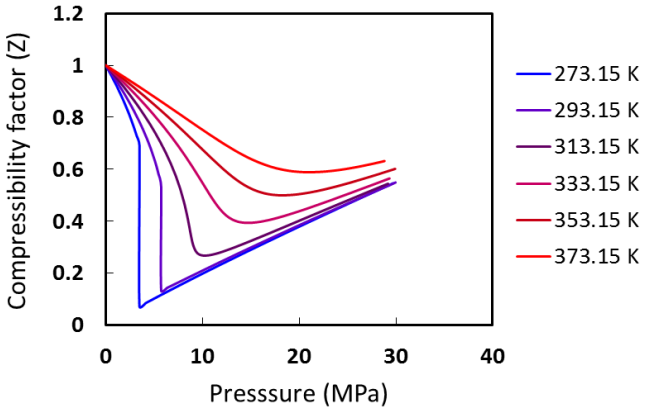

Figure 3.3.1 Deviation behavior of the CO_2 under different temperatures and pressures (Data is obtained from the NIST Standard Reference Database 23 (REFPROP: Version 8.0.))

To tentatively solve the above-mentioned issues, this work first uses a dual-site Langmuir model to describe $scCO_2$ adsorption behavior in coal by considering both the adsorbed phase and absorbed (penetrated) phase. Then, based on the assumption that the density of the adsorbed gas phase is an unknown constant, the authors build in the concept of the Gibbs excess adsorption by applying the dual-site Langmuir model. Next, the published data of high pressure $scCO_2$ adsorption in five different coals are retrieved from literature to validate the proposed model. Last, isosteric heats of adsorption for $scCO_2$ are calculated analytically by considering the real gas behavior of $scCO_2$ and the contribution of the adsorbed and absorbed phase.

3.3.2 Absolute adsorption model

Coal swelling is a pronounced phenomenon associated with CO_2 injection into coal seams, which results in the injection issues in field tests (White et al., 2005; Van Bergen, et al., 2006). Researchers used different approaches such as dilatometric, optical or strain gages, X-ray and small-angle scattering techniques to study the coal swelling effects in a laboratory scale but have not reached an agreement on whether the coal swelling is universal or not. Radlinski et al..(2009) found that coal microstructures were unaffected by exposure to CO_2 pressure over a period of days based on the SANS and USANS tests. Most other researchers agree that the uptake of CO_2 in coal will results in the swelling monotonically with pressure which can be modeled by a Langmuir-type curve based on laboratory evidence as shown in equation (1) (Levine, 1996; Palmer and Mansoori, 1998; Shi and Durucan, 2004a; Cui et al., 2007; Pini et al., 2009 & 2010),

$$\varepsilon_s = \varepsilon_0 \cdot \frac{k_s P}{1 + k_s P} \quad (1)$$

where ε_s is the swelling strain under specific pressure, ε_0 and k_s are fitting coefficients.

Based on the assumption that coal swelling is induced by the CO_2 penetration (absorption) in macrostructure of coal, a dual-site Langmuir model is used for describing both the conventional adsorption of CO_2 in coal and the CO_2 absorption in coal as shown in equation (2) (Fornstedt et al., 1996; Graham et al., 1953; Larsen, 2004; Pini et al., 2010). Figure 3.3.2 shows how the CO_2 phase changes before and after CO_2 sorption: the absolute adsorption is the sum of net adsorption

and absorption uptake. The dual-site model therefore combines both the adsorption and absorption content of CO_2 in coal and both of them show a Langmuir-type term. In addition, the absorption term essentially has similar properties with the coal swelling behavior.

$$n_a = n_{ad}\frac{K_1 P}{1+K_1 P} + n_{ab}\frac{K_2 P}{1+K_2 P} \quad (2)$$

where n_a is the absolute adsorption content under specific pressure, n_{ad} is the net adsorption content, n_{ab} is the absorption content, K_1 and K_2 are corresponding Langmuir contents ($(K_1(T) = A_1 \cdot \exp(-\frac{E_1}{RT})$ and $K_2(T) = A_2 \cdot \exp(-\frac{E_2}{RT})$)), P is pressure.

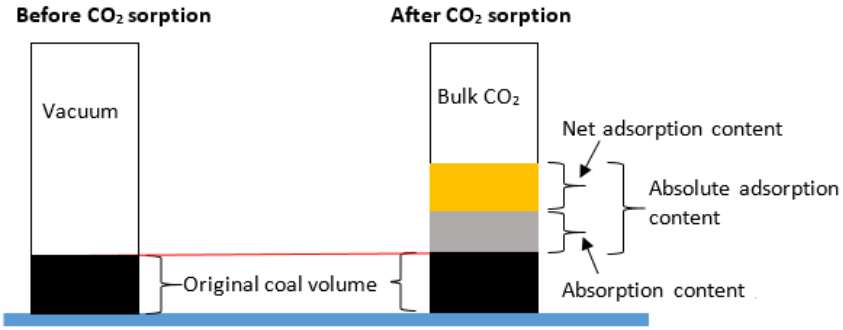

Figure 3.3.2 The difference of CO_2-coal sorption system before and after CO_2 adsorption.

If the absorbed and adsorbed phase can be weighted by a parameter, and equation (2) is rearranged, the following form can be obtained,

$$n_a = n_{\max} \cdot \left[(1-\alpha)\frac{K_1(T)P}{1+K_1(T)P} + \alpha\frac{K_2(T)P}{1+K_2(T)P})\right] \quad (3)$$

It should be pointed out that the physical meaning of $n_{\max}$ in equation (3) is different from the conventional Langmuir equation, which is composed of both the net adsorption content and the absorption content. The term "adsorbed" will be used in the following sections as a simplification which actually refers to both adsorbed and absorbed phases.

3.3.3 Gibbs excess adsorption model and isosteric heat of adsorption

3.3.3.1 Gibbs excess adsorption model

For a pure gas and solid sorption system, the excess adsorbed amount (n_e) can be shown by the Gibbs equation (4),

$$n_e = n_a - V_a \cdot \rho_g = \mathrm{n}_a(1-\frac{\rho_g}{\rho_a}) \qquad (4)$$

where n_e is the excess adsorption content, n_a is the absolute adsorption content, V_a is the total volume of both adsorbed and absorbed phase, ρ_a is the density of adsorbed phase and ρ_g is the density of bulk phase under specific temperature and pressure,. When the V_{ad} is very small, the contribution of the adsorbed gas phase can be neglected and n_e is the approximation of the n_a (Zhou et al., 2001). However, for a high pressure sorption system, the contribution of the adsorbed phase must be taken into consideration to physically interpret the adsorption behavior such as the decreasing observed adsorption uptake with increasing pressures after the maximum observed adsorption uptake. Therefore, it is imperative to find a reasonable approach for obtaining the absolute isotherms from Gibbs excess isotherms considering properties of adsorbed gas phase for gas-solid sorption system under high pressures and temperatures.

Considering the accepted assumption that the density of adsorbed gas phase can be treat as an unknown constant (Agarwal et al., 1988; Zhou et al., 2001; Do et al., 2003; Stadie et al., 2012; Schell et al., 2012; Stadie et al., 2013 & 2015; Tang et al., 2016), the volume of the adsorbed gas phase can be obtained by equation (5),

$$V_a = \frac{n_a}{\rho_a} \qquad (5)$$

Combining equation (3), equation (5) can be rewritten as,

$$V_a = V_{\max} \cdot \left[(1-\alpha)\frac{K_1(T)P}{1+K_1(T)P} + \alpha \frac{K_2(T)P}{1+K_2(T)P}) \right] \qquad (6)$$

where V_a is the total volume of adsorbed gas phase under specific temperature and pressure, V_{max} is the maximum volume at maximum adsorption content, $V_{\max} = n_{\max}/\rho_a$. Combining equation (3), (4) and (6), both excess adsorption (n_e) and surface coverage (θ) equation can be obtained as shown in equation (7) and (8)

$$n_e(P,T) = (n_{\max} - V_{\max} \cdot \rho_g) \cdot \left[(1-\alpha)(\frac{K_1(T)P}{1+K_1(T)P}) + \alpha(\frac{K_2(T)P}{1+K_2(T)P}) \right] \quad (7)$$

$$\theta = (1-\alpha)\frac{K_1(T)P}{1+K_1(T)P} + \alpha\frac{K_2(T)P}{1+K_2(T)P}) \quad (8)$$

If the observed adsorption isotherms (Gibbs excess adsorption isotherms) are obtained through isothermal adsorption tests, equation (8) is able to describe the adsorption behavior where the parameters ($V_{\max}$, $n_{\max}$, $K(T)$) can be easily obtained via curve fitting. The absolute adsorption content can then be obtained via equation (5).

3.3.3.2 Isosteric heat of adsorption

Based on the Clapeyron relationship, it is known,

$$\Delta H_{ad} = (\frac{dP}{dT})_{n_a} \cdot T \cdot \Delta v = (\frac{dP}{dT})_{n_a} \cdot T \cdot (v_a - v_g) \quad (9)$$

Where ΔH_{ad} is the isosteric heat of adsorption, $\Delta v (= (v_a - v_g))$ is the volume change of phase change, v_g is the molar volume of bulk gas phase, v_a is the molar volume of adsorbed gas phase, and T is temperature.

In order to obtain ΔH_{ad}, the $(\frac{dP}{dT})_{n_a}$ must be obtained first (Chakraborty et al., 2006; Stadie et al., 2015). Based on the surface coverage concept (equation (3)), the following relationship can be obtained (Stadie et al., 2014 & 2015),

$$(\frac{dP}{dT})_{n_a} = (\frac{\partial P}{\partial \theta})_{n_a} \cdot (\frac{\partial \theta}{\partial K})_{n_a} \cdot (\frac{\partial K}{\partial T})_{n_a} \quad (10)$$

Combining with equation (10) and (11) and applying the ideal gas law ($Pv_g = RT$), we can obtain one form of isosteric heat of adsorption mathematically (equation 11),

$$-\Delta H_{ads(n_a),IGL} = (\frac{\partial P}{\partial \theta})_{n_a} \cdot (\frac{\partial \theta}{\partial K})_{n_a} \cdot (\frac{\partial K}{\partial T})_{n_a} \cdot T \cdot (\frac{RT}{P} - \rho_a^{-1}) \quad (11)$$

If we combine equation (10) and (11) and apply the real gas law, another analytical form of the isosteric heat of adsorption can be obtained (equation (12),

$$-\Delta H_{ads(n_a),RGL} = \left(\frac{\partial P}{\partial \theta}\right)_{n_a} \cdot \left(\frac{\partial \theta}{\partial K}\right)_{n_a} \cdot \left(\frac{\partial K}{\partial T}\right)_{n_a} \cdot T \cdot (\rho_g^{-1} - \rho_a^{-1}) \qquad (12)$$

Equation (12) and (13) are much easier to solve using the analytical approach. Equation (13) shows the analytical solution of $\left(\frac{dP}{dT}\right)_{n_a}$ (Stadie et al., 2013 & 2015),

$$\left(\frac{\partial P}{\partial \theta}\right)_{n_a} \cdot \left(\frac{\partial \theta}{\partial K}\right)_{n_a} \cdot \left(\frac{\partial K}{\partial T}\right)_{n_a} = \frac{\frac{(1-\alpha)P}{(1+K_1(T)P)^2} \cdot \frac{-E_1 K_1(T)}{RT^2} + \frac{\alpha P}{(1+K_2(T)P)^2} \cdot \frac{-E_2 K_2(T)}{RT^2}}{\frac{(1-\alpha)K_1(T)}{(1+K_1(T)P)^2} + \frac{\alpha K_2(T)}{(1+K_2(T)P)^2}} \qquad (13)$$

Using dual-site Langmuir adsorption model, absolute adsorption isotherms can be obtained without any subjective assumptions from the excess adsorption isotherms. The isosteric heat of adsorption can be calculated considering the real gas behavior and the contribution of adsorbed and absorbed phase, and both of them are not considered in the classic Clausius-Clapeyron approximation.

3.3.4 Data set acquisition and processing

The study of $scCO_2$ adsorption in coals are limited in literature. Two data sets are directly retrieved from the literature (Song et al. (2015); Ottiger et al., 2006). All these data were measured using gravimetric approach to obtain the $scCO_2$ sorption isotherms in dry coal under different temperatures and pressure (>=15MPa). Detailed information about these tests are referred the original publications. The pertinent data from these papers are shown in Figure 3.3.3.

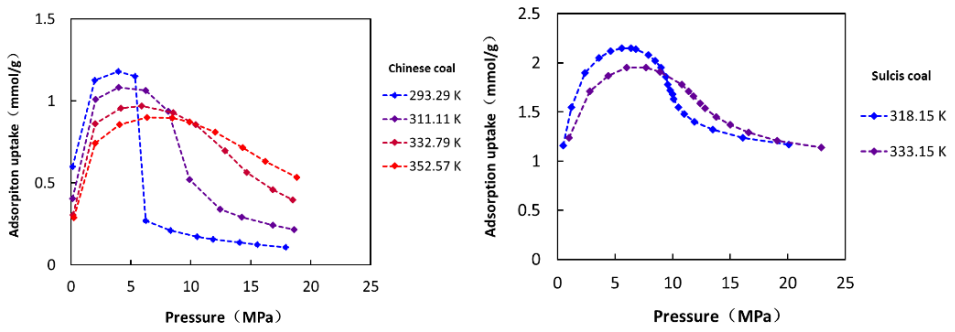

Figure 3.3.3 Experimental data retrieved from Song et al.(2015), Ottiger et al.(2006); the dotted line is to connect data points for visualization.

The observed adsorption isotherms under different temperatures are fitted simultaneously using equation (7) within the limits of the fitting parameters ($0<n_{max}<100$ mmol/g, $0<V_{max}<100$ cm^3/g,

$0 < \alpha < 1$, 10 kJ/mol <E_1, E_2<100 kJ/mol, 0<A_1, A_2). The test data is processed using the Universal Global Optimization method of the Auto2Fit software (*7D*-soft High Technology Inc., China), and the UGO can find the global maximal/minimal value of any functions without using the initial start values. The obtained fitting parameters are shown in Table 3.3.1.

Table 3.3.1 Fitting parameters (equation (7)) for coal samples

Samples	Temperatures (K)	n_{max}(mmol/g)	V_{max}(cm^3/g)	α	E_1(kJ/mol)	E_2(kJ/mol)	A_1(MPa^{-1})	A_2(MPa^{-1})
Chinese coal	293.29, 311.11, 332.79, 352.55	1.6675	0.0752	0.4941	26.702	25.497	2.15E-04	1.10E-05
Sulcis coal	318.15, 333.15	6.3932	0.2220	0.6612	28.019	36.940	5.16E-05	1.54E-08

Once all the fitting parameters are obtained from fitting the observed adsorption isotherms using equation (7), the absolute adsorption isotherm can be obtained using equation (5). Then, the isosteric heat of adsorption can also be obtained using equations (11) & (12) analytically.

3.3.5. Modeling results and discussions

3.3.5.1 Observed and absolute adsorption isotherms

Figure 3.3.4 shows the dual-site Langmuir model fits observed adsorption isotherms very well. It is clear that the predicted absolute adsorption content of $scCO_2$ increases continuously with increasing pressures. The absolute adsorption content is much higher than Gibbs excess adsorption isotherms. The distinguishable difference between observed and absolute adsorption isotherm implies the significant contribution of the adsorbed layer of $scCO_2$ in coal for absolute adsorption content.

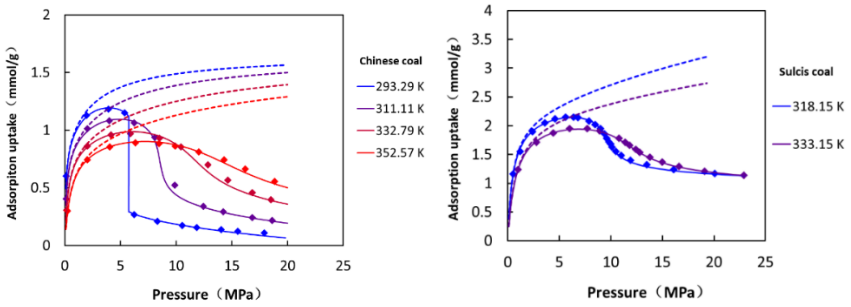

Figure 3.3.4 Fitting adsorption isotherms using dual-site Langmuir model for five coals; solid line: Gibbs excess fitting (equation (8)) and dotted line: absolute adsorption uptake (equation (5))

For both coals, a consistent observed phenomenon is that there are crossovers of the observed adsorption isotherms under different temperatures after the observed adsorption content reached the maximum value. After the crossover, the observed adsorption content at higher temperature is higher than that at low temperatures under same pressure, which cannot reflect the nature of adsorption under different temperatures. However, the nature of adsorption under different temperatures can be shown via the absolute adsorption uptake, where the higher the temperature the lower the adsorption uptake. The abnormal crossover phenomenon of the observed adsorption isotherms appears because the pressure is used as the independent variable, instead of the density of $scCO_2$. Two components of Gibbs excess adsorption uptake (equation (7)), surface coverage (Θ) and the term (n_{max}-V_{max}*ρ (P,T), as a function of pressure and density are shown in Figure 3.3.5. When the pressure is treated as a variable, the term (n_{max}-V_{max}*ρ(P,T)) show temperature as well as pressure dependency feature because of the density of $scCO_2$, ρ(P,T) . However, when the pressure is treated as a density, the term (n_{max}-V_{max}*ρ (P,T) only show pressure-independency feature. Therefore, the cross-over is simply caused by the PVT behavior of $scCO_2$.

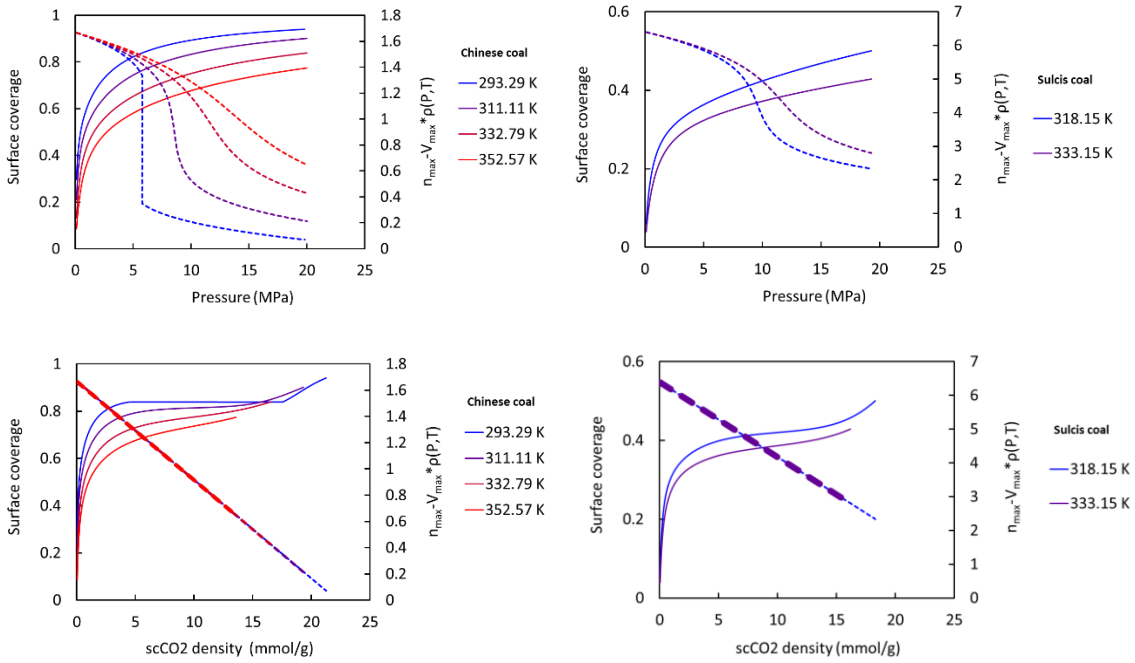

Figure 3.3.5 Surface coverage (solid line, left axial) and the term (n_{max}-V_{max}*ρ (P,T)) (dotted lines, right axial) with increasing pressure (density) for both Chinese and Sulcis coals

3.3.5.2 Adsorption isotherm prediction

For geological storage of carbon dioxide in the subsurface, such as unminable coal seams and shale formations, one of the crucial questions is how to estimate the storage capacity of carbon dioxide under real geological conditions. With increasing depth, both in-situ reservoir pressure and geothermal effects become pronounced, and there will be a phase change of carbon dioxide from subcritical status to supercritical status. Thus, carbon dioxide storage capacity must take high pressure and high temperature conditions into consideration. However, it is impractical to measure all isotherms under different temperatures. Therefore, finding an adsorption model to predict higher temperature adsorption isotherms using lower temperature data also arises researcher's interests.

Predicting isotherms under different temperatures is possible using the proposed model because the temperature dependency of adsorption isotherms are only shown through the Langmuir constant ($K_1(T)$ and $K_2(T)$). Figure 3.3.6 (left part) shows the predicted adsorption isotherms have the same feature of the observed adsorption isotherms, where both the crossovers and the abnormal phenomenon (the higher the temperature the higher the observed adsorption uptake) occur. When the adsorption isotherms are plotted as a function of bulk density, the crossovers disappear, which means the higher the temperature the lower the observed adsorption uptake. This behavior can also be shown in the predicted adsorption isotherms (Figure 3.3.6, right part).

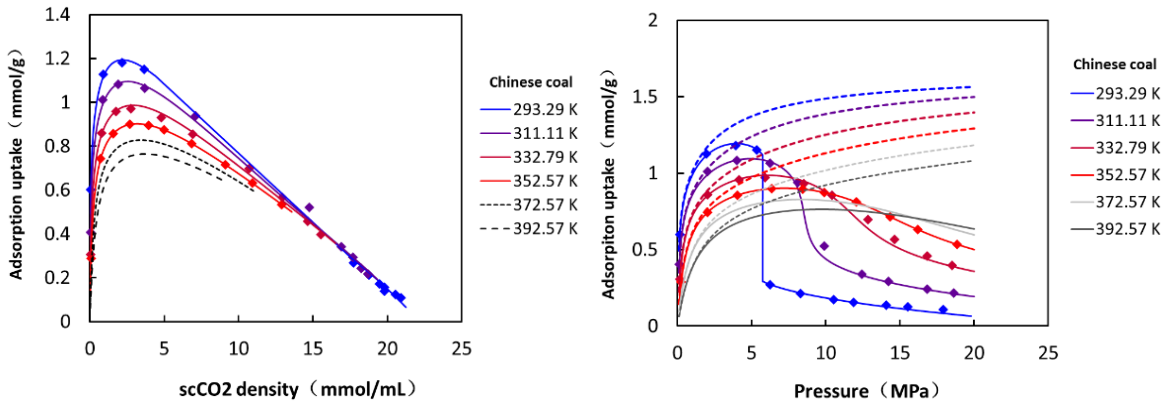

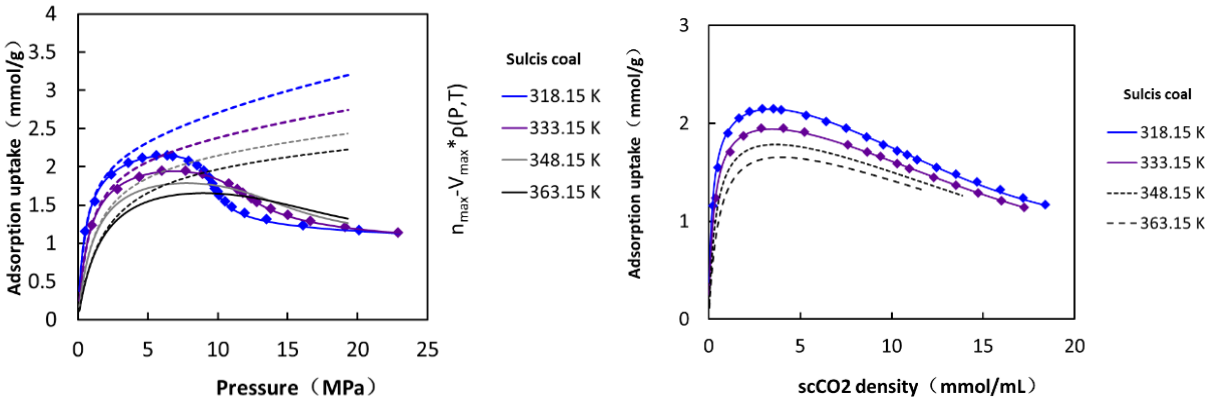

Figure 3.3.6 Prediction of adsorption isotherms (black lines) beyond test data; left: adsorption uptake as a function of pressure, right; adsorption uptake as a function of bulk density.

3.3.5.3 Confidence of the predicted adsorption isotherms

In order to validate the prediction ability of the proposed model, the Chinese coal sample is taken as an example to show the confidence of the predicted adsorption isotherms. First, only three adsorption isotherms from four isotherms are fitted using the proposed method. Then, the predicted adsorption isotherms are compared with the test data to see the difference. Table 3.3.2 shows the fitting parameters use only three adsorption isotherms. Figure 3.3.7 shows all predicted absolute isotherms are consistent with test data. The predicted adsorption isotherms beyond test data are approximately the same. Comparing with Figure 3.3.4, it can be seen the fitting results using four isotherms are always better than predictions using three isotherms. This also means the best-fit parameter can only be achieved using a large set of measured data.

Table 3.3.2 Fitting parameters (equation (7)) for observed adsorption isotherms using only three adsorption isotherms

Samples	Fitting isotherms (K)	Predicted isotherms (K)	n_{max}(mmol/g)	V_{max}(cm^3/g)	α	E1(kJ/mol)	E2(kJ/mol)	A1(MPa^{-1})	A2(MPa^{-1})
Chinese coal	293.29, 311.11, 332.79	352.55, 392.57	1.6837	0.0760	0.5345	26.593	27.244	6.08E-06	1.54E-04
	293.29, 332.79, 352.55	311.11, 392.57	1.6521	0.0745	0.5033	27.632	24.941	1.66E-04	1.44E-05
	293.29, 311.11, 352.55	332.79, 392.57	1.6471	0.0742	0.5050	26.962	25.192	2.05E-04	1.41E-05

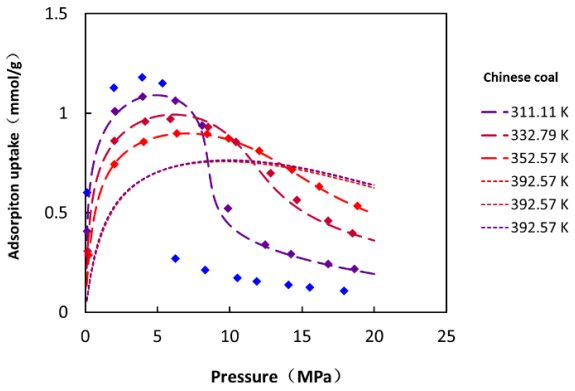

Figure 3.3.7 Adsorption isotherms comparison between fitting data using three low temperature isotherms (dotted dark lines) and fitting data using four temperature adsorption isotherms (solid color lines). Solid symbol represents test data.

3.3.5.4 Thermodynamic analysis of isotherms

Figure 3.3.8 shows isosteric heats of adsorption calcualted using equations (11) and (12) and it can be seen that (i) the isosteric heat of adsorption decreases with increasing absolute adsorption uptake and (ii) temperature dependence of the isosteric heat of adsorption. It is also clear that the isosteric heats of adsorption using the ideal gas law are always higher than that using the real gas law at the same temperature. This means the isosteric heats of adsorption using the ideal gas law always overestimate the isosteric heat of adsorption. Both the temperature dependency and adsorption uptake dependency of the isosteric heat can also be readily shown using the proposed approach.

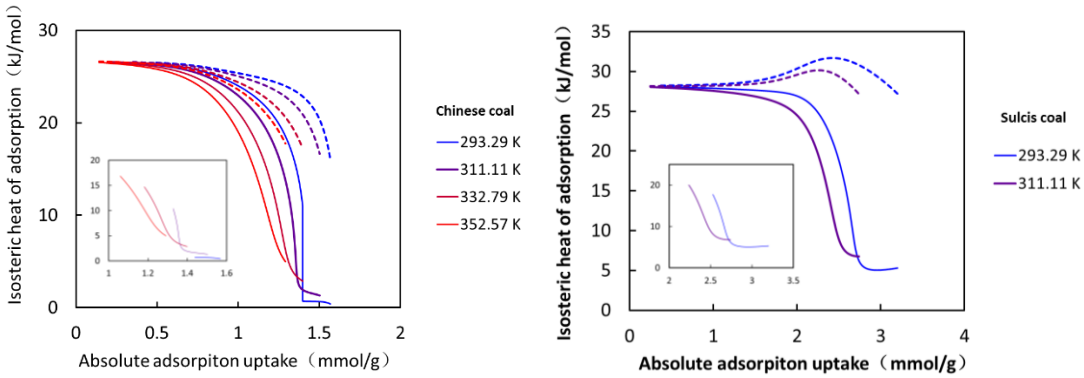

Figure 3.3.8 Comparison of different isosteric heats of adsorption for $scCO_2$ in coal: isosteric heat of adsorptions using ideal gas law (dotted lines) and real gas law (solid lines), and the gas phases are supercritical and liquid in the magnified area.

After carbon dioxide becomes $scCO_2$ (or liquid CO_2), the heat of adsorption shows different behaviors as shown in the magnified area in Figure 3.3.8. When the CO_2 is in liquid phase, the isosteric heat of adsorption is the lowest compared with $scCO_2$. When the CO_2 becomes $scCO_2$, the isosteric heat of adsorption decreases with increasing absolute adsorption uptake but there are crossovers of isosteric heat of adsorption under different temperatures, which has not been reported for other gases in literature. This can be attributed to the enhanced interaction among adsorbed phase over the coal surface at higher density (Schaef et al, 2013). Figure 3.3.9 shows the density at low temperature is much higher than that at high temperature for $scCO_2$, which may strengthen the enhanced interaction effect.

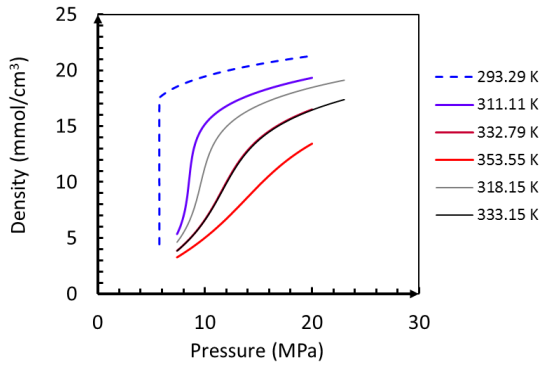

Figure 3.3.9 Density of liquid and $scCO_2$; dotted line represents liquid carbon dioxide and solid line represents $scCO_2$

3.3.6 Implications for geological carbon dioxide storage

Caron dioxide storage in deep unminable coal seams and deep shale formations are two of the promising geological sites for onshore carbon sequestrations. Since the adsorption phase of carbon dioxide in coal is one of the main components of the total carbon dioxide gas-in-place in the subsurface, the accurate prediction of adsorption carbon dioxide in coal is crucial. With increasing depth, high pressure and high temperature geological situation has to be accounted for. Such geological conditions result in the phase change of carbon dioxide from subcritical phase to supercritical phase, and an optimized model is needed to model such behavior of carbon dioxide. The proposed dual-site Langmuir model can describe both the observed adsorption and the absolute adsorption of sub- and super-critical carbon dioxide adsorption in coal. In order to accurately assess the storage capacity of $scCO_2$ in coal, the equation (14) should be used for the total carbon dioxide gas-in-place (GIP) in the subsurface (Tang et al., 2016),

$$GIP = n_e + V_{tot}\rho_g \quad (14)$$

Where n_e is the observed adsorption uptake (Gibbs excess adsorption uptake), V_{tot} is the total pore space of coal, ρ_g is the density of bulk gas. Equation (14) supports that if the observed adsorption isotherms are obtained from laboratory tests, the carbon dioxide storage capacity can be accurately assessed and there is no need to differentiate absolute adsorption content from observed adsorption isotherms. However, this is only valid for estimating the total storage capacity of coal seams. In order to understand the existing status of injected carbon dioxide in coal and carbon dioxide transport behavior under reservoir conditions, the true ratio between bulk carbon dioxide and adsorbed phase must be known. Using the observed adsorption isotherms (Gibbs excess adsorption isotherms) will always underestimate the true content of adsorbed phase as shown in Figure 3.3.4. The dual-site Langmuir model can solve this problem by extrapolating the true content of the adsorbed phase (equation (3)) from observed adsorption isotherms. Furthermore, for large scale carbon dioxide injection test in subsurface coal seams, one of the fundamental questions is to understand how the injected carbon dioxide transports in the coal seams (Tang et al., 2015). Since carbon dioxide existed in coal seams mainly in two phases (free gas and adsorbed gas), the adsorbed phase does influence the transport behavior of carbon dioxide because it not only occupies spaces in nanopores but also interacts with pore walls. It has been found that the adsorbed gas phase significantly affects adsorptive gas (methane) transport in coal seams and shale formations (Yu et al., 2014; Akkutlu et al., 2012; Civan et al., 2011; Singh et al., 2016; Naraghi et al., 2015; Wu et al., 2016). This situation will occur for carbon dioxide transports in coal. Therefore, in order to build a reasonable gas transport model for carbon dioxide transport in coal seams, the very first step is to obtain the true ratio of free phase to adsorbed phase (Tang et al., 2016). The proposed single-site Langmuir adsorption model will make this possible.

3.3.7 Conclusions

This work uses a dual-site Langmuir adsorption model to describe high pressure carbon dioxide adsorption in coal by considering both adsorbed phase and absorbed phase based on the assumption the density of the adsorbed and absorbed phase is an unknown constant. Then, the isosteric heat of adsorption are calculated analytically by considering both the real gas behavior and the adsorbed gas phase. Last, the published data for high pressure carbon dioxide adsorption in coal are retrieved to verify the proposed model.

Modeling results reveal the proposed model can not only reasonably address observed test phenomena but also has the intrinsic ability to extrapolate adsorption isotherms under different temperatures beyond test data. It was found that the crossovers of the observed adsorption isotherms under different temperatures are caused by the changing volume of the adsorbed and absorbed gas phase during adsorption process.

Both the temperature dependence and absolute adsorption uptake dependence of the isosteric heat of adsorption are readily investigated for $scCO_2$ adsorption in coal; for subcritical carbon dioxide, the higher the temperature the lower the isothersteric heat of adsorption and the higher the absolute adsorption uptake the lower the isothersteric heat of adsorption. The gas behavior significantly affects the quantity of isosteric heat of adsorption: the isosteric heat of adsorption using ideal gas law always overestimates isosteric heat of adsorption for $scCO_2$ adsorption in coal. For $scCO_2$ adsorption in coal, there exists an abnormal phenomenon that the higher the temperature the higher the isosteric heat of adsorption, which has not been reported in literature.

The proposed adsorption model lays the foundation for accurately estimating the storage capacity of carbon dioxide, differentiating the true ratio between adsorbed phase and bulk phases and developing gas transport by considering adsorbed phase effect. The thermodynamic analysis is helpful for interpreting temperature related phenomena associated with carbon dioxide adsorption in coal.

Acknowledgements

Financial assistance for this work was provided by the U.S. Department of Energy through the National Energy Technology Laboratory's Program under Contract No. DE-FE0006827.

References

Grubb, M. (1995). Seeking fair weather: ethics and the international debate on climate change. International Affairs (Royal Institute of International Affairs 1944), 463-496.

Stern, N. (2009). The global deal: Climate change and the creation of a new era of progress and prosperity. PublicAffairs.

Morgan, J., Dagnet, Y., & Tirpak, D. (2014). Elements and ideas for the 2015 Paris agreement. Washington, DC: Agreement for Climate Transformation.

The Paris Protocol – A blueprint for tackling global climate change beyond 2020 (2015): http://eur-lex.europa.eu/legal-content/EN/TXT/?qid=1425546396765&uri=COM:2015:81:FIN

Herzog, H. J. (2001). Peer reviewed: what future for carbon capture and sequestration?. Environmental science & technology, 35(7), 148A-153A.

White, C. M., Strazisar, B. R., Granite, E. J., Hoffman, J. S., & Pennline, H. W. (2003). Separation and capture of CO2 from large stationary sources and sequestration in geological formations—coalbeds and deep saline aquifers.*Journal of the Air & Waste Management Association*, *53*(6), 645-715.

Metz, B., Davidson, O., de Coninck, H., Loos, M., & Meyer, L. (2005). Carbon dioxide capture and storage.

Benson, S. M., & Cole, D. R. (2008). CO2 sequestration in deep sedimentary formations. Elements, 4(5), 325-331.

Orr, F. M. (2009). Onshore geologic storage of CO2. Science, 325(5948), 1656-1658.

Figueroa, J. D., Fout, T., Plasynski, S., McIlvried, H., & Srivastava, R. D. (2008). Advances in CO 2 capture technology—the US Department of Energy's Carbon Sequestration Program. International journal of greenhouse gas control, 2(1), 9-20.

White, C. M., Smith, D. H., Jones, K. L., Goodman, A. L., Jikich, S. A., LaCount, R. B., ... & Schroeder, K. T. (2005). Sequestration of carbon dioxide in coal with enhanced coalbed methane recovery a review. Energy & Fuels,19(3), 659-724.

Mazzotti, M., Pini, R., & Storti, G. (2009). Enhanced coalbed methane recovery. The Journal of Supercritical Fluids, 47(3), 619-627.

Busch, A., & Gensterblum, Y. (2011). CBM and CO2-ECBM related sorption processes in coal: a review. International Journal of Coal Geology, 87(2), 49-71.

Godec, M., Koperna, G., & Gale, J. (2014). CO2-ECBM: A Review of its Status and Global Potential. Energy Procedia, 63, 5858-5869.

Hedges, S. W., Soong, Y., McCarthy Jones, J. R., Harrison, D. K., Irdi, G. A., Frommell, E. A., ... & Brown, T. D. (2005). CO2 Sequestration in Unmineable Coal Seams: Potential Environmental

Impacts (No. DOE/NETL-IR-2005-215; NETL-TPR-1225). National Energy Technology Laboratory (NETL), Pittsburgh, PA, Morgantown, WV, and Albany, OR.

Reucroft, P. J., & Sethuraman, A. R. (1987). Effect of pressure on carbon dioxide induced coal swelling. Energy & Fuels, 1(1), 72-75.

Pan, Z., & Connell, L. D. (2007). A theoretical model for gas adsorption-induced coal swelling. International Journal of Coal Geology, 69(4), 243-252.

Pan, Z., Connell, L. D., & Camilleri, M. (2010). Laboratory characterisation of coal reservoir permeability for primary and enhanced coalbed methane recovery. International Journal of Coal Geology, 82(3), 252-261.

Cui, X., Bustin, R. M., & Chikatamarla, L. (2007). Adsorption-induced coal swelling and stress: Implications for methane production and acid gas sequestration into coal seams. Journal of Geophysical Research: Solid Earth (1978–2012), 112(B10).

Day, S., Fry, R., & Sakurovs, R. (2008). Swelling of Australian coals in supercritical CO 2. International Journal of Coal Geology, 74(1), 41-52.

Stevens, S. H., Spector, D., & Riemer, P. (1998, January). Enhanced coalbed methane recovery using CO2 injection: worldwide resource and CO2 sequestration potential. In SPE International Oil and Gas Conference and Exhibition in China. Society of Petroleum Engineers.

Yamasaki, A. (2003). An overview of CO2 mitigation options for global warming-Emphasizing CO2 sequestration options. Journal of Chemical Engineering of Japan, 36(4), 361-375.

Gunter, W. D., Mavor, M. J., & Robinson, J. R. (2004, September). CO2 storage and enhanced methane production: field testing at Fenn-Big Valley, Alberta, Canada, with application. In Proceedings of the 7th International Conference on Greenhouse Gas Control Technologies (GHGT-7) (pp. 413-422).

Sams, W. N., Bromhal, G., Jikich, S., Ertekin, T., & Smith, D. H. (2005). Field-project designs for carbon dioxide sequestration and enhanced coalbed methane production. Energy & fuels, 19(6), 2287-2297.

van Bergen, F., Pagnier, H., & Krzystolik, P. (2006). Field experiment of enhanced coalbed methane-CO2 in the upper Silesian basin of Poland. Environmental Geosciences, 13(3), 201-224.

Wong, S., Law, D., Deng, X., Robinson, J., Kadatz, B., Gunter, W. D., ... & Zhiqiang, F. (2007). Enhanced coalbed methane and CO 2 storage in anthracitic coals—micro-pilot test at South Qinshui, Shanxi, China. International Journal of Greenhouse Gas Control, 1(2), 215-222.

Ripepi, N. S. (2009). Carbon dioxide storage in coal seams with enhanced coalbed methane recovery: geologic evaluation, capacity assessment and field validation of the central appalachian basin (Doctoral dissertation, Virginia Polytechnic Institute & State University).

Connell, L. D., Pan, Z., Shangzhi, M., Camilleri, M., Down, D., Carras, J., ... & Lupton, N. (2013). Description of a CO 2 Enhanced Coal Bed Methane Field Trial Using a Multi-Lateral Horizontal Well. Energy Procedia, 37, 6760-6768.

Gilliland, E. S., Ripepi, N., Conrad, M., Miller, M. J., & Karmis, M. (2013). Selection of monitoring techniques for a carbon storage and enhanced coalbed methane recovery pilot test in the Central Appalachian Basin. International Journal of Coal Geology, 118, 105-112.

Wei, N., Li, X., Fang, Z., Bai, B., Li, Q., Liu, S., & Jia, Y. (2015). Regional resource distribution of onshore carbon geological utilization in China. Journal of CO2 Utilization.

Goodman, A. L., Busch, A., Duffy, G. J., Fitzgerald, J. E., Gasem, K. A. M., Gensterblum, Y., ... & Robinson, R. L. (2004). An inter-laboratory comparison of CO2 isotherms measured on Argonne premium coal samples. Energy & Fuels, 18(4), 1175-1182.

Goodman, A. L., Busch, A., Bustin, R. M., Chikatamarla, L., Day, S., Duffy, G. J., ... & Jing, C. (2007). Inter-laboratory comparison II: CO 2 isotherms measured on moisture-equilibrated Argonne premium coals at 55 C and up to 15 MPa. International Journal of Coal Geology, 72(3), 153-164.

Gensterblum, Y., Van Hemert, P., Billemont, P., Battistutta, E., Busch, A., Krooss, B. M., ... & Wolf, K. H. (2010). European inter-laboratory comparison of high pressure CO2 sorption isotherms II: natural coals. International Journal of Coal Geology, 84(2), 115-124.

Siemons, N., & Busch, A. (2007). Measurement and interpretation of supercritical CO2 sorption on various coals. International Journal of Coal Geology, 69(4), 229-242.

Pini, R., Ottiger, S., Burlini, L., Storti, G., & Mazzotti, M. (2010). Sorption of carbon dioxide, methane and nitrogen in dry coals at high pressure and moderate temperature. International Journal of Greenhouse Gas Control, 4(1), 90-101.

Krooss, B. M., Van Bergen, F., Gensterblum, Y., Siemons, N., Pagnier, H. J. M., & David, P. (2002). High-pressure methane and carbon dioxide adsorption on dry and moisture-equilibrated Pennsylvanian coals. International Journal of Coal Geology, 51(2), 69-92.

Toribio, M. M., Oshima, Y., & Shimada, S. (2004). Evaluation of sequesterable carbon dioxide in Japanese coal samples at sub-critical and supercritical conditions. Studies in Surface Science and Catalysis, 153, 375-380.

Sudibandriyo, M., Pan, Z., Fitzgerald, J. E., Robinson, R. L., & Gasem, K. A. (2003). Adsorption of methane, nitrogen, carbon dioxide, and their binary mixtures on dry activated carbon at 318.2 K and pressures up to 13.6 MPa.Langmuir, 19(13), 5323-5331.

Fitzgerald, J. E., Pan, Z., Sudibandriyo, M., Robinson Jr, R. L., Gasem, K. A. M., & Reeves, S. (2005). Adsorption of methane, nitrogen, carbon dioxide and their mixtures on wet Tiffany coal. Fuel, 84(18), 2351-2363.

Ottiger, S., Pini, R., Storti, G., Mazzotti, M., Bencini, R., Quattrocchi, F., ... & Deriu, G. (2006). Adsorption of pure carbon dioxide and methane on dry coal from the Sulcis Coal Province (SW Sardinia, Italy). Environmental Progress, 25(4), 355-364.

Bae, J. S., & Bhatia, S. K. (2006). High-pressure adsorption of methane and carbon dioxide on coal. Energy & Fuels, 20(6), 2599-2607.

Sakurovs, R., Day, S., Weir, S., & Duffy, G. (2007). Application of a modified Dubinin-Radushkevich equation to adsorption of gases by coals under supercritical conditions. Energy & fuels, 21(2), 992-997.

Day, S., Duffy, G., Sakurovs, R., & Weir, S. (2008). Effect of coal properties on CO 2 sorption capacity under supercritical conditions. International Journal of Greenhouse Gas Control, 2(3), 342-352.

Weniger, P., Kalkreuth, W., Busch, A., & Krooss, B. M. (2010). High-pressure methane and carbon dioxide sorption on coal and shale samples from the Paraná Basin, Brazil. International Journal of Coal Geology, 84(3), 190-205.

Song, Y., Xing, W., Zhang, Y., Jian, W., Liu, Z., & Liu, S. (2015). Adsorption isotherms and kinetics of carbon dioxide on Chinese dry coal over a wide pressure range. Adsorption, 21(1-2), 53-65.

Pini, R. (2014). Interpretation of net and excess adsorption isotherms in microporous adsorbents. Microporous and Mesoporous Materials, 187, 40-52.

Pan, H., Ritter, J. A., & Balbuena, P. B. (1998). Examination of the approximations used in determining the isosteric heat of adsorption from the Clausius-Clapeyron equation. Langmuir, 14(21), 6323-6327.

Chakraborty, A., Saha, B. B., Koyama, S., & Ng, K. C. (2006). On the thermodynamic modeling of the isosteric heat of adsorption and comparison with experiments. Applied physics letters, 89(17), 171901.

Stadie, Nicholas. "Synthesis and thermodynamic studies of physisorptive energy storage materials." PhD diss., California Institute of Technology, 2012.

Stadie, N. P., Murialdo, M., Ahn, C. C., & Fultz, B. (2013). Anomalous isosteric enthalpy of adsorption of methane on zeolite-templated carbon. Journal of the American Chemical Society, 135(3), 990-993.

Stadie, N. P., Murialdo, M., Ahn, C. C., & Fultz, B. (2015). Unusual Entropy of Adsorbed Methane on Zeolite-Templated Carbon. The Journal of Physical Chemistry C, 119(47), 26409-26421.

Radlinski, A. P., Busbridge, T. L., Gray, E. M., Blach, T. P., Cheng, G., Melnichenko, Y. B., ... & Esterle, J. (2009). Dynamic micromapping of CO2 sorption in coal. Langmuir, 25(4), 2385-2389.

Tang, X., Ripepi, N., & Gilliland, E. (2015). Isothermal adsorption kinetics properties of carbon dioxide in crushed coal. Greenhouse Gases: Science and Technology.

Palmer, I., Mansoori, J., 1998. How permeability depends on stress and pore pressure in coalbeds: a new model. SPE Reserv. Eval. Eng. 1, 539–544.

Shi, J.Q., Durucan, S., 2004a. Drawdown induced changes in permeability of coalbeds: a new interpretation of the reservoir response to primary recovery. Transp. Porous Media 56, 1–16.

Cui, X.J., Bustin, R.M., Chikatamarla, L., 2007. Adsorption-induced coal swelling and stress: implications for methane production and acid gas sequestration into coal seams. J. Geophys. Res. [Solid Earth] 112, 1–16.

Pini, R., Ottiger, S., Burlini, L., Storti, G., Mazzotti, M., 2009. Role of adsorption and swelling on the dynamics of gas injection in coal. J. Geophys. Res. [Solid Earth] 114, B04203.

Larsen, J. W. (2004). The effects of dissolved CO2 on coal structure and properties. International Journal of Coal Geology, 57(1), 63-70.

Agarwal, R. K., & Schwarz, J. A. (1988). Analysis of high pressure adsorption of gases on activated carbon by potential theory. Carbon, 26(6), 873-887.

Zhou, L., Zhou, Y., Bai, S., Lü, C., & Yang, B. (2001). Determination of the adsorbed phase volume and its application in isotherm modeling for the adsorption of supercritical nitrogen on activated carbon. Journal of colloid and interface science, 239(1), 33-38.

Do, D. D., & Do, H. D. (2003). Adsorption of supercritical fluids in non-porous and porous carbons: analysis of adsorbed phase volume and density. Carbon, 41(9), 1777-1791.

Do, D. D., & Do, H. D. (1997). A new adsorption isotherm for heterogeneous adsorbent based on the isosteric heat as a function of loading. Chemical engineering science, 52(2), 297-310.

Ozdemir, E., Morsi, B. I., & Schroeder, K. (2003). Importance of volume effects to adsorption isotherms of carbon dioxide on coals. Langmuir, 19(23), 9764-9773.

Romanov, V. N., Goodman, A. L., & Larsen, J. W. (2006). Errors in CO2 adsorption measurements caused by coal swelling. Energy & fuels, 20(1), 415-416.

Jakubov, T.S., Mainwaring, D.E., 2002. Adsorption-induced dimensional changes of solids. PCCP 4, 5678–5682.

Herbst, A., & Harting, P. (2002). Thermodynamic description of excess isotherms in high-pressure adsorption of methane, argon and nitrogen. Adsorption, 8(2), 111-123.

Luo, X., Wang, S., Wang, Z., Jing, Z., Lv, M., Zhai, Z., & Han, T. (2015). Adsorption of methane, carbon dioxide and their binary mixtures on Jurassic shale from the Qaidam Basin in China. International Journal of Coal Geology, 150, 210-223.

Levine, J., 1996. Model study of the influence of matrix shrinkage on absolute permeability of coal bed reservoirs. In: Gayer, R., Harris, I. (Eds.), Coalbed Methane and Coal Geology, vol. 109. Geological Society Special Publication, London, pp. 197–212.

Yu, W., & Sepehrnoori, K. (2014). Simulation of gas desorption and geomechanics effects for unconventional gas reservoirs. Fuel, 116, 455-464.

Akkutlu, I. Y., & Fathi, E. (2012). Multiscale gas transport in shales with local kerogen heterogeneities. SPE Journal, 17(04), 1-002.

Civan, F., Rai, C. S., & Sondergeld, C. H. (2011). Shale-gas permeability and diffusivity inferred by improved formulation of relevant retention and transport mechanisms. Transport in Porous Media, 86(3), 925-944.

Singh, H., & Javadpour, F. (2016). Langmuir slip-Langmuir sorption permeability model of shale. Fuel, 164, 28-37.

Schell, J., Casas, N., Pini, R., & Mazzotti, M. (2012). Pure and binary adsorption of CO2, H2, and N2 on activated carbon. Adsorption, 18(1), 49-65.

Naraghi, M. E., & Javadpour, F. (2015). A stochastic permeability model for the shale-gas systems. International Journal of Coal Geology, 140, 111-124.

Wu, T., & Zhang, D. (2016). Impact of Adsorption on Gas Transport in Nanopores. Scientific Reports, 6.

Tang, X. (2016). Comments on paper "Langmuir slip-Langmuir sorption permeability model of shale". Fuel, 181, 1095.

Tang, X., Ripepi, N., Stadie, N. Yu, L. & Hall, M. (2016) A dual-site Langmuir equation for accurate estimation of high pressure deep shale gas resources. Fuel. DOI:10.1016/j.fuel.2016.07.088.

Schaef, H. T., Glezakou, V. A., Owen, A. T., Ramprasad, S., Martin, P. F., & McGrail, B. P. (2013). Surface condensation of CO2 onto kaolinite. Environmental Science & Technology Letters, 1(2), 142-145.

Chapter 4 Gas adsorption kinetics analysis and pore characterization of coal

4.1 Isothermal adsorption kinetics properties of carbon dioxide in crushed coal

Xu Tang[a]*, Nino Ripepi[a], Ellen Gilliland[a,b]

(a Department of Mining and Minerals Engineering, Virginia Polytechnic Institute and State University, Blacksburg, Virginia, 24060, USA; b Virginia Center for Coal and Energy Research (0411), Virginia Polytechnic Institute and State University, Blacksburg, Virginia 24061, USA)

Abstract: Understanding the dynamic response of coal to carbon dioxide sorption is crucial for optimizing carbon dioxide sequestration in unmineable coal seams and enhanced coalbed methane recovery. In order to explore the adsorption kinetics of carbon dioxide in coal, fifteen isothermal adsorption tests were conducted on bituminous and subbituminous coals at 50℃ for increasing equilibrium pressures (up to 4 MPa). The pseudo-second order (PSO) model is introduced to approximate the carbon dioxide sorption kinetics in coal, and the kinetics properties are then investigated via the PSO model. The linear relationship between (t/q) and (t) is validated and confirmed with a high correlation coefficient (> 99%). The kinetics parameter, k2, decreases with both increasing equilibrium sorption pressure and increasing pressure difference. The sorption equilibrium content, Qe, in each sorption stage depends on both the final equilibrium pressure and the pressure difference. Based on the relationship between sorption content and time, the sorption content for different pressure ranges is predicted using different time intervals. The analysis indicates that the adsorption process for carbon dioxide in coal is a combination of both bulk diffusion-controlled and surface interaction-controlled processes; the former dominates the initial stage while the latter controls the majority of the overall process.

Key words: Coal, Carbon dioxide, Kinetics, Adsorption, Pseudo-second order model

Published in Greenhouse Gases: Science and Technology, DOI: 10.1002/ghg.1562.

4.1.1 Background and introduction

Understanding the carbon dioxide sorption properties of coal is crucial for carbon dioxide sequestration in unmineable coal seams and enhanced coalbed methane recovery.[1] Extensive studies have been conducted to determine what influence moisture, coal rank, temperature and pressure have on the sorption properties of coal gases.[2-8] However, most of the studies focus on the thermodynamic properties of the sorption process (sorption content of gas in coal), which only relates to the ultimate state of the sorption system. Few studies consider the sorption kinetics, which describe changes in the sorption process with respect to time, or the gas transport rate. Having an understanding of sorption kinetics is critical for understanding the sorption mechanism of gas in coal.

Many key research questions surrounding the geological sequestration process relate to the sorption kinetics of carbon dioxide in coal. For example, how quickly the injected CO_2 plume will migrate through a coal seam during injection, how the sorption process will affect the transportation of carbon dioxide in the coal seam, whether continuous injection or intermittent injection is more effective for maximizing storage, and how long it takes for the reservoir to reach new gas-coal sorption equilibrium. All of these issues are related to the kinetics characteristics of gas and coal interactions. Field studies of these variables are costly and time-consuming. Controlled laboratory studies of system kinetics, including isothermal tests, provide the best way to investigate the mechanisms behind these phenomena.

To understand the kinetic properties of the coal and gas sorption system, the gas transport characteristics of the system must be defined in order to determine which factors are influential. Generally, the gas transport in coal can be divided into three stages: ① gas flow in the macropore/cleat system of the coal, ② gas diffusion within the cleat system of coal, and ③ physical interaction of the coal and gas (gas adsorption and desorption on the coal surface). The overall rate of the sorption process may be controlled by any of these three steps or a combination of them. At the laboratory level, the time associated with gas transport in the macropore system can be neglected because of the millimeter-scale coal sample in the test. Thus, step ② and step ③ or their combination controls the entire process. How gas is transported through the micropore system of coal, especially at a nanolevel, is still unknown. Even though the CO_2 desorbs from the

coal surface in only 10 to 50 ms,[9] whether it will influence the overall dynamic equilibrium sorption process is still unknown.

The purpose of this study is to investigate the adsorption processes for carbon dioxide and two types of coal (bituminous and subbituminous coal). Fifteen isothermal adsorption tests were conducted at 50℃ for increasing equilibrium pressures, and the test data were gathered at specific time intervals for up to 14 days. The test data were analyzed using the pseudo-second-order (PSO) kinetics model.

4.1.2 PSO sorption kinetics model

There are only three isothermal adsorption kinetics models which have been applied for gas and coal interactions (shown in Table 4.1.1): the unipore model,[10-19] the bidisperse model,[3, 20-23] and the dynamic diffusion model.[24-26] The first two models are widely used in the CBM industry. The unipore model is used as a theoretical foundation for estimating the lost content during drilling via the Square-Root-Time method. The unipore model is better for high rank coal and the bidisperse model is better for low rank coal.[3]

Table 4.1.1 Comparison of different adsorption kinetics models for gas in coal

Model	Assumptions	Reference
Intraparticle/ Unipore diffusion	Isothermal process; Homogenous pore structure of coal; Independence of diffusion coefficient on gas concentration and location in coal.	10-19
Bidisperse diffusion	Isothermal process; Two distinct pore structures of coal; Independence of diffusion coefficient on gas concentration, time and location in coal.	3, 20-23
Dynamics diffusion	Isothermal process; Natural pore structure of coal; Time-dependent diffusion coefficient	24-26
Surface interaction (PFO and PSO)	Langmuir's sorption assumptions; Sorption kinetics is controlled by the rate of ad/desorption process.	28, 32-35

Many kinetics models for the solid/solution interaction system exist in chemical engineering.[27-31] The kinetics models used in physical chemistry may be used for gas-solid sorption system. There are currently three classic and widely used kinetics models used to describe the adsorption rate for different sorption systems: the pseudo-first-order model, [28,32-33] the pseudo-second-order model,[33-

[34] and the intraparticle diffusion model (unipore model). The PFO and PSO models have been widely used for the solid/solution interaction system to explain the kinetics phenomena occurring in a chemical reaction. This interaction is based on the assumption that the surface interaction (Step ③) dominates the kinetics process, and the rate at which molecule of the adsorbate enter the adsorbed phase either controls the overall rate of the sorption process or is involved in it. Here, the surface interaction includes the actual chemical bond reaction on the surface of the adsorbent and the physical interaction such as van der Waals forces.[27] Both Azizian (2004)[28] and Liu et al (2008)[33] show that the PFO and PSO models are special cases for the Langmuir rate equation. They also point out that these models can be used to describe chemical or biosorption systems in addition to other sorption systems. [28-30, 33]

(1) Pseudo-first-order model (PFO)

The PFO, also called Lagergren equation has the following differential form, [32]

$$\frac{dQ_t}{dt} = k_1(Q_e - Q_t) \qquad (1)$$

where Q_t is the amount of gas adsorbed on the surface of adsorbent, Q_e is the equilibrium value of Q_t, t is time, and k_1 is the PFO rate coefficient, or the time-scaling factor describing how fast equilibrium can be reached in the system. In Integral equation (2), the PFO model is obtained.

$$Q_t = Q_e(1 - \exp(-k_1 t)) \qquad (2)$$

The published literature shows that the PFO model is more reasonable when the change in adsorbed gas density is small or the change of surface area covered in sorbent is small.[28-33] This condition does not apply to the gas and coal sorption system. However, as a parallel model, the PSO model is more applicable when the change of the gas adsorbate density is significant. The PSO model may be used for the gas-solid interaction system.

(2) Pseudo-second-order model (PSO)

The PSO model was first empirically proposed by Blanchard et al (1984)[35] and was later theoretically proven by Azizian (2004)[28]. The PSO model has the following form,[34]

$$\frac{dQ_t}{dt} = k_2(Q_e - Q_t)^2 \qquad (3)$$

where Q_t is the amount gas adsorbed on the surface of adsorbent, Q_e is the equilibrium value of Q_t, t is time, and k_2 is the PSO rate coefficient, a complex function of the density of adsorbed gases. Integral equation (3) produces the PSO model.

$$Q_t = \frac{k_2 Q_e^2 t}{1 + k_2 Q_e t} \qquad (4)$$

Equation (4) can be rearranged in the following form, which is most favorable,

$$\frac{1}{Q_t} = \left(\frac{1}{k_2 Q_e^2}\right) \cdot \frac{1}{t} - \frac{1}{Q_e} \quad (5)$$

Plotting 1/Qt and 1/t gives a linear relationship, where $1/Q_e$ is the intercept of the obtained line and $1/(k_2 Q_e^2)$ is the slope.

Generally, the PFO and PSO models are used for describing the adsorption/desorption kinetics (Step③) when the entire sorption process is controlled by the surface interaction, instead of by the adsorbate mass transfer, as with the unipore model (Step②). Rudzinski et al (2007)[36] proposed a theoretical interpretation for the difference between the diffusion and surface controlled processes via the statistical rate theory method. Miyake (2013)[37] also pointed out that a relationship exists between the PSO rate coefficient, k_2, and the diffusion coefficient within spherical homogenous adsorbent microspheres in the unipore model. This implies that the PSO model may be used to interpret the sorption kinetics for carbon dioxide in coal. Therefore, the PSO model is used here to analyze the kinetics data throughout the sorption process.

4.1.3 Experimental section

4.1.3.1 Sample preparation

The blocks of coal used in this study were obtained from the Pocahontas No. 3. coal seam (bituminous coal) and Eagle Butte coal mine (subbituminous coal). The coal specimens were ground and sieved by 1.0 mm-1.7mm (12-18 U.S. mesh) metal sifters with natural weathering for the isothermal testing. The proximate and ultimate analysis results for the test samples are shown in Table 4.1.2.

Table 4.1.2 Proximate and ultimate analysis of coal (Unit: %)

Proximate analysis				
Coal type	Bituminous coal		Subbituminous coal	
Test samples	As received	Dry basis	As received	Dry basis
Moisture	0.45	--	29.08	--
Sulfur	1.40	1.41	0.64	0.90
Volatile	13.72	13.78	40.89	57.66
Fixed Carbon	67.23	67.53	24.43	34.45
Ash	18.61	18.69	5.60	7.89

Ultimate analysis				
Coal type	Bituminous coal		Subbituminous coal	
Test samples	As received	Dry basis	As received	Dry basis
Moisture	0.45	--	29.08	--
Carbon	72.55	72.88	47.08	66.38
Hydrogen	3.42	3.44	4.00	5.64
Nitrogen	0.83	0.83	0.70	0.99
Oxygen	2.74	2.75	12.91	18.20

4.1.**3.2 Test approach**

All tests were conducted using high temperature and pressure (HTHP) isothermal test equipment made by GoldenAPP of China. The experimental design is based on the manometric method (similar with volumetric approach) using the Sieverts apparatus.[38] The schematic of the setup and the parameters of the sorption system are shown in Figure 4.1.1, and the test parameters are shown in Table 4.1.3. In this approach, a defined amount of gas is transferred from a calibrated reference cell to a test cell containing the sample. The sorption content of gas is the difference between the mass of the transferred gas and the mass of the reference gas. The mass of transferred gas is calculated based on the pressure change of the reference cell. The mass of the reference gas is calculated by multiplying the density of the gas in the test cell and the void volume, which is determined prior to the test using a helium displacement method.

The detailed test procedure is as follows:

1) The weight-measured coal sample is put into the test cell, and the desired sorption pressure equilibrium points are defined using the preset software.

2) Prior to the sorption test, the void volume of the test cell is determined by the helium displacement method. The volume and density of the coal sample can also be obtained here.

3) During the sorption test, predefined amounts of gas are continuously transferred from a calibrated reference volume into the test cell containing the sample.

4) The pressure and temperature of both cells is continuously measured and recorded at certain time intervals throughout the test. These values are used for calculating the mass of the transferred

gas and the mass of reference gas. The measured pressure is also used to determine the sorption equilibrium. A pressure measurement is recorded once the fluctuation error for the measured value in the test cell stabilizes within predefined range or the sorption time reaches the predefined interval. At this point the system is considered to be in sorption equilibrium and step (3) will be repeated for the next defined pressure point.

5) The sorption mass is calculated by the following equation, $m_{sorbed} = m_{tranfer} - m_{reference} = \rho_{tranfer} V_{tranfer} - \rho_{reference} V_{reference.}$ The density of both the free gas and the transferred gas under different pressures and temperatures is obtained from the commercial database (REFPROP) provided by the American National Standards Institute. [39-40]

6) After all defined pressure points are measured the test is complete and is terminated.

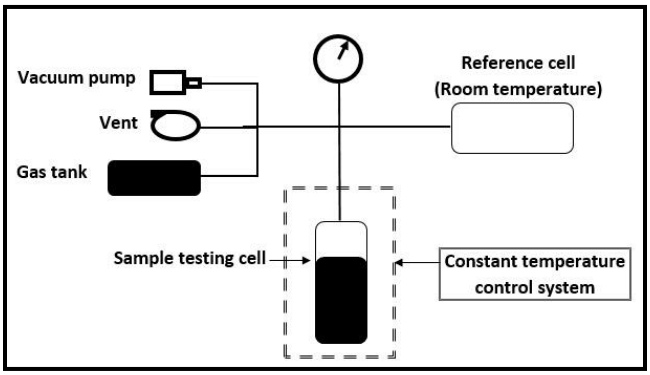

Figure 4.1.1 Schematic of high temperature and pressure (HTHP) isothermal test setup

Table 4.1.3 Test parameters for isothermal sorption system

Sample Parameters			Instrument parameters	
Sample treatment	Natural air dry		Pressure transducer	Accuracy: up to 20 MPa±0.05% F.S. Stability: 0.025% F.S.
Particle size	1.0 mm-1.7mm		Temperature Control	Air bath; Room temperature to 500±1℃
Sample weight	5-6 g		Reference cell	30.3388 mL
Gas purity (CO2)	99.999%		Sample volume	39.8314 mL
Gas purity (He)	99.999%		Dead space volume	Helium displacement tests under five different pressures (up to 5 MPa)
Equilibrium time	Subbituminous: 9-10h; Bituminous: 5-6h.		Equation of state	American National Standards Institute REFPROP data base
Vacuum prior to testing	Yes		Control system	Fully automated control

4.1.3.3 Data collection and processing

The first two sorption stages (Ⅰ) and (Ⅱ) are used as examples in Figure 4.1.2 to help explain the data measurement and recording process described in Step (4) of Section 3.2. In the first sorption stage (Figure 4.1.2), the values of both the pressure and temperature of the test cell and the reference cell are recorded at the incremental point (t_1=0, q_1), then (t_2, q_2) …… and so on (t_n, q_n) (n>1) until the process reaches the first sorption equilibrium points defined in Step 1 of 3.2 Test procedure . The second stage begins at the end point of the first and proceeds in the same way. The time interval between the first two points ($\Delta T=t_1-t_0$) and other points ($\Delta t=t_{n+1}-t_n$) (n>1) is different (Figure 4.1.2); ΔT is around 20 minutes and Δt is around 12 minutes. The ΔT is spent on transferring gas from the reference cell to the test cell, which is necessary for instrument operation. The gas refill process causes the small increase of sorption content in the ΔT. Since the first time interval ΔT is small in comparison to the entire test process, the sorption process analysis in this report will begin at the point t_1 instead of t_0, and end at the next t_0. The total sorption content (Q_t) in each sorption stage consists of two parts. Values for Q_t, Q_n and ΔQ_n (where $Q_t = Q_n+\Delta Q_n$, for n>1) are directly obtained from data recorded during this test. The test data are used to evaluate the quality of the predicted data derived from the kinetics model.

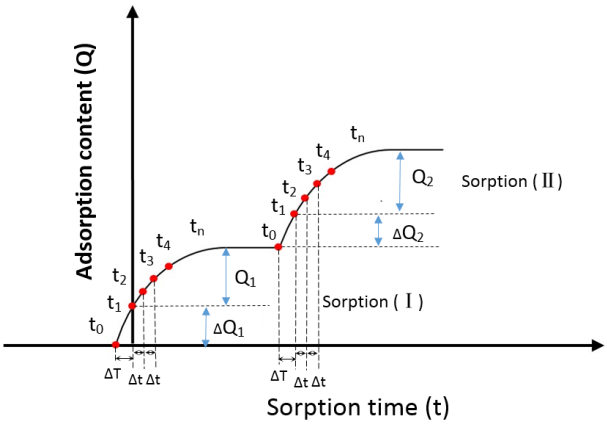

Figure 4.1.2 Time dependent sorption data recording process

4.1.3.4 Determination of sorption equilibrium

Standards for the determination of sorption equilibrium in the coal and gas sorption system have only recently been established. The true equilibrium state for sorption between the coal and gases (CO2, N2, CH4) may never be reached due to kinetics restrictions of gases in coal, but "technical

equilibrium" or "quasi-equilibrium" can be defined, reached and applied during the test.[41-42] Currently, there are two popular methods to determine the equilibrium state: a pressure monitoring approach and a sorption time monitoring approach[43-44]. The former monitors the change of the pressure in the sample cell; if the pressure change of the test cell is within a certain range, the system is treated as having reached its equilibrium state. The latter approach, determined from sorption time, is an empirical method, and different research groups use different sorption times for the isothermal adsorption test. However, both approaches are limited. The shortcoming of the pressure monitoring approach is that it neglects the temperature influence on sorption content during the sorption process. Since the temperature cannot be fully controlled during the sorption process (accuracy of temperature measurement), it may happen that the temperature variation will affect the sorption content change. Another issue is that applying the same equilibrium criteria under different pressures is not reasonable since the sorption pressure interval and sorption equilibrium pressure are different. For the empirical, time determined approach, the equilibrium time varied from laboratory to laboratory and is hard to evaluate. Generally, a longer time produces more accurate results, but too long of a waiting time cannot provide the quick turnaround needed to serve the industry. In this test, the sorption equilibrium status is determined by a sorption time monitoring approach based on the author's technical experience. The equilibrium times for subbituminous coal and bituminous coal are 9-10h and 5-6 h, respectively.

4.1.4 Test results

As shown in Figure 4.1.3, changes in the isothermal sorption content with time are recorded during the sorption process in eight different pressure ranges (MPa) under 50℃. To compare the sorption processes over different pressures, each sorption process is extracted (right side of Figure 4.1.3). Figure 4.1.4 shows the isothermal adsorption curves of both bituminous coal and subbituminous coal. The adsorption capacity of bituminous coal is higher than the subbituminous coal.

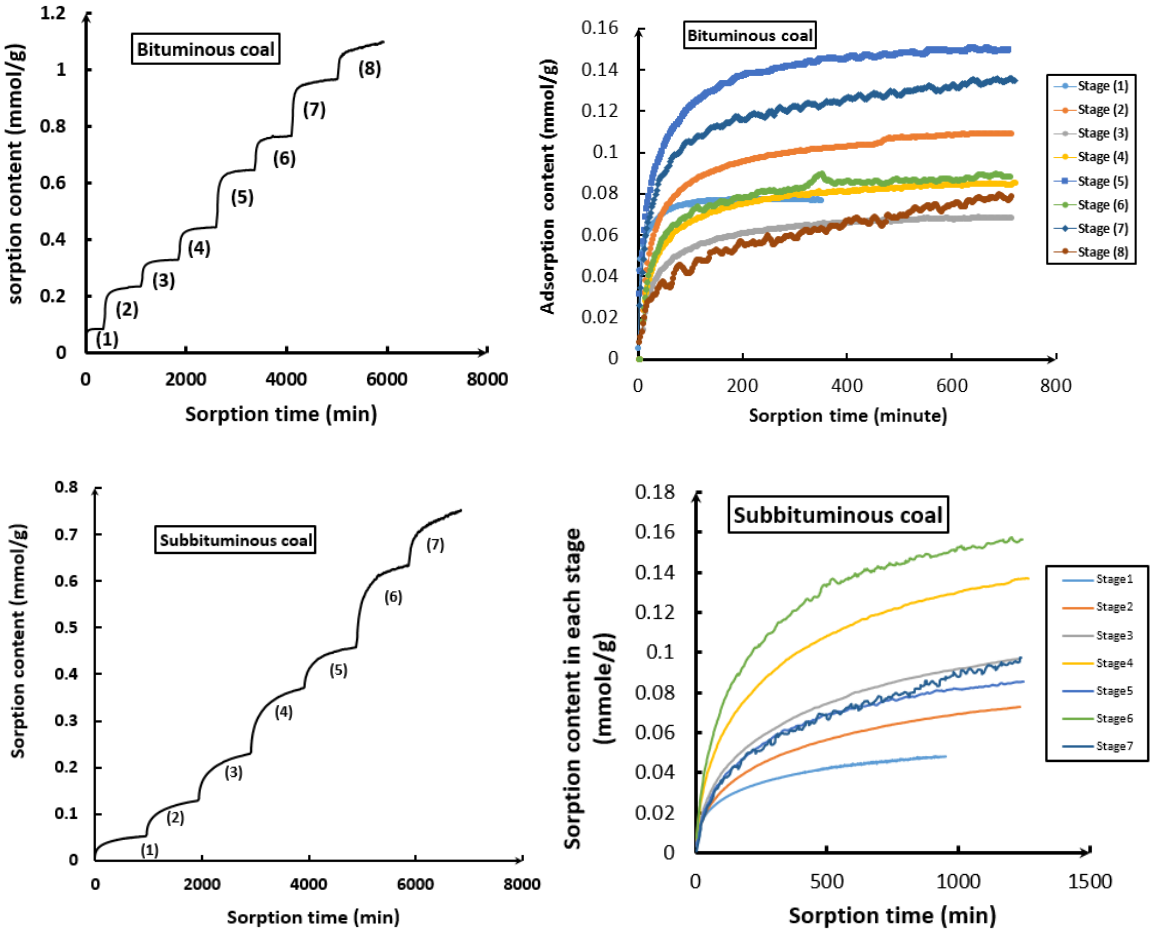

Figure 4.1.3 Relation between isothermal sorption content and time at 50℃ for bituminous and subbituminous coal

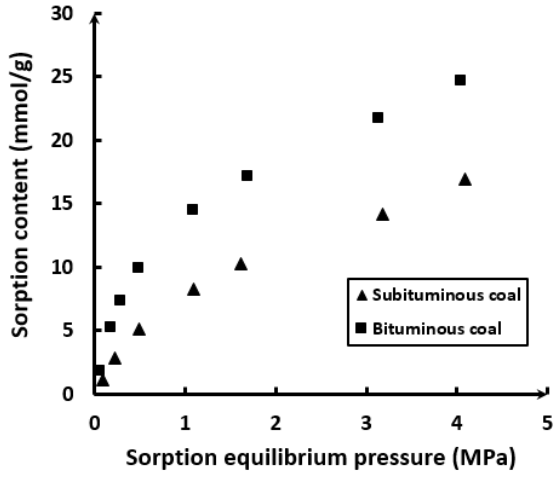

Figure 4.1.4 Isothermal adsorption curves for bituminous and subbituminous coal at 50℃

Figure 4.1.3 shows there are sorption content fluctuations when the sorption pressure increases during stages (5-8) for the bituminous coal and during stages (6-7) for the subbituminous coal. These fluctuations are inevitable and are caused by pressure measurement error and temperature influence. The pressure transducer is of very high precision (0.05% of full scale) and is able to monitor and record slight changes occurring in the test cell. When the test cell pressure increases, the corresponding measurement error also increases, ultimately causing the fluctuation in sorption content (Figure 4.1.5). It is also clear that the sorption process in stages 7-8 for the bituminous coal and stages 6-7 for the subbituminous coal are different from other processes (discussed in Section 5.1.). Another factor contributing to the fluctuations is related to the calculation of the sorption content, which is based on the density of gas under different pressures and temperatures. The fluctuation of the sorption content is the integrated effect of both temperature and pressure variation. In the later sorption stages, as the absolute sorption pressure increases, the absolute sorption content becomes smaller. The measurement error resulting from both the pressure measurement error and the temperature error will be magnified compared to the previous stages.

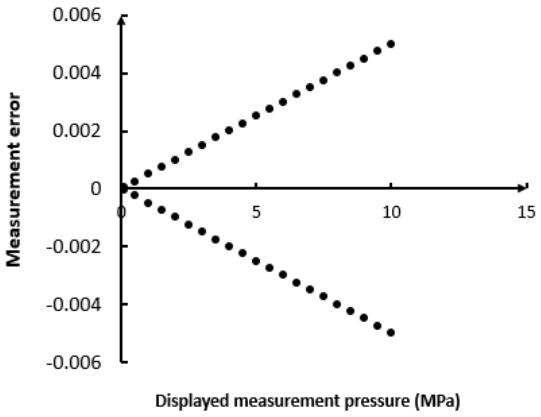

Figure 4.1.5 Measurement error of the pressure transducer

4.1.5 Discussion

4.1.5.1. PSO model application

First, the physical meaning of the kinetics parameter in equation (5) of the gas-solid system needs to be explained. Here, Q_e represents the equilibrium sorption content in each sorption stage under different pressure ranges, and the k_2 represents the other kinetics parameter used to evaluate the sorption process. The linear relationship between t/Q_t and t is used to fit the data, which correspond

very well to the test data (Figures 4.1.6 and 4.1.7, Table 4.1.4). The equilibrium sorption content (Q_e) and kinetics parameter (k_2) in each sorption stage are also obtained (Table 4.1.4).

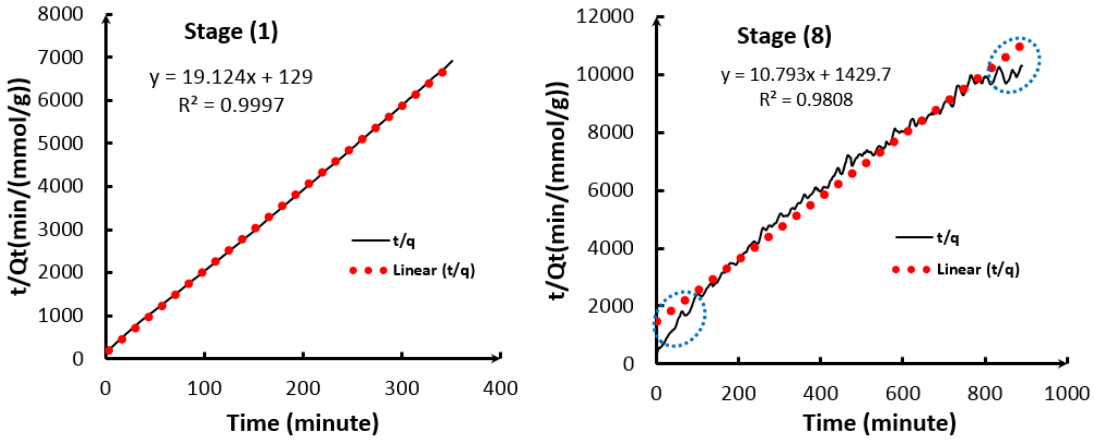

Figure 4.1.6 Linear relationship between t/Qt and t: stage (1) and stage (8) for bituminous

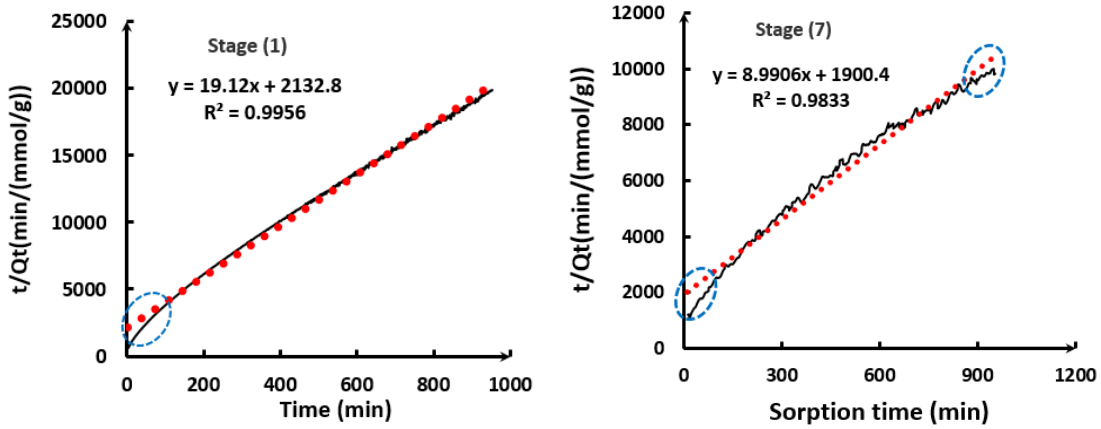

Figure 4.1.7 Linear relationship between t/Qt and t: stage (1) and stage (8) for sub-bituminous coal

Figures 4.1.6 and 4.1.7 show that, even though the curves show a very highly fitting trend (R2>0.98), there are deviations in the initial test stage and the final test stage (blue circles). In the initial test stage, the diffusion-controlled process dominates the process; carbon dioxide molecules are adsorbed on the surface of coal and/or fill pore spaces as a result of the increase of pressure in each stage. At this time, the increasing pressure increases the density of the gas molecules inside the pores of the coal and is the controlling factor in the sorption system compared to interactions among gas molecules. This is supported by the unipore model, which is applicable when $Q_t/Q_\infty<0.5$[45] and which has bulk diffusion as the controlling factor in the initial adsorption stage.

In the following stages, the interaction among the gas molecules becomes dominant (linear relationship between sorption content and time), which means the dynamic process of gas adsorption/desorption controls the system. This is the point where the PSO model can be applied. As shown in Figure 4.1.6 and 4.1.7, the diffusion-controlled process is only a small part of the total sorption process and does not significantly influence the overall sorption process.

Table 4.1.4 PSO model fitting data

Coal samples	Sorption process	PSO model linear fitting	R^2	Q_e(mmol/g)	k_2
Bituminous coal	Stage (1)	y = 19.1240x + 1290	0.9997	0.0523	2.8351
	Stage (2)	y = 8.7926x + 296.16	0.9992	0.1137	0.2610
	Stage (3)	y = 14.027x + 430.78	0.9997	0.0713	0.4567
	Stage (4)	y = 0.4195x + 13.077	0.9997	0.0883	0.3634
	Stage (5)	y = 6.4357x + 168.09	0.9999	0.1554	0.2464
	Stage (6)	y = 10.935x + 307.90	0.9992	0.0914	0.3884
	Stage (7)	y = 7.0164x + 300.72	0.9986	0.1425	0.1637
	Stage (8)	y = 10.793x + 1429.7	0.9808	0.0927	0.0815
Subbituminous coal	Stage (1)	y = 19.137x + 2122.1	0.9955	0.0562	0.1726
	Stage (2)	y = 12.236x + 1838.1	0.9925	0.0855	0.0815
	Stage (3)	y = 9.0867x + 1442.7	0.9927	0.1139	0.0574
	Stage (4)	y = 6.5057x + 924.43	0.9952	0.1577	0.0458
	Stage (5)	y = 10.431x + 1451.2	0.9963	0.0984	0.0750
	Stage (6)	y = 5.7648x + 655.78	0.9982	0.1926	0.0507
	Stage (7)	y = 9.0223x + 1880.2	0.9833	0.1332	0.0433

Reviewing the sorption content curves in Figure 4.1.3, it can be found that the sorption content in stages (7-8) of bituminous coal and stages (6-7) of subbituminous coal shows an increase compared to previous stages. This could be due to capillary condensation the mesopore system of the coal or the pore-filling phenomena which occurs in nanopores.[46-48] In addition, since the coal sample is dried naturally, the presence of residual water vapor inside the coal may also contribute to the carbon dioxide condensation.[49-50] Therefore, the conventional sorption equilibrium determination approach cannot be applied in these stages.

4.1.5.2 Kinetics parameters analysis using PSO model

As shown in Figure 4.1.8 (A & C), as the equilibrium sorption pressure increases, the equilibrium sorption content in each stage appears to initially increase and then begins to fluctuate. No consistent quantitative relationship can be obtained from current data. Figure 4.1.8 (B &D) shows that an increase in pressure difference causes a general but unstable increase in the equilibrium sorption content. When the pressure differences are approximately the same, the stage of low

sorption equilibrium pressure results in a higher sorption content than the stage of high sorption equilibrium pressure (red ellipse in Figure 4.1.8 (B)). Figure 4.1.8 (A-D) also show the sorption content in each sorption process (1-8) is controlled by both the final equilibrium pressure and the pressure difference. For the bituminous coal, the maximum sorption content occurs at a sorption equilibrium pressure of 1.0884MPa with a pressure difference of 0.6018MPa, and the minimum sorption content occurs at the first sorption pressure point of 0 MPa with a pressure difference of 0.064MPa. For the subbituminous coal, the maximum sorption content occurs at a sorption equilibrium pressure of 3.1822MPa with a pressure difference of 1.5608MPa, and the minimum sorption content occurs at the first pressure point of 0 MPa with a pressure difference of 0.0889MPa.

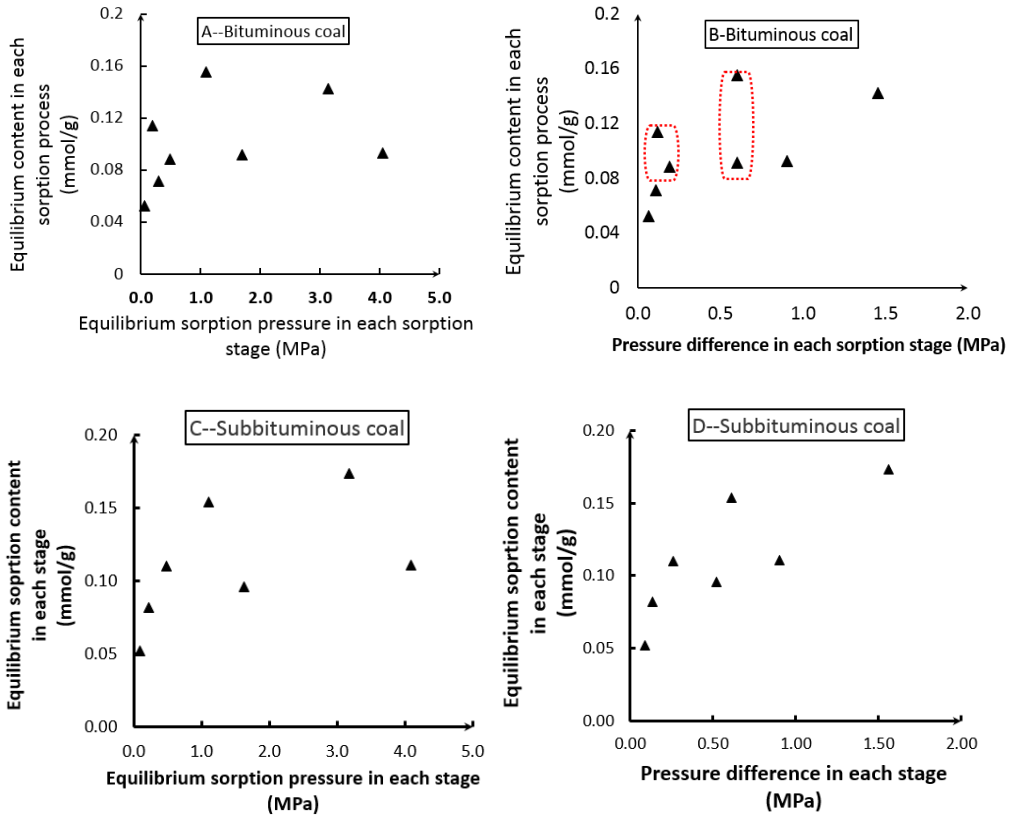

Figure 4.1.8 Relationship between pressure and kinetics parameter Qe

The kinetics parameter (k_2) decreases as the equilibrium sorption pressure and the pressure difference increase for both bituminous and subbituminous coal (Figure 4.1.9). The highest k_2 value occurs at a pressure of 0.064 MPa for bituminous coal and at a pressure of 0.0368 MPa for subbituminous coal. The lowest k_2 is 0.0815 for bituminous coal at the sorption equilibrium

pressure of 4.0451MPa with a pressure difference of 0.9018MPa, and is 0.0458 for subbituminous coal at a sorption equilibrium pressure of 3.1822MPa with a pressure difference of 1.5608MPa. Figure 4.1.9 also shows that the k_2 of bituminous coal is generally higher than the k_2 of subbituminous coal, which implies that the value of k_2 may be influenced by the coal rank or the affinity of different types of coal.[43] Since the highest k_2 value is obtained in the first sorption stage where the sorption pressure is low (0.064 MPa for bituminous coal and 0.0368 MPa for subbituminous coal), it may indicate the affinity of different types of coal or the retention properties of carbon dioxide on different types of coal.

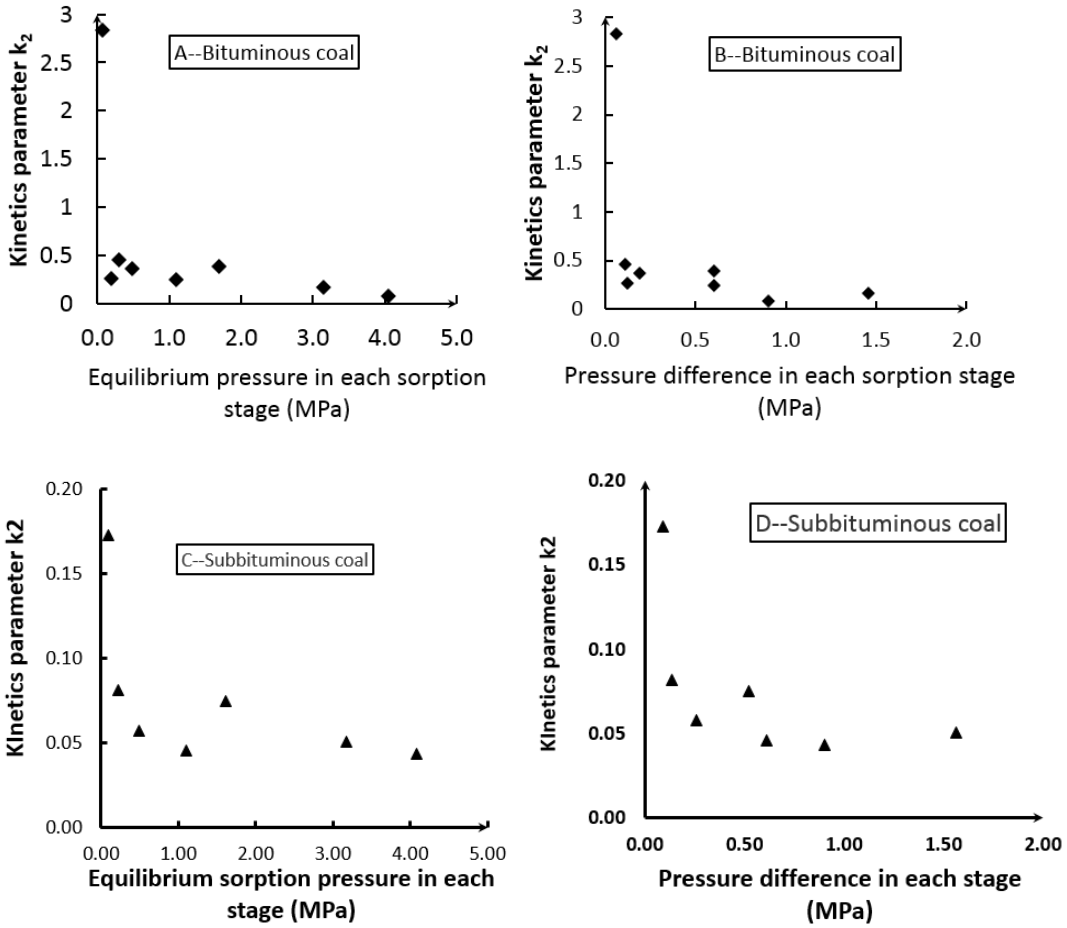

Figure 4.1.9 Relationship between pressure and kinetics parameter k_2

4.1.5.3 Sorption capacity estimation using PSO model

Since sorption equilibrium content (Q_e) is easily obtained from the time and (t/q) linear relationship, it may be possible to determine the (Q_e) using different time ranges under each pressure step. To validate this hypothesis, the initial portion of the sorption-time relationship is used to predict the

final sorption equilibrium status. The different sorption time ranges are analyzed using the PSO model for bituminous and subbituminous coal (same procedure used in Section 5.2). Figure 4.1.10 shows predicted curves for adsorption equilibrium content based on the PSO model for different time intervals (120, 180, 240, 360, 480, 600 min) compared to the measured test data.

The fitting coefficient of the PSO model for each sorption stage is extremely high (> 95%) (Detailed comparison between predicted accumulated sorption content and measured accumulated sorption content in each sorption stage is shown in the Supporting documents). Figure 4.1.10 shows the error analysis for fitting the measured data curves to the PSO model, where the error is the ratio of the difference of the calculated value and test value to test value. For bituminous coal, the lowest error is achieved using the 360-minute predicted sorption-time curve to match the measured test data. The best match for subbituminous coal is the 600-min predicted sorption-time curve. The best-fit curve for each coal type is plotted with the associated measured test data in Figure 4.1.10 and confirms the low error of each match. The predicted results are credible, and the accuracy of the maximum error is within 0.2 percent. The test results support that the sorption-time relationship can be used to predict the final equilibrium sorption content in each sorption stage.

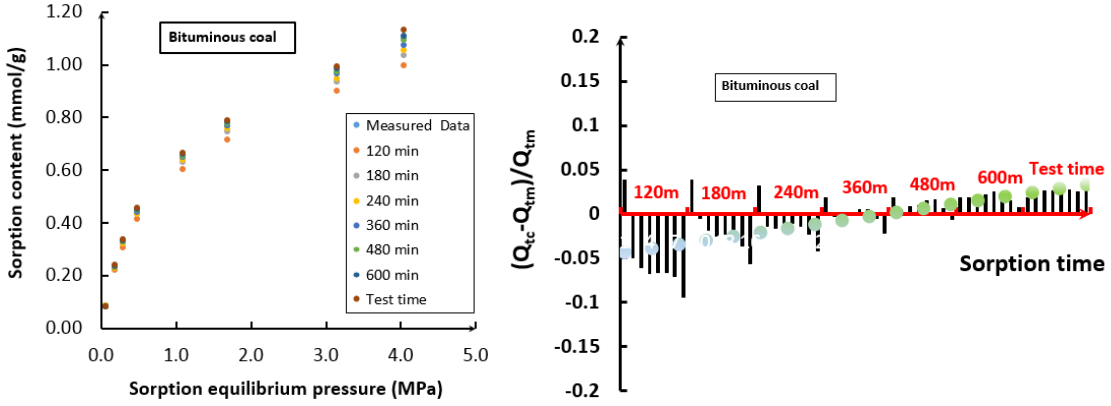

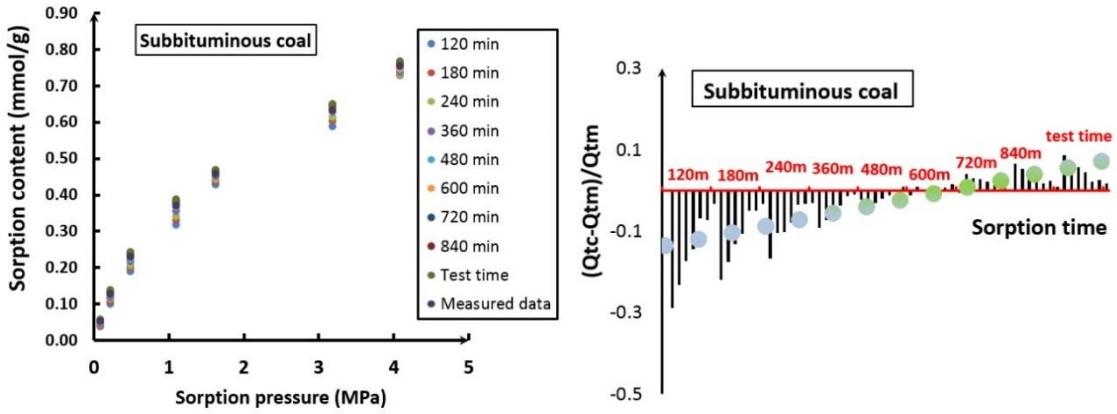

Figure 4.1.10 Isothermal adsorption curves and error analysis; Q_{tc} is the predicted value using PSO value, Q_{tm} is the measured test value.

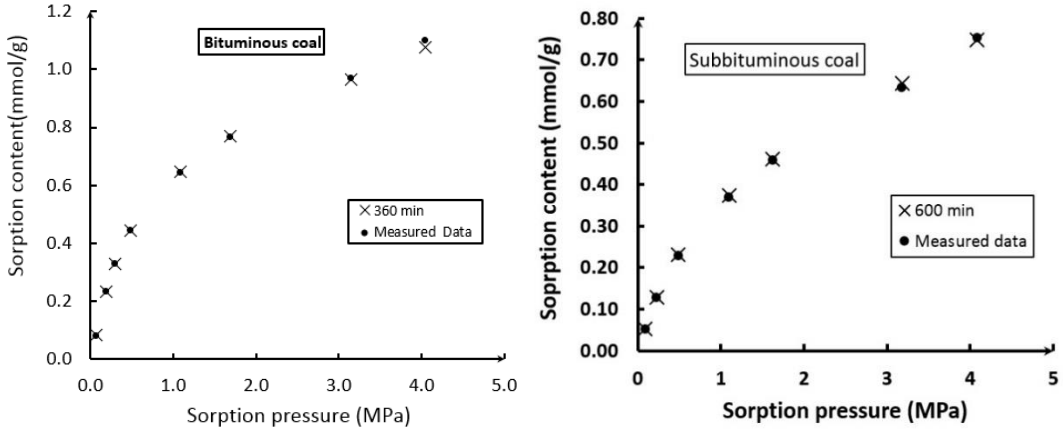

Figure 4.1.11 Comparison between predicted values and measured test data

4.1.5.4 Implication of the PSO kinetics model

Generally, the pore system of coal is complicated and consists of macropores (50nm < pore width), mesopores (2nm <pore width< 50nm), micropores (< 2 nm) (IUPAC, 2001), and submicropores (< 0.4 nm) [51]. The micropore dominates and determines the specific surface area in coal [1,52]. The different types and shapes of pores in coal also complicate gas transport in coal (Figure 4.1.12). The two-ended open pore is easy to access while the one-ended open pore (dead end pore and ink-bottle pore) and closed pore are hard to reach. For the ink-bottle pore, a high external force is needed to push the gas molecule into the pore. This may also be true for narrow channels within the pore system induced by pore wall effects.

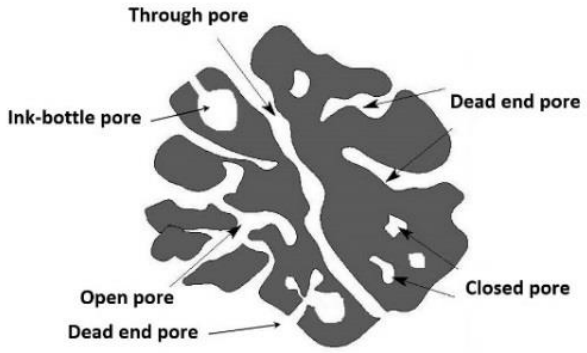

Figure 4.1.12 Generalized pore system in coal

The pressure influenced kinetics parameters (Q_e and k_2) can reveal and describe important physical properties of coal, including the complex pore system, heterogeneous properties of the coal surface, and the approximation of monolayer adsorption or pore-filling effects under low pressures. As shown in Figures 4.1.8 and 4.1.9, there is no consistent relationship between the maximum equilibrium sorption content Q_e and kinetic parameter k_2. This may be attributed to the different size and amount of pores in coal. It could also indicate that the gas easily accesses the coal but does not remain securely stored; the higher kinetic parameter does not mean the highest sorption content. The different sorption contents associated with different pressures also imply a heterogeneous nature of the coal surface. When the carbon dioxide is first exposed to the coal, it can be easily adsorbed in the high potential energy sites induced by pore wall effects. When the pressure is increased, the low sorption potential energy sites are occupied and the interaction of carbon dioxide molecules increases. Once the low sorption potential energy sites are filled, the higher external force is needed to force the carbon dioxide molecule to access the available sorption site and stay stable. The highest kinetics parameter (k_2) in the initial pressure stage implies that monolayer adsorption or pore-filling dominates the adsorption process, which is different from the following sorption stages. Multilayer adsorption or capillary condensation may occur because of the increasing external force and the interaction among gas molecules as the sorption pressure increases.

4.1.5.5 Discussion on PSO model application for the carbon dioxide-coal sorption system

The successful application of the PSO model provides a new viewpoint to understand the carbon dioxide-coal sorption system. The PSO model is based on a surface interaction assumption, which has only two kinetics parameters (Q_e and k_2) and is different than other kinetics models (shown in

Table 4.1.1). The high correlation coefficient (>99%) of the fitted data supports that this model can be used to analyze the sorption kinetics data. This model can also be used to accurately predict equilibrium sorption content under different pressures.

However, does the successful use of the PSO model mean that this model can explain how the carbon dioxide interacts with coal during the adsorption process? Is the simple fitting procedure using the PSO model sufficient for describing carbon dioxide adsorption kinetics in coal? The answer is still unclear. The experimental results suggest the adsorption process for coal and carbon dioxide to be a combination of both bulk diffusion-controlled and surface interaction-controlled processes. For the non-isobaric process associated with the carbon dioxide-coal sorption system, the initial stage is controlled by the bulk diffusion process. This is supported by the deviation of the PSO model fitting process in the initial part of each stage (Figure 4.1.7). It should be noted that this bulk diffusion-controlled process is only a small part of the total process considering the long equilibrium time (Figure 4.1.7). Following the bulk diffusion stage is the surface interaction - controlled sorption process, which requires a long time for the sorption system to reach equilibrium. The surface interaction process dominates the sorption process when the bulk diffusion process becomes less important. As mentioned earlier, the PSO model is based on the surface interaction-controlled sorption That is to say, the surface interaction dominates the sorption process, which is supported by strong curve fitting derived from the PSO model.

It should be noted that, even though the PSO model has been widely used and can reasonably explain most of the liquid-solid sorption processes, there exist some situations where the PSO model is applicable but surface interaction does not dominate the process.[53-54] Therefore, even though the PSO model may not reveal the mechanism behind the carbon dioxide-coal sorption system, it provides an accurate description of the main part of the adsorption process, which is the surface diffusion-controlled process. The relationship between the kinetics parameter (k_2) and pressure shows both the heterogeneous properties of the coal surface and the approximation of monolayer adsorption for low pressures. The linear relationship between sorption content and time can be used to predict the equilibrium sorption content (Q_e) during the sorption process.

4.1.6 Conclusions

To understand the kinetic properties of the dynamic coal-carbon dioxide sorption process, 15 isothermal adsorption tests were conducted at 50℃ for increasing equilibrium pressures (up to 4

MPa) for bituminous and subbituminous coal. The PSO model was used to approximate carbon dioxide adsorption kinetics in crushed coal. Analysis of the measured test data and comparison to model predictions produced the following results:

1) The PSO model can be used to predict credible equilibrium sorption content under different pressures for the carbon dioxide-coal sorption system.
2) A high correlation coefficient (>99%) was obtained for the linear relationship between (Time/Sorption content) and (Time) using the PSO model.
3) The kinetics parameter (k_2) decreases with the increase of both equilibrium sorption pressure and the pressure difference. The sorption equilibrium content (Q_e) in each sorption stage depends on both the final equilibrium pressure and pressure difference.
4) The adsorption diffusion process for carbon dioxide in coal is a combination of both bulk diffusion-controlled and surface interaction-controlled processes; the former is clear in the initial stage while the latter dominates the overall process.

Acknowledge

Financial assistance for this work was provided by the U.S. Department of Energy through the National Energy Technology Laboratory's Program under Contract No. DE-FE0006827.

References

1. White C. M., Smith D. H., Jones K. L., Goodman A. L., Jikich S. A., LaCount R. B., ... & Schroeder K. T. Sequestration of carbon dioxide in coal with enhanced coalbed methane recovery a review. Energy & Fuels, 19(3), 659-724 (2005).
2. Busch A., Gensterblum Y., Krooss B. M., & Siemons N. Investigation of high-pressure selective adsorption/desorption behaviour of CO< sub> 2</sub> and CH< sub> 4</sub> on coals: An experimental study. International Journal of Coal Geology, 6(1), 53-68 (2006).
3. Busch A., & Gensterblum Y. (2011). CBM and CO2-ECBM related sorption processes in coal: a review. International Journal of Coal Geology, 87(2), 49-71 (2011).
4. Goodman A. L., Busch A., Duffy G. J., Fitzgerald J. E., Gasem K. A. M., Gensterblum Y., ... & White C. M. An inter-laboratory comparison of CO2 isotherms measured on Argonne premium coal samples. Energy & fuels, 18(4), 1175-1182 (2004).
5. Goodman A. L., Busch A., Bustin, R. M. Chikatamarla, L Day, S. Duffy, G. J., ... & White C. M. Inter-laboratory comparison II: CO< sub> 2</sub> isotherms measured on moisture-

equilibrated Argonne premium coals at 55° C and up to 15 MPa. International Journal of Coal Geology, 72(3), 153-164 (2007).

6. Siemons N., & Busch A. Measurement and interpretation of supercritical CO< sub> 2</sub> sorption on various coals. International Journal of Coal Geology, 69(4), 229-242 (2007).
7. Gensterblum Y., Van Hemert P., Billemont P., Busch A., Charriere D., Li D., ... & Wolf K. H. European inter-laboratory comparison of high pressure CO< sub> 2</sub> sorption isotherms. I: Activated carbon. Carbon, 47(13), 2958-2969 (2009).
8. Gensterblum Y., Van Hemert P., Billemont P., Battistutta E., Busch A., Krooss, B. M., ... & Wolf K. H. European inter-laboratory comparison of high pressure CO< sub> 2</sub> sorption isotherms II: Natural coals. International Journal of Coal Geology, 84(2), 115-124 (2010).
9. Gawor M., & Skoczylas N. Sorption Rate of Carbon Dioxide on Coal. Transport in Porous Media, 101(2), 269-279 (2014).
10. Smith D. M., & Williams F. L. Diffusion models for gas production from coal: determination of diffusion parameters. Fuel, 63(2), 256-261 (1984a).
11. Smith D. M., & Williams F. L. Diffusion models for gas production from coals: Application to methane content determination. Fuel, 63(2), 251-255 (1984b).
12. Smith D. M., & Williams F. L. Diffusional effects in the recovery of methane from coalbeds. Society of Petroleum Engineers Journal, 24(5), 529-535 (1984c).
13. Yang Q. & Wang Y. Theory of methane diffusion from coal cuttings and its application. Journal of China Coal Society. 3:87-94 (1986).
14. Guo Y.Y., Wu S.Y. Study on the measurement of coal particle gas diffusion and diffusion coefficient. Shanxi Mining Institute Journal, 15(1), 15-19 (1997).
15. Nie B., Guo Y. Mathematical Physics Model of Gas Diffusion through Coal Particle. Journal of Liaoning Technical University (Natural Science), 18(6), 582-585 (1999).
16. Nie B. S., Guo Y. Y., & Wu S. Y. Theoretical model of gas diffusion through coal particles and its analytical solution. Journal-China University of Mining and Technology-Chinese Edition, 30(1), 19-22 (2001).
17. Li D., Liu Q., Weniger P., Gensterblum Y., Busch A., & Krooss B. M. High-pressure sorption isotherms and sorption kinetics of CH< sub> 4</sub> and CO< sub> 2</sub> on coals. Fuel, 89(3), 569-580 (2010).

18. Han F., Busch A., Krooss B. M., Liu Z., & Yang J. CH< sub> 4</sub> and CO< sub> 2</sub> sorption isotherms and kinetics for different size fractions of two coals. Fuel, 108, 137-142 (2013).
19. Tang X., Li Z., Ripepi N., Louk A. K., Wang Z., & Song D. Temperature-dependent diffusion process of methane through dry crushed coal. Journal of Natural Gas Science and Engineering, 22, 609-617 (2015).
20. Ruckenstein E., Vaidyanathan A. S., & Youngquist G. R. Sorption by solids with bidisperse pore structures. Chemical Engineering Science, 26(9), 1305-1318 (1971).
21. Cui X., Bustin R. M., & Dipple G. Selective transport of CO< sub> 2</sub>, CH< sub> 4</sub>, and N< sub> 2</sub> in coals: insights from modeling of experimental gas adsorption data. Fuel, 83(3), 293-303 (2004).
22. Yi J., Akkutlu, I. Y., & Deutsch C. V. Gas transport in bidisperse coal particles: investigation for an effective diffusion coefficient in coalbeds. Journal of Canadian Petroleum Technology, 47(10), 20-26 (2008).
23. Pone J. D. N., Halleck P. M., & Mathews J. P. Sorption capacity and sorption kinetic measurements of CO2 and CH4 in confined and unconfined bituminous coal. Energy & Fuels, 23(9), 4688-4695 (2009).
24. Zhang Y. Geochemical kinetics. Boston, Princeton University Press, 224-227, 284-298,418-434. (2008).
25. Jian X., Guan P., & Zhang W. Carbon dioxide sorption and diffusion in coals: Experimental investigation and modeling. Science China Earth Sciences,55(4), 633-643 (2012).
26. Li Z., Wang D., Song D. Influence of temperature on dynamic diffusion coefficient of CH4 into coal particles by new diffusion model [J]. Journal of China Coal Society, 40(5):1055-1064. doi:10. 13225 / j. cnki. jccs. 2014. 1218 (2015).
27. Plazinsk, W., Rudzinski W., & Plazinska A. Theoretical models of sorption kinetics including a surface reaction mechanism: a review. Advances in Colloid and Interface Science, 152(1), 2-13 (2009).
28. Azizian S. Kinetic models of sorption: a theoretical analysis. Journal of Colloid and Interface Science, 276(1), 47-52 (2004).

29. Azizian S. A novel and simple method for finding the heterogeneity of adsorbents on the basis of adsorption kinetic data. Journal of colloid and interface science, 302(1), 76-81 (2006).
30. Liu Y., Yang S. F., Xu H., Woon K. H., Lin Y. M., & Tay J. H. Biosorption kinetics of cadmium (II) on aerobic granular sludge. Process Biochemistry, 38(7), 997-1001 (2003).
31. Haerifar M., & Azizian S. Mixed surface reaction and diffusion-controlled kinetic model for adsorption at the solid/solution interface. The Journal of Physical Chemistry C, 117(16), 8310-8317 (2013).
32. Lagergren S. About the theory of so-called adsorption of soluble substances. Kungliga Svenska Vetenskapsakademiens Handlingar, 24(4), 1-39 (1898).
33. Liu Y., & Shen L. From Langmuir kinetics to first-and second-order rate equations for adsorption. Langmuir, 24(20), 11625-11630 (2008).
34. Ho Y. S., & McKay G. Pseudo-second order model for sorption processes. Process Biochemistry, 34(5), 451-465 (1999).
35. Blanchard, G., Maunaye, M., & Martin, G. Removal of heavy metals from waters by means of natural zeolites. Water Research, 18(12), 1501-1507 (1984).
36. Rudzinski, W., & Plazinski, W. Studies of the kinetics of solute adsorption at solid/solution interfaces: on the possibility of distinguishing between the diffusional and the surface reaction kinetic models by studying the pseudo-first-order kinetics. The Journal of Physical Chemistry C, 111(41), 15100-15110 (2007).
37. Miyake, Y., Ishida, H., Tanaka, S., & Kolev, S. D. Theoretical analysis of the pseudo-second order kinetic model of adsorption. Application to the adsorption of Ag (I) to mesoporous silica microspheres functionalized with thiol groups. Chemical Engineering Journal, 218, 350-357, (2013).
38. Blach T. P., & Gray E. M. Sieverts apparatus and methodology for accurate determination of hydrogen uptake by light-atom hosts. Journal of Alloys and Compounds, 446, 692-697 (2007).
39. Lemmon E. W., Huber M. L., & McLinden M. O. NIST reference fluid thermodynamic and transport properties–REFPROP (2002).

40. Lemmon E. W., Huber M. L., & McLinder M. O. NIST reference fluid thermodynamic and transport properties database (REFPROP). NIST Standard Reference Database, 23 (2007).
41. Gasparik, M., Rexer, T. F., Aplin, A. C., Billemont, P., De Weireld, G., Gensterblum, Y., ... & Zhang, T. First international inter-laboratory comparison of high-pressure CH 4, CO2 and C2H6 sorption isotherms on carbonaceous shales. International Journal of Coal Geology, 132, 131-146 (2014).
42. Gasparik, M., Gensterblum, Y., Ghanizadeh, A., Weniger, P., & Krooss, B. M. High-Pressure/High-Temperature Methane-Sorption Measurements on Carbonaceous Shales by the Manometric Method: Experimental and Data-Evaluation Considerations for Improved Accuracy. SPE Journal (2015).
43. Tang, X., Wang, Z., Ripepi, N., Kang, B., & Yue, G. (2015). Adsorption Affinity of Different Types of Coal: Mean Isosteric Heat of Adsorption. Energy & Fuels, 29 (6), pp 3609–3615.
44. Wang Z, Tang X., Yue G., Kang B., Xie C. & Li X. Physical simulation of temperature influence on methane sorption and kinetics in coal: Benefits of temperature under 273.15 K. Fuel, 185, 207–216 (2015).
45. Charrière D., & Behra P. Water sorption on coals. Journal of colloid and interface science, 344(2), 460-467 (2010).
46. Röcken P., & Tarazona P. Capillary condensation in structured pores.The Journal of chemical physics, 105(5), 2034-2043 (1996).
47. Neimark A. V., & Ravikovitch P. I. Capillary condensation in MMS and pore structure characterization. Microporous and Mesoporous Materials, 44, 697-707 (2001).
48. Weinberger B., Darkrim-Lamari F., & Levesque D. Capillary condensation and adsorption of binary mixtures. The Journal of chemical physics, 124(23), 234712 (2006).
49. Heath J. E., Bryan C. R., Matteo E. N., Dewers T. A., Wang Y., & Sallaberry C. J. Adsorption and capillary condensation in porous media as a function of the chemical potential of water in carbon dioxide. Water Resources Research, 50(3), 2718-2731 (2014).
50. Li Z., Jin Z., & Firoozabadi A. Phase Behavior and Adsorption of Pure Substances and Mixtures and Characterization in Nanopore Structures by Density Functional Theory. SPE Journal, 19(06), 1-096 (2014).

51. Hirsch P. B. X-ray scattering from coals. Proceedings of the Royal Society of London. Series A. Mathematical and Physical Sciences, 226(1165), 143-169 (1954).
52. Rouquerol J., Avnir D., Fairbridge C. W., Everett D. H., Haynes J. M., Pernicone N., ... & Unger K. K. Recommendations for the characterization of porous solids (Technical Report). Pure and Applied Chemistry, 66(8), 1739-1758 (1994).
53. Yang J., & Volesky B. Cadmium biosorption rate in protonated Sargassum biomass. Environmental science & technology, 33(5), 751-757 (1999).
54. Febrianto J., Kosasih A. N., Sunarso J., Ju Y. H., Indraswati N., & Ismadji S. Equilibrium and kinetic studies in adsorption of heavy metals using biosorbent: A summary of recent studies. Journal of Hazardous Materials, 162(2), 616-645 (2009).

4.2 How different coal particle sizes generate unreliable pore characterization from gas adsorption test

Xu Tang[a], Nino Ripepi[a], Matthew R Hall[b,c], Lee A Stevens[b], David Mee[b]

(a Department of Mining and Minerals Engineering, Virginia Polytechnic Institute and State University, Blacksburg, Virginia, 24060, U.S.; b Nottingham Centre for Geomechanics, Faculty of Engineering, University of Nottingham, Nottingham, NG7 2RD UK; c British Geological Survey, Environmental Science Centre, Keyworth, Nottingham, NG12 5GG UK)

Abstract: In gas adsorption analysis, the effect of particle size distribution in coal samples is known to result in unreliable pore characterization. This experimental artefact has led researchers to a misunderstanding of the pore network features in coals and the hysteresis mechanism that occurs during gas sorption. In this study, CO_2 and N_2 adsorption tests on five sizes of crushed Pocahontas No. 7 coal were conducted at 0 °C and -196°C under sub-atmosphere pressures. Our results show that the adsorbed uptake of CO_2 and N_2 increases non-linearly with decreasing particle diameter under the same test conditions. This is caused by the increase in volume of accessible pores and fresh surface area created by comminution during sample preparation. Comparative results from five different coal particles show that it is difficult to characterize the pore features of coal using only one coal particle size. The difference in integral area between desorption and adsorption isotherms (hysteresis loop) decreased as a function of particle diameter. The force closed desorption phenomenon was observed for all N_2 sorption tests, which may be attributed to the instability of the meniscus condensation inside pores. Unclosed hysteresis loops were observed in both CO_2 and N_2 sorption tests which may be attributed to the plasticization of un-rigid coal during gas sorption.

Key words: Coal, Carbon dioxide, Nitrogen, Pore, Particle size, Hysteresis

4.2.1 Introduction

Pore characterization of coal and organic-rich shale is of research interest because of the recent exploitation of unconventional natural gas resources and the corresponding large storage potential for carbon dioxide [1-9]. Since the pore features of coal and shale influence the gas transport in the coal seam and shale formation, it is crucial to understand how the pore features may affect (i) the production of gas and liquids, (ii) the development of enhanced gas recovery techniques, and (iii) effective deployment of carbon dioxide storage tests [5, 10-13]. Several state-of-the-art techniques have been applied to characterize the pore system of coal and shale [14-23]. Among these techniques, gas adsorption under sub-atmosphere conditions is the most common one for its applicability to the pore size range, simplicity, effectiveness and low cost [24-27]. For manmade porous materials, there are fewer issues for pore characterization (than for heterogenous natural materials) using gas sorption since the pore system can be designed in advance and the test procedure has been standardized [ISO 15901-3; ISO9277 1-1, 2, 3]. Several issues persist when the gas adsorption technique is applied for natural materials (coal and organic-rich shale) such as sorption equilibrium status evaluation and the proper particle size of sample used for testing. In particular, there is no standard for geo-materials such as gas sorption tests in coal using the volumetric approach under sub-atmosphere and high pressure [28-31], making it difficult to independently evaluate and compare published pore characterization data. The pore size distribution (PSD) data from gas adsorption tests should ideally be validated by parallel techniques such as small angle X-ray diffraction (SAXRD) or scanning transmission electron microscopy (STEM) brightfield image analysis. In addition, it is unclear how to determine whether the sorption system reaches equilibrium. An important issue is the lack of consistency in the selection of coal particle diameter for gas adsorption analysis, along with sufficient understanding of how this can affect the reliability of porosity characterization (Table 4.2.1). Therefore, it is imperative to clarify how both the different coal particle size and pseudo-equilibrium state of the sorption system will influence the pore characterization of coal.

Table 4.2.1 Different coal particle sizes used in low temperature gas adsorption analyses

Sample	Literature	Particle size (micro)	N_2 adsorption test	CO_2 adsorption test
Coal	[32]	250	Yes	Yes
Coal	[33]	250 - 425	Yes	--
Coal	[34]	180 - 250	Yes	--
Coal	[35]	250	Yes	Yes
Coal	[36]	212 -425	Yes	Yes
Coal	[37]	710 - 850	--	Yes
Coal	[38]	75	Yes	Yes
Coal	[39]	30- 80	Yes	Yes
Coal	[40]	30-80	Yes	--
Coal	[41]	212 -425	--	Yes
Coal	[42]	213 -425	--	Yes
Coal	[43]	1300-2200	--	Yes
Coal	[44]	250 - 500	--	Yes
Shale and coal	[45]	250	--	Yes
Shale	[46]	180 - 250	Yes	--
Shale	[47]	< 250	Yes	Yes
Shale	[48]	250	Yes	Yes
Shale	[19]	250	Yes	Yes
Shale	[49]	< 250	Yes	Yes
Rock	[50]	//	Yes	--
Rock	[51]	8000	Yes	--
Rock	[18]	4750; chips size; 25400	Yes	Yes

In this paper, the authors have designed a series of gas adsorption tests to parametrically assess how particle size influences the results of porosity analysis. Five different sizes of crushed coal (< 106 μm, 106-150 μm, 150-180 μm, 180-300 μm, 300-600 μm) were used to conduct CO_2 full adsorption/desorption isotherms at 0 °C, and N_2 adsorption/desorption isotherms at -196°C at sub-atmosphere pressures (4 to 750mmHg).

4.2.2 Experimental methodology

4.2.1 Sample preparation

The coal samples used in this study were all extracted from a core extracted from the Pocahontas No.7 coal seam (Buchanan County, VA, United States). The composition of the coal was evaluated (Table 4.2.2) in accordance with ASTM D7582 – 15 and ASTM D3176 - 15. The coal specimens were then ground using an agate mortar and pestle and sieved through 106, 150, 180, 300, 600 μm aperture metal sifters. Five different particle size distributions were obtained by separation as follows: (i) <106 μm, (ii) 106-150 μm, (iii) 150-180 μm, (iv) 180-300 μm, (v) 300-600 μm. The

crushed samples were placed in a drying oven (at 104℃ to 110℃) for 1 hour to dehydrate. After dehydration, the samples were stored in a vacuum desiccator for later use in accordance with ASTM D3173 - 11.

Table 4.2.2 Composition of coal samples

Proximate analysis		
Test samples	**As received**	**Dry basis**
Moisture	0.6	--
Sulfur	4.36	4.39
Volatile	19.34	19.46
Fixed Carbon	69.81	70.23
Ash	10.25	10.25

Ultimate analysis		
Test samples	**As received**	**Dry basis**
Moisture	0.6	--
Carbon	79.11	9.59
Hydrogen	4.33	4.29
Nitrogen	0.99	1
Oxygen	0.95	0.42

4.2.2.2 Test approach and data processing

Gas sorption was conducted using a Micromeritics 3Flex volumetric analyzer (Norcross GA, USA) using ultrapure N_2 and CO_2 adsorbates (BOC gases, Nottingham, UK). All samples were degassed for 15 hours at 110 ℃ using a VacPrep Degasser (Micrometritics, Norcross GA, USA). Approximately 1-2.3 gram coal samples were used for each N_2 sorption isotherms including using a filler rod. Sample tube bulbs were immersed in liquid N_2 at approximately -196 °C. For CO_2 isotherms, approximately 0.2 gram of coal sample was weighed in to a sample tube. The tubes were immersed in 50% ethylene glycol solution inside an isothermal controller (in place of the liquid nitrogen dewar) during the tests which was set to 0℃. The equilibrium state for each test was set based on the pressure measurement approach, *i.e.* when the partial pressure fluctuation inside the test tube is within 0.3%.

The BET specific surface area using N_2 was calculated by the linear BET relationship under the relative pressure ranges from Rouquerol's approach, which includes (1) both the resulting parameter C_{BET} is positive and the intercept on the ordinate of the BET-plot is positive, and (2) the term $V_{ad}(p_o-p)$ should continuously increase with p/p_o [52; ISO 9277: 2010]. Detailed calculation procedure is referred to in ISO 9277: 2010.

The pore size distribution was obtained using the non-local density functional theory (NLDFT) model applied to the adsorption branch [53-55]. The calculation approach of the pore size distribution using NLDFT and DFT method is based on the integral adsorption equation (Eq. 1).

$$N(p/p_0) = \int_{D\min}^{D\max} N(p/p_0, D) f(D) dD \qquad \text{Eq. 1}$$

where, D is the pore size (diameter or width), $N(p/p_0,D)$ is the kernel of the theoretical isotherms of different pore widths; f(D) is the PSD. Once the isothermal adsorption data is obtained, the PSD can be derived numerically by solving the integral adsorption equation. The NLDFT model is available for describing the PSD to the whole range of micro- and meso-pore sizes. Since several DFT kernels have been applied for both mesoporous activated carbons and other organic materials, it is logical to have confidence that this approach will work for coal [54-55]. In this paper, the carbon slit pore model of NLDFT kernel was applied for meso- and macro-pore using N_2 adsorption data, and the CO_2-DFT model was applied for micropore using CO_2 adsorption data.

4.2.3 Test results and discussion

4.2.3.1 Adsorption behavior of carbon dioxide for different coal particle size ranges

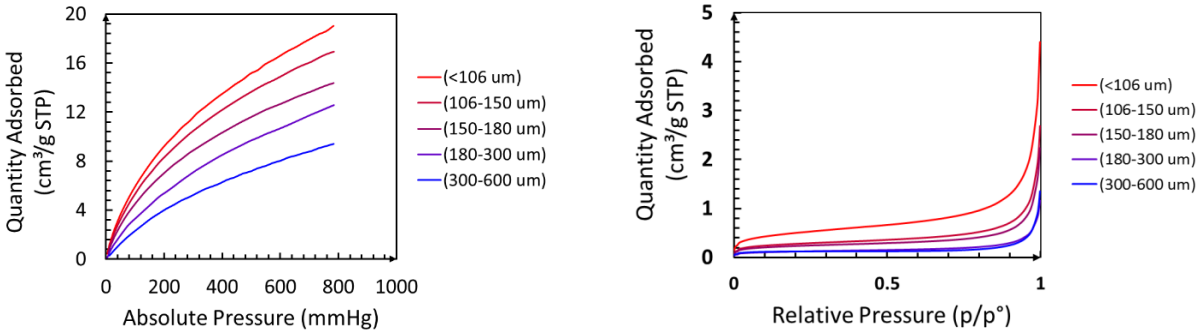

Figure 4.2.1 Adsorption behavior of carbon dioxide and nitrogen

From Figure 4.2.1, it can be seen that the adsorbed volume of both CO_2 and N_2 in coal is greater for smaller particle diameters under the same test conditions. This can be attributed to the increased surface area as well as access to fresh pores resulting from grinding. Since coal typically has a high proportion of micropores, it is important to understand how the adsorbate enters the micropore network. For microfluidic flow, the Knudsen number, Kn is given by the ratio of mean free path length to pore diameter [56] is used to classify different flow patterns. Four distinct Kn regimes have been measured as shown in Table 4.2.3. From Figure 3.3.2, it can be seen that in the micropore (0-2nm) range the free molecular flow dominates the process because the Kn is extremely high (above 10). Since surface diffusion is insignificant and configuration diffusion can be neglected after monolayer completion, Knudsen diffusion is assumed to dominate the free

molecular flow process. In the mesopores (2-50nm), both the free molecular and continuum flow with molecular diffusion occur, where the concentration-driven bulk diffusion is also included. In the macropores (50 nm<pore size), Fickian bulk diffusion may occur. Since diffusion is a time-consuming process, a longer time is needed for the sorption system of large coal particle sizes to reach equilibrium state. This is because the gas molecular moves a longer distance to access adsorption sites in larger coal particles compared with smaller coal particles. In addition, the reduction of coal particles via grinding exposes more access pores and surface area of coal particles, which increases the portion of available adsorption sites or pores during the sorption test [57].

Table 4.2.3 Microfluidic regime classified by Knudsen number (revised from [56])

<table>
<tr><th colspan="2">Gas flow regimes</th><th colspan="4">Modeling approach</th></tr>
<tr><td rowspan="3">Continuum flow</td><td rowspan="3">Kn→0</td><td>100 < Re</td><td colspan="3">Turbulent flow</td></tr>
<tr><td>(1~10) < Re< 100</td><td>Transition flow</td><td>Non-Darcy</td><td rowspan="2">Navier-Stokes equation</td></tr>
<tr><td>1 < Re< 10</td><td>Laminar flow</td><td>Darcy</td></tr>
<tr><td rowspan="2">Continuum flow (with molecular diffusion)</td><td>0.001 < Kn< 0.1</td><td>Re→0</td><td colspan="2">with slip flow</td><td rowspan="2">Burnett equation</td></tr>
<tr><td>0.1< Kn <10</td><td>Re→0</td><td colspan="2">Transition flow</td></tr>
<tr><td rowspan="3">Free-molecular flow</td><td rowspan="3">0.1 =< Kn</td><td rowspan="3">Re→0</td><td colspan="2">Knudsen diffusion</td><td rowspan="3">Maxwell-Stefen approach</td></tr>
<tr><td colspan="2">Surface diffusion</td></tr>
<tr><td colspan="2">Configural diffusion</td></tr>
</table>

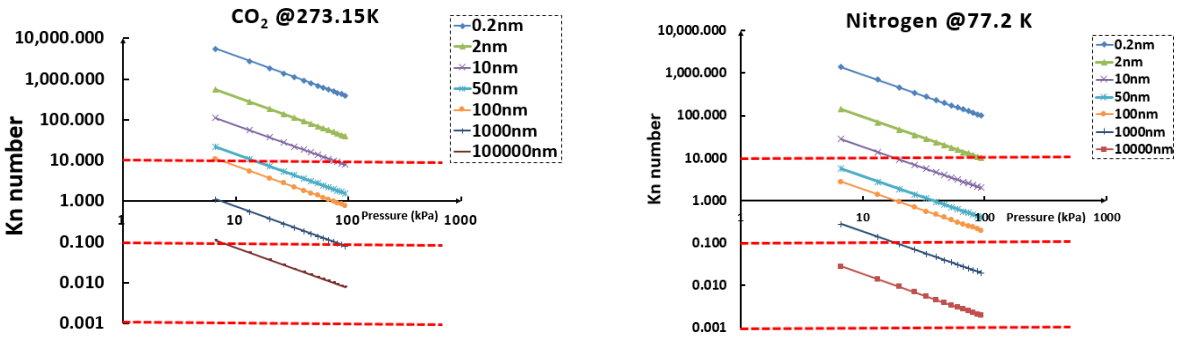

Figure 4.2.2 Knudsen number of CO_2 and N_2 in different size of pore under different test conditions

4.2.3.2 BET surface area

Even though the CO_2 adsorption test is reliable for measuring the pore size distribution of micropores in coal (based on the micropore-filling assumption), the specific surface area calculated from CO_2 adsorption isotherms is less so due to (i) uncertainties in monolayer capacity, (ii) the cross-sectional area of an adsorbed molecule in a molecular-scale pore, and (iii) the coal swelling

phenomenon [58]. Thus, the BET specific surface area obtained from CO_2 adsorption data can be unreliable for coals and so the N_2 isotherms were used instead for this study in order to minimize the error compared with the absolute value [59,60]. Following Rouquerol's approach, the maximum relative pressure for linear BET fitting in each tests ranged from 0.0088 to 0.2 p/p_0.

As shown in Figure 4.2.3, it can be seen that the BET surface area increases exponentially with decreasing coal particle size in the test results; the BET area is four times higher for coal particles less than 106 μm than for coal particles in the range of 300-600 μm. This can be attributed that the comminution of the coal particle provides more fresh surface area of the tested particles during the sample preparation stage. Figure 4.2.3 also shows the surface area of 30-50 μm and 50-80 μm coal particle are very close, and the surface area increases rapidly especially when the coal particle is less than 106 μm.

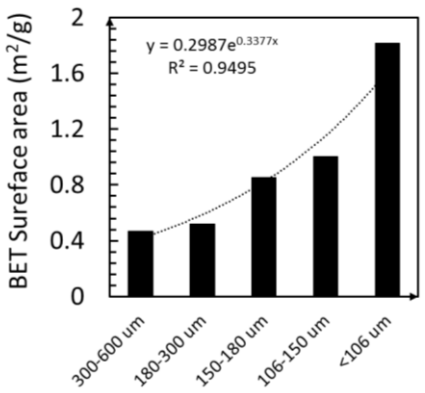

Figure 4.2.3 N_2 BET surface area comparison of different sizes of coal particles

4.2.3.3 Pore size distribution (PSD)

Figures 4.2.4-4.2.5 show the comparison of the PSD of different coal particles from CO_2 and N_2 adsorption data. From Figure 4.2.4, it can be seen that the micro pore size distribution has a similar trend with different pore width for all tested samples but the incremental pore volume of each pore size is different. The measured pore width ranges from 0.4nm to 0.9nm in all tested samples, and the smaller particle size samples have higher cumulative pore volume. The cumulative pore volume increases with the reduction of particle size as shown in the test data (Figure 4.2.4). There is a large gap for accumulative pore volume; the accumulative pore volume of coal is less than 106 μm, which is around two times that of coal particles in the range of 300-600 μm.

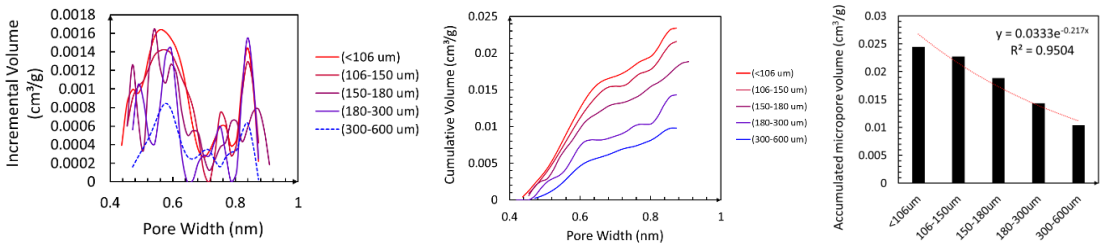

Figure 4.2.4 Comparison of micropore size distribution of different coal particles from CO_2 adsorption test

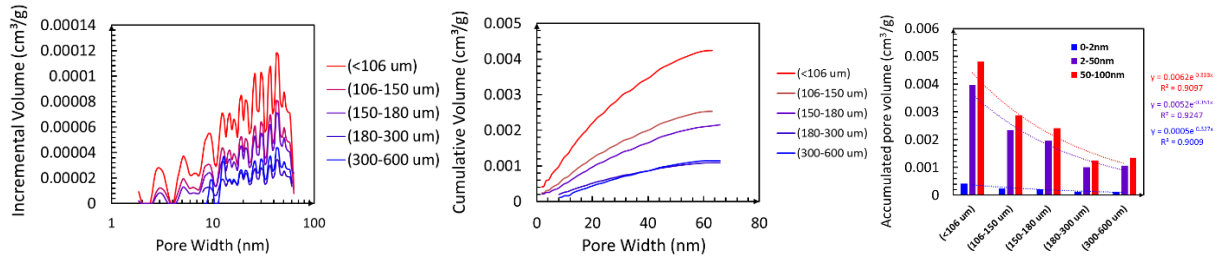

Figure 4.2.5 Comparison of pore size distribution of different coal particle size from N2 adsorption test

From Figure 4.2.5, the PSD obtained from N_2 adsorption data has a similar trend in the range of 10 nm to 80 nm, but there are marked differences for PSD in pore ranges from 2 nm to 8 nm. The measured PSD decreases with increasing particle size, and there are no pores ranging from 2 to 8nm detected for particles in 180-300 µm or 300-600 µm range. The reason why no pores less than 1 nm were detected during N_2 nitrogen adsorption is that the nitrogen molecule is prevented from entering micropores because of the diffusion restriction issue at a low temperature of -195.95℃ [ISO 15901-3]. The accumulated pore volume in micro-, meso- and macro-pores exponentially decreases and is inversely related to particle size, as shown in Figure 4.2.5. The cumulative pore volume of coal particles >105 µm diameter is almost twice that of particles in the range 300-600 µm. This can be attributed to the fact that the apparent pore volumes in smaller coal particles increased following comminution.

Comparing both Figure 4.2.4 and Figure 4.2.5, the micropores detected using carbon dioxide sorption in coal is one order of magnitude higher than that of the mesopores and macropores detected using nitrogen. It can reasonably be expected that the micropore volume measured by nitrogen does highly underestimate the micropore volume in coals [61].

4.2.3.4 Effect of particle size distribution on hysteresis

Physisorption hysteresis is mostly associated with capillary condensation in mesopores, and its apparent form is dependent on the pore feature of adsorbents and the sorption environment such as pressure and temperature [24-26, 62]. In addition, it is possible that the CO_2 is partly chemisorbed to the coal adsorbent [15,17; 63, 64].

From Figure 4.2.6, it can be seen that the extent of hysteresis decreases with particle diameter, as observed by a separate recent study [57]. The desorption isotherms do not close with their corresponding adsorption branches even under very low pressures (Figure 4.2.6). For the unclosed hysteresis loop in Figure 4.2.6, it is difficult to attribute a reason, though partial chemisorption during the test is possible. Whether the plasticization of un-rigid coal occurs or not is arguable since the unaffected coal structure has been directly observed during adsorption/desorption tests in previous studies using SAXS and USANS [15,17, 65,66]. Another reason is that the adsorbate affinity to active sites along the pore walls of coal is likely to be variable due to the heterogeneous nature of the material composition [30, 67]. CO_2 is more easily trapped in micropores compared with the meso- and macro-pores because of the accumulated adsorption potential energy.

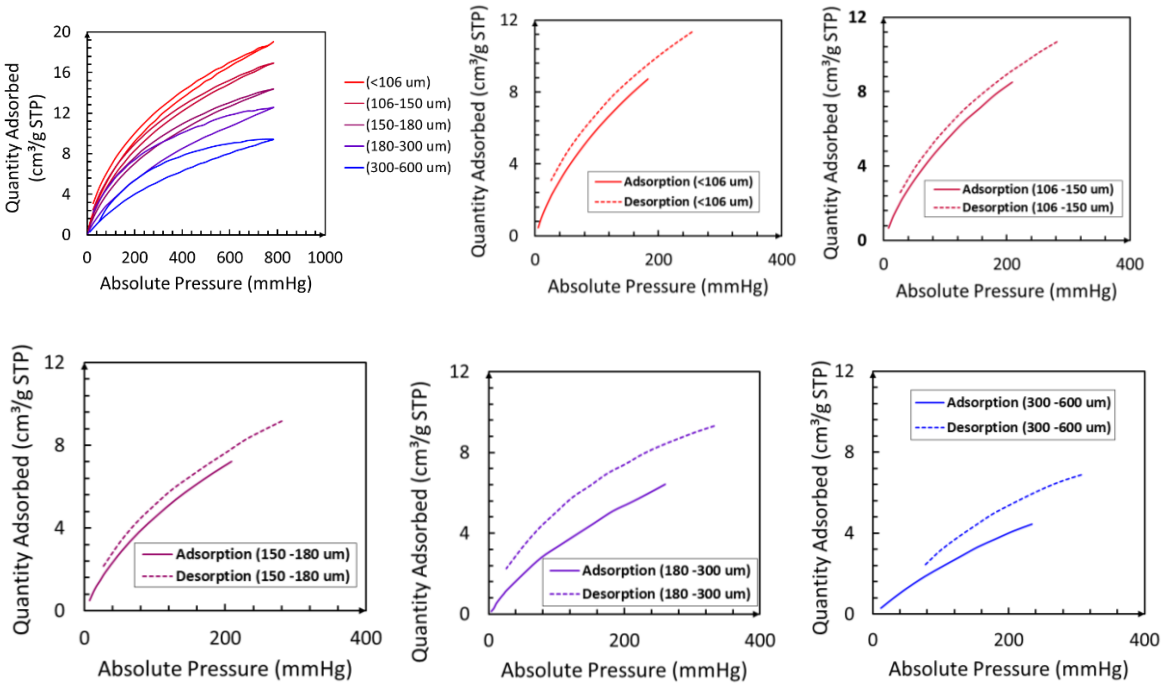

Figure 4.2.6 Hysteresis behavior of carbon dioxide in coal

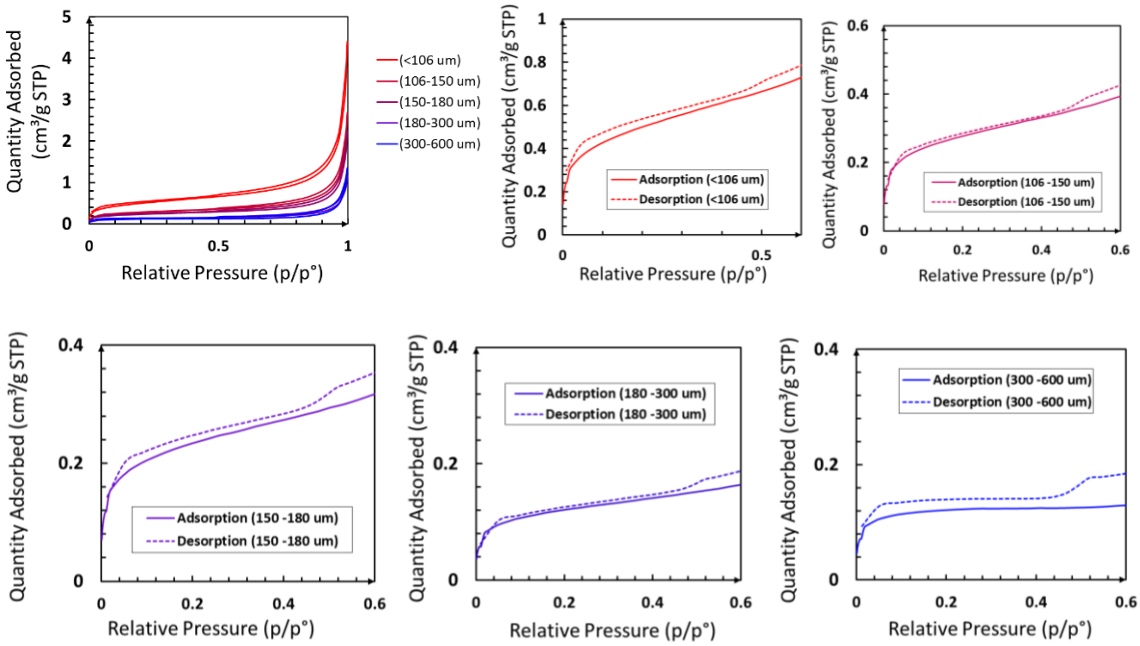

Figure 4.2.7 Hysteresis behavior of nitrogen in coal

Figure 4.2.7 shows the nitrogen isotherms of all tested samples and the hysteresis loops does not close under very low relative pressures (around 0.01 p/p_0 in this work), and the hysteresis loop may close under extremely low pressures up to 0.001 p/p_0. It is also hard to classify them to the standard H3 or H4 type hysteresis loop. For H3 hysteresis loop, the sorption isotherms do not exhibit any limiting adsorption at high relative pressure, which is usually observed with aggregates of plate-like particles with slit-shaped pores [24]. H4 hysteresis loop is similar to H3 hysteresis loop but the adsorption branch is a composite of Type 1 and Type 2. The force closed phenomenon that occurs at a relative pressure ranging from 0.4 to 0.6 p/p_0 was observed for all isotherms, which is caused by (i) the tensile strength effect, (ii) the interconnected pore features of coal, and (iii) the potential existence of the "ink bottle" pore [68]. The large particle size has a relative sharp drop compared with that in a small particle size. This can be attributed to the different stability state of multilayer nitrogen adsorption for different particle sizes [25].

From Figure 4.2.6 and Figure 4.2.7, it can be seen that both CO_2 and N_2 ad/desorption curves show specific features for different coal particle sizes. Specifically, in Figure 4.2.6, the hysteresis loops of CO_2 in the sample of 180-300 and 300-600 μm are larger than that in the sample of 150-180, 106-150, and <106 μm. In Figure 4.2.7, N_2 sorption isotherms in the sample of 300-600 and 180-300 μm are different from that in the sample of 150-180, 106-150, and less than 106 μm, i.e. the

general slope of the former is lower than the latter when the relative pressure is between 0.2 and 0.3. Therefore, it may be possible that for large coal particle sizes (up to 600 μm), the additional 'fresh' pore volume and associated surface area, due to comminution, are insignificant. However, for smaller coal particle sizes (below 180 μm), the 'fresh' pore volume and surface area due to comminution are more pronounced, as shown by the increasing adsorption content with pressure.

4.2.4 Conclusions

Carbon dioxide and nitrogen adsorption tests on five sizes of crushed Pocahontas No. 7 coal were conducted at 0 °C and -196°C in sub-atmosphere pressures to clarify how different coal particle sizes influence the pore characterization of coal. Several conclusions can be made based on the test results:

(1) The adsorption content of carbon dioxide and nitrogen in coal increases with decreasing particle size, which is mainly caused by the increasing accessible pores and fresh surface area created via comminution. The hysteresis loop decreases with the reduction in coal particle size.

(2) The measured micro-, meso- and macro-pore volume and nitrogen BET surface area all increase non-linearly as particle size is reduced. This makes it difficult to accurately characterize the real pore features of coal using only one particle size during gas adsorption analysis. Therefore, we cannot recommend the optimum coal particle size for pore characterization of coal. However, we do find that the fresh pores and surface area created via comminution significantly influence our understanding about the real pore features of natural coals. Our preliminary recommendation is that larger particle sizes are preferred, and that mean particle diameters less than 180 μm should be removed by sifting in order to minimize the error in apparent micropore volume.

(3) The 'force closed desorption phenomenon' was observed for all N_2 sorption tests, which may be attributed to the instability of the meniscus condensation inside pores. An unclosed hysteresis loop was observed in both CO_2 and N_2 sorption tests, which is perhaps due to the plasticization of un-rigid coal during gas sorption process.

Acknowledgements

This research was supported in part by the U.S. Department of Energy through the National Energy Technology Laboratory's Program (No. DE-FE0006827). The first author wants to acknowledge the Pratt Grad Study Abroad Scholarship from Virginia Tech for the travel support.

References

1. White, C. M., Smith, D. H., Jones, K. L., Goodman, A. L., Jikich, S. A., LaCount, R. B., ... & Schroeder, K. T. (2005). Sequestration of carbon dioxide in coal with enhanced coalbed methane recovery a review. Energy & Fuels,19(3), 659-724.
2. Benson, S. M., & Cole, D. R. (2008). CO2 sequestration in deep sedimentary formations. Elements, 4(5), 325-331.
3. Kang, S. M., Fathi, E., Ambrose, R. J., Akkutlu, I. Y., & Sigal, R. F. (2011). Carbon dioxide storage capacity of organic-rich shales. SPE Journal, 16(04), 842-855.
4. Tao, Z., & Clarens, A. (2013). Estimating the carbon sequestration capacity of shale formations using methane production rates. Environmental science & technology, 47(19), 11318-11325.
5. Busch, A., Alles, S., Gensterblum, Y., Prinz, D., Dewhurst, D. N., Raven, M. D., ... & Krooss, B. M. (2008). Carbon dioxide storage potential of shales. International Journal of Greenhouse Gas Control, 2(3), 297-308.
6. Busch, A., & Gensterblum, Y. (2011). CBM and CO2-ECBM related sorption processes in coal: a review. International Journal of Coal Geology, 87(2), 49-71.
7. Pashin, J. C., & McIntyre, M. R. (2003). Temperature–pressure conditions in coalbed methane reservoirs of the Black Warrior basin: implications for carbon sequestration and enhanced coalbed methane recovery. International Journal of Coal Geology, 54(3), 167-183.
8. Godec, M., Koperna, G., & Gale, J. (2014). CO 2-ECBM: A Review of its Status and Global Potential. Energy Procedia, 63, 5858-5869.
9. Ripepi, N. S. (2009). Carbon dioxide storage in coal seams with enhanced coalbed methane recovery: geologic evaluation, capacity assessment and field validation of the central appalachian basin (Doctoral dissertation, Virginia Polytechnic Institute & State University).
10. Javadpour, F., Fisher, D., & Unsworth, M. (2007). Nanoscale gas flow in shale gas sediments. Journal of Canadian Petroleum Technology, 46(10).
11. Fathi, E., & Akkutlu, I. Y. (2009). Matrix heterogeneity effects on gas transport and adsorption in coalbed and shale gas reservoirs. Transport in Porous Media,80(2), 281-304.

12. Freeman, C. M., Moridis, G. J., & Blasingame, T. A. (2011). A numerical study of microscale flow behavior in tight gas and shale gas reservoir systems.Transport in porous media, 90(1), 253-268.
13. Ross, D. J., & Bustin, R. M. (2009). The importance of shale composition and pore structure upon gas storage potential of shale gas reservoirs. Marine and Petroleum Geology, 26(6), 916-927.
14. Ravikovitch, P. I., Vishnyakov, A., & Neimark, A. V. (2001). Density functional theories and molecular simulations of adsorption and phase transitions in nanopores. Physical Review E, 64(1), 011602.
15. Radlinski, A. P., Busbridge, T. L., Gray, E. M., Blach, T. P., Cheng, G., Melnichenko, Y. B., ... & Esterle, J. (2009). Dynamic micromapping of CO2 sorption in coal. Langmuir, 25(4), 2385-2389.
16. Ravikovitch, P. I., Vishnyakov, A., Russo, R., & Neimark, A. V. (2000). Unified approach to pore size characterization of microporous carbonaceous materials from N2, Ar, and CO2 adsorption isotherms. Langmuir, 16(5), 2311-2320.
17. Radlinski, A. P., Mastalerz, M., Hinde, A. L., Hainbuchner, M., Rauch, H., Baron, M., & Thiyagarajan, P. (2004). Application of SAXS and SANS in evaluation of porosity, pore size distribution and surface area of coal.International Journal of Coal Geology, 59(3), 245-271.
18. Clarkson, C. R., Freeman, M., He, L., Agamalian, M., Melnichenko, Y. B., Mastalerz, M., ... & Blach, T. P. (2012). Characterization of tight gas reservoir pore structure using USANS/SANS and gas adsorption analysis. Fuel, 95, 371-385.
19. Clarkson, C. R., Solano, N., Bustin, R. M., Bustin, A. M. M., Chalmers, G. R. L., He, L., ... & Blach, T. P. (2013). Pore structure characterization of North American shale gas reservoirs using USANS/SANS, gas adsorption, and mercury intrusion. Fuel, 103, 606-616.
20. Jagiello, J., & Thommes, M. (2004). Comparison of DFT characterization methods based on N 2, Ar, CO 2, and H 2 adsorption applied to carbons with various pore size distributions. Carbon, 42(7), 1227-1232.
21. Ryu, Z., Zheng, J., Wang, M., & Zhang, B. (1999). Characterization of pore size distributions on carbonaceous adsorbents by DFT. Carbon, 37(8), 1257-1264.

22. Harris, L. A., & Yust, C. S. (1976). Transmission electron microscope observations of porosity in coal. Fuel, 55(3), 233-236.
23. Yao, S., Jiao, K., Zhang, K., Hu, W., Ding, H., Li, M., & Pei, W. (2011). An atomic force microscopy study of coal nanopore structure. Chinese Science Bulletin, 56(25), 2706-2712.
24. Sing, K. S. (1985). Reporting physisorption data for gas/solid systems with special reference to the determination of surface area and porosity (Recommendations 1984). Pure and applied chemistry, 57(4), 603-619.
25. Sing, K. (2001). The use of nitrogen adsorption for the characterisation of porous materials. Colloids and Surfaces A: Physicochemical and Engineering Aspects, 187, 3-9.
26. Sing, K., & Williams, R. (2004). Physisorption hysteresis loops and the characterization of nanoporous materials. Adsorption Science & Technology, 22(10), 773-782.
27. Thommes, M., Kaneko, K., Neimark, A. V., Olivier, J. P., Rodriguez-Reinoso, F., Rouquerol, J., & Sing, K. S. (2015). Physisorption of gases, with special reference to the evaluation of surface area and pore size distribution (IUPAC Technical Report). Pure and Applied Chemistry, 87(9-10), 1051-1069.
28. Gasparik, M., Rexer, T. F., Aplin, A. C., Billemont, P., De Weireld, G., Gensterblum, Y., ... & Zhang, T. (2014). First international inter-laboratory comparison of high-pressure CH 4, CO 2 and C 2 H 6 sorption isotherms on carbonaceous shales. International Journal of Coal Geology, 132, 131-146.
29. Gasparik, M., Gensterblum, Y., Ghanizadeh, A., Weniger, P., & Krooss, B. M. (2015). High-Pressure/High-Temperature Methane-Sorption Measurements on Carbonaceous Shales by the Manometric Method: Experimental and Data-Evaluation Considerations for Improved Accuracy. SPE Journal.
30. Wang Z., Tang, X., & Yue, G. et al. (2015). Physical Simulation of Temperature Influence on Methane Sorption and Kinetics in Coal: Benefits of Temperature under 273.15K. Fuel.158: pp 207–216.
31. Tang, X., Ripepi, N., & Gilliland, E. (2015). Isothermal adsorption kinetics properties of carbon dioxide in crushed coal. Greenhouse Gases: Science and Technology. DOI: 10.1002/ghg.1562.

32. Clarkson, C. R., & Bustin, R. M. (1999). The effect of pore structure and gas pressure upon the transport properties of coal: a laboratory and modeling study. 1. Isotherms and pore volume distributions. Fuel, 78(11), 1333-1344.
33. Wang, G., Wang, K., & Ren, T. (2014). Improved analytic methods for coal surface area and pore size distribution determination using 77K nitrogen adsorption experiment. International Journal of Mining Science and Technology,24(3), 329-334.
34. Nie, B., Liu, X., Yang, L., Meng, J., & Li, X. (2015). Pore structure characterization of different rank coals using gas adsorption and scanning electron microscopy. Fuel, 158, 908-917.
35. Mastalerz, M., He, L., Melnichenko, Y. B., & Rupp, J. A. (2012). Porosity of coal and shale: insights from gas adsorption and SANS/USANS techniques. Energy & Fuels, 26(8), 5109-5120.
36. Gan, H., Nandi, S. P., & Walker, P. L. (1972). Nature of the porosity in American coals. Fuel, 51(4), 272-277.
37. Radovic, L. R., Menon, V. C., Leon, C. L. Y., Kyotani, T., Danner, R. P., Anderson, S., & Hatcher, P. G. (1997). On the porous structure of coals: evidence for an interconnected but constricted micropore system and implications for coalbed methane recovery. Adsorption, 3(3), 221-232.
38. Okolo, G. N., Everson, R. C., Neomagus, H. W., Roberts, M. J., & Sakurovs, R. (2015). Comparing the porosity and surface areas of coal as measured by gas adsorption, mercury intrusion and SAXS techniques. Fuel, 141, 293-304.
39. Prinz, D., & Littke, R. (2005). Development of the micro-and ultramicroporous structure of coals with rank as deduced from the accessibility to water. Fuel, 84(12), 1645-1652.
40. Prinz, D., Pyckhout-Hintzen, W., & Littke, R. (2004). Development of the meso-and macroporous structure of coals with rank as analysed with small angle neutron scattering and adsorption experiments. Fuel, 83(4), 547-556.
41. Gürdal, G., & Yalçın, M. N. (2001). Pore volume and surface area of the Carboniferous coals from the Zonguldak basin (NW Turkey) and their variations with rank and maceral composition. International Journal of Coal Geology,48(1), 133-144.
42. Gürdal, G., & Yalçın, M. N. (2000). Gas adsorption capacity of Carboniferous coals in the Zonguldak basin (NW Turkey) and its controlling factors. Fuel,79(15), 1913-1924.

43. Linge, H. G. (1989). The surface area of coal particles. Fuel, 68(1), 111-113.
44. Senel, I. G., Gürüz, A. G., Yücel, H., Kandas, A. W., & Sarofim, A. F. (2001). Characterization of pore structure of Turkish coals. Energy & fuels, 15(2), 331-338.
45. Mastalerz, M., Drobniak, A., Strąpoć, D., Acosta, W. S., & Rupp, J. (2008). Variations in pore characteristics in high volatile bituminous coals: implications for coal bed gas content. International Journal of Coal Geology, 76(3), 205-216.
46. Tian, H., Pan, L., Xiao, X., Wilkins, R. W., Meng, Z., & Huang, B. (2013). A preliminary study on the pore characterization of Lower Silurian black shales in the Chuandong Thrust Fold Belt, southwestern China using low pressure N 2 adsorption and FE-SEM methods. Marine and Petroleum Geology, 48, 8-19.
47. Chalmers, G. R., Bustin, R. M., & Power, I. M. (2012). Characterization of gas shale pore systems by porosimetry, pycnometry, surface area, and field emission scanning electron microscopy/transmission electron microscopy image analyses: Examples from the Barnett, Woodford, Haynesville, Marcellus, and Doig units. AAPG bulletin, 96(6), 1099-1119.
48. Strapoc, D., Mastalerz, M., Schimmelmann, A., Drobniak, A., & Hasenmueller, N. R. (2010). Geochemical constraints on the origin and volume of gas in the New Albany Shale (Devonian–Mississippian), eastern Illinois Basin. AAPG bulletin, 94(11), 1713-1740.
49. Ross, D. J., & Bustin, R. M. (2009). The importance of shale composition and pore structure upon gas storage potential of shale gas reservoirs. Marine and Petroleum Geology, 26(6), 916-927.
50. Janssen, C., Wirth, R., Reinicke, A., Rybacki, E., Naumann, R., Wenk, H. R., & Dresen, G. (2011). Nanoscale porosity in SAFOD core samples (San Andreas Fault). Earth and Planetary Science Letters, 301(1), 179-189.
51. Schmitt, M., Fernandes, C. P., da Cunha Neto, J. A., Wolf, F. G., & dos Santos, V. S. (2013). Characterization of pore systems in seal rocks using nitrogen gas adsorption combined with mercury injection capillary pressure techniques.Marine and Petroleum Geology, 39(1), 138-149.
52. Rouquerol, J., Llewellyn, P., & Rouquerol, F. (2007). Is the BET equation applicable to microporous adsorbents?. Studies in surface science and catalysis, (160), 49-56.
53. Lastoskie, C., Gubbins, K. E., & Quirke, N. (1993). Pore size heterogeneity and the carbon slit pore: a density functional theory model. Langmuir, 9(10), 2693-2702.

54. Ravikovitch, P. I., Vishnyakov, A., Russo, R., & Neimark, A. V. (2000). Unified approach to pore size characterization of microporous carbonaceous materials from N2, Ar, and CO2 adsorption isotherms. Langmuir, 16(5), 2311-2320.
55. Landers, J., Gor, G. Y., & Neimark, A. V. (2013). Density functional theory methods for characterization of porous materials. *Colloids and Surfaces A: Physicochemical and Engineering Aspects*, *437*, 3-32.
56. Squires, T. M., & Quake, S. R. (2005). Microfluidics: Fluid physics at the nanoliter scale. Reviews of modern physics, 77(3), 977.
57. Chen, Y., Wei, L., Mastalerz, M., & Schimmelmann, A. (2015). The effect of analytical particle size on gas adsorption porosimetry of shale. International Journal of Coal Geology, 138, 103-112.
58. Mahajan, O. P. (1991). CO2 surface area of coals: the 25-year paradox. Carbon, 29(6), 735-742.
59. Gregg, S. J., Sing, K. S. W. (1967). Adsorption surface area and porosity. 2nd edition. London: Academic Press, 1982, 303P.
60. Rouquerol, J., Rouquerol, F., Llewellyn, P., Maurin, G., & Sing, K. S. (1999). Adsorption by powders and porous solids: principles, methodology and applications. Academic press, 467P.
61. Bartholomew, C. H., White, W. E., Thornock, D., Wells, W. F., Hecker, W. C., Smoot, L. D., ... & Williams, F. L. (1988). Surface and pore properties of ANL and PETC coals. Amer. Chem. Soc. Div. Fuel Chem. Preprints, 33(3), 24-31.
62. Neimark, A. V., Ravikovitch, P. I., & Vishnyakov, A. (2000). Adsorption hysteresis in nanopores. Physical Review E, 62(2), R1493.
63. Mirzaeian, M., & Hall, P. J. (2006). The interactions of coal with CO2 and its effects on coal structure. Energy & fuels, 20(5), 2022-2027.
64. DI, G. H., DUAN, L. J., TANG, S. H., & XIA, C. H. (2012). Experimental study on CO2-coal interactions. Journal of China Coal Society, 37(5), 788-793.
65. Larsen, J. W., Flowers, R. A., Hall, P. J., & Carlson, G. (1997). Structural rearrangement of strained coals. Energy & Fuels, 11(5), 998-1002.
66. Liu, C. J., Wang, G. X., Sang, S. X., & Rudolph, V. (2010). Changes in pore structure of anthracite coal associated with CO 2 sequestration process. Fuel, 89(10), 2665-2672.

67. Tang, X., Wang, Z., Ripepi, N., Kang, B., & Yue, G. (2015). Adsorption Affinity of Different Types of Coal: Mean Isosteric Heat of Adsorption. Energy & Fuels. 2015, 29 (6), pp 3609–3615.
68. Groen, J. C., Peffer, L. A., & Pérez-Ramírez, J. (2003). Pore size determination in modified micro-and mesoporous materials. Pitfalls and limitations in gas adsorption data analysis. Microporous and Mesoporous Materials, 60(1), 1-17.

Chapter 5 Conclusions and future work

5.1. Conclusions

In this dissertation, high pressure gas (methane and carbon dioxide) adsorption in different shale and coal samples under different temperatures were measured, modelled and analyzed to understand gas adsorption behavior, thermodynamic characteristics, and gas adsorption kinetics. Some tentative conclusions can be obtained.

- The dual-site Langmuir adsorption model can simulate methane adsorption behavior in shale under high pressure (up to 27MPa) and high temperature (up to 355.15K) conditions as well as supercritical carbon dioxide adsorption in coals under high pressure (up to 20MPa) and high temperature (up to 352.57K).
- The dual-site Langmuir adsorption model can not only interpret all observed adsorption phenomena, such as how the observed adsorption uptake first increases, reaches the maximum and then decreases with increasing pressure and the crossover of adsorption isotherms under different temperatures, but also it can extrapolate adsorption isotherms beyond test data.
- The dual-site Langmuir adsorption model can be used to differentiate the true ratio between adsorbed phase and bulk gas phase for shale gas under reservoir conditions. This can be used to obtain an accurate shale GIP resource estimation as a function of reservoir pressure and geothermal gradients.
- Based on the dual-site Langmuir adsorption model, it was found the maximum gas adsorption capacity of shale and coal is independent of temperature, and the temperature dependence of observed and absolute adsorption uptake are confirmed.
- The concept of the deep shale gas reservoir is proposed to provide a new perspective on shale gas development on the basis of the successful application of the dual-site Langmuir adsorption model.
- Neglecting either the real gas behavior or the adsorbed phase volume, such as the Clausius–Clapeyron approximation, results in an overestimation of the isosteric heat of adsorption.

- Based on the dual-site Langmuir model, the isosteric heat of adsorption for high pressure gas adsorption in shale and coal can be calculated analytically by considering both the real gas behavior and the volume effect of the adsorbed phase.
- The true isosteric heat of adsorption exhibits adsorption uptake as well as temperature dependence for high pressure gas adsorption in shale and coal, which can be readily investigated using the dual-site Langmuir adsorption model.
- The isosteric heat of adsorption in Henry's region for methane in anthracite, lean coal, and gas-fat coal is -23.31KJ/mol, -20.47 KJ/mol, -11.14 KJ/mol, respectively, are independent of temperature and can display the overall heterogenous property of different types of coal.
- Carbon dioxide adsorption kinetics in coal can be modeled by the pseudo-second order model. Modelling results indicates that the adsorption process for carbon dioxide in coal is a combination of both bulk diffusion-controlled and surface interaction-controlled processes; the former dominates the initial stage while the latter controls the majority of the overall process.
- Particle size of coal samples can significantly influence the sorption behavior of gas in coal, which affects the pore characterization of coal. It is difficult to characterize the pore features of coal using only one coal particle size.
- The differences in integral area between desorption and adsorption isotherms (hysteresis loop) for gas in coal decreases as a function of particle diameter.
- Unclosed hysteresis loops were observed in both low pressure carbon dioxide and nitrogen sorption tests which may be attributed to the plasticization of un-rigid coal during gas sorption.

These scientific conclusions provide an option for accurate estimation of the shale gas-in-place resource (total gas, adsorbed gas and free gas) in deep subsurface, accurate estimation of carbon dioxide storage capacity in coal seams, heat transfer analysis during shale gas production process, pore characterization of geo-materials such as coal and shale, and gas adsorption kinetics properties in geo-materials.

5.2. Future work

While the results and conclusions from this study provide valuable information for our understanding of high pressure gas (methane and carbon dioxide) adsorption behavior, thermodynamics and kinetics in shale and coal, these topics are far from being exhaustive. The published data for high pressure (> 15MPa) gas adsorption in shale and coal is still very limited. More experimental work should be continued to include more shale and coal samples to verify and validate the applied method in this work. Followings are some recommendations for future research work.

- **Water influence on gas adsorption capacity and transport in shale and coal**

Water treatments, such as water based drilling, hydraulic fracturing and water production with coalbed methane, accompany shale gas and coalbed methane development for subsurface reservoirs. However, water influence on these reservoirs is complex. On the one hand, water can displace the adsorbed phase of methane because of the high affinity of water on shale and coal. On the other hand, water can damage the reservoir because of the retention of water in shale and coal caused by the spontaneous imbibition effect, which can significantly impair the formation permeability and reduce the productivity. Therefore, it is critical to study the interaction among water, gas and shale/coal by simulating the real field scenarios to further enhance natural gas production in shale gas and coalbed methane reservoirs.

- **Mixture gas competitive adsorption in shale and coal**

This dissertation mainly focuses on pure gas adsorption in coal and shale. However, for enhanced coalbed methane and shale gas recovery by carbon dioxide injection and supercritical gas fracturing technique, the competitive adsorption between methane and carbon dioxide are important to recognize. Furthermore, since natural gas is a mixture gas composed of other heavier hydrocarbons like ethane, butane et al., how the natural gas quality (natural gas composition) changes with time for a shale gas well is still unclear. Since field tests for competitive adsorption behavior of mixture gases are expansive and sometimes impractical, controlled laboratory studies can provide an effective way to investigate the mechanisms behind these phenomena.

- **Validation of thermodynamic characterization of gas adsorption in shale and coal**

The thermodynamic modeling results of this work reveal that the isosteric heat of adsorption depends on both adsorption uptake and temperature. Even though the results are supported by robust theoretical derivation, direct measurement of heat release are needed to verify the modeling results. Considering the unique feature of differential scanning calorimetry in measuring heat release, heat measurement for gas adsorption in shale and coal are feasible. This future study will help further in understanding the interaction between gas and shale/coal during the adsorption process.

- **Adsorption mechanism investigation of gas in shale and coal using molecular simulation**

Shale and coal are pore-rich natural compounds containing pores from nanoscale to macroscale fractures. Therefore, it is impossible to understand the true gas adsorption behavior in different scale of pores through laboratory tests. Furthermore, there is no equation of states available for obtaining the physical properties of gas such as density in a confined nanoscale space. Considering the controllability and robust theoretical background of the molecular simulation approach, investigation of gas adsorption behavior in different scales of pore under extreme pressure and temperatures are possible. This future study will be helpful to understand and interpret observed gas adsorption behavior in shale and coal from laboratory tests.

Appendix A Supplemental materials for Section 2.2

A dual-site Langmuir equation for accurate estimation of high pressure deep shale gas resources

Supporting Information

Xu Tang[*], Nino Ripepi[*,†], Nicholas P. Stadie[‡], Lingjie, Yu[§,¶], Matthew R Hall[#,‖]

([*]Department of Mining and Minerals Engineering & [†]Virginia Center for Coal and Energy Research, Virginia Polytechnic Institute and State University, Blacksburg, Virginia, 24060, U.S; [‡]ETH Zürich, Laboratory of Inorganic Chemistry, Vladimir-Prelog-Weg 1, 8093 Zürich, Switzerland; [§]Wuxi Research Institute of Petroleum Geology of Sinopec Exploration & Production Research Institute, and [¶]Sinopec Key Laboratory of Petroleum Accumulation Mechanisms, Wuxi, Jiangsu, 214151, China); [#]Nottingham Centre for Geomechanics, Faculty of Engineering, University of Nottingham, Nottingham, NG7 2RD UK, [‖]British Geological Survey, Environmental Science Centre, Keyworth, Nottingham, NG12 5GG UK)

Corresponding author: Xu Tang

E-mail: xutang@vt.edu; Tel: 540-998-7174

Address: 100 Holden Hall Blacksburg, VA 24061-0239

Introduction

This paper introduces a dual site Langmuir model to describe and predict methane adsorption behavior under 303.15K, 318.15K, 333.15K, and 355.15K and up to 27 MPa. The dual site Langmuir is used for accurate prediction of adsorbed methane in deep shale gas reservoirs under high pressure and temperature conditions. The shale gas-in-place (GIP) content is estimated by considering the volume of the adsorbed layer at *in-situ* conditions. Our findings show that for shale formations deeper than 1000 m (> 15 MPa) below the subsurface, the GIP has historically been significantly overestimated. Also, the ratio of the adsorbed phase compared to the free gas has been significantly underestimated.

In order to support our findings in the paper, we provide the following information:

(1) Physical properties of Longmaxi shale (China)
(2) High pressure methane adsorption test data
(3) Data processing approach
(4) Geological gas-in-place estimation using conventional approach

1. Physical properties of Longmaxi shale (China)

Shale samples from the Lower Silurian Longmaxi Formation (collected at a depth of 2400.8 m) were obtained from the Fuling #1 well in the Fuling region, Sichuan Province, China. The vitrinite equivalent reflectance (Ro) of the sample is 2.2% - 2.5%. The physical properties of the shale are shown in Table A-1 (Note: TOC – total organic carbon (%), S1 – hydrocarbons evolved at 300°C (mg/g), S2 – hydrocarbons evolved between 300 and 600°C (mg/g) upon heating at 25°C/min, S3 – organic carbon dioxide evolved at 300°C and up to 390°C (mg/g), T_{max} is the maximum temperature for obtaining S2). The rock pyrolysis measurement was conducted using a Rock-Eval 6 analyzer (Vinci Technologies, France).

Table A-1 Properties of shale

Rock-Eval analysis	
TOC (%)	4.52
Tmax(°C)	344
S1(mg/g)	0.01
S2(mg/g)	0.01
S3(mg/g)	0.13

The shale specimen was ground and sieved using 0.38-0.83 mm metal sifters and placed in a drying oven at 105 °C for 24 hour to dehydrate. After dehydration, the prepared sample was stored in a desiccator prior to adsorption measurements.

2. High pressure methane adsorption tests

Methane adsorption measurements were conducted using a Rubotherm Gravimetric Sorption Analyzer IsoSORP. The methane density was obtained *via* the NIST package using the Setzmann & Wagner equation (1). The instrument can achieve pressures of up to 35 MPa and temperatures up to 150°C ±0.2℃. Ultrapure methane gas (99.99%) was used as the adsorbate. Equilibrium was defined as when the adsorption time was longer than 2 hours or when the weight change of the sample was within 30 μg over a span of 10 min. The detailed characteristics of the instrument has been extensively described anywhere else (2).

The test procedure used was as follows:

(1) Mass of the adsorption cell

The blank test (without shale samples) was first conducted in order to obtain the mass and volume of the adsorption cell (shown in Figure A-1). The whole system is pumped down to vacuum conditions, and then the measurement is conducted by dosing pure nitrogen into the adsorption cell up to 5MPa. The apparent weight of the adsorption cell can be recorded from magnetic suspension balance (MSB), which is the interaction between the weight of the adsorption cell and the buoyancy induced by the dosing N_2. Through the linear relationship between the apparent weight of the adsorption cell and the density of the nitrogen, the mass and the volume of the adsorption cell can be obtained,

$$m_{sc}^{N2} = m_s - \rho_{N2} V_s \quad \text{(S-1)}$$

where m_{sc}^{N2} is the apparent of the adsorption cell, m_s is the mass of the adsorption cell, ρ_{N2} is the density of nitrogen obtained from NIST package, and V_s is the adsorption cell volume.

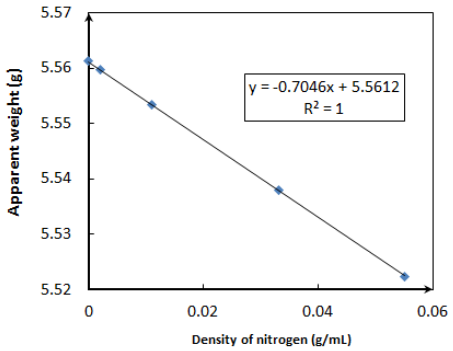

Figure A-1 Blank test results

(2) Mass of test shale sample

After the shale sample is put in the adsorption cell, the whole system is pumped down to vacuum conditions. Then, the non-adsorbed pure Helium is dosed into the system up to 5MPa (shown in Figure A-2). The apparent weight of the adsorption cell with shale can be recorded from MSB. It should be noted even though Helium adsorption in shale is very small, it still has some influence on the test results, which cannot be avoided. The Helium intrusion test is also the routine method for measuring the skeletal density of porous material. Through the similar relationship in equation (S1), the total mass of the adsorption cell and the shale sample can be obtained,

$$m_{sc}^{He} = m_{sc} - \rho_{He} V_{sc} \quad \text{(S-2)}$$

where m_{sc}^{He} is the apparent of the adsorption cell, m_{sc} is the mass of the adsorption cell, ρ_{He} is the density of nitrogen obtained from the NIST package, and V_{sc} is the adsorption cell volume.

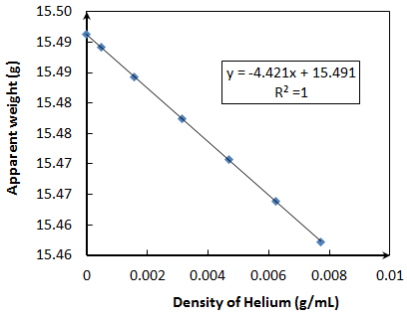

Figure A-2 Helium test results

Then, the mass and volume of the shale sample can be obtained using equation (S-3) and (S-4),

$$m_{shale} = m_{sc} - m_s \quad \text{(S-3)}$$

$$V_{shale} = V_{sc} - V_s \quad \text{(S-4)}$$

(3) Methane adsorption test

Once the mass of the shale sample is obtained, the system is then pumped to vacuum conditions. Then, the adsorption cell is dosed with methane and the apparent weight of the adsorption cell can be recorded at each equilibrium point:

$$m_t^{CH4} = m_{sc} + m_a - \rho_{CH4}(V_{sc} + V_a) \quad \text{(S-5)}$$

Where m_t^{CH4} is the apparent weight of the adsorption cell, V_a is the volume of the adsorbed methane layer, m_a is the absolute adsorption uptake, ρ_{CH4} is the density of methane obtained from NIST package. If we rewrite equation (S-5)

$$m_{Gibbs} = m_a - \rho_{CH4} V_a = m_t^{CH4} - m_{sc} + \rho_{CH4} V_{sc} \quad \text{(S-6)}$$

Where the term ($m_a - \rho_{CH4} V_a$) is called Gibbs excess mass (m_{Gibbs}), which can be easily obtained from equation (S-6). Then, we can obtain the molar excess adsorption uptake (n_{ex}) and M_{CH4} is the molar mass of methane (16.04 g/mol).

$$n_{ex} = \frac{m_{Gibbs}^{CH4}}{M_{CH4} \cdot m_{shale}} \quad \text{(S-7)}$$

This process is repeated at predefined measuring equilibrium pressure points.

Table A-2 Test data under 303.15K, 318.15K, 333.15K, and 355.15K

303.15 K	
Pressure (MPa)	**Adsorption content-test data (mmol/g)**
0.5	0.0308
1	0.0451
2	0.0621
4	0.079
6	0.0866
8	0.0893
10	0.0879
12	0.0853
15	0.0763
16	0.0754
18	0.0679
20	0.0625
22	0.058
24	0.0518
25	0.0491

318.15K	
Pressure(MPa)	**Adsorption content-test data (mmol/g)**
0.5	0.0250
1	0.0375
2	0.0531
4	0.0696
6	0.0772
8	0.0813
10	0.0813
12	0.0790
15	0.0737
16	0.0723
18	0.0670
20	0.0629
22	0.0580
24	0.0540
25	0.0509

333.15 K	
Pressure(MPa)	**Adsorption content-test data (mmol/g)**
0.5	0.0196
1	0.0308
2	0.0455
4	0.0616
6	0.0701
8	0.0754
10	0.0777
12	0.0786
15	0.0768
16	0.0759
18	0.0714
20	0.0670
22	0.0643
24	0.0616
25	0.0607
26	0.0598
27	0.0576

355.15 K	
Pressure (MPa)	**Adsorption content-test data (mmol/g)**
0.5	0.0156
1	0.0250
2	0.0384
4	0.0536
6	0.0625
8	0.0679
10	0.0705
12	0.0719
15	0.0714
16	0.0710
18	0.0692
20	0.0670
22	0.0643
24	0.0612
25	0.0621
26	0.0594

3. Data processing approach

The test data were processed using a previously developed Mathematica script (3-5); the four Gibbs excess adsorption isotherms were fitted simultaneously to the dual-site Langmuir model (equation 6 in the paper) by a least-squares residual minimization algorithm based on the Differential Evolution method. Each data point was given the same weight and none were discarded. The density of the bulk fluid as a function of temperature and pressure was obtained

from the NIST REFPROP database (1). The seven independent fitting parameters were varied to achieve the global minimum of the residual-squares value within the following limits: 0<nmax <100 mmol/g, 0< Vmax<10 cm3/g, 0<α<1, 0< E1 <100 kJ/mol, 0< E2 <100 kJ/mol, A1 > 0, A2 > 0). Minimization was performed in excess of 100 unique times by changing the random seed in order to assure that a global minimum was achieved. Once the seven fitting parameters were determined, absolute and excess adsorption uptake could be easily calculated at any temperature and pressure by use of equations 5 and 6.

4. Geological gas-in-place estimation using conventional approach

The most widely used approach for estimating the adsorbed methane content is as follows the Langmuir equation is used to fit the adsorption isotherms under intermediate pressures and temperatures (6-11). Then, based on the relationship between Langmuir constants (n_{max} and K(T)) and temperature, the adsorbed methane content is predicted using equation (S-8) at in-situ temperatures and pressures (6-11). The test isotherm data before the observed the maximum value is used to obtain the relationship between Langmuir constants and temperature (test data is shown in Table A-2), and the fitting parameters are shown in Table A-3.

$$n_a = n_{\max} \frac{K(T)P}{1+K(T)P} \quad \text{(S-8)}$$

Table A-3 Fitting parameter using two parameter Langmuir equation

Langmuir Fitting		
Temperature (K)	a (mmol/g)	K(T)(1/MPa)
303.15	0.104	0.782
318.15	0.095	0.663
333.15	0.093	0.499
355.15	0.088	0.3999
Langmuir constant-a (T)	a(T)=0.189-0.000287*T	
Langmuir constant - K(T)	K(T)=0.00723*EXP(1423.77/T)	

It is worth pointing out that in Figure 2.2.7 and 2.2.8 in the paper, there are crossover between the Absolute Adsorption curve and Conventional Absolute prediction, which should not occur theoretically. This deviation can be attributed to the empirical equation for Langmuir constants with temperatures as shown in Table A-3. The obtained empirical equation induces new uncertainties for the adsorbed methane content when it is used for prediction.

Reference

1 Setzmann, U., & Wagner, W. (1991). A new equation of state and tables of thermodynamic properties for methane covering the range from the melting line to 625 K at pressures up to 100 MPa. Journal of Physical and Chemical reference data, 20(6), 1061-1155.

2 Keller, J. U., & Staudt, R. (2005). Gas adsorption equilibria: experimental methods and adsorptive isotherms. Springer Science & Business Media.

3 Stadie, N. P., Murialdo, M., Ahn, C. C., & Fultz, B. (2013). Anomalous isosteric enthalpy of adsorption of methane on zeolite-templated carbon. Journal of the American Chemical Society, 135(3), 990-993.

4 Murialdo, M., Stadie, N. P., Ahn, C. C., & Fultz, B. (2015). Observation and Investigation of Increasing Isosteric Heat of Adsorption of Ethane on Zeolite-Templated Carbon. The Journal of Physical Chemistry C, 119(2), 944-950.

5 Stadie, N. P., Murialdo, M., Ahn, C. C., & Fultz, B. (2015). Unusual Entropy of Adsorbed Methane on Zeolite-Templated Carbon. The Journal of Physical Chemistry C, 119(47), 26409-26421.

6 Curtis, J. B. (2002). Fractured shale-gas systems. AAPG bulletin, 86(11), 1921-1938.

7 Montgomery, S. L., Jarvie, D. M., Bowker, K. A., & Pollastro, R. M. (2005). Mississippian Barnett Shale, Fort Worth basin, north-central Texas: Gas-shale play with multi–trillion cubic foot potential. AAPG bulletin, 89(2), 155-175.

8 Kuuskraa, V., Stevens, S. H., & Moodhe, K. D. (2013). Technically recoverable shale oil and shale gas resources: an assessment of 137 shale formations in 41 countries outside the United States. [J]. Natural Gas Industry, 5, 003.

9 NETL (National Energy Technology Laboratory). (2009). Modern shale gas development in the United States: A primer. US Department of Energy, Office of Fossil Energy. https://www.netl.doe.gov/File%20Library/Research/Oil-Gas/shale-gas-primer-update-2013.pdf.

10 EIA, 2016. http://www.eia.gov/dnav/ng/ng_prod_sum_dcu_NUS_a.htm

11 Andrews, I. J. (2013). The Carboniferous Bowland Shale gas study: geology and resource estimation.

Appendix B Supplemental materials for Section 4.1

Isothermal Adsorption Kinetics Properties of Carbon Dioxide in Crushed Coal

Supporting Information

Xu Tang[a]*, Nino Ripepi[a], Ellen Gilliland[a,b]

(a Department of Mining and Minerals Engineering, Virginia Polytechnic Institute and State University, Blacksburg, Virginia, 24060, USA; b Virginia Center for Coal and Energy Research (0411), Virginia Polytechnic Institute and State University, Blacksburg, Virginia 24061, USA)

The following two Tables (Table B-1 and Table B-2) support the detailed discussion in **Section 5.3 Sorption capacity estimation via PSO model**

Table B-1 Comparison between the predicted sorption content and measured data for bituminous coal

		PSO Fitting curve	R2	Equilibrium pressure (MPa)	Sorption content in each stage value	Equilibrium pressure (MPa)	Accumulated Qt (mmol/g)	Measured data (mmol/g)	(Qt-Qm)/Qm (100%)
120	Stage 1	y = 18.54x + 182.27	R^2 = 0.9994	0→0.0640	0.0851	0.064	0.0851	0.0820	0.038392141
	Stage 2	y = 10.559x + 134.96	R^2 = 0.998	0.0640→0.1851	0.1365	0.1851	0.2216	0.2332	-0.049337995
	Stage 3	y = 16.61x + 235.95	R^2 = 0.9975	0.1851→0.2951	0.0861	0.2951	0.3077	0.3278	-0.061194744
	Stage 4	y = 13.31x + 193.05	R^2 = 0.9972	0.2951→0.4866	0.105	0.4866	0.4127	0.4427	-0.067630475
	Stage 5	y = 7.326x + 108.94	R^2 = 0.997	0.4866→1.0884	0.1895	1.0884	0.6022	0.6445	-0.06569456
	Stage 6	y = 12.425x + 184.31	R^2 = 0.9978	1.0884→1.6892	0.1133	1.6892	0.7154	0.7658	-0.065746328
	Stage 7	y = 8.2933x + 129.5	R^2 = 0.9977	1.6892→3.1433	0.1842	3.1433	0.8996	0.9685	-0.071087954
	Stage 8	y = 19.192x + 390	R^2 = 0.9715	3.1433→4.0451	0.0957	4.0451	0.9954	1.0984	-0.093836682
180	Stage 1	y = 18.546x + 181.25	R^2 = 0.9998	0→0.0640	0.0851	0.064	0.0851	0.0820	0.038392141
	Stage 2	y = 9.9552x + 158.5	R^2 = 0.9985	0.0640→0.1851	0.1468	0.1851	0.2319	0.2332	-0.005160428
	Stage 3	y = 15.6x + 277.11	R^2 = 0.9979	0.1851→0.2951	0.09	0.2951	0.3219	0.3278	-0.017871956
	Stage 4	y = 12.564x + 223.7	R^2 = 0.9982	0.2951→0.4866	0.1095	0.4866	0.4314	0.4427	-0.025385002
	Stage 5	y = 6.8907x + 126.51	R^2 = 0.9981	0.4866→1.0884	0.1981	1.0884	0.6295	0.6445	-0.023337183
	Stage 6	y = 12.021x + 200.96	R^2 = 0.9986	1.0884→1.6892	0.116	1.6892	0.7454	0.7658	-0.026570218
	Stage 7	y = 8.0367x + 140.82	R^2 = 0.9988	1.6892→3.1433	0.188	3.1433	0.9334	0.9685	-0.036187645
	Stage 8	y = 16.828x + 497.77	R^2 = 0.9781	3.1433→4.0451	0.0846	4.0451	1.0365	1.0984	-0.056419815
240	Stage 1	y = 18.738x + 167.5	R^2 = 0.9998	0→0.0640	0.1454	0.064	0.0846	0.0820	0.03215653
	Stage 2	y = 9.6516x + 176.73	R^2 = 0.9989	0.0640→0.1851	0.0924	0.1851	0.23	0.2332	-0.013510656
	Stage 3	y = 15.042x + 311.29	R^2 = 0.9983	0.1851→0.2951	0.1122	0.2951	0.3224	0.3278	-0.016389662
	Stage 4	y = 12.158x + 248.59	R^2 = 0.9985	0.2951→0.4866	0.203	0.4866	0.4346	0.4427	-0.018188108
	Stage 5	y = 6.6672x + 140.43	R^2 = 0.9985	0.4866→1.0884	0.1178	1.0884	0.6376	0.6445	-0.010730273
	Stage 6	y = 11.765x + 217.43	R^2 = 0.999	1.0884→1.6892	0.1906	1.6892	0.7553	0.7658	-0.013676142
	Stage 7	y = 7.874x + 150.96	R^2 = 0.9991	1.6892→3.1433	0.1071	3.1433	0.9459	0.9685	-0.023307642
	Stage 8	y = 15.748x + 567.09	R^2 = 0.9857	3.1433→4.0451	0.0846	4.0451	1.0531	1.0984	-0.041272458
360	Stage 1	y = 19.124x + 129	R^2 = 0.9997	0→0.0640	0.0835	0.064	0.0835	0.0820	0.018736055
	Stage 2	y = 9.3353x + 204.66	R^2 = 0.9993	0.0640→0.1851	0.1489	0.1851	0.2324	0.2332	-0.003216854
	Stage 3	y = 14.507x + 358.99	R^2 = 0.999	0.1851→0.2951	0.0948	0.2951	0.3272	0.3278	-0.001745339
	Stage 4	y = 6.5513x + 151.07	R^2 = 0.9994	0.2951→0.4866	0.1152	0.4866	0.4424	0.4427	-0.000567002
	Stage 5	y = 6.5513x + 151.07	R^2 = 0.9994	0.4866→1.0884	0.2056	1.0884	0.648	0.6445	0.005405871
	Stage 6	y = 11.195x + 271.08	R^2 = 0.9977	1.0884→1.6892	0.1221	1.6892	0.77	0.7658	0.005520152
	Stage 7	y = 7.6905x + 168.25	R^2 = 0.9993	1.6892→3.1433	0.1936	3.1433	0.9636	0.9685	-0.005031445
	Stage 8	y = 14.727x + 663.06	R^2 = 0.9919	3.1433→4.0451	0.1115	4.0451	1.0752	1.0984	-0.021152926
480	Stage 1	******	******	0→0.0640	0.0835	0.064	0.0835	0.0820	0.018736055
	Stage 2	y = 9.1911x + 223.29	R^2 = 0.9995	0.0640→0.1851	0.1506	0.1851	0.2341	0.2332	0.004074589
	Stage 3	y = 14.213x + 396.9	R^2 = 0.9993	0.1851→0.2951	0.0963	0.2951	0.3304	0.3278	0.008017543
	Stage 4	y = 11.564x + 308.34	R^2 = 0.9995	0.2951→0.4866	0.1164	0.4866	0.4468	0.4427	0.009373109
	Stage 5	y = 6.4792x + 160.21	R^2 = 0.9996	0.4866→1.0884	0.2073	1.0884	0.6541	0.6445	0.01487034
	Stage 6	y = 10.975x + 296.37	R^2 = 0.9981	1.0884→1.6892	0.1239	1.6892	0.7779	0.7658	0.015836527
	Stage 7	y = 7.514x + 192.14	R^2 = 0.9991	1.6892→3.1433	0.1967	3.1433	0.9746	0.9685	0.006326643
	Stage 8	y = 13.534x + 821.72	R^2 = 0.9899	3.1433→4.0451	0.1175	4.0451	1.0922	1.0984	-0.005676364
600	Stage 1	******	******	0→0.0640	0.0835	0.064	0.0835	0.0820	0.018736055
	Stage 2	y = 8.928x + 267.7	R^2 = 0.9989	0.0640→0.1851	0.1538	0.1851	0.2373	0.2332	0.017799658
	Stage 3	y = 14.076x + 420.25	R^2 = 0.9995	0.1851→0.2951	0.0975	0.2951	0.3348	0.3278	0.021441505
	Stage 4	y = 11.425x + 332.58	R^2 = 0.9995	0.2951→0.4866	0.1174	0.4866	0.4522	0.4427	0.021572337
	Stage 5	y = 6.4474x + 165.86	R^2 = 0.9998	0.4866→1.0884	0.2081	1.0884	0.6603	0.6445	0.024489964
	Stage 6	y = 11.019x + 288.9	R^2 = 0.999	1.0884→1.6892	0.1236	1.6892	0.7838	0.7658	0.023504832
	Stage 7	y = 7.3484x + 220.95	R^2 = 0.9989	1.6892→3.1433	0.1997	3.1433	0.9835	0.9685	0.015487868
	Stage 8	y = 12.61x + 985.54	R^2 = 0.9868	3.1433→4.0451	0.1229	4.0451	1.1065	1.0984	0.007374363
Test	Stage 1	y = 19.1240x + 1290	0.9997	0→0.0640	0.0523	0.064	0.0835	0.0820	0.018750282
	Stage 2	y = 8.7926x + 296.16	0.9992	0.0640→0.1851	0.1137	0.1851	0.2391	0.2332	0.025413768
	Stage 3	y = 14.027x + 430.78	0.9997	0.1851→0.2951	0.0713	0.2951	0.3362	0.3278	0.025842488
	Stage 4	y = 0.4195x + 13.077	0.9997	0.2951→0.4866	0.0883	0.4866	0.4544	0.4427	0.026638771
	Stage 5	y = 6.4357x + 168.09	0.9999	0.4866→1.0884	0.1554	1.0884	0.6628	0.6445	0.028379294
	Stage 6	y = 10.935x + 307.90	0.9992	1.0884→1.6892	0.0914	1.6892	0.7870	0.7658	0.027628826
	Stage 7	y = 7.0164x + 300.72	0.9986	1.6892→3.1433	0.1425	3.1433	0.9931	0.9685	0.025356897
	Stage 8	y = 10.793x + 1429.7	0.9808	3.1433→4.0451	0.0927	4.0451	1.1294	1.0984	0.028217133

Table B-2 Comparison between the predicted sorption content and measured data for subbituminous coal

		PSO fitting equation	R2	Sorption process	Sorption content in each stage (mmol/g)	Accumulated Qt(mmol/g)	Measured data (mmol/g)	(Qt-Qm)/Qm (100%)
120	Stage 1	y = 30.398x + 826.88	R^2 = 0.9909	0→0.0889	0.0368	0.0368	0.0517	-0.28800008
	Stage 2	y = 23.295x + 695.14	R^2 = 0.9837	0.0889→0.2254	0.0467	0.0984	0.1281	-0.23167448
	Stage 3	y = 17.521x + 580.12	R^2 = 0.9809	0.2254→0.4871	0.0610	0.1890	0.2289	-0.1741305
	Stage 4	y = 11.939x + 391.57	R^2 = 0.9826	0.4871→1.0997	0.0878	0.3166	0.3700	-0.14426721
	Stage 5	y = 18.327x + 696.2	R^2 = 0.9804	1.0997→1.6214	0.0571	0.4270	0.4580	-0.06754876
	Stage 6	y = 9.0444x + 362.57	R^2 = 0.9762	1.6214→3.1822	0.1297	0.5876	0.6338	-0.07283536
	Stage 7	y = 13.741x + 1091.4	R^2 = 0.8422	3.1822→4.0845	0.0952	0.7288	0.7533	-0.03260822
180	Stage 1	y = 27.406x + 976.42	R^2 = 0.9911	0→0.0889	0.0404	0.0404	0.0517	-0.21858108
	Stage 2	y = 19.898x + 842.88	R^2 = 0.984	0.0889→0.2254	0.0540	0.1057	0.1281	-0.17445773
	Stage 3	y = 14.951x + 687.16	R^2 = 0.9842	0.2254→0.4871	0.0708	0.1988	0.2289	-0.1312689
	Stage 4	y = 10.209x + 463.09	R^2 = 0.9851	0.4871→1.0997	0.1020	0.3308	0.3700	-0.10590458
	Stage 5	y = 15.866x + 800.23	R^2 = 0.9852	1.0997→1.6214	0.0656	0.4355	0.4580	-0.04906817
	Stage 6	y = 7.9366x + 407.94	R^2 = 0.9864	1.6214→3.1822	0.1452	0.6030	0.6338	-0.04848409
	Stage 7	y = 13.61x + 1102.5	R^2 = 0.9521	3.1822→4.0845	0.0959	0.7295	0.7533	-0.0316784
240	Stage 1	y = 25.54x + 1107.3	R^2 = 0.9916	0→0.0889	0.0431	0.0431	0.0517	-0.16705199
	Stage 2	y = 16.854x + 1057.3	R^2 = 0.9853	0.0889→0.2254	0.0631	0.1148	0.1281	-0.1035927
	Stage 3	y = 13.561x + 773.22	R^2 = 0.9859	0.2254→0.4871	0.0776	0.2057	0.2289	-0.1013175
	Stage 4	y = 9.2495x + 522.58	R^2 = 0.9859	0.4871→1.0997	0.1121	0.3410	0.3700	-0.07844101
	Stage 5	y = 14.366x + 893.9	R^2 = 0.9861	1.0997→1.6214	0.0722	0.4421	0.4580	-0.03469837
	Stage 6	y = 7.3391x + 444.76	R^2 = 0.9899	1.6214→3.1822	0.1554	0.6133	0.6338	-0.03229825
	Stage 7	y = 13.356x + 1117.8	R^2 = 0.9788	3.1822→4.0845	0.0973	0.7309	0.7533	-0.02982355
360	Stage 1	y = 23.195x + 1339	R^2 = 0.9923	0→0.0889	0.0471	0.0471	0.0517	-0.09053903
	Stage 2	y = 15.772x + 1168	R^2 = 0.9869	0.0889→0.2254	0.0672	0.1189	0.1281	-0.07181391
	Stage 3	y = 11.816x + 932.48	R^2 = 0.9865	0.2254→0.4871	0.0885	0.2165	0.2289	-0.0539906
	Stage 4	y = 8.1097x + 625.22	R^2 = 0.9876	0.4871→1.0997	0.1273	0.3562	0.3700	-0.03737154
	Stage 5	y = 12.569x + 1054.7	R^2 = 0.9876	1.0997→1.6214	0.0821	0.4520	0.4580	-0.01296763
	Stage 6	y = 6.6113x + 511.24	R^2 = 0.9916	1.6214→3.1822	0.1704	0.6283	0.6338	-0.0086305
	Stage 7	y = 12.315x + 1213.6	R^2 = 0.9886	3.1822→4.0845	0.1036	0.7372	0.7533	-0.02142222
480	Stage 1	y = 21.732x + 1542.9	R^2 = 0.9929	0→0.0889	0.0500	0.0500	0.0517	-0.0344397
	Stage 2	y = 14.533x + 1333.2	R^2 = 0.9886	0.0889→0.2254	0.0726	0.1243	0.1281	-0.0296123
	Stage 3	y = 10.85x + 1059.6	R^2 = 0.988	0.2254→0.4871	0.0961	0.2241	0.2289	-0.02082184
	Stage 4	y = 7.5244x + 701.76	R^2 = 0.9901	0.4871→1.0997	0.1369	0.3658	0.3700	-0.01144675
	Stage 5	y = 11.724x + 1165.6	R^2 = 0.9907	1.0997→1.6214	0.0879	0.4578	0.4580	-0.00044651
	Stage 6	y = 6.1676x + 569.04	R^2 = 0.9922	1.6214→3.1822	0.1813	0.6392	0.6338	0.00853913
	Stage 7	y = 11.327x + 1343.2	R^2 = 0.9884	3.1822→4.0845	0.1107	0.7443	0.7533	-0.01202031
600	Stage 1	y = 20.701x + 1728	R^2 = 0.9933	0→0.0889	0.0522	0.0522	0.0517	0.009857373
	Stage 2	y = 13.681x + 1481.1	R^2 = 0.9896	0.0889→0.2254	0.0768	0.1286	0.1281	0.003843098
	Stage 3	y = 10.151x + 1179.2	R^2 = 0.9885	0.2254→0.4871	0.1024	0.2305	0.2289	0.006905163
	Stage 4	y = 7.1306x + 769.12	R^2 = 0.9915	0.4871→1.0997	0.1442	0.3731	0.3700	0.008390949
	Stage 5	y = 11.27x + 1243.7	R^2 = 0.9932	1.0997→1.6214	0.0913	0.4612	0.4580	0.00705622
	Stage 6	y = 5.9931x + 598.62	R^2 = 0.995	1.6214→3.1822	0.1860	0.6439	0.6338	0.015988204
	Stage 7	y = 10.761x + 1440.7	R^2 = 0.9902	3.1822→4.0845	0.1153	0.7489	0.7533	-0.00585639
720	Stage 1	y = 20.025x + 1876.3	R^2 = 0.9942	0→0.0889	0.0539	0.0539	0.0517	0.041377667
	Stage 2	y = 13.063x + 1613.1	R^2 = 0.9905	0.0889→0.2254	0.0803	0.1320	0.1281	0.030840841
	Stage 3	y = 9.6907x + 1276.5	R^2 = 0.9898	0.2254→0.4871	0.1071	0.2352	0.2289	0.027348009
	Stage 4	y = 6.8703x + 824.15	R^2 = 0.9929	0.4871→1.0997	0.1496	0.3784	0.3700	0.022751988
	Stage 5	y = 10.921x + 1318.3	R^2 = 0.9945	1.0997→1.6214	0.0941	0.4640	0.4580	0.013247809
	Stage 6	y = 5.8993x + 618.64	R^2 = 0.9967	1.6214→3.1822	0.1887	0.6465	0.6338	0.020174457
	Stage 7	y = 10.181x + 1564.9	R^2 = 0.9887	3.1822→4.0845	0.1206	0.7542	0.7533	0.001170989
840	Stage 1	y = 19.525x + 2006.4	R^2 = 0.995	0→0.0889	0.0552	0.0552	0.0517	0.066095696
	Stage 2	y = 12.603x + 1730	R^2 = 0.9914	0.0889→0.2254	0.0831	0.1348	0.1281	0.052655113
	Stage 3	y = 9.3773x + 1355.2	R^2 = 0.9914	0.2254→0.4871	0.1105	0.2386	0.2289	0.042415135
	Stage 4	y = 6.6867x + 870.37	R^2 = 0.9941	0.4871→1.0997	0.1536	0.3824	0.3700	0.033553849
	Stage 5	y = 10.649x + 1386.4	R^2 = 0.9953	1.0997→1.6214	0.0965	0.4664	0.4580	0.018354748
	Stage 6	y = 5.8332x + 635.47	R^2 = 0.9976	1.6214→3.1822	0.1906	0.6485	0.6338	0.023205336
	Stage 7	y = 9.5442x + 1726.1	R^2 = 0.9843	3.1822→4.0845	0.1272	0.7608	0.7533	0.00987023
Test time	Stage 1	y = 19.137x + 2122.1	R^2 = 0.9955	0→0.0889	0.0562	0.0562	0.0517	0.086166938
	Stage 2	y = 12.236x + 1838.1	R^2 = 0.9925	0.0889→0.2254	0.0855	0.1372	0.1281	0.0712354
	Stage 3	y = 9.0867x + 1442.7	R^2 = 0.9927	0.2254→0.4871	0.1139	0.2419	0.2289	0.057018658
	Stage 4	y = 6.5057x + 924.43	R^2 = 0.9952	0.4871→1.0997	0.1577	0.3866	0.3700	0.044799541
	Stage 5	y = 10.431x + 1451.2	R^2 = 0.9963	1.0997→1.6214	0.0984	0.4683	0.4580	0.022640083
	Stage 6	y = 5.7648x + 655.78	R^2 = 0.9982	1.6214→3.1822	0.1926	0.6505	0.6338	0.026414853
	Stage 7	y = 9.0223x + 1880.2	R^2 = 0.9833	3.1822→4.0845	0.1332	0.7668	0.7533	0.017915467

Appendix C Copyright releasing documents from publishers

Copyright Clearance Center RightsLink®

Account Info | Help

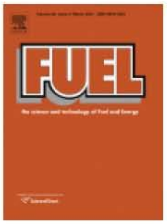

Title: A dual-site Langmuir equation for accurate estimation of high pressure deep shale gas resources

Author: Xu Tang,Nino Ripepi,Nicholas P. Stadie,Lingjie Yu,Matthew R. Hall

Publication: Fuel

Publisher: Elsevier

Date: Dec 1, 2016

Logged in as:
Xu Tang
Account #:
3001075328
LOGOUT

Order Completed

Thank you for your order.

This Agreement between Xu Tang ("You") and Elsevier ("Elsevier") consists of your order details and the terms and conditions provided by Elsevier and Copyright Clearance Center.

License number	Reference confirmation email for license number
License date	Nov 01, 2016
Licensed Content Publisher	Elsevier
Licensed Content Publication	Fuel
Licensed Content Title	A dual-site Langmuir equation for accurate estimation of high pressure deep shale gas resources
Licensed Content Author	Xu Tang,Nino Ripepi,Nicholas P. Stadie,Lingjie Yu,Matthew R. Hall
Licensed Content Date	1 December 2016
Licensed Content Volume	185
Licensed Content Issue	n/a
Licensed Content Pages	8
Type of Use	reuse in a thesis/dissertation
Portion	full article
Format	both print and electronic
Are you the author of this Elsevier article?	Yes
Will you be translating?	Yes
Number of languages	>10
Languages	Chinese
Order reference number	
Title of your thesis/dissertation	Measurements, Modeling and Analysis of High Pressure Gas Sorption in Shale and Coal for Unconventional Gas Recovery and Carbon Sequestration
Expected completion date	Dec 2016
Estimated size (number of pages)	180
Elsevier VAT number	GB 494 6272 12
Requestor Location	Xu Tang 505 Sunridge Drive Apt I BLACKSBURG, VA 24060 United States Attn: Xu Tang

Title: Adsorption Affinity of Different Types of Coal: Mean Isosteric Heat of Adsorption

Author: Xu Tang, Zhaofeng Wang, Nino Ripepi, et al

Publication: Energy & Fuels

Publisher: American Chemical Society

Date: Jun 1, 2015

Logged in as:
Xu Tang
Account #:
3001075328
LOGOUT

PERMISSION/LICENSE IS GRANTED FOR YOUR ORDER AT NO CHARGE

This type of permission/license, instead of the standard Terms & Conditions, is sent to you because no fee is being charged for your order. Please note the following:

- Permission is granted for your request in both print and electronic formats, and translations.
- If figures and/or tables were requested, they may be adapted or used in part.
- Please print this page for your records and send a copy of it to your publisher/graduate school.
- Appropriate credit for the requested material should be given as follows: "Reprinted (adapted) with permission from (COMPLETE REFERENCE CITATION). Copyright (YEAR) American Chemical Society." Insert appropriate information in place of the capitalized words.
- One-time permission is granted only for the use specified in your request. No additional uses are granted (such as derivative works or other editions). For any other uses, please submit a new request.

BACK CLOSE WINDOW

JOHN WILEY AND SONS LICENSE TERMS AND CONDITIONS

Nov 03, 2016

This Agreement between Xu Tang ("You") and John Wiley and Sons ("John Wiley and Sons") consists of your license details and the terms and conditions provided by John Wiley and Sons and Copyright Clearance Center.

License Number	3980370249330
License date	Nov 01, 2016
Licensed Content Publisher	John Wiley and Sons
Licensed Content Publication	Greenhouse Gases: Science and Technology
Licensed Content Title	Isothermal adsorption kinetics properties of carbon dioxide in crushed coal
Licensed Content Author	Xu Tang,Nino Ripepi,Ellen Gilliland
Licensed Content Date	Nov 16, 2015
Licensed Content Pages	15
Type of use	Dissertation/Thesis
Requestor type	Author of this Wiley article
Format	Print and electronic
Portion	Full article
Will you be translating?	No
Title of your thesis / dissertation	Measurements, Modeling and Analysis of High Pressure Gas Sorption in Shale and Coal for Unconventional Gas Recovery and Carbon Sequestration
Expected completion date	Dec 2016
Expected size (number of pages)	180
Requestor Location	Xu Tang 505 Sunridge Drive Apt I BLACKSBURG, VA 24060 United States Attn: Xu Tang
Publisher Tax ID	EU826007151
Billing Type	Invoice
Billing Address	Xu Tang 505 Sunridge Drive Apt I BLACKSBURG, VA 24060 United States Attn: Xu Tang
Total	0.00 USD